Construction and employment of a system for the in vivo and in vitro analysis of NER in chromatin

Rebecca Johnson

ProQuest LLC
789 East Eisenhower Parkway
P.O. Box 1346
Ann Arbor, MI 48106-1346

Abbreviations

BER	Base Excision Repair
CPD	Cyclobutane pyrimidine dimer
CS	Cockayne syndrome
DNA	Deoxyribonucleic acid
dsDNA	Double-stranded DNA
GG-NER	Global genome Nucleotide excision repair
HAT	Histone acetyltransferase
HDAC	Histone deacetylase
ML *endo*	*Miccrococcus luteus* CPD endonuclease
MPC	Magnetic particle concentrator
mRNA	Messenger RNA
NER	Nucleotide excision repair
NTS	Non-transcribed strand
ORF	Open reading frame
PCR	Polymerase chain reaction
6-4 photoproducts	Pyrimidine-pyrimidone (6-4) photoproducts
PR	Photoreactivation
PTM	Post-translational modification
RNA	Ribonucleic acid
RNAPII	RNA polymerase II
ROS	Reactive oxygen species
RPA	Replication protein A
r.t	Room temperature
SGD	Saccharomyces cerevisiae Genome Database
ssDNA	Single-stranded DNA
TC-NER	Transcription coupled nucleotide excision repair
TS	Transcribed strand
TTD	Trichothiodystrophy
UAS	Upstream activation sequence
URS	Upstream regulatory sequence
UV	Ultraviolet (light)
WT	Wild type
XP	Xeroderma pigmentosum
YPD	Yeast extract/Peptone/Dextrose medium

CONTENTS

Chapter 1

Chapter 2

Chapter 5

Chapter 6

Chapter 1

General Introduction

1.1 DNA damage

1.1.1 Endogenous DNA damage

Multiple agents within our environment can act to damage our DNA. These damaging factors can be grouped into endogenous and exogenous genotoxic agents, with both groups able to cause significant damage to the DNA double helix. These agents can produce a multitude of DNA lesions, giving rise to altered DNA which although the basis of genetic diversification, can also be disadvantageous to an organism. Any lesion which can affect the integrity of DNA is likely to cause genomic instability, a prerequisite to detrimental mutations and carcinogenesis (Friedberg 2001, 2003).

Endogenous damage which arises within the cell can take various forms, from simple point mutations, transitions (purine-purine or pyrimidine-pyrimidine) or transversions (purine-pyrimidine and vice versa) to extensive insertions or deletions of genetic material. The most common forms of damage result from errors in DNA replication along with spontaneous changes to the DNA bases. DNA polymerase fidelity is less than 100% and it often makes mistakes when inserting complimentary bases. This, along with the inherent margin of error found in 2'-5' exonuclease proofreading enzymes, reduces the fidelity of the DNA replication process. The inability to remove erroneous bases results in base mismatch, which can lead to same-sense, mis-sense or nonsense mutations, with various cellular outcomes. Following a subsequent round of replication the mis-incorportated bases will form a permanent mutation within the genome (Friedberg et al. 2006; Watson et al. 2004).

Spontaneous changes to the DNA bases can be exemplified by the base Cytosine which is prone to hydrolytic damage, a process of deamination, which converts the base to Uracil. Adenine, Guanine and 5-Methylcytosine are also capable of deamination, to Hypoxanthine, Xanthine and Thymine respectively; however these

conversions are less frequent than that of Cytosine. The presence of an incorrect base has implications for the replication of genetic information (Friedberg et al. 2004). Another major form of endogenous damage is the spontaneous loss of bases due to hydrolysis of the N-glycosyl linkage, referred to as depurination or depyrimidination, depending on the lost base. These modifications result in abasic sites within the DNA sequence, a structure which must be rectified for DNA metabolism to take place. Both forms of hydrolytic damage, deamination and depurination form unnatural structures not expected within DNA, and can therefore be detected by repair systems, apart from 5-methylacytosine which is a hotspot for spontaneous mutations. Of increasing interest with respect to DNA damage are the ubiquitous reactive oxygen species (ROS) including $O_2^{\cdot-}$, H_2O_2 and $OH^{\cdot}$ species. ROS are created during cellular metabolism and are able to damage all intracellular macromolecules from proteins to nucleic acids. 8-oxoguanine (8-oxoG) formed from the oxidation of guanine is a common result of ROS, and leads to transversion mutations, as it has the ability to base pair with not only cytosine, but also adenine during replication (Friedberg 2003, 2005).

1.1.2 Exogenous DNA damage

Chemical induced damage

Many chemicals exist which can damage the structure of DNA. These can be broadly divided into alkylating agents, cross-linking agents, electrophilic reactants and agents which cause strand breaks.

Alkylating agents act by electrophilic attack of the nucleophilic centres of nitrogen and to a lesser extent oxygen within the bases of DNA. These agents can also react with other chemical groups which have less nucleophilic centres such as the phosphodiester DNA backbone. N-methyl-N'-nitro-N-nitrosoguanidine (MNNG), N-methyl-N-nitrosourea (MNU) and methyl methanesulfonate (MMS) are monofunctional alkylating agents which have the ability to form various O-alkylated and N-alkylated DNA products. A vulnerable site of alkylation damage is the C6 atom of guanine, which becomes alkylated to produce O^6-methylguanine, and then incorrectly base pairs with thymine (Friedberg 2005).

Perhaps one of the most deleterious of damages is the formation of DNA cross links, these can be either interstrand crosslinks or intrastrand adducts. DNA

replication and transcription are inhibited in the presence of interstrand crosslinks, which prevent the separation of DNA strands. A number of cancer chemotherapy drugs have exploited this crosslinking property such as Cisplatin, which has proven effective in the treatment of bladder, testicular and ovarian cancers (Friedberg et al. 2006). DNA is also capable of crosslinking with proteins, such as histones, exemplified by the process of formaldyhyde crosslinking used in the experimental technique of chromatin immunoprecipitation. DNA-protein links also provide a barrier to metabolic processes.

Intracellular chemicals can damage the cell directly, however many substances are metabolised, often by the cytochrome P-450 system, to form genotoxic electrophilic reactants which may be mutagenic as well as carcinogenic. Strand breaks within the DNA structure may also be induced by a variety of chemicals and enzymes (Friedberg et al. 2006).

Ionising radiation

Perhaps the most devastating cause of exogenous damage is radiation. Ionising radiation exists naturally in the form of radon in the Earths' atmosphere, and is also present in cosmic rays. Doses of radiation received by individuals can vary greatly, depending on factors such as locality (certain parts of the world are especially rich in soil radiation) and factors such as long-haul flights and lifestyle. Ionising radiation can also be created artificially, and is used routinely in diagnostic x-rays and nuclear medicine treatments, for visualisation and radiotherapy procedures in the healthcare service. Ionizing radiation is particularly detrimental to DNA, resulting in base damage, single-strand breaks (SSBs) and double-strand breaks (DSBs). Double strand breaks arise due to the ionisation of the deoxyribose backbone component, and are not repaired as readily as other forms of damage, proving lethal to a cell unless corrected (Friedberg 2003). Reactive oxygen species are also a possible consequence of ionising radiation, causing additional damage. Like many damaging agents ionizing radiation is also exploited therapeutically to kill rapidly proliferating cells (Watson et al. 2004).

UV Radiation

UV light has been shown to be responsible for a range of DNA lesions and is therefore used routinely as a paradigm to study DNA damage and repair.

The UV light spectrum is beyond that of the visible light spectrum, and has been designated into three categories, UVA, UVB and UVC. UVA has the longest wavelength of the three (400-320nm) and is often referred to as black light. UVB light is referred to as medium wave (320-295nm), with UVC (295-100nm) referred to as short wave (Friedberg et al. 2006). The majority of the UV light to reach the Earths' surface is UVA and UVB, as the ozone layer is fairly impenetrable to wavelengths of less than 300nm. UVC light is used within laboratories experimentally as it is easily accessible from germicidal lamps, and has a DNA specific wavelength, with DNA having an absorption peak of 260nm. Although UVA light does not cause burning of the skin, it has been shown to contribute to the premature aging of the skin, including the formation of wrinkles. UVB does have some beneficial effects, such as the induction of vitamin D formation. However, of interest to this study is the fact that UVB and UVC radiation can have deleterious effects on DNA molecules, causing DNA lesions which are mutagenic and carcinogenic.

The most frequent photoproduct lesions produced by UV light at 260nm are cyclobutane pyrimidine dimers (CPDs) and pyrimidine-pyrimidone (6-4) photoproducts ((6-4) PP). CPDs constitute 70-85% of the UV induced photoproducts at 260nm, formed by the covalent bonding of the C5 and C6 bonds with an adjacent pyrimidine (shown in Figure 1) (Friedberg et al. 2006). Upon saturation of the C5-C6 double bonds, a four membered ring persists (Li et al. 2006). The ratio of CPD induction following UVC irradiation is noted as follows T-T, T-C, C-T, C-C in a ratio of 68:16:13:3 (Mitchell et al. 1992). There are four main isomeric forms of CPDs, with the cis-syn isoform being most prevalent in B-form DNA (Friedberg 2005), creating a bulky adduct which is more pH and temperature stable than the native DNA. A CPD lesion causes a sharp 30° bend in the helical axis towards the major groove of DNA and a 9° kink due to the unwinding of the strand containing the lesion (Kim et al. 1995; Park et al. 2002a). CPDs are however accommodated well, not displacing DNA from histones (Gale et al. 1987; Svedruzic et al. 2005). The induction of CPDs is affected by the local DNA sequence, with a more flexible substrate

supporting CPD formation (Thoma 1999). CPDs have been shown to have a periodicity of 10.3 bases, positioned facing away from the histone interfaces (Pehrson 1989). The resulting distortion of the DNA helix in the presence of CPDs leads to stalling of RNA and DNA polymerases (Friedberg et al. 2006; Kim et al. 1995). CPDs can be recognized by the enzyme pyrimidine dimer DNA glycosylase which forms a single strand nick at sites of dimers. This enzyme has allowed UV-induced CPD formation to be studied extensively.

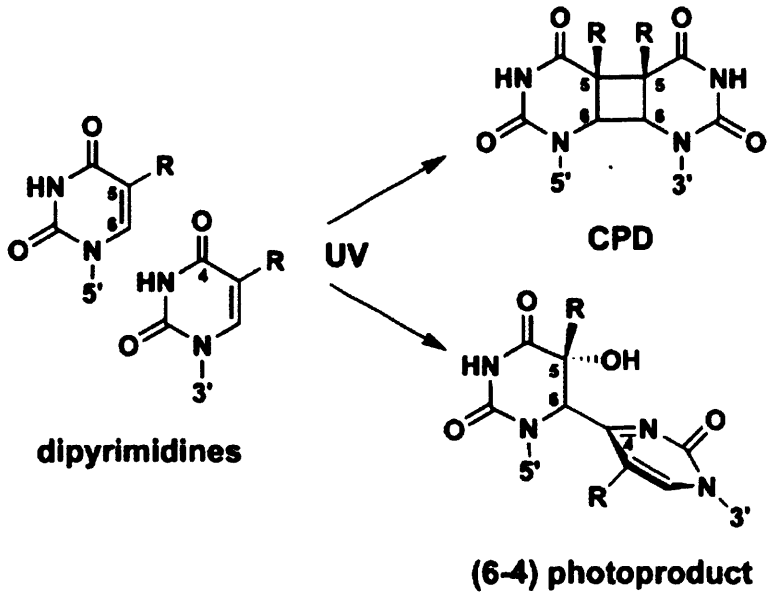

Figure 1: Absorption of UV light by DNA induces two main forms of mutagenic lesions in DNA between adjacent pyrimidines. These are cyclobutane pyrimidine dimers (CPDs) in predominantly the T-T form, where the double bonds between C5 and C6 carbon atoms of any two adjacent pyrimidines become saturated to produce a four-membered ring. (6-4) photoproducts are formed between the 5' C4 position and the 3' C6 position of two adjacent pyrimidines, most frequently T-C sites (Li et al. 2006).

As well as CPDs, the lower incidence (6-4) photoproduct also gives rise to a helix-distorting lesion. (6-4) photoproducts induce a significant alteration of DNA structure, resulting in an exaggerated 44° bending of the helix, a more marked distortion than the 9° kink seen in CPDs (Kim et al. 1995). Constituting 15-25% of DNA lesions following 260nm UV light, (6-4) photoproducts involve the bonding of the 5' C4 and 3' C6 positions on adjacent pyrimidines (see Figure 1), with the pyrimidine planes being almost perpendicular. Where CPDs occur evenly throughout chromosomal DNA, 6-4 photoproducts have a six-fold incidence in nucleosomal

linker regions compared with core nucleosomal regions (Mitchell et al. 1990). Heterogeneity of photoproduct formation can result from protein-DNA interactions, exemplified by TBP binding at the TATA box altering UV-induced lesion formation (Aboussekhra and Thoma 1999; Thoma 1999), as well as the DNA structure, for example, within a TATA box where the DNA is bent (6-4) photoproduct formation is favoured as opposed to CPD formation (Thoma 1999).

It should be noted that UV radiation can also cause DNA cross links with proteins or less frequently DNA-DNA links and strand breaks.

1.1.3 The effects of DNA damage in a cellular context

In eukaryotic cells DNA damage initiates a cascade of signalling pathways referred to as the DNA damage response (Friedberg 2001). The response includes (i) the activation of cell-cycle checkpoint pathways and subsequent signalling pathways slowing or stopping the progression of the cell cycle to allow for eficient repair and tolerance mechanisms, which mitigate the possible outcomes of arrested DNA replication (ii) enzymatic DNA repair pathways (iii) up-regulation of specific genes, of which the function of many of the gene subsets is not yet established (Friedberg 2005). *Escherichia coli* which have been subjected to DNA damage undergo an extensively documented SOS response, with the induction of a large subset of well defined genes (Janion 2001). In *Saccharomyces cerevisiae*, the transcriptional response to DNA damage can be exemplified by the RNR genes, which mediate the rate-limiting step in dNTP production required for DNA synthesis and DNA repair mechanisms. The onset of damage results in a modest increase in the RNR gene transcript levels (Fu et al. 2008). In mammalian cells, if the damage is extensive then (iv) activation of mechanisms to tolerate mutations, bypassing damage or (v) apoptosis can occur (Friedberg 2005). The responses to DNA damage are often combined, with little known about the DNA damage response triggers, and whether there is 'cross-talk' between pathways.

The ways in which a cell can react to DNA damage are generally classed as DNA repair and DNA damage tolerance (Friedberg et al. 2004; Friedberg 2005). Damage tolerance plays a vital role in promoting Darwinian evolution by ensuring natural variance. DNA tolerance mechanisms enable the replicative bypass of replication-blocking lesions without actually removing the damage. This is of

particular importance, as stalled replication forks can lead to cell lethality or major chromosomal abnormalities (Ulrich 2007). Damage tolerance can be exemplified by the translesion DNA synthesis pathway (TLS), which acts to bypass lesions utilising low-fidelity DNA polymerases (Friedberg 2005). TLS acts to prevent a block in the replication process, however the specialised polymerases employed insert free bases, often introducing mutations (Friedberg 2003). As well as TLS, an error-free tolerance pathway has recently emerged involving the ubiquitination of the sliding clamp protein PCNA. Monoubiquitination appears to be involved with the activity of all damage-tolerant polymerases, with polyubiquitinaion a pre-requisite for the error-free pathway (Ulrich 2007). The most disruptive of damages suffered in mammalian cells are almost always eradicated by apoptosis (programmed cell death) to prevent the replication of cells and subsequent propagation of incorrect genetic information.

The repair of DNA damage encompasses three major repair mechanisms, each involving multiple proteins. In humans, when these repair pathways are defective, disease can result exemplified by the cancer-prone disorder Xeroderma pigmentosum (XP), an outcome of faulty nucleotide excision repair (NER). The relationship between DNA repair, transcription and the onset of disease if these are disrupted outlines the importance of the basal transcription machinery in the DNA repair process. This is reinforced by the variant form of XP (XP-V), where disease arises from a defective variant low-fidelity DNA polymerase. Defects in Mismatch repair (MMR) give rise to Hereditary non-polyposis colon cancer (HNPCC), further validating the somatic mutation hypothesis, whereby mutations in specific genes, namely tumour suppressor genes and oncogenes lead to neoplastic transformation (Friedberg 2003).

Cell cycle checkpoints

The accurate propagation of genetic material between mother and daughter cells is essential for cell viability. To ensure correct progression, cell cycle checkpoints exist, with the G1/S and G2/M transitions and an intra S-phase checkpoint playing significant roles in the DNA damage response. When cell cycle checkpoints and their regulatory factors fail to function properly, genomic instability may arise, leading to disease states, exemplified by the human autosomal recessive neurodegenerative disorder Ataxia Telangiecasia (AT).

The ATR (Ataxia Telangiecasia and Rad3p-related) and ATM (Ataxia Telangiecasia mutated) protein kinases were found to be involved in the DNA damage response, in particular the response to ionising radiation. The ATR-mediated signalling cascade acts to regulate the cell cycle and is generally associated with the cellular response to double strand breaks (DSBs). ATM acts more in the response to UV damage and replication stalls, only contributing a minor role in the DSB response. A major factor in the damage response is the presence and detection of ssDNA, placing the single-strand binding protein PRA with a central role in the ATR signalling cascade (Brush and Kelly 2000; Friedberg et al. 2004).

ATR and ATM have roles in each step of the cell cycle, mediated by the phosphorylation of downstream targets such as Brca1, Chk1, p53 and Rad17, factors which mediate inhibition of the cell cycle therefore promoting repair (Abraham 2001; Friedberg et al. 2004; Harrison and Haber 2006). The G1/S checkpoint has been extensively studied, acting to prevent the replication of damaged DNA. Following ionising radiation damage ATM and ATR mediate the accumulation and activation of the p53 transcription factor, via Chk2 kinase mediated phosphorylation. The presence of elevated levels of activated p53 in turn up-regulates multiple targets including p21, which acts to arrest the cell cycle at G1 preventing cells from entering S phase (Abraham 2001). Along with a role in cell cycle delay to allow for repair, p53 has also been implicated directly in the regulation of NER (Rubbi and Milner 2003).

The S-phase checkpoint enables the reduction of the rate of DNA synthesis following DNA damage. Generally DSBs can be repaired at this stage by homologous recombination (HR) or the error-prone non-homologous end joining mechanism (NHEJ). ATM again has a role in the S-phase checkpoint, via interactions with Chk2, mediating cyclin A-cdk2 activation. ATM/ATR phosphorylation of *BRCA1* also mediates the recombinational repair required for S-phase progression, along with the NBS1-Mre11-Rad50 protein complex. The final checkpoint is the G2 cell cycle checkpoint, which acts to prevent the entry of DNA damaged cells into mitosis. The cdc2 cyclin dependant kinase controls entry into mitosis, the phosphorylation of which is mediated by ATM and ATR. Along with AT, Nijmegen breakage syndrome (NBS) and an increased susceptibility to breast cancer highlight the importance of cell cycle checkpoints in human disease (Abraham 2001).

The *S. cerevisiae* ATR and ATM homologues are *MEC1* and *TEL1* respectively, and although similar in structure, the precise checkpoint regulatory roles are not as defined (Harrison and Haber 2006).

1.2 DNA repair mechanisms

Various repair mechanisms have evolved to ensure the correct replication of DNA, each repairing different subsets of DNA lesions. These repair mechanisms are conserved across eukaryotic species, and have been studied in most model organisms, from yeast to human cells. Here, I will concentrate on the repair mechanisms in yeast, with reference to the human counterparts.

In order to prevent accumulation of genetic mutations DNA damage may be (i) directly reversed, (ii) excised from DNA and replaced, or (iii) tolerated and bypassed in cellular processes.

Cellular response to DNA damage	**Repair/ Tolerance mechanism**
Direct reversal of DNA damage	Enzymatic photoreactivation Repair of alkylated base damage Ligation of DNA strand breaks
Excision of DNA damage	Base Excision Repair (BER) Nucleotide Excision Repair (NER) Mismatch Repair (MMR)
Tolerance of DNA damage	Replicative bypass of template damage (gap formation and recombination) Translesion DNA synthesis

Table 1.1: Cellular responses to DNA damage, adapted from (Friedberg et al. 2006).

1.2.1 DNA repair involving the reversal of damage

The simplest of the repair mechanisms is the reversal of a damaged DNA base by a single step reaction and a single enzyme. This reversal of DNA damage is considered an efficient, generally error-free mechanism, particularly useful for the

removal of UV-induced damage and alkylation damage. Reversal pathways can be assumed to be advantageous, kinetically faster than a multi-step process, thereby reducing the risk of genetic instability.

Alkylation damage, such as O^6-alkylguanine and O^4-alkylthymine products impose a great genetic risk within a genome, having potential to mis-pair during semi-conservative DNA synthesis. The reversal of such damage has been demonstrated in *E. coli*, utilising a group of enzymes named methyltransferases (MTases). These enzymes allow the direct reversal of O-alkylated and N-alkylated bases following the transfer of the methyl groups from the base to enzyme, restoring the native chemistry of the base (Kleibl 2002; Xiao and Samson 1992). This process is however energetically unfavourable, as the accepting alkyltransferase protein can only undergo the reversal reaction once, requiring additional repair proteins for extensive alkylation damage (Friedberg et al. 2006).

The repair of single-strand breaks within DNA can also be considered as reversal of damage. Agents such as ionising radiation are capable of promoting the hydrolysis of the phosphodiester bond within the DNA backbone, with single-strand breaks being the most prevalent form of damage within a cell. The reversal of such single-strand breaks requires the actions of a DNA ligase enzyme, which acts to rejoin DNA ends with free 3'OH and 5' phosphate groups. However, ionising radiation, as one example does not necessarily provide clean cut substrates, and the DNA ends often require further processing to repair adjacent damaged bases before the DNA can be ligated (Friedberg et al. 2006). The direct reversal of single-stranded breaks therefore only applies to a small subset of DNA substrates.

The reversal of UV induced damage

As described previously, UV light is a major source of DNA damage, and an exogenous agent which has resulted in the evolutionary development of multiple adaptive mechanisms. The most common UV-induced products, 6-4 photoproducts and cyclobutane pyrimidine dimers are a major threat for an organism's genetic integrity, resulting in diverse mechanisms for the efficient repair of photoproducts.

The ability of cells to recover from UV induced damage was realised prior to the discovery of DNA structure in 1953 (Dulbecco 1949; Kelner 1949a), and this recovery of cells was in turn shown to be light dependant (Kelner 1949b), leading to

the discovery of photoreactivation. This was acheived via an enzyme-catalysed reaction in *E. coli* and *S. cerevisiae* (Rupert 1960). The enzymes are referred to as photolyases which can act on CPDs (CPD photolyase) or 6-4 PPs (6-4 PP photolyase). The photolyases act to monomerise the dimers into their constituent pyrimidines so reversing the damage (Sancar 1990, 2000). The photolyase enzyme first binds to the target dimer, before utilising the energy yeilded from UV-A (320-400nm) and blue light (400-500nm) to excite the cofactor $FADH^-$. Photolyases contain chromophores, light harvesting proteins namely MTHF or 8-HDF, which in turn transfer energy to excite $FADH^-$ and this energy is then used to split the dimer (Eker et al. 1990; Malhotra et al. 1992). This light-dependant reaction therefore restores the original pyrimidines by photolysis of the dimer.

Photolyases are seen to be active across the majority of organisms, and are grouped according to function (Goosen and Moolenaar 2008), however placental mammals appear to lack both CPD and (6-4) PP photolyase activity (Todo et al. 1993; Todo et al. 1996; Weber 2005). The human genome contains two photolyase homologs, namely the CRY genes, however these are not involved in photoreactivation (Weber 2005). Light-dependant removal of CPDs has however been reported in human skin (Sutherland et al. 1980), suggesting a similar mechanism may persist in human cells.

1.2.2 DNA repair involving the excision of damage

The major excision repair pathways are Base Excision Repair (BER), Nucleotide Excision Repair (NER) and Mismatch Repair (MMR). These repair mechanisms are so-called due to the incision of damage-containing DNA, and subsequent removal of the damage by excision. As this study focuses on NER, attention will be paid to MMR and BER, with NER being explored in further detail in subsequent sections.

1.2.2.1 Mismatch Repair (MMR)

The metabolic processes of a cell provide sources of mismatched bases within the DNA double helix, including DNA replication errors, heteroduplex formation during recombination and imperfect hairpin formations. The mismatch repair (MMR)

system has been shown to improve the fidelity of the DNA replication process, detecting mismatches in bases which can otherwise escape detection by DNA proofreading proteins.

The MMR pathway has been well characterised in *E. coli*, where the responsible protein factors have been defined. The DNA base mismatch is first recognised as a distortion in the DNA backbone, recruiting the MutS repair factor to initiate the ATP-dependant removal of the incorrect base (Lamers et al. 2003; Natrajan et al. 2003). The binding of MutS results in a conformational change of the protein, and an associated kink in the DNA. MutL is then recruited to the site, which upon binding recruits and activates the endonuclease MutH. MutH acts to incise the unmethylated daughter DNA strand containing the mispaired base. Uvr D, a member of the DNA helicase II family, then unwinds the DNA duplex from the nick generated by MutH, followed by the action of one of three exonucleases which removes the mismatched base-containing ssDNA. The single-stranded gap is then refilled by DNA polymerase III and re-joined by the actions of a DNA ligase. This mechanism is aided by the Dam methylase enzyme, to ensure excision of the newly mis-incorporated base, rather than the parental strand (Jun et al. 2006; Kunkel and Erie 2005; Watson et al. 2004). Although humans cells do not produce a Dam methylase enzyme, PCNA and the conformation of newly synthesised DNA, in the form of Okazaki fragments are thought to play a role in distinguishing the parental strand (Watson et al. 2004).

Although the MMR system is conserved from prokaryotes to eukaryotes, the eukaryotic system is more complex with five MutS homologues (MSH proteins) as well as four MutL homologues identified which function as heterodimers with multiple proteins (Jun et al. 2006; Waters 2006). Defects in MMR result in a 'mutator' phenotype, with an increase in spontaneous mutations and increased microsatellite instability (Peltomaki 2001). This can be exemplified in humans, with defects in hMSH2 and hMLH1 giving rise to hereditary nonpolyposis colorectal cancer (HNPCC), and more recently identified, breast cancer (Lynch and de la Chapelle 1999; Wasielewski et al. 2009).

1.2.2.2 Base excision repair (BER)

Base excision repair is the predominant DNA repair pathway for the removal of small base lesions, such as those induced by oxidative and alkylation damage. BER is defined by the actions of DNA glycosylase enzymes (either mono- or bi-functional), which are each capable of recognising specific modifications to bases, or the incorrect incorporation of bases. For example, the bacteriophage T4 encodes a CPD-specific endonuclease, T4 pyrimidine dimer glycosylase (T4-Pdg), and along with the *Micrococcus luteus* pyrimidine dimer glycosylase (Mlu-Pdg) provide tools to detect and quantify CPDs in numerous organisms. DNA glycosylases act to hydrolyse the N-glycosidic bond between a damaged base and deoxyribose-phosphate component to create an apurinic/apyrimidimic (AP) site. This allows the subsequent cleavage of the phosphodiester bond 5' to the AP site by an AP endonuclease. The resulting gap can then be tailored by the removal of the 5' terminal deoxyribose-phosphate (5'dRP) by either the endonuclease or a deoxyribosephosphodiesterase (dRPase) (Almeida and Sobol 2007). Bi-functional glycosylases catalyse the incision 3' to the AP site as well as removal of the damaged base. DNA Polymerase (Pol ß in mammals) is then able to insert a new nucleotide into the gap (Goosen and Moolenaar 2008), followed by subsequent restoration of the DNA strand by DNA ligase.

BER can be sub-divided into two pathways in humans, the more predominantly used short patch BER, where one nucleotide is replaced, or long-patch BER, replacing up to thirteen nucleotides (Almeida and Sobol 2007).

1.2.2.3 Nucleotide excision repair (NER)

Nucleotide Excision Repair (NER) allows for efficient repair of a wide range of DNA lesions, mainly including bulky helix distorting lesions such as those induced by UV as well as chemical adducts. NER is therefore extensively required to act on multiple substrates, with defects in this pathway in humans giving rise to the cancer prone syndrome Xeroderma Pigmentosum (XP). NER, like other excision repair mechanisms follows a general pathway, consisting of damage recognition, incision of DNA either side of the damage, excision of the damage containing DNA segment, restoration of the resulting gap and ligation to seal the DNA. Much of how NER

operates has been determined using UV damage (CPDs and 6-4 PPs) as a substrate for repair (Friedberg et al. 2006).

1.2.2.4 NER in a prokaryotic system

Bacterial NER was first observed in *E. coli* and the mechanism was shown to involve the UvrA, UvrB and UvrC proteins, as displayed in Figure 1.2. UvrA and UvrB associate and are responsible for damage recognition, the expression levels of which are controlled by the SOS response (Janion 2001). The UvrABC proteins have the ability to recognise and cleave damaged DNA in an ATP dependant reaction. The *E. coli* UvrA protein contains two ABC ATPase domains, with the binding of ATP required for dimerisation of UvrA and the subsequent binding of UvrA to DNA. The hydrolysis of ATP is then required for the release of UvrA from undamaged DNA (Goosen and Moolenaar 2008; Truglio et al. 2006). It is believed that the C-terminal zinc finger region of the protein is responsible for the damage-specific binding of UvrA (Croteau et al. 2008), with mutations in which giving rise to a highly UV sensitive phenotype (Truglio et al. 2006). It has been shown that 6-4 photoproducts are more helix distorting than CPDs, and are incised at a higher rate, suggesting DNA distortion is a major factor in NER machinery recognition (Chandrasekhar and Van Houten 2000).

UvrA forms the initial contacts with the DNA (DellaVecchia et al. 2004); however the UvrAB complex has a higher affinity for damaged DNA than UvrA alone. UvrB interacts with UvrA, UvrC, UvrD, DNA polymerase I and DNA, and is the most conserved of the UvrABC proteins (Goosen and Moolenaar 2008), therefore a central component of the NER mechanism. UvrB in complex with UvrA is involved in the second stage of damage recognition, damage verification, forming the preincision complex, which in turn is recognised by UvrC. UvrB has six helicase motifs along with an ATPase actvity, however, it is thought that UvrB does not use its helicase domains to scan along DNA, but to distort the DNA at lesion sites, referred to as strand destabilisation (Skorvaga et al. 2004) as to allow for recognition and recruitment of the UvrABC proteins (Truglio et al. 2006).

UvrB must be in an ATP bound form before a dual incision step carried out by the third protein UvrC can take place. In *E. coli* the precise positioning of the incisions has been shown to cut at the fourth or fifth phosphodiester bond 3' to the

damage, and the eighth phosphodiester bond 5' to the damage. The UvrC endonuclease is responsible for the incision at both the 3' and 5' sides of the lesion. The catalytic sites are located in the C-terminal and N-terminal parts of the protein, responsible for 5' and 3' incisions respectively, which are separated by a highly variable linker region (Truglio et al. 2006). Towards the N-terminal 3' catalytic domain is the UvrB-binding domain. *E. Coli* also contains an additional protein, Cho, which is homologous to the N-terminal 3' domain of UvrC. It is thought that this protein acts as a backup for the 3' incision of the damaged DNA (Goosen and Moolenaar 2008).

The incision reactions subsequently result in release of UvrC, and the recruitment of UvrD (DNA helicase II) which enables the release of the damage-containing oligonucleotide. DNA polymerase I restores the gap and releases UvrB. DNA ligase then completes the NER mechanism with the resealing of the DNA gap (Goosen and Moolenaar 2008; Truglio et al. 2006).

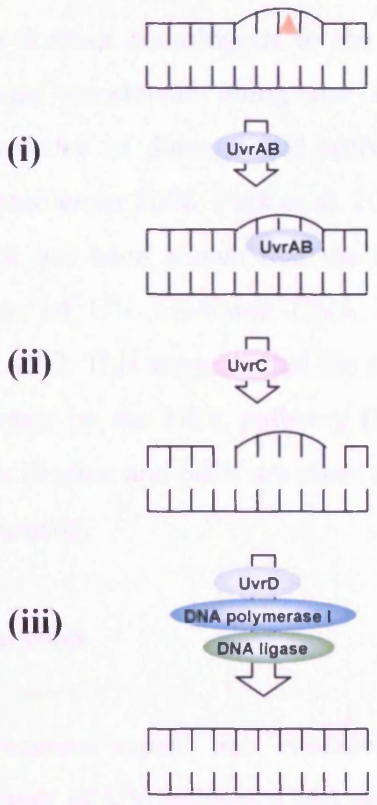

Figure 1.2: Schematic of the Prokaryotic NER mechanism. (i) DNA damage is recognised by the UvrAB complex, which acts to destabilise DNA contacts. (ii) UvrC is then recruited which acts to incise the DNA strand flanking the DNA lesion. (iii) UvrD then promotes the excision of the damage containing DNA. The actions of DNA polymerase I and DNA ligase then restore the DNA duplex.

Heterogeneity exists within the NER mechanism in prokaryotes, with a difference in rate of repair seen between transcribed regions and non-transcribed regions of the genome. Transcription coupled-NER (TC-NER) can be distinguished from Global genome-NER (GG-NER) marked by the presence of a stalled RNA polymerase. GG-NER is mediated by UvrA and UvrB, which exist in low cellular concentrations. When the SOS stress response is activated by DNA replication arrest, UvrA and UvrB transcription is upregulated allowing proficient GG-NER (Crowley and Hanawalt 1998; Hanawalt and Spivak 2008).

TC-NER involves a targeted recruitment of repair proteins. Transcription repair coupling factor (TRCF) encoded by the *mfd* (mutation frequency decline) gene has been shown to be a key signalling component of the TC-NER pathway, recruiting NER proteins to the DNA lesion (Deaconescu et al. 2007). Interestingly TRCF has

sequence and structural homology with the UvrB protein, with RNA polymerase binding ability and a domain homologous to the RecG helicase, giving rise to the theory that TRCF can translocate along the DNA, displacing a stalled RNA polymerase in the presence of damage and recruiting UvrA and subsequent NER factors (Goosen and Moolenaar 2008; Park et al. 2002b; Selby and Sancar 1994).

Interestingly, it has been shown that the binding of *E.coli* CPD photolyase stimulates the incision of UV irradiated DNA by the nucleotide excision repair enzyme complex UvrABC. This suggests that the structure of the DNA is altered after binding, favouring repair by the NER pathway (Sancar et al. 1984). It is therefore possible that photoreactivation and NER are more efficient when the pathways coexist and are able to act in unison.

1.2.2.5 NER in Eukaryotes

Nucleotide excision repair has evolved to become the primary repair mechanism for the repair of UV induced DNA damage, as well as other intrastrand DNA helix-distorting lesions; and appears across all studied eukaryotes. The eukaryotic NER mechanism echoes that seen in prokaryotes, however is far more complex, involving at least 30 individual proteins, evolved to contend with the increased challenges provided by the chromatin environment (see Section 1.3.5). The NER mechanism in the yeast *S. cerevisiae* and in humans is homologous, with many identical facets, allowing *S. cerevisiae* to be used as a model to study NER. Although not as well understood as the bacterial system, the best characterised components of the NER pathway are those proteins shown to be defective in the inherited cancer prone disorder Xeroderma pigmentosum (XP) (Friedberg et al. 2006).

NER in Saccharomyces cerevisiae

The genes involved in NER in *S. cerevisiae* can be divided into two distinct groups, determined by the degree of sensitivity to UV light and other DNA damaging agents. Those genes considered essential for effective incision of UV induced damage are referred to as Class I genes and include *RAD1*, *RAD2*, *RAD4*, *RAD10* and *RAD14*, along with the genes encoding the subunits of *RPA* (*RFA1*, *RFA2* and *RFA3*), and the genes encoding the core subunits of TFIIH (*RAD3*, *RAD25/SSL2*, *SSL1*, *TB1*, *TFB2*,

TFB3), mutations of which confer a high degree of UV sensitivity. Class II genes are not considered essential for the NER incision reaction, however increase the efficiency of the mechanism and give rise to a moderate UV sensitivity. The class II genes are the *RAD7* and *RAD16* genes, along with *RAD23* and *MMS19* (Prakash et al. 1993; Prakash and Prakash 2000).

The NER mechanism elucidated in yeast has been shown to be homologous to that in human cells, with mutations in homologous genes giving rise to similar defects in the NER reaction. Some subtle differences may be noted between the yeast and human genes involved. Human homologues of the yeast genes *RAD7* and *RAD16*, required for the repair of non-transcribed regions of the genome and *MMS19* have yet to be structurally defined. Deletion of *RAD4*, a class I gene gives rise to a highly UV sensitive phenotype, defective in NER, however the human counterpart XPC is only required for the repair of non-transcribed regions of the genome. Interestingly, unlike the mammalian genome, the majority of the yeast genome is transcriptionally active (Holstege et al. 1998). The differences between TC-NER and GG-NER can be equally displayed in *E. coli,*. yeast and humans (Mellon et al. 1986; Prakash and Prakash 2000).

Molecular mechanism of NER in eukaryotes

The molecular mechanism for nucleotide excision repair has been extensively studied and can be divided into five main steps namely (i) damage recognition, (ii) open complex formation, (iii) dual incision, (iv) excision of the damage containing oligonucleotide and (v) repair synthesis and gap ligation (Prakash and Prakash 2000). As this project was carried out using yeast as a model, the focus will be on the molecular mechanism elucidated in *S. cerevisiae*, with reference to the human counterparts (see Table 1.2).

S. cerevisiae	Human gene	Function
RAD4	XPC	Lesion recognition in GG-NER (and TC-NER in yeast) in complex with Rad23
RAD23	RAD23B RAD23A	In complex with and stabilises Rad4/XPC
RAD14	XPA	Binds and stabilises open complex, recognises DNA damage
RFA1	RPA1 (RPAp70)	RPA stabilises ssDNA during formation of the open complex (with Rad14)
RFA2	RPA2 (p32)	
RFA3	RPA3 (p14)	
RAD2	XPG(ERCC5)	Endonuclease (3' incision); stabilises full open complex
RAD10	ERCC1	Part of endonuclease (5' incision) complex with Rad1
RAD1	XPF (ERCC4)	Part of endonuclease (5' incision) complex with Rad10
CDC9	LIG1	
RAD28	CSA (CKN1)	TC-NER
RAD26	CSB (ERCC6)	TC-NER, DNA dependant ATPase
	DDB1	Forms a complex with DDB2, with similarities to Rad7/16 complex
	DDB2	GG-NER. Lesion recognition, recruits XPC. Defects give rise to XPE
MMS19	MMS19L	Influences TFIIH as upstream regulatory element?
RAD7	unknown	Forms a GG-NER complex with Rad16 and Abf1
RAD16	unknown	DNA dependant ATPase, complex with Rad7 and Abf1
ABF1	unknown	Essential DNA binding protein
TFIIH subunits:		
RAD25/Ssl2	XPB	3' to 5' helicase
RAD3	XPD	5' to 3' helicase
TFB1	GTF2H1/p62	
SSL1	GTF2H2/p44	Zn finger, DNA binding
TFB4	GTF2H3	Ring finger, DNA binding
TFB2	GTF2H4/p52	
TFB5	GTF2H5, TTD-A	Stabilization of TFIIH. Defects give rise to TTD
KIN28	CDK7	CDK, C-terminal domain kinase, CAK
CCL1	CCNH	Cyclin
TFB3	MNAT1	CDK assembly factor

Table 1.2: Genes involved in NER of the yeast *S. cerevisiae* and the human homologues. The biochemical activity for each gene is described if known.

DNA damage recognition

Of perhaps the most important and as yet less understood mechanistic stage of nucleotide excision repair is the initial damage recognition process. Decades of research have elucidated that the recognition of DNA damage is determined by the precise temporal and spatial location of the DNA lesion, in terms of cell cycle, chromatin environment and local metabolic processes. In terms of genes involved, the NER pathway can be divided into two distinct pathways, Transcription coupled- NER (TC-NER), acting on actively transcribed regions of the genome, and global genome-NER (GG-NER) acting on the genome as a whole, especially noted in all non-transcribed regions of the genome, differing only in the DNA lesion recognition mode. This crucial primary step in the NER mechanism is the only divergence of the pathway, with the mechanism converging into a single pathway beyond damage recognition. The two sub-pathways are explored in more detail below, and shown in Figure 1.3.

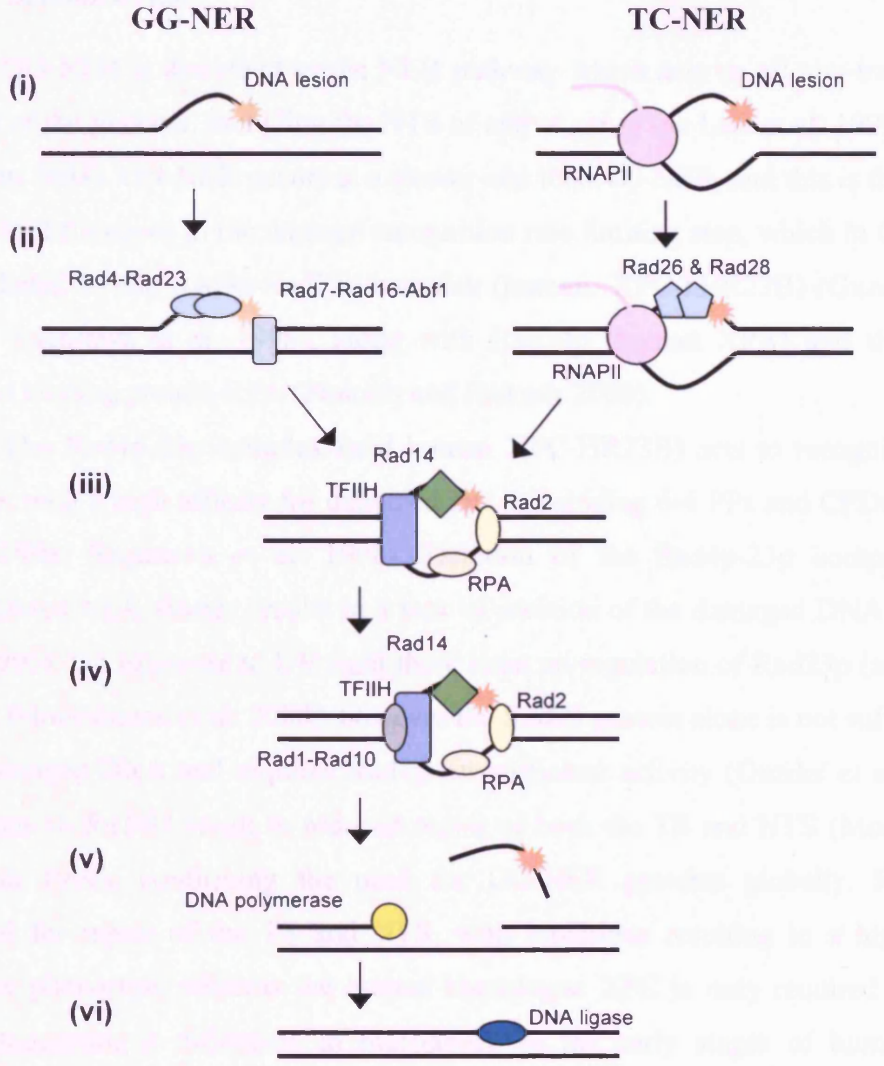

Figure 1.3: A schematic of the major factors involved in the mechanistic stages of NER. (i) DNA lesion induction results in the (ii) recognition of DNA damage. In GG-NER this step is mediated by the Rad4p-Rad23p and Rad7p-Rad16p-Abf1p protein complexes. In TC-NER Rad26p and Rad28p along with a stalled RNAPII are responsible for recognition. (iii) Beyond damage recognition the pathways converge, and the Rad14p, Rad2p, RPA and TFIIH factors are recruited, forming an open complex (iv) Rad1p-Rad10p and Rad2p then incise the DNA 5' and 3' to the damage respectively. (v) The DNA damage containing oligonucleotide is excised, and the native DNA restored by DNA polymerase. (vi) DNA ligase then completes the reaction, sealing the DNA duplex.

Global Genome-NER

GG-NER is described as the NER pathway which acts on all non-transcribed regions of the genome, including the NTS of active genes (de Laat et al. 1999; Li and Smerdon 2004). GG-NER occurs at a slower rate than TC-NER, and this is thought to be due to differences in the damage recognition rate limiting step, which in GG-NER is mediated by the Rad4p-Rad23p complex (human XPC-hHR23B) (Guzder et al. 1998a; Sugasawa et al. 1998), along with Rad14p (human XPA) and the single stranded binding protein RPA (Prakash and Prakash 2000).

The Rad4p-23p complex (and human XPC-HR23B) acts to recognise DNA damage, with a high affinity for damaged DNA including 6-4 PPs and CPDs (Jansen et al. 1998; Sugasawa et al. 1998). Deletion of the Rad4p-23p complex in a reconstituted NER system results in a lack of incision of the damaged DNA (Guzder et al. 1995). On exposure to UV light there is an up-regulation of Rad23p (and XPC) mRNA (Hoogstraten et al. 2008), however the Rad23 protein alone is not sufficient to bind damaged DNA and requires Rad4p for sufficient activity (Guzder et al. 1995). Mutations in *RAD23* result in reduced repair of both the TS and NTS (Mueller and Smerdon 1996), confirming the need for GG-NER proteins globally. Rad4p is essential for repair of the TS and NTS, with mutations resulting in a highly UV sensitive phenotype, whereas the human homologue XPC is only required for GG-NER, suggesting a difference in mechanism in the early stages of human NER (Venema et al. 1991).

In yeast, Rad23p interacts with TFIIH and Rad14p, acting to recruit the NER factors to the site of damage (Ramsey et al. 2004). Rad23p also interacts with the proteosome via its ubiquitin-like (UbL) domain (Russell et al. 1999), acting to regulate cellular levels of Rad4p by inhibiting its proteosomal degradation (Araujo and Wood 1999; Batty and Wood 2000; Chen and Madura 2002; Guzder et al. 1995; Rouse and Jackson 2002). Therefore it is suggested that Rad23p's role is regulatory in the NER mechanism, stabilising the Rad4p-23p complex required for NER factor assembly (Sweder and Madura 2002). It should be noted that the presence of the UbL domain did not mark Rad23p itself for degradation suggesting a non-proteolytic role for Rad23p (Watkins et al. 1993). Two distinct pathways emerged, the first non-proteolytic pathway involving the Rad23p/19S subunit of the proteosome, and the second requiring *de novo* protein synthesis and the damage-induced ubiquitination of

Rad4p via a Rad7p-16p contained E3 ubiquitin ligase (Gillette et al. 2006; Reed and Gillette 2007).

In *S. cerevisiae* the Rad7p-16p complex is also required for GG-NER (Bang et al. 1992; Terleth et al. 1990; Verhage et al. 1994), and is estimated to be responsible for repair of 20-50% of the genome (Verhage et al. 1994). The Rad7-16 proteins form a complex, thought to interact with the essential protein autonomously replicating sequence-binding factor 1 (Abf1), to form the so-called GG-NER complex. Rad7p-16p has roles in ATP-dependant damage recognition (Guzder et al. 1998b) as well as in the post-incision events, with Rad7p and Rad16p mutants being deficient in repair synthesis and incision (Reed et al. 1998; Wang et al. 1997).

Rad7p-16p binding is thought to be mediated by the zinc binding motifs of Rad16p. Rad16p has DNA-dependant ATPase activity with homology to the Snf2 chromatin remodelers, an activity which is inhibited by the presence of UV lesions (Guzder et al. 1998b). This gave rise to the concept that Rad7p-16p complex may track along DNA, inhibited by damage, providing a nucleation site for NER factors (Prakash and Prakash 2000). The Rad16p component of the GG-NER complex is required for the generation of superhelical torsion required for the excision of the damage containing oligonucleotide *in vitro* (Reed et al. 1998; Yu et al. 2004). Rad16p has also been more recently implicated in the histone H3 acetylation required for efficient GG-NER in a chromatin substrate (Teng et al. 2008).

In humans the XPE/DDB2 may also play a role in the specific recognition of UV induced photoproducts. The DDB complex (DDB1 and DDB2) encoded by the XPE gene binds to minor and major helix distorting lesions, creating a kink in the DNA, enhancing the recognition by the NER factors XPC, hHR23B and Cen2 (Tang and Chu 2002). It is thought that the DDB complex may be a functional homologue of Rad7-Rad16.

It should be noted that although much research has been carried out into the early stages of damage recognition in the global genome, the intricacies of how the NER machinery gains access to DNA within a chromatin environment is far from understood.

Transcription Coupled-NER

The NER of DNA damage within regions of DNA undergoing active transcription is termed Transcription coupled NER (TC-NER), and it is defined by the presence of a stalled RNA polymerase (RNAP) (Hanawalt 1994; Laine and Egly 2006). Much current understanding of TC-NER is derived from CS cells, those from patients with a rare photosensitive disease Cockayne syndrome. CS cells have an inherent delayed recovery of RNA synthesis following DNA damage, due to a defect in the repair of transcribed genes (Mayne and Lehmann 1982; Venema et al. 1990b), and subsequently found to be due to a defect in TC-NER (Troelstra et al. 1992; Venema et al. 1990a).

The repair found in transcriptionally active regions was found to be more efficient than repair in non-transcribed regions (Bohr et al. 1985; Mellon et al. 1986) and this finding was echoed in *S. cerevisiae* (Smerdon and Thoma 1990) and bacterial systems (Mellon and Hanawalt 1989). In mammalian systems enhanced repair of the transcriptionally active genes may be due to factors which govern the accessibility of RNA polymerase II (RNAPII) to the control regions, such as the specific localisation of chromatin remodelling factors and TFIIH, or perhaps in the catalysis of mRNA (Gao et al. 1994; Tu et al. 1996). The RNAPII- mediated transcription of genes is intimately linked with the NER pathway, with a temperature sensitive mutant of RNAPII in *S. cerevisiae* resulting not only in an inhibition of transcription, but also an inhibition of TC-NER (Sweder and Hanawalt 1992). TFIIH, a major part of the transcription initiation complex also acts as an integral component of the NER machinery (Feaver et al. 1999). Repair was found to be faster at sites proximal to the transcription initiation site, with repair gradually slowing towards the 3' end of the gene (Tu et al. 1996). The interface between GG-NER and TC-NER differs depending on the gene studied, and can occur before the start of transcription, a few hundred base pairs upstream, or 23 nucleotides down-stream (Tijsterman et al. 1996).

Cockayne syndrome A (CSA) and Cockayne syndrome B (CSB) genes were shown to be essential for efficient TC-NER in humans. The *S. cerevisiae* CSA and CSB homologues were subsequently cloned, designated *RAD28* and *RAD26* respectively (Bhatia et al. 1996; van Gool et al. 1994). Rad28p is not essential for TC-

NER (Bhatia et al. 1996), and precise roles of this protein are yet to be elucidated fully.

In *E. coli* the TRCF protein acts to displace a stalled RNAP molecule and recruit NER machinery. In yeast it is postulated that Rad26p plays this role, and like the human CSB gene, is required for removal of UV lesions from the transcribed strand (van Gool et al. 1994; van Hoffen et al. 1993). Both Rad26p and CSB have inherent DNA dependant ATPase activity (Guzder et al. 1996a; Selby and Sancar 1997), suggesting a role in the alteration of chromatin structure to allow access for NER machinery. However, CSB has not been shown to displace RNAP (Selby and Sancar 1997), but it does interact with TFIIH and XPA, key components of the pre-incision complex. An over-expression of Rad26 protein increases both TC-NER, as well as overcoming the requirement for GG-NER protein Rad7 in the repair of the NTS. It is thought that this over-expression increases accessibility of DNA within chromatin to NER factors, attributed to the DNA dependant ATPase activity of Rad26p (Bucheli and Sweder 2004).

Rad26p has been implicated in multiple roles of the TC-NER pathway, all of which confirm the intimate link between transcription and repair. It is suggested that the priority of the transcription factor TFIIH for either repair or transcription is mediated by Rad26p (You et al. 1998). Rad26p has also been implicated in transcription elongation (Selby and Sancar 1997), and an alternative damage response, promoting repair though damaged bases (Lee et al. 2002), independent of excision repair pathways.

In *S. cerevisiae*, Rad26p and Rbp9p, a subunit of RNAPII appear to be involved in two sub-pathways of TC-NER (Li and Smerdon 2002, 2004; van Gool et al. 1994). *RBP9* shares sequence identity with TFIIS, a transcription elongation factor, which in mammalian cells aids in the reactivation of a stalled polymerase, however, TFIIS does not appear to have this role in *S. cerevisiae* (Verhage et al. 1997). The concept of multiple pathways was bought about by studies which showed that *rad26rad7* or *rad26rad16* double mutants were not as UV sensitive as NER deficient strains (Rad14) (Verhage et al. 1996). The Rbp9p-mediated Rad26p-independent pathway has been shown to have different efficiencies in different genomic regions (Li and Smerdon 2002). It should be noted that repair of the actively transcribed strand is detected to some degree in multiple yeast genes studied to date in a Rad26p mutant, such as *RPB2* (Bhatia et al. 1996; Gregory and Sweder 2001;

Verhage et al. 1996) and *MFA2* (Teng and Waters 2000), however this is thought to be largely attributed to GG-NER.

Rad26p is almost dispensable for TC-NER in highly induced genes (Li and Smerdon 2002, 2004), and Rad26p is required for the efficient Rad16p-independent repair of many repressed regions of the yeast genome, including the *GAL1-10*, *PHO5* and *ADH2* genes (Li et al. 2007b). Taken together, multiple factors may contribute to the repair of different genomic domains.

In yeast TC-NER of RNAPII transcribed genes requires *RAD4*, a component also needed for lesion recognition in GG-NER, suggesting that once the initial damage factors are alerted to a stalled polymerase, GG-NER factors are recruited, including those for lesion recognition (Hanawalt and Spivak 2008). In human cells however, the need for GG-NER recognition proteins is removed in the presence of a stalled RNAP. CSB is a SNF2 family member which interacts with the elongating RNAP II, stimulating transcription. Upon transcriptional arrest however CSB binding is enhanced (van Gool et al. 1997). It is thought that following RNAPII arrest the polymerase regresses, rather than dissociating, to allow for the recruitment of NER factors (Hanawalt and Spivak 2008). TC-NER in mammals requires the actions of CSA, CSB, XAB2, TFIIS, HMGN1 and p300 in concert with RNAPII. CAF1 is also required for the restoration of nucleosome structure post repair (Hanawalt and Spivak 2008).

Repair of RNA pol I transcribed rDNA is an emerging field, with two further genes, Rad34p (homolgous to Rad4p) and Rad33p implicated in TC-NER and total NER respectively. Interestingly, Rad33p plays an additional role in repair of RNA pol II transcribed genes, with a potential association with Rad4p/23p (den Dulk et al. 2006; Tremblay et al. 2008).

DNA unwinding and open complex formation

Once the DNA lesion has been recognised by the various early acting factors, the formation of an open complex takes place. This creates a 'bubble' of open chromatin surrounding the DNA damage region, allowing the binding of NER proteins in close proximity to the damaged base.

The open complex formation is achieved primarily by the transcription factor TFIIH. This is a multi-protein complex containing two DNA helicase subunits

Rad25p (XPB) and Rad3p (XPD), which are both essential for transcription. TFIIH is either recruited by associations with the Rad4p-23p complex or is present due to stalled transcription machinery. Rad25p and Rad3p possess 3' to 5' and 5' to 3' polarity respectively (Guzder et al. 1994; Sung et al. 1987), functioning together to actively unwind approximately 20-30 base pairs surrounding the DNA damage (de Laat et al. 1999). In yeast, although *RAD3* is an essential gene a mutation within the 5'-3' helicase domain is not lethal, but renders NER defective (Qiu et al. 1993). This open complex formation is also dependant on ATP hydrolysis and the cooperative binding of Rad14p (XPA) and RPA for stabilization of the open structure (Guzder et al. 1995; He et al. 1995). The binding of RPA to ssDNA promotes the opening of the structure, as well as acting to stabilise it. RPA has also been shown in mammalian cells to bind in a specific orientation, interacting specifically with the 5' side binding XPG, and the 3' side binding ERCC1-XPF, and provides a structure to ensure strand specificity of the endonucleases (de Laat et al. 1999).

Next comes a role for Rad14p which has a higher affinity for damaged DNA than human XPA (Guzder et al. 1993; Jones and Wood 1993), which in turn increases when binding in concert with RPA. Rad14p is crucial in the formation of the pre-incision complex consisting of Rad4p-23p, Rad14p, RPA, the transcription factor TFIIH, Rad3p and Rad25p, Rad1p-10p complex and Rad2p (Prakash and Prakash 2000).

Dual incision and excision of damaged DNA

The main stage of NER, which gives rise to the mechanisms name, is the dual incision of the DNA strand containing the DNA damage, and the subsequent turning out and excision of the damage containing oligonucleotide. Having recruited the pre-incision complex at the site of DNA damage, the RPA and Rad14 proteins subsequently recruit the ssDNA-dsDNA junction endonucleases Rad1-10 complex and Rad2p, which act to incise the DNA at the 5' and 3' sides of the DNA damage respectively. Rad1p-10p must be in a complex to function as single-stranded DNA endonuclease (Tomkinson et al. 1993).

Rad1p-10p exists as a complex with Rad14p *in vivo*, with Rad2p associating with TFIIH (Guzder et al. 1996b), suggesting that the sequential steps may not be as clear cut, with multiple proteins recruited together at the nucleation site. As well as

providing the essential endonucleolytic activities to ensure dual incision of the damage containing oligonucleotide, Rad1p-10p and Rad2p are required for the assembly of the full complement of the NER machinery at the damage site (Prakash and Prakash 2000). Rad2p has sequence homology to *E. coli* DNA pol I, which has inherent 5'-3' nuclease function to remove RNA primers formed during lagging strand DNA synthesis, cleaving the 5'ended ssDNA junction with duplex DNA (Habraken et al. 1995).

NER results in the excision of a damage-containing oligonucleotide 27-30 nucleotides in length (Guzder et al. 1995; Guzder et al. 1996b; Habraken et al. 1996; Mu et al. 1997). The Rad7-16-Abf1 GG-NER complex has been implicated in the generation of superhelical torsion, mediated by the Snf2-family member Rad16p, which plays a key role in the *in vitro* excision of the fragment (Reed et al. 1998; Yu et al. 2004), suggesting DNA conformation aids in the timely excision of the damage containing oligonucleotide.

Repair synthesis and gap ligation

Once the damage has been removed, the DNA double helix must then be restored to ensure genomic stability. Replicative synthesis takes place to allow the resulting gap to be sealed. This takes place using the polymerase δ or ε holoenzyme found in mammalian and yeast cells (Budd and Campbell 1995), along with RPA, PCNA (Shivji et al. 1992) and RFC. The phosphate backbone is then sealed via DNA ligase I to reform a functional DNA double helical structure.

1.2.2.6 NER deficiencies and human disease aetiology

Defects in the NER genes can give rise to 7 known clinical entities, arising from at least 10 causative genes. These clinical disorders can arise from mutations in multiple genes, and different mutations in a single gene may give rise to different disorders. All diseases present with increased UV sensitivity, and a spectrum of other pathologies generally encountered in old age (Niedernhofer 2008). The three main disorders associated with NER are the rare autosomal recessive Xeroderma pigmentosum (XP), Cockayne syndrome (CS) and trichothiodystropy (TTD) (Leibeling et al. 2006).

Xeroderma Pigmentosum (XP)

The recessive inherited disorder Xeroderma pigmentosum (XP) affects approximately 1:125000 people worldwide (Lichon and Khachemoune 2007) and is characterised by parchment-like skin (xeroderma) and sunlight-induced freckles (pigmentosum). The skin changes in XP patients can present as young as 6 months, with progressive diffuse erythema and edema and subsequent onset of xerosis and scaling. Of importance in clinical assessment are the UV-induced skin changes, generally noted as an extreme sensitivity to sunlight, with significant sun burn which persists beyond the time expected to heal. Increased freckling in also a diagnostic marker, with hyperpigmented macules being detected from a young age especially in regions exposed to UV light including hands, face and tongue. The majority of XP patients will suffer from ocular abnormalities, including inflammation, erythema, loss of eye lashes, and neoplasms of the eye lids, conjunctiva, cornea and iris.

XP presents with an early onset of skin cancers, with a 1000-fold increased risk of malignant neoplasms. The onset of cancers including basal and squamous cell carcinoma and cutaneous melanoma occur at a mean age of ten years old predominantly in regions exposed to UV light (Kraemer et al. 2007). XP does however also present with an increased risk of other tumour types.

XP encompasses two disorders, that of classic XP, and a more severe disorder which is referred to as XP neurological, in which patients also suffer from a variety of degenerative neurological abnormalities. Approximately 20-30% of XP sufferers present with neurological dysfunction (Kraemer et al. 2007), which can vary greatly, from microcephaly, cerebral dysfunction, to sensorineural deafness and peripheral neuropathy (de Boer and Hoeijmakers 2000; Lehmann 2003).

NER is a heterogeneous disorder, which provides a complex relationship between clinical diseases and molecular defects in NER. XP exhibits seven complementation groups XPA to XPG, as well as a variant form of the disease XPV. The complementation groups correspond to individual proteins which are involved in the multi-faceted NER mechanism. XPV does not have a defect in NER but arises due to a defective DNA polymerase η, a polymerase which can bypass UV-induced DNA damage (Leibeling et al. 2006).

The genes generally associated with XP neurological are XPA, XPB, XPD and XPG, genes which have crucial roles in NER and basal transcription. XPA complementation group patients present with severe symptoms, as XPA is indispensible for both GG-NER and TC-NER. The GG-NER specific XPE protein mutation gives rise to a mild XP phenotype. The clinical outcomes identified to date for XPF mutations are mild, however it is thought that those studied are mis-sense mutations, and may still possess functional protein (Lehmann 2003). XPB and XPD proteins hold a role in transcription and NER, therefore give rise to a variety of clinical outcomes when mutated. Defects in XPD can give rise to any of the six major NER-associated diseases, XP, XP neurological, TTD, XP/CS, XP/TTD or COFS (Kraemer et al. 2007).

Neurological aetiology is highly debated in XP, as UV light does not penetrate to the brain tissue, and not all complementation groups have essential roles in basal transcription. Although, it is worth noting that neurons do not divide. It is widely considered that the neurological defects are due to an inability to repair oxidative lesions (Brooks 2007). Following this research, XP patients are advised to avoid where possible exposure to exogenous damaging agents, especially cigarette smoke.

Cockayne Syndrome (CS)

Cockayne syndrome (CS) is characterised by a sensitivity to sunlight, however it presents as a rash opposed to the hyperpigmented macules seen in XP (Kraemer et al. 2007). CS patients do not have an increased risk of carcinomas, and present with microcephaly, gait ataxia, cachectic dwarfism, leukodystrophy along with developmental delay and optic atropy, deafness, osteoporosis, and characteristic facial features such as sunken eyes, beaked nose and large ears (Leibeling et al. 2006). The primary histological finding in CS is demyelinisation of neurons rather than the primary neuronal degeneration seen in XP (Kraemer et al. 2007). There is also a severe form of CS, now known as a distinct disease, COFS (cerebral, ocular, facial, skeletal syndrome).

CS does not arise due to a lack of total NER, as an XPA mutant does not give rise to CS. Most CS patients belong to groups A and B due to mutations in the human CSA and CSB genes. CSA and CSB have been shown by a yeast two-hybrid system to interact *in vitro* (Henning et al. 1995). CSA and CSB have also been shown to

interact with p44 subunit of TFIIH and XPG respectively as well as associating with RNA polymerase II, helping to overcome obstacles in transcription (see Section 1.2.2.5).

A subset of patients present with both CS and XP symptoms, described as a separate clinical entity, XP/CS. Upon genetic testing it was found that no CS mutations were present, however the defect lay within an XP gene. The genes involved are XPB, XPD and the endonuclease encoding XPG. The defect can therefore be assumed to be involved in NER and oxidative damage repair (Leibeling et al. 2006) and not in transcription.

Trichothiodystrophy (TTD)

One of the defining characteristics of patients with TTD is brittle hair, due to a deficit of sulphur caused by a reduced level of cysteine-rich matrix proteins. Sufferers also exhibit a short stature (cachetic dwarfism), ichthyosis, developmental abnormalities, unusual facial features as well as photosensitivity (Kraemer et al. 2007; Lehmann 2003). The patients who are sun sensitive do not exhibit the pigmental abnormalities seen in XP and the causative mutations have been found to be in TFIIH subunits, XPD, XPB or TTDA (Leibeling et al. 2006). Like CS, TTD does not give rise to an increased risk in UV-induced cancers (Kraemer et al. 2007). The majority of patients have mutations in the XPD gene, which has a role in transcription initiation and is part of the TFIIH complex. Most XPD mutations are found within the C-terminal third of the protein, affecting the association with the p44 component of the TFIIH core. This interaction stimulates the helicase activity of the XPD protein. Patients who do not present with photosensitivity can be ascribed to mutations in TTDN1 or other unknown genes (de Boer and Hoeijmakers 2000).

A further clinical entity of XP/TTD has the combined features of the two diseases, with the characteristic facial features and developmental abnormalities of TTD along with an increased risk of UV-induced cancers and pigmental changes. It is thought that XP/TTD patients carry compound heterozygous XPD mutations, giving rise to a defect in basal transcription and in NER (Leibeling et al. 2006).

There is also a subset of patients with mild clinical manifestations, but without developmental or neurological abnormalities. These patients have a mild sensitivity to UV light, and are designated $UV^{S}S$ (UV sensitive syndrome). As described, the

aetiology of the NER-associated diseases is varied. CS and $UV^{S}S$ can be attributed solely to a deficiency in TC-NER and interestingly these syndromes do not have an enhanced susceptibility to cancer. The TC-NER defect results in high levels of apoptosis following UV damage, however proficient GG-NER helps to reduce mutagenesis and therefore carcinogenesis (Hanawalt and Spivak 2008).

Defects in GG-NER, such as an XPC mutation results in high levels of mutagenesis, however the GG-NER–cancer link is not observed in those TTD patients with GG-NER defects. It is speculated that an increased cancer rate may also arise in XP patients due to a deficient immune response or low catalase activity (Gaspari et al. 1993; Quilliet et al. 1997).

1.3 Transcription and NER in a chromatin context

1.3.1 Chromatin structure

In order to understand the complexities of DNA damage, it is a necessity to first understand the manner in which DNA is tightly compressed within the nucleus of our cells. The DNA in eukaryotic species is packaged within the nucleus, in complex structures named chromosomes. The condensation of the DNA double helix at the most basic level involves the wrapping of 146bp of DNA around 2 copies each of H2A, H2B, H3 and H4 histone proteins, to form a nucleosome core particle (NCP). The interstitial nucleosome complexes then fold further to produce chromatin 30nm fibres. In eukaryotes (but not *S. cerevisiae*) this structure is stabilised by the addition of histone H1 in the linker DNA region between nucleosomes. Figure 1.4 displays the additional stages of folding and coiling required for the condensation of chromatin into chromosomes.

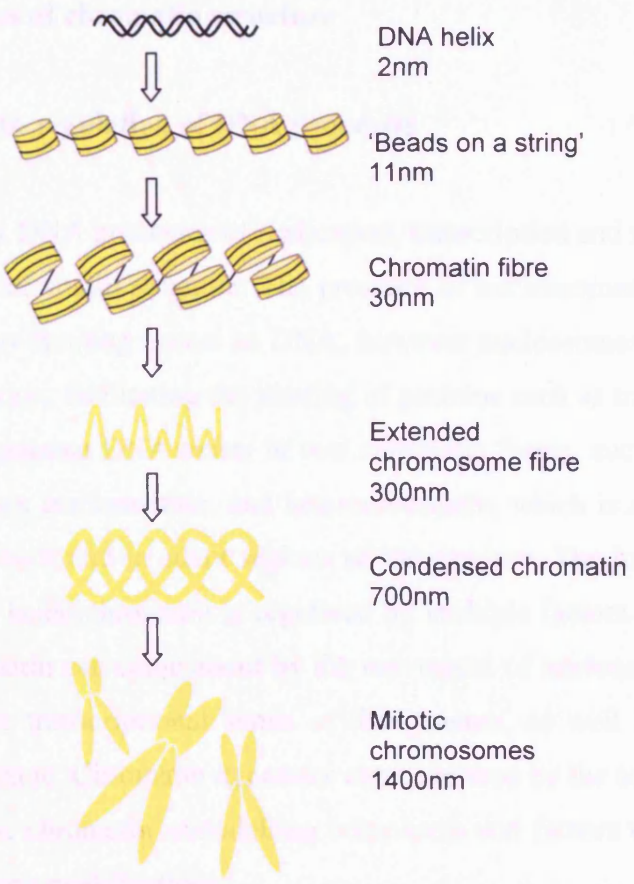

Figure 1.4: The DNA double helix associates with histones to form nucleosomes, arranged in a 'beads on a string' manner. Further folding into a solenoid results in a chromatin fibre. Additional coiling condenses the compacted chromatin structure to form chromosomes. Adapted from (Alberts et al. 2002).

A heterogeneity of nucleosome distribution has been noted with promoter regions having a lower density of nucleosomes compared with coding regions (Sekinger et al. 2005), with a 200bp nucleosome free region identified in gene promoters in yeast (Yuan et al. 2005). A chromatin environment affords protection for genomic DNA, but it is an obstacle for factors such as the transcription machinery and repair proteins. For cellular metabolism to efficiently take place nucleosome remodelling factors and histone covalent modification enzymes have been identified which act to overcome the chromatin structure.

1.3.2 Implications of chromatin structure

1.3.2.1 Chromatin regulation of DNA processes

The major DNA processes of replication, transcription and repair are mediated by the dynamic chromatin structure. The presence of nucleosomes can act to repress these processes by limiting access to DNA, however nucleosomes may also provide an activator function, facilitating the binding of proteins such as transcription factors. Throughout the genome DNA exists in two chromatin forms, euchromatin, which is considered an open conformation, and heterochromatin, which is a condensed closed conformation often found in silent regions of the genome. The interchange between euchromatin and heterochromatin is regulated by multiple factors. The local changes induced in chromatin can come about by the movement of nucleosomes and can alter depending on the transcriptional status of the genome, as well as the progression through the cell cycle. Chromatin dynamics can be altered by the actions of chromatin modifying agents; chromatin remodelling complexes and factors which induce post-translational histone modifications.

Transcription has been extensively investigated in terms of chromatin rearrangements and modifications, and has shed light on the regulatory roles chromatin plays in DNA repair.

1.3.2.2 Transcription in a chromatin environment

Much of our understanding of chromatin biology has emerged from transcriptional studies. Eukaryotic transcription follows the same general pattern, requiring not only an active RNAPII, but also a subset of basal transcription factors. RNAPII directed transcription begins with the recruitment and binding of activator proteins in the upstream TATA box and transcription start site regions of a core promoter. The transcription initiation step subsequently involves the binding of activator proteins to recruit co-activators such as Swi/Snf, SAGA and mediator which in turn provide a chromatin environment suitable for general transcription factor (GTF) recruitment. The recruitment of RNAPII then takes place, which is positioned at the core promoter by TBP (a component of TFIID), TFIIA and TFIIB. These

transcription factors assemble along with TFIIF to form the closed pre-initiation complex. On recruitment of TFIIH and TFIIK, 11-15bp of DNA is then melted to form a single-stranded region by the actions of the helicase activity of TFIIH. Once the single-stranded template is positioned in the RNAPII cleft, the complex is referred to as the 'open complex', and RNA synthesis can then proceed (Friedberg 1996; Li et al. 2007a). The multi-subunit TFIIH complex is also responsible for the phosphorylation of the carboxy-terminal domain (CTD) of RNAPII, which occurs during the first 30bp of transcription, to allow dissociation of the GTFs. As RNAPII proceeds to the elongation phase the phosphorylated CTD acts to recruit elongation and mRNA processing factors for efficient transcription completion (Buratowski 2003).

The initial recruitment of transcription factors (TFs) must overcome chromatin structure to gain access to the recognition sites. This is able to occur on a rapid time scale via spontaneous unwrapping of nucleosomes (Bucceri et al. 2006), however TF binding is stimulated by the addition of chromatin remodelling complexes (Utley et al. 1997). It is now largely accepted that chromatin modifying agents exist to aid in the binding and subsequent progression of the transcriptional machinery. The requirement for chromatin modifying agents in transcription can be exemplified by increased histone acetylation which mobilises nucleosomes, seen at active promoters. In *S. cerevisiae* it was shown that the histone H3 and H4 acetylation level at promoters was proportional to the rate of transcription, bought about by the increased recruitment of histone acetyltransfereases (HATs) Gcn5 and Esa1 (Pokholok et al. 2005; Robert et al. 2004).

The recruitment of HATs and chromatin remodelling complexes takes place in a coordinated manner, with activator-recruited complexes such as Swi/Snf playing a major role in DNA accessibility (Cosma et al. 1999). Two mechanisms for DNA access in transcription initiation can be proposed. Firstly, nucleosomes may be lost to allow for the pre-incision complex (PIC) to assemble, with nucleosome restoration following transcription (Adkins et al. 2007; Reinke and Horz 2003). The alternative model involves the formation of a partial PIC at the promoter site, with the association of TFIIH and RNAPII disrupting adjacent nucleosomes (Zanton and Pugh 2006).

Histone modifications are also well documented throughout transcription, such as H3K4 methylation, H2B monoubiquitination and H3K36 methylation. RNAPII is

not able to transcribe through a nucleosomal template, but the loss of at least one H2A/H2B dimer allows RNAPII progression (Kireeva et al. 2005). The progression of RNAPII through a nucleosomal environment results in multiple transcriptional pause sites, which induce subtle regression of the RNAPII particle. TFIIS has been implicated in the reactivation of RNAPII elongation to allow RNAPII to transcribe through a nucleosomal template (Kireeva et al. 2005). The RSC ATP-dependant chromatin remodelling complex has also been implicated in RNAPII transcription through nucleosomes, stimulated by SAGA and NuA4 mediated histone acetylation (Carey et al. 2006).

1.3.2.3 Interplay between transcription and repair

The relationship between transcription and repair can be clearly shown by the preferential repair of transcriptionally active genes (Mellon et al. 1986). The TC-NER pathway (as discussed in Section 1.2.2.5) is responsible for the repair of DNA lesions within actively transcribed regions of the genome. The initiating factor for TC-NER is thought to be a stalled RNAPII, although it is plausible that the phenomenon of transcription-associated repair may also take place due to the conformation of chromatin and accumulation of repair factors during transcription. It can be suggested that an open chromatin configuration is a more efficient substrate for repair processes to take place. However it should be kept in mind that the non-coding strand is not repaired to the same rate as the transcribed strand, and this strand specificity is not easily explained in terms of chromatin structure. It is worth bearing in mind that GG-NER also acts on the TS of active genes ahead and behind of the RNAPII complex, further enhancing the rate of repair of the TS.

The transcription factor TFIIH is not only involved in transcription, but also in NER, with two of the TFIIH subunits, namely Rad25 and Rad3 (XPB and XPD respectively in human cells) being required for efficient repair (both TC-NER and GG-NER pathways). This does provide a direct coupling of transcription and repair, however it has been shown that TFIIH dissociates from an elongating RNAPII, retracting from a plausible mechanism for a direct dual role for TFIIH (Friedberg 1996).

In transcription, the helicase activity of TFIIH is required for the unwinding of the DNA template to allow for the correct positioning of RNAPII to initiate

transcription (Holstege et al. 1996). The CTD kinase activity of TFIIH also plays a role in the transition from initiation to elongation stages of transcription (Buratowski 2003). A model whereby a core TFIIH complex exists with a dynamic kinase and repair component has been suggested, whereby the complex exists with kinase function during transcription, and when damage is encountered the kinase can dissociate and the repair form can persist (Svejstrup et al. 1995). However, the model of a repairosome has been overshadowed by emerging evidence of a sequential assembly of repair factors (Araujo and Wood 1999; Guzder et al. 1996b; Prakash and Prakash 2000).

It is possible that the stalled transcriptional machinery actually hinders the access of repair proteins, as has been shown in *E. coli in vitro* (Selby and Sancar 1990). It should also be remembered that the vital link between transcription and repair attributed to TFIIH can be exemplified by the range of clinical disorders arising due to defective TFIIH (Kraemer et al. 2007).

Multiple repair proteins also aid in the correct transcriptional process, independent of their role in NER, ensuring correct posttranslational modifications, further entwining the link between transcription and repair (Le May et al. 2010a; Le May et al. 2010b), and introducing further questions in how the cell is able to retain distinct cellular processes.

1.3.3 Chromatin remodelling factors

Chromatin remodelling complexes can be divided into two main groups, those which modify histones, mostly at the N-terminal tails; and those that use ATP hydrolysis to disrupt positioned nucleosomes.

1.3.3.1 Histone post-translational modifications

Histone proteins, predominantly histone tails are subject to a broad spectrum of post-translational modifications, including methylation, acetylation, ubiquitination, ADP-ribosylation, sumolation and phosphorylation. These modifications allow nucleosomes to interact with non-histone proteins, and have an effect on the stability and packaging abilities of chromatin. Modifications to the histone proteins can be classed into those associated with transcription, often referred to as euchromatin

modifications, exemplified by histone H3 and H4 acetylation and methylation of H3K4. Heterochromatin modifications conversely are associated with silent regions of the genome including inactive genes, such as methylation of H3K9 and H3K27 (Li et al. 2007a). The roles of histone modifications are diverse, with much still to uncover. Histone modifications, except methylation, generally act to mobilise nucleosomes, altering the net charge of the nucleosomal surfaces to loosen the DNA-histone interactions both *in vivo* (Reinke and Horz 2003) and *in vitro* (Hassan et al. 2006). As well as directly influencing chromatin structure (Shogren-Knaak et al. 2006), histone modifications are thought to provide a distinct epigenetic code, influencing not only chromatin dynamics but also protein recruitment (Jenuwein and Allis 2001; Strahl and Allis 2000).

In terms of transcription, the histone code has been well defined, for example, the entire ORF of active genes methylated at H3K4 is mediated by a specific complex, Set1. The degree of H3K4 methylation, mono-, di- or trimethylation occurs at different sites within a gene, itself stimulated by a further modification H2B monoubiquitination (Sun and Allis 2002).

Histone variants have also been a subject of much recent research. These differ from canonical histones in that they are expressed outside of S-phase and incorporated into chromatin in a DNA replication-independent manner. The variant histone Htz1 is enriched at promoters primed for transcription initiation, generally in the two nucleosomes flanking the 200bp nucleosome free region. Htz1 is displaced upon transcription initiation, a pre-requisite for transcription to take place (Li et al. 2005; Zhang et al. 2005). Maintaining the histone epigenetic landscape and the deposition of histone proteins ensures memory and maintenance of the genome.

1.3.3.2 Histone acetylases (HATs) and deacetylases (HDACs)

Perhaps the most extensively studied histone modification is that of acetylation, involved in both gene regulation and nucleosome assembly (Wade et al. 1997). This acetylation is conducted by a group of enzymes named histone acetyltransferases (HATs) via the transfer of an acetyl group from acetyl coA to the ε-amino group of specific lysine residues in the amino-termini of histone tails, which neutralises the positive charge. The positive charge can be restored by the actions of a second group of enzymes histone deacetylases (HDACs), and therefore acetylation

status is a reversible process. The acetylation of specific residues is thought to create a more permissive chromatin structure, allowing accessibility to transcriptional proteins and those for other DNA mediated processes (Roth et al. 2001). Therefore deacetylation is associated with the repression of chromatin structure and transcription.

The relationship between acetylation and transcription can be further supported as many transcriptional activators possess HAT activity, for example, Gcn5 in yeast (Kuo et al. 1996). The diverse implications of histone acetylation in cellular processes provide an interesting area of research (Roth et al. 2001).

1.3.3.3 ATP-dependant chromatin remodelling complexes

As well as being subject to histone modifications, chromatin can also be mediated by the actions of ATP-dependant chromatin remodelling agents (Saha et al. 2006). The SWI/SNF (mating-type switching and sucrose fermentation in yeast) superfamily of chromatin remodelers has been extensively studied, with family members including SWI/SNF, ISWI, CHD and IO80 (Morrison and Shen 2009). Genome wide studies proposed a role for SWI-SNF in gene regulation (Holstege et al. 1998), and recruitment of the complex was shown to be an essential step in transcriptional regulation (Cosma et al. 1999). SWI/SNF complexes utilise the energy from ATP to remodel nucleosome structure, providing an increased affinity for transcription factor binding, with the remodelled chromatin state persisting after dissociation of the SWI/SNF complex (Cote et al. 1998; Schnitzler et al. 1998). SWI/SNF may also function along with ATP hydrolysis to return chromatin structure to its former un-modelled state (Schnitzler et al. 1998). Homologs of the ATP-dependant SWI/SNF have been identified in higher eukaryotes, including the SWI2 homologs Brahma in *Drosophila melongaster* (Tamkun et al. 1992), and Brahma and BRG1 in humans (Chiba et al. 1994). Further ATP-dependant chromatin remodelling complexes containing helicase-like domains include the RSC complex, which has been shown to allow RNAPII progression through paused sites in nucleosome templates, a reaction stimulated by SAGA and NuA4 mediated histone acetylation (Carey et al. 2006).

The SWI/SNF complex mode of action was thought to be one of two possible mechanisms, with the first utilising the complexes ability to generate superhelical

torsion (Havas et al. 2000) resulting in DNA being twisted over nucleosomes altering the rotational setting, often referred to as twist defect diffusion. However, further studies suggest that a second mechanism, involving the formation of a loop or bulge in the DNA, also referred to as bulge diffusion, is more likely (Bazett-Jones et al. 1999). These diffusion models appear energetically favourable within a cellular context, when compared to the process of histone dissociation (Thoma 2005), and although remodelled chromatin has a reduced DNA-histone affinity, the four core histones are retained (Schnitzler et al. 1998).

In humans the Swi/Snf complex is approximately 2MDa, containing at least 9 subunits which include a bromodomain-containing ATPase subunit, either BRM (Brahma) or BRG1 (brama-related gene 1) (Halliday et al. 2009). The diverse regulatory roles of SWI/SNF in DNA methylation, replication, recombination and repair are of clinical importance, with subunits of SWI/SNF implicated as tumour suppressor genes, linking chromatin remodelling with carcinogenesis (Halliday et al. 2009).

1.3.3.4 UV-induced DNA damage formation in chromatin

It has been long understood that a modulation of UV-induced DNA damage formation is seen within a chromatin environment. The presence of nucleosomes acts to protect some regions of DNA from damage, whilst those regions which are exposed such as the linker regions are subject to potential damage. The ability of UV light to damage a base is determined in part by the flexibility of the DNA (Thoma 1999), with bending of DNA towards the minor groove reducing CPD formation (Pehrson and Cohen 1992). The B-form structure of DNA can also be affected by DNA binding proteins which when bound induce a morphological alteration to the DNA structure. DNA-binding proteins can therefore modulate DNA damage formation, giving rise to a heterogeneous distribution of DNA lesions (Thoma 1999). As DNA-binding complexes can alter the induction of DNA damage, it is of no surprise that DNA within a nucleosomal structure incurs a distinct modulation of damage formation. It has been shown in nucleosome core particles isolated from human cells by nuclease digestion that induction of CPD formation was distributed with a periodicity of 10.3 bases (Gale et al. 1987). A similar modulation was seen in DNA which was engineered to form a loop (Pehrson and Cohen 1992), but not in linker DNA (Pehrson

1989). It was later found that bending of the DNA around the histone octamer facilitates the formation of CPDs at sites where the DNA minor grooves face outside. In contrast to CPDs, there does not appear to be modulation of 6-4 PP formation, which occurs at 20-30% of the yields of CPDs, in a nucleosomal background (Friedberg et al. 2006; Gale and Smerdon 1990). Interestingly CPDs do not displace DNA from histones, and are accommodated well within chromatin (Gale et al. 1987; Svedruzic et al. 2005).

1.3.4 NER in a chromatin environment

As damage must be repaired within a chromatin environment, it is thought that various factors must be in place to remodel chromatin structure. NER requires multiple proteins simply to act on naked DNA, but extensive work into the details of how chromatin is modified to enable NER still remains elusive. This complex question was originally investigated by (Smerdon and Lieberman 1978), yet whilst a lot of work has been carried out into the chromatin rearrangements involved with transcription, those for repair are less understood.

In terms of NER, lesions encountered by a RNAPII complex within regions undergoing active transcription are repaired by TC-NER. The GG-NER pathway acts on both the TS and NTS of active and repressed genes, however only GG-NER must engage in the repair of nucleosomal DNA (Hanawalt et al. 2003). It is thought that the open chromatin conformation inherent with active transcription promotes efficient NER in transcribed genes. It has been established for some years that the presence of nucleosomes inhibit efficient nucleotide excision repair both *in vitro* and *in vivo*, greatly reducing repair synthesis (Wang et al. 1991). A modulation of repair is seen within chromatin, with repair slower in the centre of nucleosomes, and becoming relatively faster towards the periphery and within the linker regions (Svedruzic et al. 2005). Linker regions in *S. cerevisiae* cells are often short, about 15bp, not allowing much space for repair, thereby leading to the assumption that nucleosome mobility applies to multiple adjacent nucleosomes.

Repair in a chromatin environment requires fulfilment of the three stages of the proposed access-repair-restore model (Smerdon 1991). The first and perhaps most elusive stage is the recognition of the DNA lesion within a chromatin background. Secondly, the NER machinery must access the site of lesion, followed by restoration

of the original chromatin structure to preserve crucial epigenetic information (Gong et al. 2005; Zhu et al. 2009).

In a study of mammalian cells, p53 was shown to mediate a global chromatin relaxation response to facilitate NER (Rubbi and Milner 2003), although multiple other studies support a local chromatin remodelling model (Gaillard et al. 2003; Gontijo et al. 2003; Groth et al. 2007; Meijer and Smerdon 1999; Osley et al. 2007; Smerdon 1991; Yu et al. 2005). In yeast access is provided by the concerted actions of histone modifying enzymes and chromatin remodelling complexes (Meijer and Smerdon 1999).

1.3.5 NER and chromatin remodelling

Chromatin remodelling in respect to DNA repair was first shown in 1978 where it was postulated that the NER mechanism demands a space of approximately 100bp for the complete excision of a 30bp damage-containing oligonucleotide (Smerdon and Lieberman 1978). Following the access-repair-restore model (Smerdon 1991) nucleosomes must therefore be modified for mobilisation or evicted to allow for factor binding. In yeast it has been shown that long-range effects in chromatin take place following DNA damage, exemplified by the redistribution of SIR proteins following double strand breaks (DSBs), which results in the loss of telomeric silencing (Mills et al. 1999).

It is postulated that nucleosomes inhibit NER at a point beyond lesion detection, as although the damage recognition factors XPC, XPA and RPA are able to bind to nucleosomal DNA *in vitro*, efficient repair does not take place in absence of chromatin remodelling (Hara and Sancar 2002). This is confounded in *S. cerevisiae* as SWI/SNF and Gcn5-dependant chromatin modifications occur independently of damage recognition by Rad4 or Rad14, with the deletion of these recognition proteins simply delaying chromatin restoration to the pre-UV state (Yu et al. 2005).

A series of *in vitro* and *in vivo* studies demonstrated the actions of chromatin remodelling complexes such as INO80, RSC and the ySWI/SNF and ISWI (Kent et al. 2001) in NER. The incision step of human NER within dinucleosome substrates was enhanced by the presence of the ACF chromatin remodelling factor, which acted to move nucleosomes to create larger linker regions (Ura et al. 2001). In a human NER reconstituted mononuclesome system it was shown that SWI/SNF activity

enhances repair of an AAF-G adduct, and that NER factors in turn enhance SWI/SNF activity (Hara and Sancar 2002). Repair by photolyase was also shown to be enhanced by the actions of SWI/SNF and ISWI (Gaillard et al. 2003), however an over-expression of photolyase saw efficient repair of transcribed and non-transcribed regions of the genome, except centromeric regions, suggesting that chromatin remodelling is not required in this instance (Bucceri et al. 2006). The involvement of SWI/SNF in human NER appears lesion specific, with no enhanced removal of CPDs seen (Hara and Sancar 2003). However human SWI/SNF has been shown to enhance the removal of CPDs by ML UV endonuclease and T4 endonuclease V mediated repair (Lee et al. 2004). SWI/SNF acts to increase the accessibility of DNA to restriction endonucleases over time following UV, which is attenuated by approx 50% in a swi2delta mutant, placing SWI/SNF with a role in the repair of UV lesions (Yu et al. 2005).

The destabilisation of higher order chromatin structures by histone tail hyperacetylation (Shogren-Knaak et al. 2006) is exploited following UV irradiation to enhance damage recognition and repair (Ramanathan and Smerdon 1989). Following UV irradiation histones H3 and H4 are acetylated throughout the genome (Yu et al. 2005). At the repressed *MFA2* promoter UV induced H3 hyperacetylation results in a relaxed chromatin structure, being more accessible to restriction enzymes, with the chromatin structure and acetylation levels returning to a pre-UV state with increasing time post-UV. The histone acetylation and chromatin remodelling were found to be at least in part due to the actions of the histone acetyltransferase Gcn5, and Swi2 (Yu et al. 2005). In mammalian cells a family of proteins named IG proteins play a role in UV responses such as cell proliferation, NER and p53 directed apoptosis, with p33ING2 enhancing NER by histone H4 acetylation and recruitment of XPA to damage (Wang et al. 2006b).

The Rad7-Rad16-Abf1 GG-NER complex acts to repair non-transcribed regions of the genome, including nucleosomal DNA and is believed to be functionally homologous to the human DDB protein. Whilst Rad7 has been shown to interact with the Sir3 protein, involved in the chromatin organisation of silenced genes (Paetkau et al. 1994), Rad16 has been implicated with multiple roles in the chromatin regulation of NER. Rad16 has inherent DNA-dependant ATPase activity, thought to provide a molecular motor for the GG-NER complex to translocate DNA in search of DNA lesions (Guzder et al. 1997). Rad16 is a member of the SWI/SNF chromatin

remodelling family, suggesting a role in the unwinding of the local chromatin environment to allow for access to NER machinery (Prakash and Prakash 2000; Thoma 1999). As well as aiding in the early stages of NER the GGR-complex has been shown to generate superhelical torsion in naked DNA, which is required for removal of the excision product in the later stages of the NER mechanism (Reed et al. 1998; Yu et al. 2004). Interestingly Rad16 has also been implicated with E3 ubiquitin ligase function, acting in concert with Rad23 to regulate the cellular levels of the damage recognition factor Rad4 (Ramsey et al. 2004).

Recently it has been displayed that Rad16 mediates UV-dependant histone H3 acetylation, and that this is required for efficient GG-NER (Teng et al. 2008). The absolute requisite for Rad7 and Rad16 during GG-NER was abolished by constitutively elevating the levels of H3Ac in the *MFA2* gene. Although many attributes of Rad7/Rad16 suggest a role in chromatin arrangement, the complex is also required for the repair of the NTS of active genes, where the chromatin arrangement is de-repressed, but where nucleosomes may still be associated with this strand. These proteins may play multiple roles within NER.

Chromatin provides an obstacle for eukaryotic NER however this is less of a problem for TC-NER, as the chromatin environment is transiently opened to allow for the translocation of RNAP. However, histone acetylation and chromatin remodelling also have suggested roles in TC-NER displayed by the enhancement of repair of the TS and NTS in Rad26 (CSB homolog) over-expressed cells. This over-expression of Rad26 also partially suppresses Rad7 deficient cells (Bucheli and Sweder 2004). In human cells CSB is recruited to stalled RNAP, and is required for recruiting NER factors XPA, XPF, RPA and TFIIH as well as p300 (HAT) and HMGN1 (Fousteri et al. 2006). CSB is also a member of the SWI/SNF2 member of ATP-dependant chromatin remodellers, thought to act by increasing accessibility to DNA lesions (Hara and Sancar 2002).

Following repair the chromatin structure must then be restored with nucleosome reassembly carried out either by histone recycling or *de novo* deposition can take place. Although it is not agreed upon whether histone proteins are lost to allow for repair machinery access, it has been shown that new histone H3-H4 dimers are incorporated at UV damage sites, dependant on functional NER and CAF-1 (Polo et al. 2006). However, this was for NER shortly after UV and in human cells where the majority of NER is coupled to transcription. CAF1 (chromatin assembly factor 1)

is dependant on the incision step of NER, therefore involved in the later stages of local rather than global chromatin reassembly following repair (Green and Almouzni 2003). It is thought that the newly incorporated histones undergo a mechanism to restore the local epigenetic information, such as the restoration of acetylation status by the actions of HDACs, as shown following DSBs (Tamburini and Tyler 2005). Hence it is of interest to determine the intricate details of the chromatin biology associated with NER.

1.4 The present study

The aim of my project was to provide an understanding of the complexities surrounding the NER mechanism within a chromatin environment. Much work had been carried out on one sub-pathway of NER, namely Transcription coupled NER (TC-NER), where chromatin exists in an open conformation. In TC-NER damage is recognised by an elongating RNA polymerase, to promote repair. Global genome NER (GG-NER), on the other hand, is described as repair of the non-transcribed regions of the genome, including the NTS of actively transcribed regions. The damage recognition signal within GG-NER is yet to be elucidated. This study focused on the GG-NER pathway, attempting to unravel the precise regulation of the chromatin environment, and uncover the factors involved in efficient NER. Of interest was how the NER machinery is able to access chromatin without initiating transcription.

In order to provide a tool for studying the NER mechanism in a chromatin complex, a plasmid has been constructed containing *MFA2* as a model gene. *MFA2* is an ideal gene with which to study repair in a chromatin environment, as its transcription is easily controlled. *MFA2* is an **a**-specific gene, producing a2 factor which is involved in the pheromone response pathway. In WT**a** haploid cells, *MFA2* is expressed, therefore the chromatin exists in an open, relaxed, state to allow transcription to take place. In WTα cells, however, the chromatin is repressed, and the gene is not transcribed. By simply studying the *MFA2* gene in the different mating types it is possible to look at the same gene in different chromatin environments. The gene is also an ideal size for studying, with the entire gene and upstream control sequences being able to be analysed on a single sequencing gel.

The regulation of *MFA2*, as with other **a**-specific genes, is well understood. Upstream of the *MFA2* initiation site is the P-box, an mcm1-binding site. This is flanked by two α2 binding sites. In **a**-cells mcm1 dimeric protein binds to the P-box to allow activation of transcription. In α -cells, however, α2 protein is produced, and this binds cooperatively with the mcm1 protein, resulting in repression of transcription. The repression is further brought about by the recruitment of the Tup1-Ssn6 general repressor complex, which stabilises nucleosomes across the promoter region via interactions with histone tails.

An inconvenience to understanding how GG-NER operates within the context of chromatin has been the absence of a suitable reporter system that will enable *in vivo* and *in vitro* analyses. The latter analyses will be essential to unravel the biochemistry behind how chromatin is metabolised to facilitate NER. Hence I have constructed a model plasmid based system to enable such approaches and report of its construction and employment *in vivo* to provide a basis for its use in future *in vitro* research.

Chapter 2

Materials and Methods

The methods described in this chapter relate to the storage and growth conditions of yeast strains, as well as the detailed techniques applied during this study. These include the UV treatment of cells, probe preparation and blotting techniques, as well as the high resolution DNA repair technology developed to study NER at the level of the nucleotide. Any additional materials and methods used are described in the relevant chapters pursuing.

2.1 Yeast Strains

The haploid yeast strains used in this study are:

PSY316 *(MATα ade2-101 ura 3-52 leu 2-3, 112 Δhis 3-200 lys2 trp1)*

Δtup1 (MATα ade2-101 ura 3-52 leu 2-3, 112 HIS::TUP1 lys2 trp1)

Δgcn5 (MATα ade2-101 ura 3-52 leu2-3, 112 Δhis 3-200 lys2 trp1)

Δrad16 (MATα ade2-101 URA::RAD16 leu2-3, 112 Δhis 3-200 lys2 trp1)

PSY316 *(MAT**a** ade2-101 ura 3-52 leu 2-3 112 Δhis 3-200 lys2 trp1)*

The PSY316 strains were obtained from Dr. Yumin Teng, Cardiff University, School of Medicine, Heath Park, Cardiff, UK.

2.2 Storage and growth conditions

All fore mentioned strains were grown and stored in Yeast Complete Medium (see Appendix I), or in synthetic complete media (see Appendix I), with Tryptophan drop-out supplement used for strains containing the TAM plasmid.

When long-term storage was required, cells were grown to exponential phase in the appropriate media, and frozen and kept at -70°C upon the addition of 30% glycerol. Pre-cultures were formed by inoculating strains into 10ml of appropriate media, and allowed to shake at 30°C, until at stationary phase. These pre-cultures could then be stored for short periods at 4°C until required. Large scale cultures such as those required for DNA repair experiments (200ml) were obtained by inoculating a pre-calculated amount of pre-culture overnight as to achieve a cell density of 2-4 x 10^7 cells/ml the following morning.

The yeast media, all glassware and implemented equipment for use in this study was autoclaved to sterilise where appropriate. All manipulations were carried out under the standard aseptic conditions.

2.3 Transformation

To incorporate the TAM plasmid construct into the various yeast strains, transformation was carried out employing a polyethene glycol-based method, to allow the incorporation of the plasmid into the cells. The transformation procedure is described below.

1) A single yeast colony was inoculated for overnight growth in 10ml YPD, shaking at 30°C
2) The following morning, the cells were diluted to achieve an OD_{600}0.1 in 50ml YPD, and allowed to grow to logarithmic phase (OD_{600} 0.5)
3) Cells were collected for 5 minutes at 3600 rpm in an Avanti centrifuge, washed with 1ml sterile water, then resuspended in 1ml Solution A (Appendix I)
4) The cells were then incubated in Solution A for 45-60 minutes at room temperature

5) Cells were collected for 3 minutes at 3600 rpm, and resuspended in 50µl Solution A per transformation point
6) The following transformation mix was prepared for each sample:
   1-5µl DNA to be transformed (dependant on concentration and size of DNA fragment)
   50µl of cells in Solution A
   5µl denatured Salmon sperm DNA
   300µl Solution B
7) The transformation mixture was incubated at room temperature on a turning wheel for 30 minutes, before heat shock treatment of cells at 42°C for 15 minutes, followed by placing on ice for 3 minutes
8) After heat shock 1ml sterile water was added, mixed gently by inversion, then cells were collected at 3600 rpm for 3 minutes
9) The cells were resuspended in 1ml YPD and left at room temperature to allow for recovery
10) On collection of the cells, and resuspension in 500µl sterile water, different amounts of the cell mixture were spread onto agar plates containing selection for the DNA transformed (Synthetic Complete medium lacking tryptophan for the TAM plasmid)
11) The plates were left at 30°C for 48 hours growth, and any colonies were screened for transformants

2.4 Analysis of UV sensitivity - Cell survival

UV-induced DNA damage can be repaired by the cell. However, if a mutation is present which may affect DNA repair processes, a particular yeast strain may show higher, or lower, sensitivity to UV light. The UV sensitivities of the strains used throughout this study were tested and compared by exposing samples to various doses of UV light and monitoring the survival of cells by counting the number of colonies after 3 days growth. For ease and accuracy, the cultures were diluted appropriately, to achieve about 200 colonies per plate. The details of the procedure were as follows:

1) YPD agar plates were prepared (see Appendix I) and labelled in advance. 10ml of cell cultures were grown overnight to give a density of $2\text{-}4\times10^7$ cells/ml. Serial dilutions were prepared according to the strain.
2) The diluted cell suspensions were mixed well using a vortex before pipetting 100µl onto the agar plates. Triplicates of each sample were prepared. Glass beads (diameter 3mm) were added to the plates and shaken laterally to spread the cells evenly across the surface of the agar. The plates were then turned upside down.
3) The 245nm UV lamp (VL-215G, Vilber Lourmat, France) was switched on 30 minutes in advance and calibrated. One plate at a time was then placed centrally under the UV lamp and treated at a dose rate of $10J/m^2{\cdot}s$. Usually, doses of 0, 10, 30, 50 and $100J/m^2$ were applied.
4) Following irradiation, the plates were immediately placed in darkness to avoid repair by photoreactivation and were incubated at 30°C for 3 days. The number of colonies on each plate was then counted and survival curves created to determine UV sensitivity.

2.5 The UV treatment of yeast cells

The UV spectrum is divided into three parts, UV-A (400 – 320nm), UV-B (320-290nm) and UV-C (290-100nm). The shorter the UV wavelength the greater the frequency and therefore energy it emits. Solar radiation consists mainly of UV-A and UV-B radiation since penetration of the ozone layer drops dramatically for wavelengths of radiation below 320nm. UV-C radiation is usually used for experimental studies, emitting radiation of a 254nm wavelength. Since this wavelength is close to the absorption maximum of DNA at about 260nm, UV-C induces damage such as CPDs more efficiently (Friedberg, *et al.*, 2005). As the UV irradiation of the cells is to be carried out in liquid PBS solution, care must be taken to ensure an even distribution of irradiation, which can be achieved by using a shallow dish, and maintaining a swirling action.

In order to induce DNA damage, yeast cells were exposed to UV irradiation prior to DNA extraction. This protocol was adjusted from (Teng et al. 1997). Cell cultures were grown to exponential phase as described in section 2.2, resuspended in

chilled phosphate buffered saline (1 x PBS, see Appendix I), and adjusted with PBS to achieve a cellular concentration of 2 x 10^7 cells/ml. A sample of untreated cells was always taken as an untreated control. Having switched the UV lamp on 30 minutes prior to use to ensure that the UV dose was stable, 50ml aliquots were then irradiated with 254nm UV light at a dose of 100J/m^2. A UV treated sample was taken immediately to measure the damage induced and the remaining cells subsequently stored on ice in the dark to prevent repair by photoreactivation. After resuspending the treated cells in appropriate media, the cells were allowed to repair for various time intervals at 30°C in a shaking incubator. At each repair time, a sample was collected by centrifugation at 4°C using a Beckman Avanti J-25 centrifuge. All samples were kept in the dark until DNA could be extracted. The protocol for UV irradiation of yeast cells is as follows:

1) Yeast cells from an overnight culture were counted to ensure a density of 2-4 x 10^7 cells/ml. The cells could then be collected by centrifugation using a Beckman Avanti J-25 centrifuge, JA-10 rotor, at 4000rpm for 5 minutes.
2) Cells were washed and resuspended in chilled PBS. The addition of 1ml of 0.5M EDTA aided in separating cells, and brief sonication was applied to ensure a homogenous cell suspension. PBS was then used to adjust the cell density to 2 x 10^7 cells/ml.
3) A 30ml sample was taken from the cell suspension to use as an untreated (U) control. This was kept on ice in the dark.
4) A 50ml batch of the cells was placed in a 14cm diameter Pyrex dish, with the cells achieving a depth of approximately 3mm. These cells were then irradiated under a calibrated (UVP Inc., CA, USA) VL-215G lamp (Vilber Lourmat, France) for 10 seconds at a dose rate of 10 J/m^2.s. Throughout the irradiation process, the dish was gently swirled to ensure an even UV dose to all cells. This irradiation step was repeated with additional 50ml batches of cells until the required amount of cells was achieved. All UV treated batches were pooled together into a sterile container on ice, and kept in the dark.
5) After UV irradiation, a 30ml sample was collected immediately for zero repair time (0).
6) The remaining treated cells were collected by centrifugation and resupended in the same volume of appropriate media, and allowed to repair at 30°C with

shaking in the dark. A sample was taken at each repair time (0.5, 1, 2, 4 hours).

7) All samples were collected by centrifugation, resuspended in chilled PBS once more, and kept on ice in the dark.

2.6 Preparation of yeast DNA

In order to extract yeast DNA, zymolyase solution was used first to create spheroplasts, which could then be lysed by the addition of lysis buffer containing sodium dodecyl sulphate (SDS) (see Appendix I). RNA and protein were then digested using DNase-free RNase A and Pronase respectively, with the DNA being extracted following phenol/chloroform extractions and ethanol precipitation. The full extraction procedure is as follows:

1) Cells in PBS were collected by centrifugation, and washed in 5ml of Sorbitol-TE solution (Appendix I)
2) Cells were resuspended in 1ml per sample of freshly prepared zymolyase 20T (10mg/ml in sorbitol-TE solution, ICN Biochemicals, Inc.) containing 8µl of 0.28M β-mercaptoethanol (Sigma), and left to incubate at 4°C in the dark overnight. The production of spheroplasts can be monitored under the microscope. For an additional check, small tester samples were added to sorbitol-TE solution, which resulted in a cloudy solution. If SDS was also added, the solution turned clear.
3) Spheroplasts were gently centrifuged at 3000rpm for 5 minutes and pellets resuspended in 1ml lysis buffer/PBS 1:1 (v/v) solution. 100µl of DNase-free RNase A (10mg/ml in TE buffer, incubated at 95°C for 10 min, Sigma) was added to each sample, mixed well and incubated at 37°C for 1 hour with occasional agitation.
4) Following RNase A treatment, 60µl Pronase (20mg/ml in TE buffer, Sigma) was added to each sample, and incubated at 37°C for 1 hour, followed by 65°C for a further hour, with occasional agitation.
5) An equal volume (approximately 1ml) of phenol:chloroform:isoamyl alcohol (25:24:1 in volume, Sigma) was added. The tubes were shaken vigorously and then centrifuged at 10000 rpm for 10 minutes. The aqueous upper phase

containing the nucleic acids was then transferred to a fresh polypropylene tube, with care taken not to disturb the interface.

6) To ensure complete deproteinisation, a second extraction with phenol/chloroform and a third with chloroform:isoamyl alcohol (24:1 in volume, Sigma) was performed as the first extraction. No protein precipitate at the interface between layers was the sign of complete deproteinisation. Finally, the aqueous phase was transferred to a fresh tube.
7) DNA precipitation was carried out by adding 2 volumes (2ml) of pre-chilled 100% ethanol to each sample with gentle shaking. The samples were kept at -20°C overnight in order to precipitate the DNA.
8) DNA pellets were collected by centrifugation at 5000 rpm for 10 minutes. The pellets were resuspended in 1ml TE buffer. 1 volume of chilled isopropanol (-20°C) was added for a second DNA precipitation, with gentle shaking. The samples were left at room temperature for 30 minutes, followed by centrifugation to collect the DNA pellet. When thoroughly dried the DNA was resuspended in 500µl TE buffer.
9) The quality of the DNA could be checked by running a non-denaturing agarose gel (Section 2.7.1), with clean DNA samples displaying a sharp band when run on an agarose gel stained with ethidium bromide (EtBr), and viewed using a UV transilluminator.
10) The DNA samples could be stored at 4°C if to be used immediately, or -20°C for longer term storage.

2.7 DNA electrophoresis

2.7.1 Non-denaturing gel electrophoresis

The quality of yeast DNA obtained from extraction was determined by electrophoresis on a non-denaturing 1% agarose gel which was subsequently viewed under a UV transilluminator. The presence of sharp, bright bands indicated clean genomic DNA samples.

1) 5µl of each DNA sample was mixed with 5µl of H_2O and 5µl of non-denaturing loading buffer (see Appendix I).

2) Samples were loaded onto a 1% (gram/ml) agarose gel which was prepared in 1×TAE buffer (see Appendix I) and contained EtBr (0.1µl/ml, Sigma). Gels were electrophoresed under 1×TAE at 70-90V for 30-60 minutes.
3) Gels were viewed under a UV transilluminator. Genomic DNA runs as a discrete high molecular weight band, hence sharp bright bands are visible.

Non-denaturing gel electrophoresis was also employed for the analysis of other DNA fragments, such as size determination of PCR products (see Chapter 3) and of sheared DNA following sonication (see Chapter 5).

2.7.2 Denaturing gel electrophoresis

Within this project, denaturing gel electrophoresis could be used to visualise DNA repair at a global level. Briefly, cells were treated with UV and allowed to repair for various time points, before extraction of total DNA (as in Sections 2.4 and 2.5). UV-treated genomic DNA preparations were subjected to digestion with *Micrococcus luteus* (ML) endonuclease, a CPD-specific endonuclease which cuts DNA specifically at CPD sites. These digested samples could then be run directly onto a denaturing gel, with DNA repair represented by the recovery of high molecular weight genomic bands, with repair time.

1) A denaturing gel mixture (2.25g agarose, 146ml H_2O, 3.7ml 2M NaCL, 300µl 0.5M EDTA) was heated using a microwave until the mixture was molten. The gel is allowed to cool to ~50°C, before pouring the mixture into a gel mould, and inserting a multi-well comb. The gel was allowed to set for 1 hour.
2) The gel was soaked in denaturing running buffer (986ml H_2O, 2ml 0.5M EDTA, 12ml 3M NaOH) for 30 minutes to equilibrate
3) The samples could then be applied to the wells and the gel run at 20V overnight to ensure separation of bands
4) When the electrophoresis was complete, the gel was then neutralised by soaking in 1M Tris-HCl, pH 7.5, 1.5M NaCl for 30 minutes
5) The gel can then be stained using EtBr, and viewed in a UV transilluminator.

2.8 Southern blotting

In order to visualise the presence and quantity of a specific DNA sequence within yeast cells, firstly a glass bead mediated rapid DNA preparation was carried out to obtain cellular DNA. This was then subject to digestion using a specific restriction endonuclease to obtain a DNA fragment of a defined size. The DNA samples could then be resolved on a 1.2% non-denaturing agarose gel, and subsequently blotted onto a hybond membrane. The specific DNA sequence of interest could be detected via hybridisation of a radiolabelled DNA probe (see section 2.10) to the membrane, and visualised using a phosphoimaging screen and Typhoon scanner system.

A Southern blotting technique is also employed for the low resolution detection of positioned nucleosomes, detailed in section 2.12.

2.8.1 Rapid glass beads DNA preparation

1) Yeast cells were grown overnight in 10ml of appropriate media. The following morning, cells were collected via centrifugation, and the cell pellet was washed with 0.5ml sterile water
2) The pellet was resuspended in 200µl of Beads lysis solution (Appendix I), to which 200µl of phenol/chloroform 1:1 (v/v), and 0.3g glass beads (acid washed, Sigma) were added. The mixture was then subject to a vigorous vortex for 4 minutes.
3) 200µl 1 x TE buffer was added to the mixture, mixed, then centrifuged for 5 minutes at 10000 rpm
4) The upper aqueous layer was transferred to a fresh eppendorf, taking care not to disturb the interface. 1ml of chilled 100% ethanol was then added to the new tube, mixed by inversion and allowed to precipitate at -20°C for at least 1 hour.
5) The samples were spun for 10 minutes as above, and the supernatant discarded. The pellet was resuspended in 0.4ml TE buffer and 1µl RNase A

(10mg/ml) added. The sample was incubated for 15 minutes at room temperature

6) DNA was obtained using a phenol/chloroform extraction, followed by precipitation involving the addition of 40µl 3M NaAc and 1ml chilled isopropanol, placed at -20°C for at least 1 hour.
7) After centrifugation and removal of the supernatant, the pellets were allowed to dry, and then resuspended in 50µl TE buffer.

2.8.2 DNA transfer

DNA samples may need to be treated with an appropriate restriction enzyme to generate fragments of interest, before resolving on a non-denaturing gel. The molecular weight-distributed bands can then be transferred to a membrane via Southern blotting, to provide a substrate which can be subject to hybridisation with a radiolabelled probe. The Southern blotting and hybridisation stages are described below.

1) After resolving the samples on a 1.2% non-denaturing agarose gel at 70V for 1.5 hours, the gel was rinsed in 0.4M NaOH for 20 minutes with gentle shaking. The Southern blotting platform was then constructed, placing filter paper, pre-soaked in 0.4M NaOH on the platform, followed by the gel, top-side down. A Hybond-xl (Perkin Elmer) membrane was cut slightly smaller than the region of interest on the gel, soaked in 0.4 M NaOH, and placed on top of the gel, ensuring no air bubbles.
2) Addition of soaked filter paper on top of the membrane, followed by further dry filter paper, absorbent tissue and an evenly distributed weight ensured that on addition of 0.4 M NaOH to the tank the capillary chromatography process could begin. The blotting process was allowed to proceed overnight (Figure 2.1).

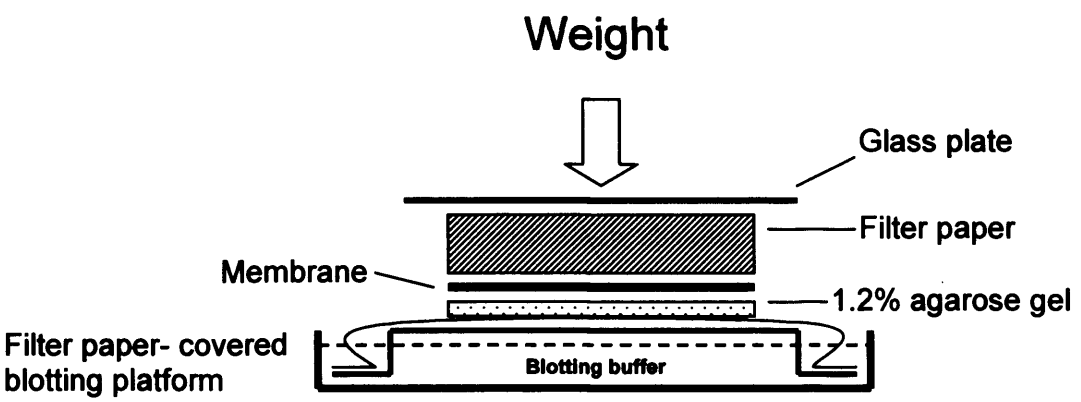

Figure 2.1: The standard blotting apparatus. For both Southern and Northern blotting techniques, the samples are loaded, and run in a 1.2% agarose gel, which is rinsed in appropriate buffer, and placed upside down on the blotting platform. A soaked transfer membrane is placed directly onto the gel, ensuring no air bubbles. Filter paper and absorbent tissue can be placed on top, followed by an evenly distributed weight. The tank is filled with appropriate blotting buffer (0.4M NaOH for Southerns, 10 x SSC for Northerns), and the chromatography process is able to take place, transferring the DNA (or RNA in the case of Northern blotting) onto the membrane.

2.8.3 Hybridisation

1) The southern blotting was stopped, and the membrane carefully removed (cutting one corner for orientation). The membrane was rinsed in 0.1 x SSC, then put under low power UV light (UV-A) for 2 minutes to allow cross-linking between the DNA and the membrane
2) The membrane was gently rolled up and inserted into a hybridisation tube, with the stained side facing inwards. 10ml Dextran hybridisation buffer (Appendix I) was added into the tube, for pre-hybridisation to proceed in the 65°C oven with rotation for at least 15 minutes. This pre-hybridisation was repeated with fresh buffer, and the procedure allowed to continue for at least a further 15 minutes.
3) A strand-specific radiolabelled probe was then constructed, as in Section 2.10, which can be added into the hybridisation chamber along with the remainder of the hybridisation buffer. The probe was left to hybridise to the membrane overnight, in the 65°C hybridisation chamber with rotation.

2.8.4 Phosphoimaging and scanning

1) After hybridisation, the membrane was rinsed twice with 10ml of southern washing buffer (2 x SSC, 1% SDS) in the rotating hybridisation tube, followed by a rinse in 0.1 x SSC in a tray with gentle shaking.
2) The membrane could was then wrapped in clingfilm wrap, and placed in a folder with a phosphorscreen for a couple of hours or overnight.
3) The phosphor screen was scanned using the Typoon phosphoimager (Storm 860, Molecular Dynamics, Inc.) to acquire the image, and visualised using Imagequant software (Molecular Dynamics, Inc.).

2.9 Analysis of gene expression

To detect mRNA levels within yeast cells, northern blot analysis was carried out. This procedure is in essence similar to that of Southern blotting, only involving the transfer of RNA opposed to DNA. This procedure involves the isolation of clean RNA from cells via an SDS and hot phenol method, which specifically allows extraction of single stranded molecules. When working with RNA, standard advised precautions were taken and all glassware and equipment was autoclaved twice to eliminate RNAse. This procedure is detailed below:

2.9.1 Extraction of total yeast RNA

1) 10ml of YPD medium was inoculated and grown overnight at 30°C on a shaking platform, to a density of $2\text{-}4\times10^7$cells/ml. The cells were collected by centrifugation at 3500rpm for 5 minutes and washed with 0.5ml of sterile H_2O.
2) The cells were transferred to a 1.5ml Eppendorf. 0.5ml of RNA lysis buffer (see Appendix I), and an equal volume of equilibrated phenol (pH 4.3±0.2, Sigma) were added and mixed well by vortex.
3) The mixture was transferred to 65°C to incubate for 1 hour with occasional vortex. Following this, the samples were immediately placed on ice for 10

minutes, then 1/10th volume of 3M NaAc was added to maintain the correct pH conditions, and the sample was centrifuged for 10 minutes at 10000 rpm

4) The upper layer was collected, and transferred to a new Eppendorf. The samples was then subjected to two phenol:chloroform:isoamyl alcohol (25:24:1 in volume, Sigma) extractions, followed by one extraction with chloroform:isoamyl alcohol (24:1) as described previously.
5) The RNA could then be precipitated with 2.5 volumes of chilled 100% ethanol at -20°C, overnight.
6) The samples were collected via centrifugation, allowed to dry and resuspended in 50µl sterile H_2O.

2.9.2 Northern blotting technique

The transfer of RNA involves the northern blotting technique. Extracted RNA is first separated using formaldehyde-agarose (FA) gel electrophoresis, and then transferred to a membrane. This was subsequently hybridised with a radioactively labelled probe, which could then be scanned and analysed.

2.9.2.1 Formaldeyde-agarose (FA) gel electrophoresis

1) To prepare the gel, 1.8g agarose was melted in 15ml 10 x FA buffer (see Appendix I) and 150ml RNase-free H_2O. This was cooled to 65°C before adding 2.7ml formaldehyde (Sigma) and 2µl EtBr. The solution was mixed thoroughly before pouring.
2) The gel was poured into a gel mould (Bio-Rad), and a multi-tooth comb inserted to create wells for loading. The gel was allowed to cool and set in the mould for 45 minutes before adding 1 x FA running buffer to equilibriate for a further 45 minutes.
3) 10µl of 5×RNA loading buffer (see Appendix I) was added to each RNA sample before carefully loading into the wells. (For subsequent gels, the loading was adjusted based on quantification of the initial gel, or RNA amount checked using a Nanodrop spectrophotometer (Thermo Scientific), to equalise the amount of RNA in each sample). The gel was then run at 50-60V for 3-4 hours, or until the dye visibly reached the centre of the gel.

4) The gel was rinsed three times in distilled H_2O and viewed under a UV transilluminator to visualise the characteristic bands of RNA.

2.9.2.2 Northern blotting, detection and analysis of RNA

1) The gel was soaked in 0.1 x SSC, and applied to the blotting platform (as for Southern blotting). A pre-soaked membrane, filter paper, absorbant tissue paper and a weight were applied, using 10 x SSC as a transfer buffer. The blotting was left overnight to proceed (Figure 2.1).

2) Following blotting, the membrane was placed under a UV transilluminator (UV-A) for 2 minutes to fix the RNA

3) Radioactively labelled probes were prepared as described in Section 2.10, using the appropriate PCR products and primers. Two probes were created, one to bind to transcribed fragments (thus detecting mRNA levels) of the gene of interest (*MFA2)* and another to detect mRNA levels of a known control gene (*ACT1).*

4) RNA was hybridised with the first probe as described in Section 2.8.3, using Dextran hybridisation buffer, overnight.

5) The membrane was wrapped in Clingfilm and placed into a cassette against a phosphorimager screen (Molecular Dynamics, Inc.). Exposure was allowed overnight at room temperature. The image was then generated by scanning the screen using a phosphorimager scanner (Storm 860, Molecular Dynamics, Inc.). Finally, mRNA levels were quantified using ImageQuant software (Molecular Dynamics, Inc.).

6) After hybridisation with one probe, the membrane was boiled twice with stripping solution (0.1×SSC, 1% SDS) for 20 minutes to strip the probe from the membrane. The hybridisation process was then repeated with the second probe. Thus mRNA levels of both the gene of interest and the control gene were detected and compared using the same membrane.

2.10 Preparation of strand-specific radiolabelled probes

The probes used in this study were designed to detect separately the transcribed strand (TS) and non-transcribed strand (NTS) of the *MFA2* fragment of interest. The technique uses 5' biotinylated primers and Dynabeads to purify single stranded DNA. Dynabeads are coated with streptavidin which binds tightly to biotin. In turn, the Dynabead-biotin complex can be isolated from the remainder of a mixture using a magnetic particle concentrator (MPC) which collects the beads against the side of an Eppendorf by creating a magnetic field (Figure 2.2).

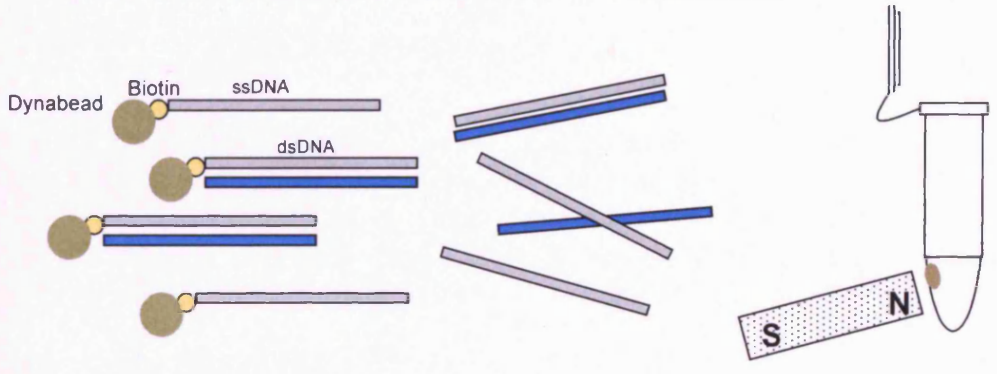

Figure 2.2: Dynabeads are coated in Streptavidin, which binds specifically to Biotin. By incorporating a biotin tag at the 5' of DNA primers, biotin labelled dsDNA fragments can be collected by the binding to the Dynabeads. The dynabead-biotin-DNA can then be collected at the side of an Eppendorf using a Magnetic particle concentrator (MPC) which creates a magnetic field.

The main steps of the probe synthesis procedure are outlined below and illustrated in Figure 2.3.

1) The DNA sequence of interest was downloaded from the *Saccharomyces cerevisiae* Genome Database (SGD^{TM}). Primers were designed using Oligo software (Version 3.4 MedProbe, Normay), one of which was biotinylated, the other unbiotinylated (Eurofins MWG Operon).

2) The DNA sequence was amplified by PCR, the conditions of which were optimized to obtain the best quality PCR product. Genomic DNA was used as

a template, and the resulting PCR products were then checked on a 1% agarose gel to ensure good quality.

3) The double-stranded PCR products were isolated using Dynabeads and a MPC, then denatured by incubation with 0.1M NaOH.

4) The biotinylated and unbiotinylated strands were separated by collecting the Dynabeads (bound to the biotinylated strand) using the MPC and using a pipette to remove the supernatant containing the unbiotinylated strand.

5) The probe was synthesised upon the biotinylated single stranded DNA template by primer extension using Sequenase Version 2.0 T7 DNA Polymerase (Amersham Pharmacia Biotech) and a α-[^{32}P] dATP (6000 Ci/mmol, Perkin Elmer) spiked dNTP mixture. The mixture was heated at a denaturing temperature and immediately placed in the MPC so that the [^{32}P] incorporated probe could be collected with a pipette as a supernatant.

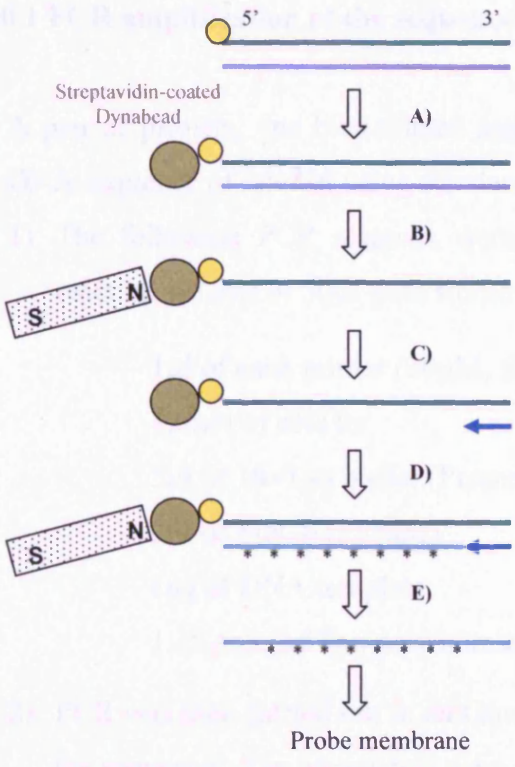

A) Biotin (●) labelled dsDNA is allowed to bind to Streptavidin-coated Dynabeads

B) dsDNA is denatured, and the biotin/bead-bound strand is collected using a magnet

C) Allow primer to bind 3' end of DNA

D) Primer-directed sequencing reaction using [^{32}P]dATPs

E) Denature strands, collect biotin/bead-labelled strand using magnet, and use supernatant containing radio-labelled probe to detect specific sequence on membrane

Figure 2.3: PCR directed amplification of a dsDNA fragment of choice is carried out, with primers designed to incorporate a biotin label at the 5' end of one strand. This dsDNA fragment should be between 300-500bp long for maximum efficiency. The addition of biotin allows a means of separation via Streptavidin coated Dynabeads. (B) On denaturing the dsDNA, and using a magnetic particle collector (MPC), the Dynabead and bound biotin labelled strand can be purified. This strand is then used for a sequencing reaction using a primer against the 3' end and radiolabelled dATPs (D). This results in a complementary strand of DNA interdispersed with radioactive dATPs. These strands were then denatured as previous and separated once again using the MPC (E). The supernatant was collected containing the radioactive probe against the DNA sequence (and strand) of interest, and this was used to probe a membrane.

For Southern blotting techniques, the probe was made against either the transcribed (TS) or non-transcribed strand (NTS) of DNA. For use in Northern blotting, the biotin label was added to the 5' end of the NTS, resulting in a TS probe to detect the NTS sequence (mRNA).

2.10.1 PCR amplification of the sequence of interest

A pair of primers, one biotinylated and one unbiotinylated, was used to amplify the DNA sequence of interest using standard PCR reactions.

1) The following PCR reagents were mixed together and made up to a total reaction volume of 50µl with sterile H_2O.

   1µl of each primer (20µM, for sequence see individual chapters)
   1µmol of dNTPs
   5µl of 10×Taq buffer (Promega)
   3µl of $MgCl_2$ (25 mM)
   1ng of DNA template
   1.25 units of Taq polymerase (Promega)

2) PCR was then carried out in an OmniGene thermal cycler (Hybaid) to amplify the sequence. The parameters were programmed as:

   First denaturation: 2 min at 95°C

   30 cycles of: Denaturation: 30 seconds at 95°C

   Annealing: 30 seconds at 57°C

   Extension: 20-30 seconds at 72°C

   Samples left for 4 mins at 72°C to complete the DNA synthesis

The quality of the PCR products obtained was then checked by loading 3µl onto a 1% agarose gel (as described in section 2.6).

2.10.2 Preparation of the radiolabelled probe

1) Take 30µl of Dynabeads solution, and use an MPC to collect the beads. Wash twice in H_2O, followed by 2 washes in 1 x BW (see Appendix I).
2) 50µl 2 x BW buffer was used to wash the beads, which were then resuspended in 10µl 2 x BW. 5µl of the relevant PCR product (see Section 2.10.1), which has a biotin tagged end was then added to the beads and incubated at room

temperature for 10 minutes, with an occasional mix. During the incubation, the Dynabeads bound to the PCR product via the biotin tag.

3) An MPC was used to collect the beads, and the supernatant was discarded. The beads were washed twice with 50µl H_2O, resuspended in 40µl 0.1M NaOH to denature DNA strands and incubated at room temperature for 10 minutes with occasional mixing. The biotinylated strand associated with the beads was kept on the Eppendorf wall using a MPC, and the supernatant containing the other strand was discarded.
4) The beads were washed with 50µl of H_2O, follow by a wash in 1 x BW. The beads were then resuspended in 20µl of 1 x BW buffer.
5) 2µl of the appropriate non-biotinylated primer (10µM) was added to the beads, mixed well and left to incubate in a small 65°C water bath, which was allowed to cool naturally, for at least 30 minutes. This step allowed the binding of the primer to the Dynabead-bound ssDNA strand.
6) The beads were then collected with an MPC, washed twice with 50µl H_2O, and resuspended in 16µl H_2O. The following components were then added for the sequencing reaction, and mixed well:

    8µl reaction buffer
    6µl dilution buffer
    4µl 5 x dATP buffer (0.1mM dTTP,dGTP,dCTP)
    2.8µl 0.1M DTT
    1µl T7 polymerase

7) 2µl α-[^{32}P] dATP was then added, and gently mixed using a 50µl pipette.
8) The mixture was incubated at 37°C for 10 minutes. The beads and associated dsDNA fragment were collected using the MPC and the supernatant was discarded.
9) Following a wash with sterile H_2O, the supernatant was discarded. The beads were resuspended in 20µl 0.1M NaOH and incubated at 37°C for at least 10 minutes to denature the dsDNA, releasing the radiolabelled ssDNA probe into the supernatant.
10) The supernatant could was then collected using the MPC, and the probe used for hybridisation with the membrane as described in Section 2.8.3.

2.11 Examining DNA repair at nucleotide resolution

To study DNA repair of UV-induced damage, an end-labelling technique described by (Teng et al. 1997) was utilised to examine and quantify CPDs at a specific nucleotide position. This technique again involved the application of specifically designed probes and Dynabead technology, and is outlined below and in Figure 2.4.

1) Genomic DNA was digested with appropriate restriction endonucleases.
2) The obtained fragment of interest was then cut at the sites of CPDs by a CPD-specific endonuclease (ML *endo*) (Y Teng) and the DNA was denatured to obtain the resulting ssDNA fragments of varying lengths.
3) A specifically designed probe was used to isolate the ssDNA fragments and also provide a template for end-labelling. The probe was complementary to the 3' end of the DNA sequence of interest and biotinylated at its 5' end. A short oligonucleotide was inserted between the complementary sequence and the 5' biotinylated end. This consisted of a six dT overhang adjacent to the complementary sequence, to provide a template to incorporate radioactive dATPs into the isolated ssDNA fragments, and six random nucleotides between the dTs and the 5' biotinylated end which eliminated any steric hindrance from the Dynabeads while radioactive dATPs were incorporated.
4) The radioactively labelled ssDNA fragments were then separated using denaturing polyacrylamide gel electrophoresis.

Finally, the gel was scanned and the resulting image quantified using ImageQuant software (Molecular Dynamics, Inc.).

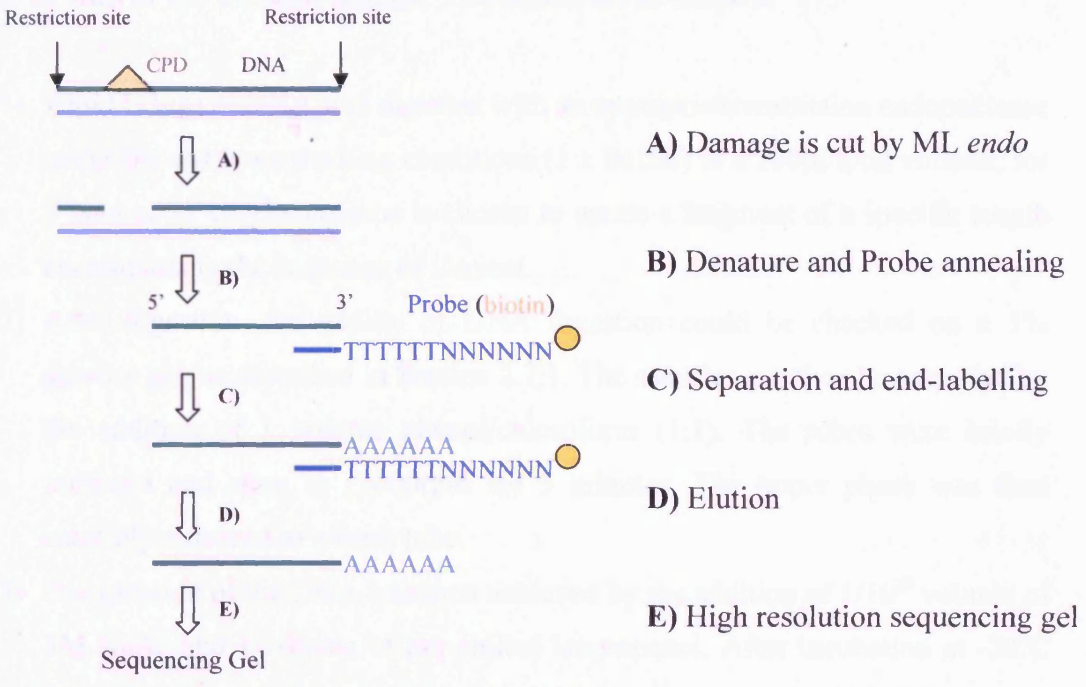

Figure 2.4: Schematic of the end-labelling procedure for detecting DNA damage and repair on high resolution sequencing gels, figure adapted from (Teng et al. 2005). **A)** After DNA extraction the *MFA2* region of interest could be obtained by cutting with the *Hae*III restriction endonuclease. The UV-induced CPD damage can then be cut with *Micrococcus Luteus* CPD-specific endonuclease. **B)** A probe specific for the 3' end of one strand of the restriction fragment is then allowed to anneal to the fragment. The probe has been designed to incorporate a region complementary to the 3'end, as well as a TTTTTT overhang, a buffer sequence and a biotin label at the 5' end. **C)** This probe and complementary fragment were separated via streptavidin coated Dynabeads and the use of a magnet. The purified fragments were then end-labelled with the incorporation of 6 [^{32}P]dATPs using the 6T overhang as a template. **D)** This labelled strand was eluted from the biotin strand again using Dynabeads, and subjected to electrophoresis on a polyacrylamide sequencing gel (**E**).

2.11.1 DNA digestion with restriction and CPD-specific enzymes

Yeast DNA samples are digested with an appropriate restriction enzyme, and DNA extracted and precipitated. Restriction endonucleases were used to obtain a fragment containing a particular *MFA2* sequence of interest. The *Hae*III restriction enzyme was chosen, which cuts at positions -517 and +83 (where +1 denotes the start codon ATG of *MFA2*), yielding a 600bp fragment containing the *MFA2* promoter

region. Following this, the DNA is cut with the CPD-specific endonuclease to cut the DNA at sites of UV-induced damage. The details are as follows:

1) 20µl (1-3µg) of DNA was digested with an appropriate restriction endonuclease under the enzymes working conditions (1 x buffer) in a 100µl total volume, for 1 hour at 37°C. The enzyme is chosen to create a fragment of a specific length encompassing the sequence of interest.
2) After digestion, the quality of DNA digestion could be checked on a 1% agarose gel, as described in Section 2.7.1. The samples can then be extracted by the addition of 1 volume phenol/chloroform (1:1). The tubes were briefly vortexed and spun at 12000rpm for 5 minutes. The upper phase was then carefully removed to a fresh tube.
3) Precipitation of the DNA was then achieved by the addition of $1/10^{th}$ volume of 3M NaAc and 1 volume of pre-chilled isopropanol. After incubation at -20°C for 2 hours, the samples can be collected by centrifugation at 12000rpm for 10 minutes, and dried thoroughly.
4) The DNA pellets were resuspended in 110µl 1 x TE buffer. 10µl of CPD-specific *ML endo* was then added to cut the DNA fragments at CPD sites, at 37°C for 1 hour.
5) Phenol/chloroform and chloroform extractions were again performed as described previously and the samples were transferred to 0.5ml Eppendorfs.

2.11.2 Purification of CPD-incised single stranded DNA fragments

Isolation of single-stranded DNA fragments was achieved using streptavidin-coated Dynabeads.

1) 30µl of 5M NaCl was added to the above 120µl DNA solution, resulting in a final sodium concentration of 1M (for optimal Dynabead-biotin binding)
2) 1µl of biotinylated probe (2µM) complementary to the 3' end of the TS was added and vortexed briefly to mix. After a brief spinning, samples were incubated at 95°C for 5 minutes to denature the DNA. This was followed by incubation at 55°C for 15 minutes to enable the primer to anneal to the DNA fragments.

3) 10µl of Dynabeads per sample were washed twice in 1 x BW buffer (see Appendix I), then resuspended in 1 volume 1 x BW buffer. 10µl of Dynabeads were added to each sample to bind the 5' biotin at room temperature for 10 minutes with occasional mixing by pipette. The beads were collected by placing the tubes in an MPC for at least 30 seconds (the supernatant can be removed to another tube for analysis of the NTS at a later date). The Dynabeads associated with *MFA2* fragments were resuspended in 50µl of 1 x BW buffer
4) 50µl of bead suspension in 1 x BW buffer was incubated at 57°C for 5 minutes to decrease non-specific annealing of fragments other than *MFA2*. The beads were collected with an MPC and the supernatant was discarded. Two washes were carried out with 60µl of water, and care was taken to remove all of the liquid before resuspending the beads in 4.3µl water
5) For the isolation of the NTS, steps 2-4 were repeated but using a different probe, complementary to the 3' end of the NTS; and incubation at 55°C for 15 minutes for annealing.

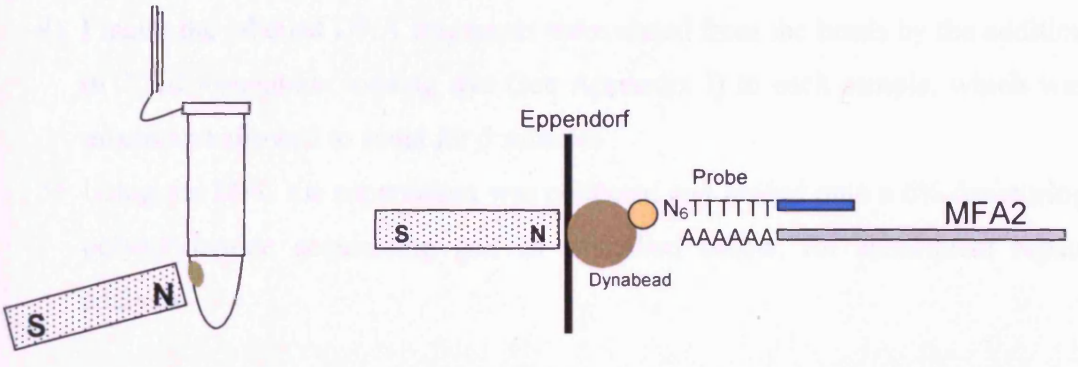

Figure 2.5: Specifically designed primers incorporating an overhang of a hexadT, then a 5' biotin-hexadN with no 3' dT, are annealed to *MFA2* restriction fragments. These *MFA2* bead-bound fragments can then be radiolabelled with exactly 6 α-[^{32}P] dATP molecules using DNA polymerase. These labelled fragments are eluted from the beads and resolved on a DNA sequencing gel.

2.11.3 End-labelling the fragments with α-[32P] dATP

All work involving the use of radio-labelled nucleotides was carried out in a radioactive laboratory, under appropriate conditions. Deoxyadenosine 5'-triphosphate α-[^{32}P] dATP (Perkin Elmer) was used to end-label the DNA fragments with radio-labelled dATPs.

1) A labelling master mix was made as follows:

	X 10	X 14
Reaction buffer	24μl	28μl
Dilution buffer	24μl	28μl
DTT	8.4μl	9.8μl
α-[^{32}P] dATP	2μl + 10μl H_2O	3μl + 9μl H_2O
Sequenase	1μl	1μl

2) 5.7μl of master mix was added to each sample, mixed well, and the reaction was allowed to proceed for 10 minutes at 37°C
3) The beads were collected using the MPC, and washed with 40μl water
4) Finally the labelled DNA fragments were eluted from the beads by the addition of 2.5μl formamide loading dye (see Appendix I) to each sample, which was mixed and allowed to stand for 5 minutes
5) Using the MPC the supernatant was collected and loaded onto a 6% denaturing polyacrylamide sequencing gel, as described below, for subsequent repair analysis

2.11.4 Denaturing polyacrylamide gel electrophoresis

A 0.4 mm thick denaturing polyacrylamide gel was used in this study to resolve the single stranded DNA fragments.

1) To create the gel, two glass plates measuring 20cm × 60cm and 20cm × 62cm were used to construct a mould. The plates were washed thoroughly with detergent and water and then washed using absolute ethanol. Dimethyldichlorosilane solution (2% in 1,1,1-trichloroethane, BDH

Chemicals) was applied to the inner surface of the shorter plate to later enable easy separation of the gel from the glass plates following electrophoresis. The plates were separated at the edges with 0.4 mm thick spacers and firmly sealed with vinyl insulation tape.

2) 75ml of 6% acrylamide gel (19:1 acrylamide:bis-acrylamide, 7M urea, 1×TBE, Severn Biotech Ltd.) was mixed with 600µl of 10% APS and 50µl of TEMED in a small conical flask.

3) The solution was slowly poured into the gel mould, taking care to avoid any bubbles that might form in the gel. A comb was immediately inserted into the top of the gel to create the loading wells, and the gel was left to set for at least 1 hour.

4) A GIBCO electrophoresis system (Model SA) and a Pharmacia power pack (EPS 3500) were used to run each sequencing gel. To achieve the optimum temperature of the gel for electrophoresis to separate the ssDNA, 50°C, it was pre-run in 1×TBE buffer for 30 minutes at an output of 70W.

5) 2.5µl of loading buffer (see Appendix I) was added to the DNA samples and they were carefully loaded into the gel. Electrophoresis was carried out for 2 hours at an output of 70W.

6) The glass plates were then separated carefully so that the gel was only stuck to one plate and a piece of Whatman filter paper, previously cut to size, was placed on top of the gel to allow a close attachment to it. The supporting paper and gel were cautiously peeled from the glass plate and a piece of Clingfilm carefully placed on top of the gel. The gel was dried using a BioRad gel dryer for two hours under vacuum at 80 °C.

7) Once dried, the gel was exposed to a phosphorimager screen in a cassette and left overnight. The screen was then scanned with a phosphorimager screen scanner (Storm 860, Molecular Dynamics, Inc.) to obtain the resulting image, which was then quantified as described below.

2.11.5 Quantification and repair analysis

Quantification of the repair at specific CPDs was carried out using ImageQuant software version 5.0 (Molecular Dynamics Inc.).

1) The intensity of each band reflected the frequency of DNA damage at a specific site and was measured as collective pixel values. To account for any slight variation in the loading of DNA samples in each lane, which may have clouded true repair effects, an adjustment was made as the total signal from individual lanes was multiplied by a factor to give equal values, and then the signal of each band was accordingly multiplied.

2) The value from the non-irradiated DNA sample was subtracted as non-specific background. The damage remaining after particular repair times was presented as a percentile with respect to the initial damage (0 lane, 100% damage).

$$\% \text{ Damage} = \frac{[\text{Damage}]_t}{[\text{Damage}]_0} \times 100$$

(where t = a given repair time, 0 = the starting time point of repair)

3) To generate repair curves, data points representing the percentage of damage at defined sites at each repair time were applied to an exponential curve.

4) Finally the time point where 50% of the damage was removed ($T_{50\%}$ value), was calculated to compare repair rates of individual CPDs.

2.12 Nucleosome mapping techniques

The mapping of nucleosomes in the various yeast strains was carried out at both low and high resolution. These techniques utilised the enzyme MNase (Micrococcal nuclease, nuclease S7, Roche), which preferentially cuts the linker DNA between nucleosomes. Regions protected from MNase digestion of 140-200bp are interpreted as positioned nucleosomes (Thoma 1996).

2.12.1 Preparation of yeast chromatin and treatment with MNase

1) Cells were inoculated into 1L of appropriate media, and grown overnight to achieve a cell density of 1-2 x 10^{10} cell/ml. The cells were collected by centrifugation at 4000rpm for 5 minutes, washed in cold water, and then in cold 1M sorbitol. After tipping of the washing solution, the wet cells were weighed.
2) Cell pellets were resuspended in 5ml lysis solution (1M sorbitol, 5mM 2-mercaptoethanol) containing 25mg zymolyase per 1g cells. Incubation was carried out at 30°C for 20 minutes with slight agitation.
3) The presence of spheroplasts was checked via microscopy, and spheroplasts were collected by centrifugation at 3000rpm for 5 minutes. Pellets were washed in cold 1M sorbitol, then resuspended in 7ml Ficoll solution (18% w/v Ficoll, 20mM KH_2PO_4 pH6.8, 1mM $MgCl_2$, 0.25mM EGTA, and 0.25mM EDTA) per 1g cells. The cell solution was then lysed using one stroke with a syringe.
4) The nuclear fraction was pelleted by centrifugation at 17000rpm at 4°C for 30 minutes. The upper white layer was carefully removed, along with the supernatant. The nuclear pellet was washed in MNase digestion buffer (15mM Tris-HCL pH7.4, 75mM NaCl, 3mM $MgCl_2$, 1.5mM $CaCl_2$, 1mM 2-mercaptoethanol) and resuspended in 1.5ml MNase digestion buffer.
5) The sample was then divided into aliquots of 250µl for MNase digestion (and 2 aliquots kept on ice for naked DNA samples).
6) Chromatin was digested by the addition of various amounts of MNase (Nuclease S7 from *Staphylococcus aureus*, Roche), and incubated for 10 minutes at 37°C.
7) The reaction was terminated by the addition of stop solution, to a final concentration of 1% SDS and 5mM EDTA in 250µl of 20mg/ml Pronase. The mixture was incubated at 55°C for at least 2 hours.
8) DNA was then purified from the samples by one phenol/chloroform and one chloroform extraction, as described previously. The subsequent upper phase was then precipitated by the addition of three volumes of ethanol overnight at -20°C.

9) DNA pellets can then be collected by centrifugation at 10000 rpm for 10 minutes, then re-dissolved in 0.5ml TE buffer, and re-precipitated with 40µl 3M NaAc and 1ml of cold ethanol at -20°C overnight.
10) The pellets were collected once again by centrifugation at 10000 rpm for 10 minutes, and the DNA dissolved in 0.5ml TE buffer.

2.12.2 Extraction and MNase treatment of the naked DNA

1) Using aliquots from step (5) above, which have been kept on ice, 1 x TE and 250µl of 20mg/ml Pronase were added, and incubated at 55°C for 2 hours.
2) DNA was purified via phenol and phenol/chloroform extractions and then precipitation as described previously, then resuspend in 250µl MNase digestion buffer.
3) The naked samples were then treated with appropriate amounts of MNase for 10 minutes at 37°C.
4) The digestion reaction was again stopped with the addition of 10% SDS and 0.5M EDTA.
5) Upon further phenol, phenol/chloroform extractions and overnight precipitation, the DNA was collected. The pellet was allowed to dry thoroughly before resuspending in 0.5ml TE buffer.

2.12.3 Low resolution nucleosome mapping

As the low resolution nucleosome mapping technique was employed to study the nucleosome distribution in the TAM plasmid, the plasmid must first be linearised using a restriction endonuclease with a unique site in the TAM sequence. *Bgl*II was chosen, and the DNA was treated as specified below.

2.12.3.1 Preparation of samples

1) 20µl of each sample (from above) was digested with an appropriate restriction endonuclease in a 100µl total reaction volume. The reaction was allowed to proceed for at least 1 hour at 37°C.

2) The DNA was extracted with one phenol/chloroform and one chloroform extraction, followed by precipitation by the addition of 10µl 3M NaCl and 110µl chilled isopropanol
3) The samples were resuspended in 30µl TE buffer, and loading buffer added appropriately.
4) All samples were then loaded onto a 1.2% agarose gel, alongside pre-constructed ladder of defined sizes, and DNA 1KB ladder (NEB).

2.12.3.2 Gel electrophoresis, blotting and probe hybridisation

1) A 1.2%(w/v) agarose gel was constructed in a large gel tank, to allow for good separation of DNA bands, and a multiple well comb inserted to allow for multiple samples to be run. The gel was left to cool and set for 45 minutes, before soaking in 1 x TBE running buffer.
2) The samples in loading buffer were then carefully loaded into the wells, and the gel run at 30V overnight, at 4°C, to prevent overheating.
3) Following electrophoresis, the EtBr stained DNA was visualised in a UV transilluminator, to ensure the bands were well distributed.
4) The gel was soaked in 0.4M NaOH, and then subject to Southern blotting, as described in Section 2.8.2.
5) A α-[^{32}P] dATP- labelled probe, designed to detect the 5' end of the *Bgl*II restriction fragment was then hybridised to the membrane, as described in Sections 2.8.3 and 2.10.
6) Finally, the membrane was placed with a phosphor screen to detect the radioisotope labelling, and imaged using a Typhoon phosphoimager (Section 2.8.4).

2.12.4 High resolution Nucleosome mapping

The nucleotide resolution method previously described to detect UV-induced cyclobutane pyrimidine dimers (CPDs) (Teng et al. 1997) can be applied to footprint the MNase sensitive sites (Teng et al. 2001).

The procedure briefly comprises:

1) Extraction of yeast chromatin and subsequent treatment with MNase (Section 2.12.1)
2) DNA digestion using restriction enzymes (as in Section 2.11.1), using the *Hae*III restriction endonuclease in a 100µl total reaction volume
3) The MNase digested fragments are then purified using specific probes and Dynabead technology, as for high resolution CPD analysis (Section 2.11.2).
4) The Dynabead-bound ssDNA fragments are then end-labelled with 6 α-[^{32}P] dATP molecules, and resolved by denaturing polacryalmide gel electrophoresis (Sections 2.11.3 and 2.11.4)
5) The resulting gel image is analysed using ImageQuant software (Molecular Dynamics Inc.) to determine the MNase sensitive sites.

Chapter 3

The construction and employment of the TAM plasmid

3.1 Introduction

Nucleotide excision repair (NER) is a fundamental DNA repair mechanism responsible for the repair of bulky DNA lesions (Prakash and Prakash 2000). NER can be divided into two sub-pathways Global Genome NER (GG-NER) which surveys the entire genome for helix-distorting lesions and Transcription Coupled NER (TC-NER) which repairs damage that disrupts an elongating RNA polymerase (reviewed in Chapter 1). Many contributing factors have been associated with efficient NER, such as chromatin structure, covalent histone modifications, histone variants and the global damage response pathway.

Cellular DNA is compacted into the eukaryotic nucleus as chromatin; in complex with both histone and non-histone proteins. The relative level of compaction is thought to be dependant on factors such as the cell cycle and the transcriptional activity of the DNA. The ability of the NER machinery to access DNA in a heterogeneous chromatin environment, without the induction of spurious transcription is not yet understood. This multi-protein mechanism has been studied for many years, and the intimate links with chromatin related factors are slowly emerging.

Chromatin is largely thought to provide a repressive structure which acts to limit the access of DNA-binding proteins. This is exemplified in repair terms by modulation of lesion removal across a region containing positioned nucleosomes, such that slow repair occurs in the internal protected region of the nucleosome, and faster repair is seen in linker regions (Wellinger and Thoma 1997). DNA processes such as transcription and repair require access to chromosomal DNA, and eukaryotic cells have developed chromatin remodelling activities to afford this access. Links

have been established between NER and chromatin remodelling (Smerdon and Lieberman 1978; Yu et al. 2005), allowing the inhibitory effect of nucleosomes to be overcome. Chromatin remodelling both *in vivo* and *in vitro* on a mononucleosome substrate (Gaillard et al. 2003; Hara and Sancar 2002) has implied that the SWI/SNF family of chromatin remodelling factors enhances repair of UV damage, with the yeast SWI/SNF complex physically interacting with the damage-recognition heterodimer Rad4-Rad23 (Gong et al. 2006).

It has been suggested that a global damage response network not only effects the induction of transcription of repair proteins, but also acts to regulate the general chromatin response. This study hopes to shed light on the complex early mechanistic stages which allow efficient repair in a repressive chromatin environment.

The yeast Saccharomyces cerevisiae MFA2 gene

Previous work within the Waters' laboratory has seen the employment of *MFA2* as a model gene for studying NER. Work carried out at *MFA2* has allowed a progression in the field of DNA repair, showing a relationship between transcriptional activity and NER at this gene. The high resolution analysis of cyclobutane pyrimidine dimer (CPD) repair at specific nucleotide positions, along with high resolution nucleosome mapping of the gene has also led to intimate links being established between repair and chromatin structure *in vivo*. However, as yet there are no model systems being employed for *in vivo* and *in vitro* analyses.

Transcriptional regulation of yeast mating type genes

In the yeast *S. cerevisiae*, haploid cells exist as two distinct phenotypes, mating type **a** cells and mating type α cells. Each cell type expresses a number of specific gene products, such as pheromones and signalling proteins, which give rise to the phenotypic mating type. The determination of mating type is defined by the presence of either MAT**a** or MATα alleles at the mating type MAT locus, located near the centromere of chromosome III. In **a** cells, the MAT**a** allele expresses the **a**1 and **a**2 genes, whilst in α cells, α1 and α2 are expressed from the MATα allele. Yeast mating type can be successfully switched from **a** to α or vice versa by replacing the distinct central Y region of one MAT allele with an alternative copy carrying the

opposite mating information, which is located in the storage loci HMR(**a**) or HML(α) (Haber 1998).

The suppression and expression of mating type specific genes has been attributed to many cellular regulators. Mating type specific genes contain upstream operator sequences, located approximately 30bp upstream of the TATA box, which act to regulate the transcriptional activity of the gene products. These operator sequences, or P boxes, differ in structure between **a** and α mating type specific genes. In mating type α specific genes, the operator sequence contains a mcm1 (minichromosome maintenance protein 1) binding site and a α1 factor binding site. Mcm1 is an essential protein, involved not only in the regulation of mating type specific genes, but also in the transcription of many other yeast genes. The mcm1 binding site within the operator deviates from a palindromic sequence, resulting in an imperfect binding site for the dimeric mcm1 protein. In **a** cells mcm1 fails to bind to this imperfect sequence, and transcription of the gene is unable to take place. In α cells, however, α1 factor (MATα1 product) is produced, which binds cooperatively with mcm1 at the operator sequence, allowing transcription of the α-specific genes.

As this project focuses on the **a**-specific *MFA2* gene, particular attention will be paid to the transcriptional regulation of mating type **a**-specific genes, represented in Figure 3.1. The upstream operator sequence of mating type **a**-specific genes is organised into a mcm1 binding site, flanked by two α2 binding sites. In **a** cells mcm1 is able to bind its consensus sequence, without the need for an additional factor and transcription can take place. In α cells, however, the homeodomain α2 factor is produced, which binds cooperatively with mcm1, causing a repression of gene transcription (Johnson 1995). The cooperative binding of α2 and mcm1 is not entirely sufficient to repress **a**-gene transcription in α cells, where full repression requires the actions of the general yeast repressor proteins Tup1 and Ssn6 (Patterton and Simpson 1994) and histone deacetylases (Herschbach et al. 1994).

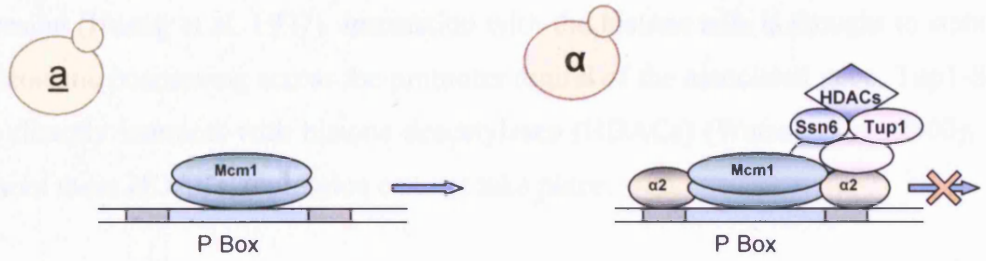

Figure 3.1: Transcriptional regulation of **a**-specific genes in haploid yeast cells. In mating type **a**-cells, the mcm1 protein complex is able to bind to its' constitutive binding site, allowing efficient transcription. In mating type α cells however, α2 factor is produced, and this binds cooperatively with the mcm1 protein. This recruits the general repressor proteins Ssn6 and Tup1, which in turn recruits histone deacetylases, resulting in a repressed gene.

The *TUP1* gene was first characterised in 1990 as a mediator of glucose repression within *Sacchromyces cerevisiae*. Tup1 mutants are so called due to the capacity for thymidine uptake (tup) from the surrounding growth medium. Tup1 mutants exhibit mating-type defects in MATα cells and de-repression of many enzymes under glucose repression, a phenomenon whereby the regulation of a subset of genes is controlled by the external glucose concentration (Williams and Trumbly 1990). The Ssn6-Tup1 repressor is a highly conserved system of transcriptional repression in eukaryotes, providing an especially important regulatory complex in budding yeast. Studies have shown that an N-terminal portion of α2 interacts directly with Tup1 (WD40 repetitive sequence), whilst a turn in the α2 homeodomain (towards C terminus, between helices 2 and 3 of the homeodomain) interacts directly with Ssn6 (Smith and Johnson 2000).

Three distinct mechanisms have been suggested for the repressive role of the Ssn6-Tup1 protein complex: (i) direct interaction with transcriptional machinery, (ii) nucleosome positioning through interactions with histone protein tails, and (iii) recruitment of HDACs (Smith and Johnson 2000; Zhang and Reese 2004b). These mechanisms arise from a plethora of studies, and lead to the suggestion that the repression is a chromatin structure-mediated event. It has been shown that Tup1-Ssn6 regulation of a subset of genes results in highly positioned nucleosomes (Cooper et al. 1994; Fleming and Pennings 2001; Li and Reese 2001; Roth et al. 1990), with deletion of either Tup1, or the Ssn6-Tup1 complex resulting in a loss of positioned nucleosomes. Tup1 has been shown to bind histone tails *in vitro*, and mutations in

histone H3 and H4 tails *in vivo* causes a compromise of Tup1-Ssn6 mediated represion (Huang et al. 1997). Interaction with the histone tails is thought to stabilise nucleosome positioning across the promoter region of the associated gene. Tup1-Ssn6 also directly interacts with histone deacetylases (HDACs) (Watson et al. 2000), and without these HDACs, repression can not take place.

MFA2 as a model gene

MFA2 is a mating type **a**-specific gene located on the left arm of chromosome XIV, encoding a putative 38 amino acid **a**-factor precursor. The mature **a**2 factor, a dodecapeptide, is a protein involved in the pheromone response pathway (Michaelis and Herskowitz 1988). There are two active species of **a** factor, *MFA1* and *MFA2*, differing only by a few residues. The **a**-factors interact with α cells to cause cell cycle arrest and physiological responses to promote efficient mating. Single mutants in either mfa1 or mfa2 still produce ample **a** factor, however, a *mfa1mfa2* double mutant has an absolute mating defect (Chen et al. 1997). *MFA2* and its regulation are well understood, with the gene being transcriptionally active in haploid mating type **a** cells, and repressed in α cells. As described previously, the regulation of **a**-specific genes is well documented, involving a subset of repressor proteins. This regulation provides an attractive quality of *MFA2* to study repair with respect to chromatin structure, as when the gene is active it exists in an 'open' chromatin structure (Chen-Cleland et al. 1993), and when repressed, the chromatin conformation closely resembles heterochromatin. The effect of chromatin environment on NER provided a focus for this study.

Hence my study used *MFA2* as a model gene, in part because it had previously been studied extensively in the field of nucleotide excision repair. Work with *MFA2* has led to a great understanding of the genes' transcriptional regulation (Chen-Cleland et al. 1993), as well as the chromatin structure and repair profiles (Teng et al. 2005; Yu and Waters 2005).

```
MQPITTASTQ ATQKDKSSEK KDNYIIKGLF WDPACVIA*
```

Figure 3.2: Amino acid sequence of the *MFA2* gene (obtained from SGD)

MFA2 is a small gene, comprising a coding region of 117bp and a transcribed region of 328bp, and this allows for the study of DNA repair across the entire gene using high resolution sequencing gels. Along with the transcriptional regulation and repair profiles of the gene, the chromatin structure has also been characterised by nucleosome mapping (Teng et al. 2001).

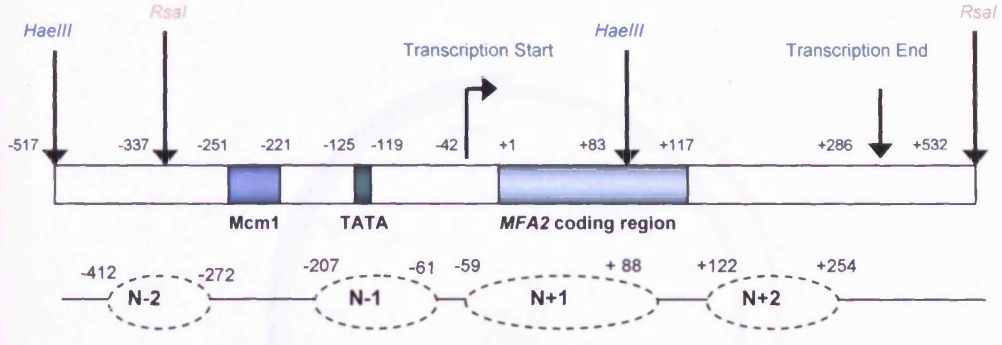

Figure 3.3: Endogenous *MFA2* restriction map, detailing the positions of the upstream operator sequence (mcm1 binding site) and TATA box. Nucleosome positions are also displayed, as mapped by (Teng et al. 2001).

Nucleosomes have been mapped to the repressed *MFA2* gene, N-2 (-412 to -272) and N-1 (-207 to -61) being located in the promoter region, and N+1 (-59 to +88) and N+2 (+122 to +254) positioned across the coding region and downstream of the coding region respectively. These highly positioned nucleosomes are lost when the gene is undergoing active transcription.

The TRP1R1 plasmid

Originally constructed in 1981, the TRP1-R1 circle is a multiple-copy synthetic plasmid derived from *Saccharomyces cerevisiae* chromosomal DNA. The 1453bp plasmid contains the *TRP1* gene and the ARS1 (autonomously replicating sequence). The TRP1 gene allows the plasmid to be selected for in a tryptophan negative background. The ARS1 sequence is responsible for promoting high frequency transformation and extra-chromosomal maintenance of plasmid DNA. ARS

sequences act as initiation sites for replication in yeast chromosomal DNA. The TRP1-R1 circle exists in 100-200 copies per cell, replicating along with the chromosomal replication process, requiring the same gene products needed for the replication of chromosomal DNA. It was found that the TRP1 R1 circle was organised into nucleosomes, having the same replicative and structural properties expected of a chromosomal origin of replication (Pederson et al. 1986; Zakian and Scott 1982).

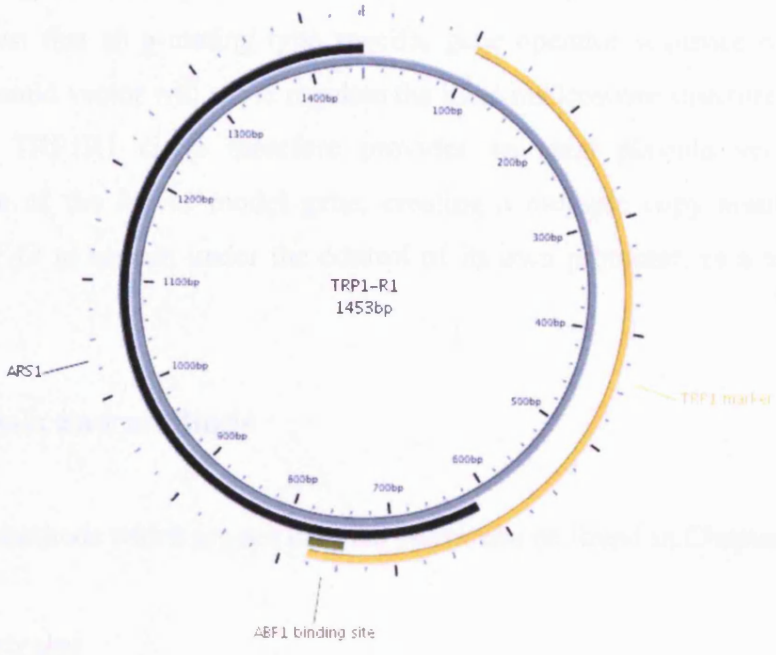

Figure 3.4: TRP1R1 plasmid (1453bp) schematic, detailing the TRP1 gene in orange, and ARS1 sequence in black. Also shown is the ABF1 consensus sequence (constructed using Plasmapper software).

The TRP1-R1 circle has been the focus of many studies into nucleosome positioning, DNA-histone interactions and chromatin folding. The characterisation of the plasmid in 1981 showed using Micrococcal nuclease digestion that nucleosomes were present on the plasmid (Zakian and Scott 1982). Indirect end-labelling analysis predicted seven nucleosomes on the plasmid (Thoma et al. 1984). The subsequent isolation of the plasmid as chromatin in 1986 (Pederson et al. 1986) confirmed the presence of seven nucleosomes, and that the chromatin structure did not differ greatly between copies of the plasmid. Later, it was discovered that four unstable

nucleosomes formed in the region of the *TRP1* gene, and three stable nucleosomes were positioned over the ARS1 region. Two hypersensitive regions to digestion with nuclease, 5' and 3' to the *TRP1* gene were also shown (Roth et al. 1990).

TRP1R1 derived plasmids were subsequently constructed to study nucleosome positioning in relation to mcm1/α2 regulated promoter regions. They showed that the α2 operator and α2 protein are responsible for nucleosome positioning, by insertion of the STE6 promoter region (including operator sequence) into the TRP1R1 circle. In this TALS (TRP-ARS-LAC-STE) plasmid one less nucleosome was found to be positioned in **a** cells, compared to those found in α cells (Roth et al. 1990). These results suggest that an **a**-mating type specific gene operator sequence placed in the TRP1R1 plasmid vector will act to regulate the local nucleosome structure.

This TRP1R1 circle therefore provides an ideal plasmid vector for the incorporation of the *MFA2* model gene, creating a multiple copy number plasmid allowing *MFA2* to remain under the control of its own promoter, as a tool to study NER.

3.2 Materials and methods

Any methods which are not detailed below can be found in Chapter 2.

3.2.1 Yeast strains

PSY316 *(MATα ade2-101 ura 3-52 leu 2-3, 112 Δhis 3-200 lys2 trp1)*
PSY316 *(MAT**a** ade2-101 ura 3-52 leu 2-3 112 Δhis 3-200 lys2 trp1)*

3.2.2 Fusion PCR of TAM plasmid

A fusion PCR method was utilised for the generation of a model plasmid. Fusion PCR involves the PCR-based amplification of two DNA fragments of interest, incorporating primers designed to create a region of complementation between the two fragments. Following the initial amplification reaction, a subsequent PCR reaction using primers for the distant ends of the total DNA allowed for the fusion of

the two fragments via the complementary region. The fused DNA fragment was then ligated to form a closed circular plasmid (detailed in Figure 3.5).

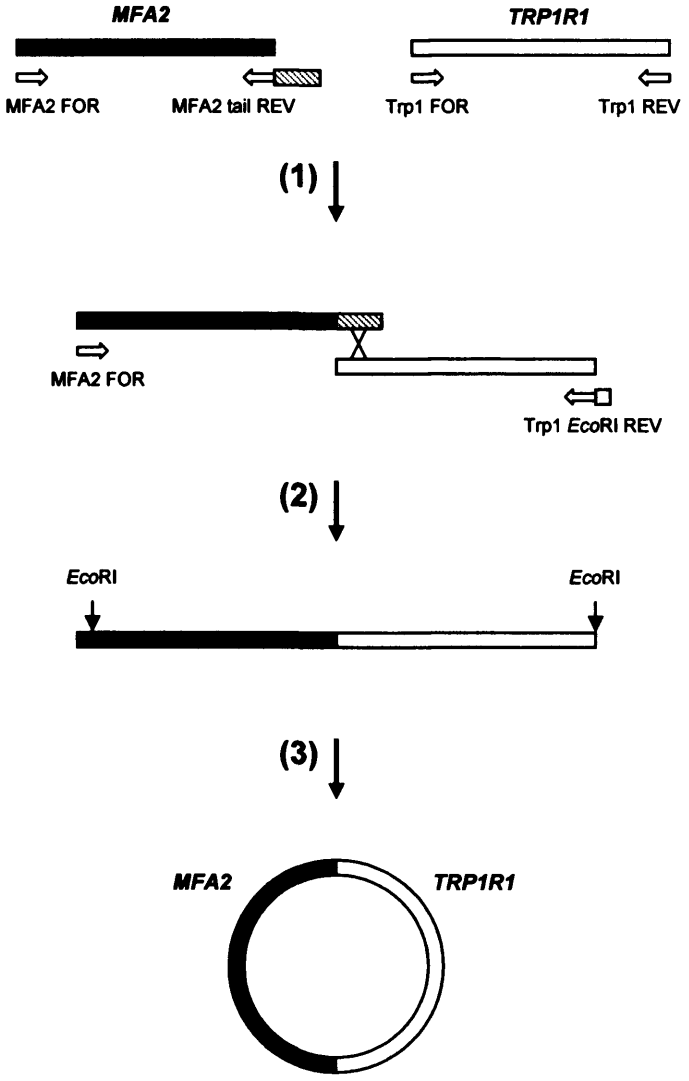

Figure 3.5: Schematic of the fusion PCR reaction. Firstly the *MFA2* region of interest was PCR amplified directly from genomic DNA using a primer set which was designed to incorporate a tail of homology at the 3' end, homologous to the 5' end of the TRP1R1 sequence. The Trp1R1 sequence was directly amplified from genomic DNA, and digested with *Eco*RI to create TRP1R1 DNA. (1) The two resulting products were than substrates for the fusion PCR reaction. (2) On amplification using a 5' MFA2 FOR primer and 3' Trp1 *Eco*RI primer, under fusion PCR conditions, the region of homology allowed for the fusion of the PCR products. (3) Subsequent digestion with *Eco*RI endonuclease and ligation resulted in a plasmid construct.

Fusion PCR primers

PCR amplification, following standard PCR conditions, allowed for the construction of the TRP1R1 and *MFA2* DNA fragments to use as substrates for the fusion PCR reaction.

TRP1 FOR: TGACGCCAGATGGCAGTAGTGG
TRP1 REV: TGTGATGGCTTGGCATGGCG

***MFA2* FOR**: AATGACATTTCAAGAACTACTGCCACGA
***MFA2* tail REV**: TAGTCACCAATGCCCTCCCTCTTGGCCCTCTCCTTTTCTTT
TTTCGACCGAATTAGAAAAGTTAAACCGTGGCAATGAAGAT

The fusion PCR reaction utilised the following primers:

***MFA2* FOR**: AATGACATTTCAAGAACTACTGCCACGA
TRP *Eco*RI REV: TAAGAATTCCCACATGTTAAAATAGTGAAGGAGCAT
GT

The fusion PCR reaction was run on a FUSION PCR cycle on a Hybaid thermal cycler under the parameters stated:

1) 94°C 2 minutes
2) 94°C 15 minutes
3) 45°C 30 seconds
4) 68°C 2 minutes
5) Go to (2) for 9 cycles
6) 94°C 15 seconds
7) 55°C 30 seconds
8) 68°C 2 minutes + 5 seconds/cycle
9) Go to (6) 15 times
10) 72°C 7 minutes

3.2.3 Plasmid confirmation

To confirm the correct construction of TAM, PCR-based checks were carried out using the primers below, under standard PCR parameters.

Plasmid confirmation primers

TAM p1: GATAGCTTTTTTCGCATACGCTACAATGACCCGATTCTT
MFA2 REV: CCGGTATACGAGGGAACAGGAAGG

3.2.4 Sequencing TAM

To ensure the PCR reactions amplified the various DNA fragments correctly, the final TAM plasmid was sequenced using the BigDye 3.1 sequencing kit.

Sequencing reaction

In a thin-walled 0.5ml eppendorf the following reaction was set up:

Template DNA
Primer - 3.2pmol
Ready Reaction Premix - 4 µl
BigDye Sequencing buffer - 2 µl
PCR-grade water – to 20 µl

The PCR reaction was allowed to proceed using a Hybaid thermal cycler and the following sequencing PCR parameters:

1) 96°C 1 min
2) 96°C 10 secs
3) 50°C 5 secs
4) 60°C 4 mins
5) Go to (2) for 25 cycles

Sequencing primers

1: AGTAATAATAACAGGCCCTCATC
2: TATATAATCAAGGGCCTCTTCTG
2a REV: AAATTAAGCGATAACACAGGCGG
3: CCGCAGGAAATGAAAGATGAACC
4: GTACTCAACGTCCGCATTCTCAT
5: ATGTGTGCCCAATAGAAAGAGAA
6: GGCGTTATTGGTGTTGATGTAAG
7: CTACAATGACCCGATTCTTGCTA
8: GGTCCACTGTGTGCCGAACATGC
8a REV: TAGTGAAGGAGCATGTTCGGCAC

Following the sequencing reactions, the PCR products were precipitated using 5µl 125nM EDTA and 60µl 100% ethanol, and the pellets collected and dried, before sending the samples for analysis by CBS.

3.2.5 Determination of TAM copy number

To evaluate the relative copy number of the TAM plasmid within the PSY316 (WT) strains, a simple assay was employed. A glass bead-mediated DNA preparation was carried out to obtain cellular DNA (Chapter 2.8.1). Total DNA was then cut using a restriction enzyme, chosen to linearise the TAM plasmid, and create a fragment of a different size encompassing the endogenous *MFA2* gene. This restricted sample could then be resolved on a non-denaturing agarose gel, transferred to a membrane via a southern blotting technique, and the *MFA2*-containing fragments detected using a radiolabelled probe (Chapter 2.10).

DNA was digested using the *Eco*RI restriction endonuclease in a 40µl total reaction volume, under the appropriate conditions (NEB) to create a 1570bp fragment of genomic *MFA2*, and a 2973bp linear TAM fragment.

Primer pair to make a probe which detects MFA2 sequence

N1379: CTATCATCTTCATACAACAATAACTACCA
P3352*: BIOTIN-GATAGCTTTTTTCTAATGATGAGAGAATTGGAATAAATTAG

A standard PCR amplification using WT DNA as a template, and the primer pair above results in a dsDNA fragment, biotin labelled on the TS. Following the probe preparation procedure outlined in Chapter 2.10.2, this dsDNA product was denatured, and the NTS probe (N1379) was hybridised to the biotinylated strand, allowing a primer-directed sequencing reaction using radiolabelled dATPs to proceed. The resulting fragment was again denatured, creating a radioactive ssDNA fragment complementary to the TS of the *MFA2* region.

3.2.6 *MFA2* mRNA analysis

Following total RNA extraction, using the hot phenol method described in Chapter 2.9, samples were run on a FA gel (see Appendix I). The gel was then transferred to a membrane via a northern blotting technique, and allowed to hybridise to a radiolabelled probe to detect *MFA2* mRNA levels. The primers were designed to incorporate a biotin label on the NTS strand, to allow the TS primer to detect mRNA. As a Northern blot control, primers were also designed to detect the *ACT1* gene mRNA (primers displayed below).

Primer pair to make probe to detect mRNA

MFA2 mRNA:
P3351: CTAATGATGAGAGAATTGGAATAAATTAG
N1380*: BIOTIN-GATAGCTTTTTTCTATCATCTTCATACAACAATAACTACCA

ACT1 mRNA:
ACT1a*: BIOTIN–GCCGGTTTTGCCGGTGACG
ACT1b: CCGGCAGATTCCAAACCCAAAA

3.3 Results

To investigate the roles and implications of chromatin in NER, it was decided that a versatile tool be constructed, which allowed ease of use, and potential for both *in vivo* and *in vitro* studies. This project has seen the incorporation of the *MFA2* model gene into a yeast plasmid. In order to successfully utilise a plasmid for studying NER, it was decided that a multiple copy number plasmid should be employed. These properties allow for the endogenous *MFA2* gene to be statistically disregarded in many of the experimental procedures undertaken.

It was decided that the *MFA2* gene, and the upstream operator sequences and downstream flanking region should be incorporated into the yeast TRP1R1 circle multiple copy number plasmid. This plasmid contains an ARS1 region, conferring extra-chromosomal maintenance of the plasmid, ensuring a multiple copy number persists. The presence of the *TRP1* gene also provided selection in a tryptophan negative background, and allowed for retention of the plasmid.

Preparation of DNA substrates for Fusion PCR reaction

The TRP1R1 circle could be directly amplified from yeast genomic DNA, using primers TRP1 FOR and TRP1 REV listed in Section 3.2, which encompass the region, and a standard PCR reaction (see Chapter 2). The fragment of interest containing the *MFA2* gene (Figure 3.6) was also generated via PCR amplification, using MFA2 FOR and MFA2 tail REV primers. This resulted in a 1587bp *MFA2* fragment, with a 54bp 3' tail of homology to the 5' end of the TRP1R1 sequence.

```
   1 AATGACATTT CAAGAACTAC TGCCACGATT TTACAAAAAG AATTCAAACT CAGTTAGTAA
  61 TAATAACAGG CCCTCATCTA TTTTCTCGGA AAACTTGGTG GATTTTGATG ATGTTAACAT
 121 GGTCGATAAG ACCAGACTGT TTATTTTTTT ATTTTTCAGT TTCATCATTA CTATACCGTT
 181 TATGGTATAA ATTAGAAAAG TTAAAGCAGC ATGTTTTCAT TTGAAACAAA TACTAATGCA
 241 ATAATAGGTA CACCATCTAC TACATAATTA ATTGATAGTT TCCTTTTCCG TTAAGTGCAT
 301 GCATAGGACG CCCATAATTT TTTAAGTTAA AAAAGCATGT ATTTACCTAT TCGGGAAATT
 361 TACATGACAT GGATGCCATA AGGAACGAAA ATGAAACATG CATGTCAGAG GAAAAAGAAC
 421 AAAGCGAGAG GAAAAAGCTG TTGCATTACC ACGTAATTTT GTATATAAAT ATCTGATAAA
 481 TAACCATTTT ATTTCCATCC ACTTCTTCTG TCGTTCATCC GTTCATTGAC ATCACTAGAG
 541 ACACCAGCGA GCTATCATCT TCATACAACA ATAACTACCA ACCTTAATGC AACCGATCAC
 601 CACTGCTTCC ACACAAGCCA CTCAGAAGGA TAAATCCTCT GAAAAGAAAG ACAACTATAT
 661 AATCAAGGGC CTCTTCTGGG ATCCCGCCTG TGTTATCGCT TAATTTTTGA CGACAACCAA
 721 GAGGTCAAAT CAATATCTAC CCTTTCATTT ATTACGTGTT GCTGGCAAAC TAATTTATTC
 781 CAATTCTCTC ATCATTAGCT CACCCTTTCC ATACTTTTTC ATACTTTTAT ACATATGTAT
 841 TTGTAGTTAT CACTTTAACA GATTTTTTCA TGTTTTTCTT TTCTGATACG CCTTTCCCTC
 901 CGCAGGAAAT GAAAGATGAA CCACCCATTA CATTCGATTT TTTTTTAAT TATATTTTTG
 961 ACTATTATTT AATCATTAAA AACACATATA TTTCATAAAT TCGTAAGGTC GTTAGTTCTA
1021 TCGTAAAAGT GAAAAAGTTT TGAGCCAGTT TTCAAAAACC CGCAGGATCC CACTATGTAT
1081 GGCTTTAAAT AATGGTTTTT CACGTGCATC AAGTCCGTAC TATCTTCACC ACTATAAACT
1141 CTTATAGGTG GATTATTCGT TTCGAATGCT GGTGGCAGTG CCGGTTTGAA AATAATCTTA
1201 CCTACCCATG GGTGGTCTTC CGTTAACGGT TTGATGCATC TTAATGAGTC TTTGATATAT
1261 CTTTTCCTTG AAACTAGTTG TGTCGCCGGT GCCCACTTCG AATCGTTACT GGATTGATTC
1321 TTATTTCCAC ATTTTAGTGA CAATTTCTTT GGAAAATCAT GATTTAAACA ACCAGTCACG
1381 GAAAAGCTTT TCGTACTGAA TATTGTACCG TACTCAACGT CCGCATTCTC ATAGCGAGAT
1441 TCTCTTTCAT CCAAATATAC CAATCTATTG ATGTCATCAT CCTCAACATA TCCATCTTCA
1501 TCATCCTCTT CGTAATTAGC ATCGTCTTCG TCTTCGTCAT CATCTTCATC TCCATTTACA
1561 TCTTCATTGC CACGGTTTAA CTTTTCT
```

Figure 3.6: Sequence of 1587bp of the *MFA2* region of interest, chosen to be incorporated into the plasmid. Highlighted in grey are the mcm1 binding site and TATA box, with the *MFA2* coding region shown in blue. The PCR amplification reaction generated this *MFA2*-containing sequence, with an additional 54bp on the 3' end, as a tail of homology to the TRP1R1 sequence.

The generation of the TRP1R1 and *MFA2* PCR products were checked on an agarose gel, alongside a DNA ladder to ensure that the correct size products have been produced.

Figure 3.7: Upon PCR amplification from genomic DNA, the *MFA2* region of interest, including the tail of homology (*MFA2*), and the TRP1-R1 containing fragment (TRP1-R1) were subjected to 0.8% TBE agarose gel electrophoresis, to check the PCR product sizes.

The resulting 1594bp TRP1R1 fragment (Figure 3.7) from genomic DNA (chromosome IV 461839-463189) could then be digested with *Eco*RI endonuclease to produce TRP1-R1 (Figure 3.8). The resulting 1453bp fragment self-ligates to form the TRP1-R1 circular plasmid.

```
   1 AATTCGGTCG AAAAAAGAAA AGGAGAGGGC CAAGAGGGAG GGCATTGGTG ACTATTGAGC
  61 ACGTGAGTAT ACGTGATTAA GCACACAAAG GCAGCTTGGA GTATGTCTGT TATTAATTTC
 121 ACAGGTAGTT CTGGTCCATT GGTGAAAGTT TGCGGCTTGC AGAGCACAGA GGCCGCAGAA
 181 TGTGCTCTAG ATTCCGATGC TGACTTGCTG GGTATTATAT GTGTGCCCAA TAGAAAGAGA
 241 ACAATTGACC CGGTTATTGC AAGGAAAATT TCAAGTCTTG TAAAAGCATA TAAAAATAGT
 301 TCAGGCACTC CGAAATACTT GGTTGGCGTG TTTCGTAATC AACCTAAGGA GGATGTTTTG
 361 GCTCTGGTCA ATGATTACGG CATTGATATC GTCCAACTGC ATGGAGATGA GTCGTGGCAA
 421 GAATACCAAG AGTTCCTCGG TTTGCCAGTT ATTAAAAGAC TCGTATTTCC AAAAGACTGC
 481 AACATACTAC TCAGTGCAGC TTCACAGAAA CCTCATTCGT TTATTCCCTT GTTTGATTCA
 541 GAAGCAGGTG GGACAGGTGA ACTTTTGGAT TGGAACTCGA TTTCTGACTG GGTTGGAAGG
 601 CAAGAGAGCC CCGAAAGCTT ACATTTTATG TTAGCTGGTG GACTGACGCC AGAAAATGTT
 661 GGTGATGCGC TTAGATTAAA TGGCGTTATT GGTGTTGATG TAAGCGGAGG TGTGGAGACA
 721 AATGGTGTAA AAGACTCTAA CAAAATAGCA AATTTCGTCA AAAATGCTAA GAAATAGGTT
 781 ATTACTGAGT AGTATTTATT TAAGTATTGT TTGTGCACTT GCCTGCAGGC CTTTTGAAAA
 841 GCAAGCATAA AAGATCTAAA CATAAAATCT GTAAAATAAC AAGATGTAAA GATAATGCTA
 901 AATCATTTGG CTTTTTGATT GATTGTACAG GAAAATATAC ATCGCAGGGG GTTGACTTTT
 961 ACCATTTCAC CGCAATGGAA TCAAACTTGT TGAAGAGAAT GTTCACAGGC GCATACGCTA
1021 CAATGACCCG ATTCTTGCTA GCCTTTTCTC GGTCTTGCAA ACAACCGCCG GCAGCTTAGT
1081 ATATAAATAC ACATGTACAT ACCTCTCTCC GTATCCTCGT AATCATTTTC TTGTATTTAT
1141 CGTCTTTTCG CTGTAAAAAC TTTATCACAC TTATCTCAAA TACACTTATT AACCGCTTTT
1201 ACTATTATCT TCTACGCTGA CAGTAATATC AAACAGTGAC ACATATTAAA CACAGTGGTT
1261 TCTTTGCATA AACACCATCA GCCTCAAGTC GTCAAGTAAA GATTTCGTGT TCATGCAGAT
1321 AGATAACAAT CTATATGTTG ATAATTAGCG TTGCCTCATC AATGCGAGAT CCGTTTAACC
1381 GGACCCTAGT GCACTTACCC CACGTTCGGT CCACTGTGTG CCGAACATGC TCCTTCACTA
1441 TTTTAACATG TGG
```

Figure 3.8: TRP1-R1 sequence (1453bp), produced via *Eco*RI digestion of the chromosome IV 461839-463189 fragment obtained by PCR amplification, directly from yeast genomic DNA.

Fusion PCR of TAM plasmid

The fusion PCR approach was employed as an alternative to the classical cloning methods previously undertaken. This eliminates the need to amplify the yeast plasmid under construction within a bacterial vector. As described the MFA2 FOR and MFA2 Tail REV primers were used to amplify the *MFA2* fragment of choice from a genomic template. The primers were designed to encompass an *Eco*RI restriction site at the 5' of the fragment, and a 'tail' of homology to the 5' of the TRP1R1 sequence at the 3' end. This tail creates a region for recombination, ensuring correct orientation and positioning of the *MFA2* and TRP1R1 fragments in the fusion PCR reaction. The TRP1R1 fragment and the resulting *MFA2*-containing PCR product were used as the DNA templates, in a 1:1 ratio for the fusion PCR reaction. The fusion PCR reaction utilised the 5' MFA2 FOR primer and the 3' TRP *Eco*RI REV primer, in a fusion PCR cycle (parameters stated in section 3.2). The TRP EcoRI REV primer was designed to contain additional nucleotide residues to ensure that the

*Eco*RI endonuclease could function correctly to produce a sticky end, to allow for future ligation.

On verification of a fusion PCR product of the correct size, the DNA fragment was subsequently digested with *Eco*RI to create a linear DNA fragment, consisting of TRP1R1 and the *MFA2* region. Upon ligation to create a circular DNA construct, the plasmid was transformed directly into yeast PSY316 cells. Transformation reactions were spread onto plates containing selective media (TRP^-) to allow for retention of the plasmid.

Positive colonies from the transformation reaction were subject to a rapid yeast glass bead preparation (see Chapter 2) to obtain cellular DNA. The resulting samples could then be run on an agarose gel, and the two species of plasmid (relaxed and supercoiled) could be observed. As a further check, unique primers were designed which amplify a region of the plasmid containing both TRP1R1 and *MFA2* (Figure 3.9). As the two regions are spatially distinct within the genome, the amplification of the correct size PCR products will verify the fusion of the regions, and therefore the presence of the TAM plasmid.

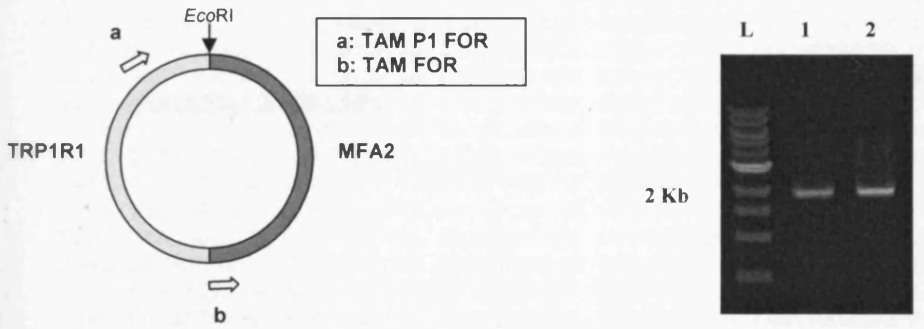

Figure 3.9: PCR was conducted using primers to amplify a unique plasmid sequence. The predicted 2Kb PCR product fragment can be seen in all samples (1 and 2 shown), verifying the presence of the TAM plasmid (L:NEB 1Kb ladder).

The final TAM plasmid (Figure 3.10 and 3.11) was also sequenced, using multiple sequencing primers and Big Dye 3.1 sequencing kit, to ensure that the plasmid had been incorporated without error.

```
   1 AATTCAAACT CAGTTAGTAA TAATAACAGG CCCTCATCTA TTTTCTCGGA AAACTTGGTG
  61 GATTTTGATG ATGTTAACAT GGTCGATAAG ACCAGACTGT TTATTTTTTT ATTTTTCAGT
 121 TTCATCATTA CTATACCGTT TATGGTATAA ATTAGAAAAG TTAAAGCAGC ATGTTTTCAT
 181 TTGAAACAAA TACTAATGCA ATAATAGGTA CACCATCTAC TACATAATTA ATTGATAGTT
 241 TCCTTTTCCG TTAAGTGCAT GCATAGGACG CCCATAATTT TTTAAGTTAA AAAAGCATGT
 301 ATTTACCTAT TCGGGAAATT TACATGACAT GGATGCCATA AGGAACGAAA ATGAAACATG
 361 CATGTCAGAG GAAAAAGAAC AAAGCGAGAG GAAAAAGCTG TTGCATTACC ACGTAATTTT
 421 GTATATAAAT ATCTGATAAA TAACCATTTT ATTTCCATCC ACTTCTTCTG TCGTTCATCC
 481 GTTCATTGAC ATCACTAGAG ACACCAGCGA GCTATCATCT TCATACAACA ATAACTACCA
 541 ACCTTAATGC AACCGATCAC CACTGCTTCC ACACAAGCCA CTCAGAAGGA TAAATCCTCT
 601 GAAAAGAAAG ACAACTATAT AATCAAGGGC CTCTTCTGGG ATCCCGCCTG TGTTATCGCT
 661 TAATTTTTGA CGACAACCAA GAGGTCAAAT CAATATCTAC CCTTTCATTT ATTACGTGTT
 721 GCTGGCAAAC TAATTTATTC CAATTCTCTC ATCATTAGCT CACCCTTTCC ATACTTTTTC
 781 ATACTTTTAT ACATATGTAT TTGTAGTTAT CACTTTAACA GATTTTTTCA TGTTTTTCTT
 841 TTCTGATACG CCTTTCCCTC CGCAGGAAAT GAAAGATGAA CCACCCATTA CATTCGATTT
 901 TTTTTTTAAT TATATTTTTG ACTATTATTT AATCATTAAA AACACATATA TTTCATAAAT
 961 TCGTAAGGTC GTTAGTTCTA TCGTAAAAGT GAAAAAGTTT TGAGCCAGTT TTCAAAAACC
1021 CGCAGGATCC CACTATGTAT GGCTTTAAAT AATGGTTTTT CACGTGCATC AAGTCCGTAC
1081 TATCTTCACC ACTATAAACT CTTATAGGTG GATTATTCGT TTCGAATGCT GGTGGCAGTG
1141 CCGGTTTGAA AATAATCTTA CCTACCCATG GGTGGTCTTC CGTTAACGGT TTGATGCATC
1201 TTAATGAGTC TTTGATATAT CTTTTCCTTG AAACTAGTTG TGTCGCCGGT GCCCACTTCG
1261 AATCGTTACT GGATTGATTC TTATTTCCAC ATTTTAGTGA CAATTTCTTT GGAAAATCAT
1321 GATTTAAACA ACCAGTCACG GAAAAGCTTT TCGTACTGAA TATTGTACCG TACTCAACGT
1381 CCGCATTCTC ATAGCGAGAT TCTCTTTCAT CCAAATATAC CAATCTATTG ATGTCATCAT
1441 CCTCAACATA TCCATCTTCA TCATCCTCTT CGTAATTAGC ATCGTCTTCG TCTTCGTCAT
1501 CATCTTCATC TCCATTTACA ATTCGGTCGA AAAAAGAAAA GGAGAGGGCC AAGAGGGAGG
1561 GCATTGGTGA CTATTGAGCA CGTGAGTATA CGTGATTAAG CACACAAAGG CAGCTTGGAG
1621 TATGTCTGTT ATTAATTTCA CAGGTAGTTC TGGTCCATTG GTGAAAGTTT GCGGCTTGCA
1681 GAGCACAGAG GCCGCAGAAT GTGCTCTAGA TTCCGATGCT GACTTGCTGG GTATTATATG
1741 TGTGCCCAAT AGAAAGAGAA CAATTGACCC GGTTATTGCA AGGAAAATTT CAAGTCTTGT
1801 AAAAGCATAT AAAAATAGTT CAGGCACTCC GAAATACTTG GTTGGCGTGT TTCGTAATCA
1861 ACCTAAGGAG GATGTTTTGG CTCTGGTCAA TGATTACGGC ATTGATATCG TCCAACTGCA
1921 TGGAGATGAG TCGTGGCAAG AATACCAAGA GTTCCTCGGT TTGCCAGTTA TTAAAAGACT
1981 CGTATTTCCA AAAGACTGCA ACATACTACT CAGTGCAGCT TCACAGAAAC CTCATTCGTT
2041 TATTCCCTTG TTTGATTCAG AAGCAGGTGG GACAGGTGAA CTTTTGGATT GGAACTCGAT
2101 TTCTGACTGG GTTGGAAGGC AAGAGAGCCC CGAAAGCTTA CATTTTATGT TAGCTGGTGG
2161 ACTGACGCCA GAAAATGTTG GTGATGCGCT TAGATTAAAT GGCGTTATTG GTGTTGATGT
2221 AAGCGGAGGT GTGGAGACAA ATGGTGTAAA AGACTCTAAC AAAATAGCAA ATTTCGTCAA
2281 AAATGCTAAG AAATAGGTTA TTACTGAGTA GTATTTATTT AAGTATTGTT TGTGCACTTG
2341 CCTGCAGGCC TTTTGAAAAG CAAGCATAAA AGATCTAAAC ATAAAATCTG TAAAATAACA
2401 AGATGTAAAG ATAATGCTAA ATCATTTGGC TTTTTGATTG ATTGTACAGG AAAATATACA
2461 TCGCAGGGGG TTGACTTTTA CCATTTCACC GCAATGGAAT CAAACTTGTT GAAGAGAATG
2521 TTCACAGGCG CATACGCTAC AATGACCCGA TTCTTGCTAG CCTTTTCTCG GTCTTGCAAA
2581 CAACCGCCGG CAGCTTAGTA TATAAATACA CATGTACATA CCTCTCTCCG TATCCTCGTA
2641 ATCATTTTCT TGTATTTATC GTCTTTTCGC TGTAAAAACT TTATCACACT TATCTCAAAT
2701 ACACTTATTA ACCGCTTTTA CTATTATCTT CTACGCTGAC AGTAATATCA AACAGTGACA
2761 CATATTAAAC ACAGTGGTTT CTTTGCATAA ACACCATCAG CCTCAAGTCG TCAAGTAAAG
2821 ATTTCGTGTT CATGCAGATA GATAACAATC TATATGTTGA TAATTAGCGT TGCCTCATCA
2881 ATGCGAGATC CGTTTAACCG GACCCTAGTG CACTTACCCC ACGTTCGGTC CACTGTGTGC
2941 CGAACATGCT CCTTCACTAT TTTAACATGT GGG
```

Figure 3.10: Sequence of the resulting TAM plasmid (*Eco*RI digestion shown). Highlighted in order are the Mcm1 binding site, TATA box, the fusion homologous region and the Abf1 binding site. The *MFA2* coding region is displayed in blue text.

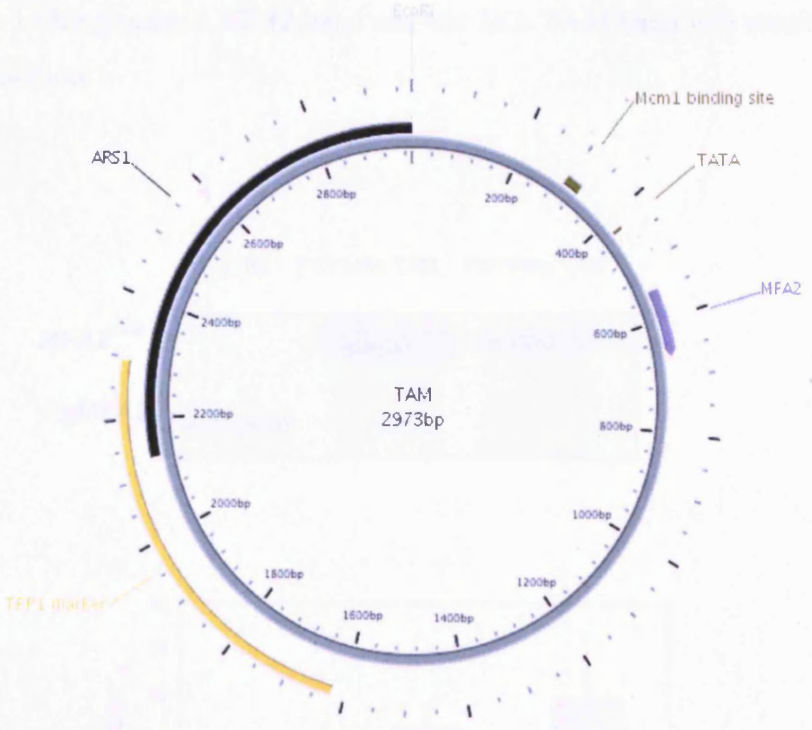

Figure 3.11: Schematic of the resulting TAM plasmid. The EcoRI restriction site is designated position 1, with the *MFA2* Mcm1 binding site, TATA box and coding region labelled. The *TRP1* gene and ARS1 sequence are also displayed.

Maintenance of multiple copy number

As originally described by Zakian and Scott, the Trp1R1 circle exists in approximately 100-200 copies per cell (Zakian and Scott 1982). To ensure that the newly constructed TAM plasmid was replicating along with the cell cycle, aided by the ARS1 sequence, the copy number of the plasmid was studied.

Relative copy number was determined by a simple assay, carried out using restriction endonuclease digestion. The TAM plasmid has been designed to have a unique *Eco*RI restriction site, with digestion resulting in a 3Kb linear molecule. There are also *Eco*RI sites flanking the endogenous copy of *MFA2*, creating a fragment of 1.5Kb. Utilising *Eco*RI, therefore, a total DNA preparation can be digested and run on an agarose gel. This can then be blotted, following a standard Southern blotting

technique, and probed using a radiolabelled probe specific for *MFA2*. The ratio between the 1.5Kb genomic *MFA2* band and the 3Kb TAM band will result in a copy number estimation.

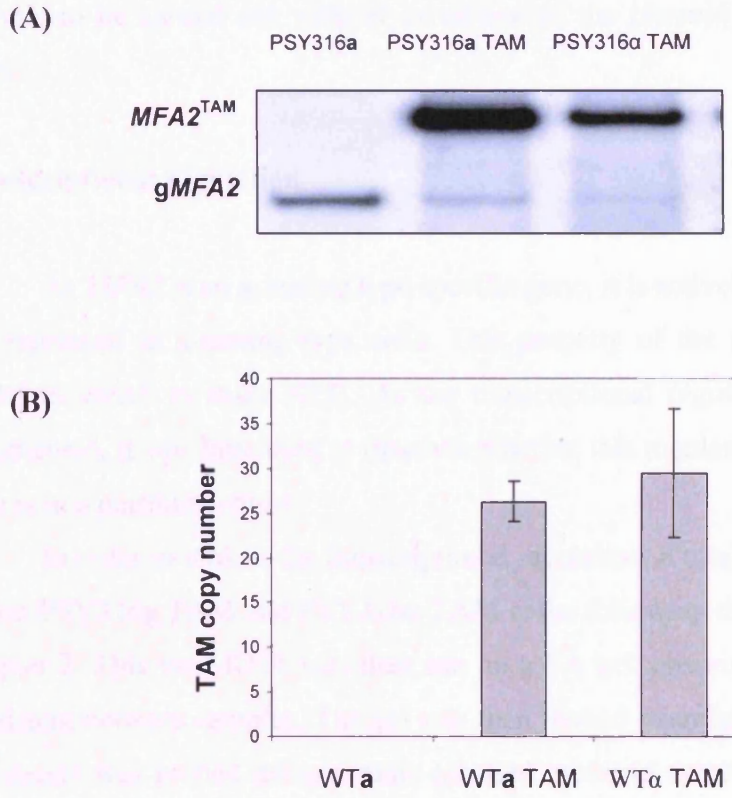

Figure 3.12: Southern blot analysis to determine the copy number of the TAM plasmid **(A)** Southern blot probed for *MFA2*, displaying the 3Kb TAM borne *MFA2* fragment and 1.5Kb endogenous *MFA2* fragment. The ratio between these two band intensities (as quantified using Imagequant software) is an approximation of plasmid copy number. PSY316 (WT) cells showed the g*MFA2* band, whereas TAM-containing strains display the higher molecular weight $MFA2^{TAM}$ band as well as the g*MFA2* band. Analysis carried out for both WT**a** TAM and WTα TAM cells. **(B)** Graphical representation of the relative copy number of TAM, obtained from three biological repeats (Appendix II).

Analysis of the copy number assay shows that the TAM plasmid exists in 26-29 copies per cell in WT**a** TAM and WTα TAM cells. A slight variation was seen across biological repeats, as indicated by the error bars, however, no substantial difference ($p>0.01$, Appendix II) was seen in the copy number properties of the

transformed TAM plasmid, suggesting that the plasmid is stable, and able to replicate along with the cell cycle. The extent of multiplicity was lower than expected from the original TRP1R1 circle plasmid studies, however, the addition of the *MFA2* region acted to double the size of the plasmid, and may go some way to explain the reduction in copy number. The resulting copy number will still allow for high resolution repair analysis to be carried out without extraction of the plasmid from the total cellular DNA.

Transcriptional regulation

As *MFA2* is an **a**-mating type specific gene, it is actively transcribed in **a** cells, and repressed in α-mating type cells. This property of the gene makes it an ideal model in which to study NER. As the transcriptional regulation of *MFA2* is well documented, it was important to discover whether this regulation still exists when the gene is in a plasmid context.

In order to look at the transcriptional regulation, a total RNA prep was carried out on PSY316**a** TAM and PSY316α TAM cells, following the protocol described in Chapter 2. This total RNA was then run on a FA gel, ensuring that the loading was consistent between samples. The gel was then blotted overnight in 10 x SSC, and the membrane was probed using a radio-labelled probe to detect *MFA2* mRNA. These levels could then be quantified using actin as an internal control, to look at the relative levels of *MFA2* mRNA.

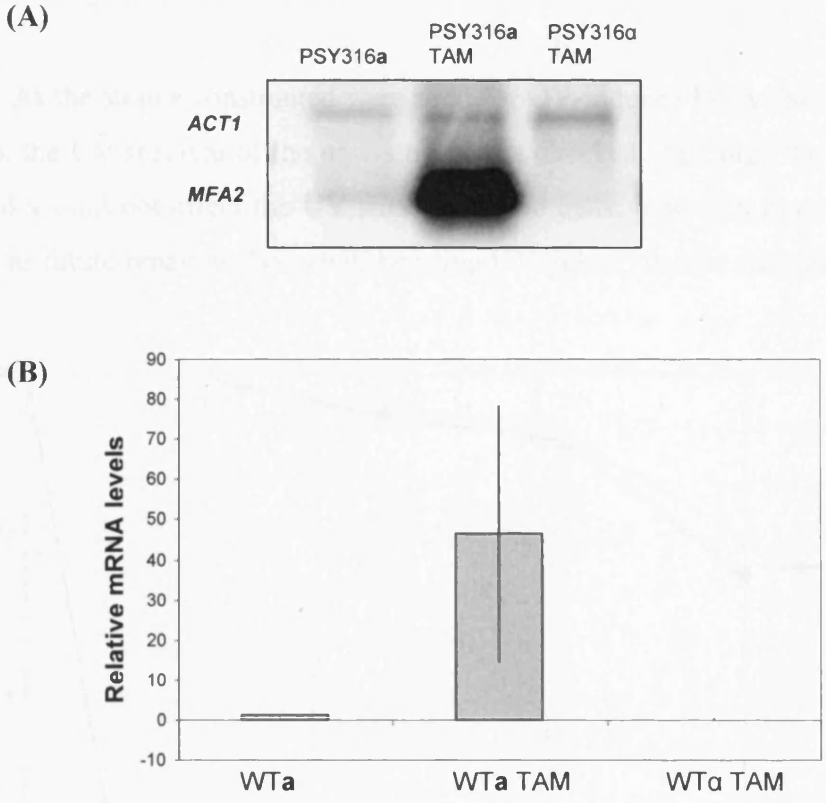

Figure 3.13: Northern blot analysis utilising a radio-labelled probe for *MFA2* mRNA. **(A)** Northern blot membrane, probed for *MFA2* mRNA, and *ACT1* mRNA. Actin is displayed as a loading control. The relative mRNA levels were detected in WT**a** cells, alongside WT**a** TAM and WTα TAM cells **(B)** Graphical representation of the Northern blot, bands quantified using Imagequant software from three repeats (Appendix II).

The relative levels of *MFA2* mRNA showed an increase in the TAM-transformed **a** cells, compared with the WT**a** cells. With the data normalised to show the level of mRNA in WT**a** cells as 1, there was approximately 64 times increase in the plasmid containing strain. These data shows that the *MFA2* gene within the plasmid context is being transcribed. In WTα TAM cells, no significant levels of *MFA2* mRNA were detected.

UV sensitivity of the WT strains

As the strains constructed were used for UV-induced DNA damage and repair studies, the UV survival of the new strains was checked. Although the presence of a plasmid should not effect the UV survival of the cells, it was an important factor to assess, as future repair analyses will be using UV light to induce damage.

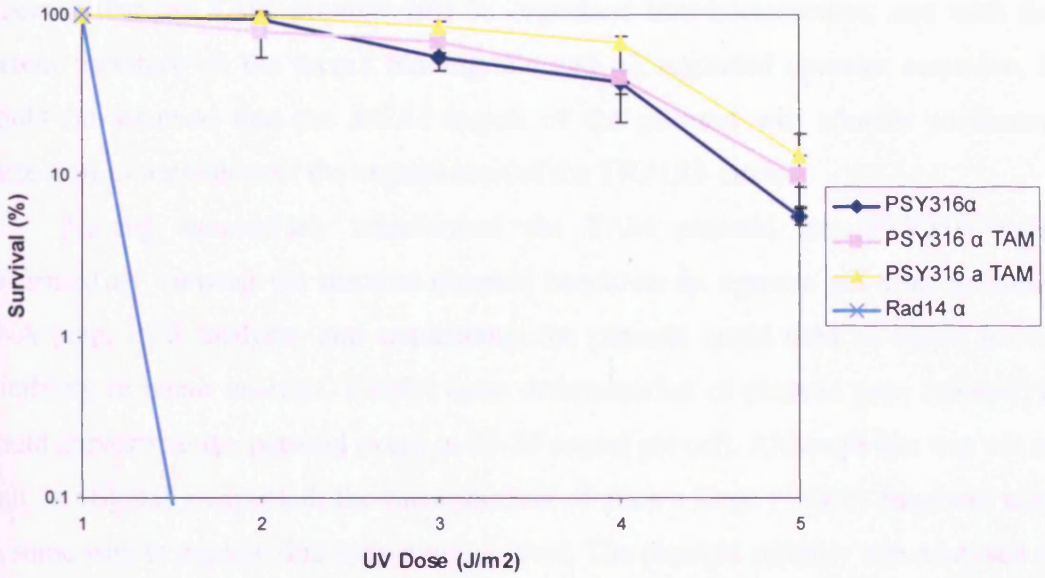

Figure 3.14: UV survival. Cells were plated onto selective plates, allowed to air dry, then treated with increasing doses of UV light. After 3 days growth colonies were counted, and UV survival recorded as a percentage. TAM-containing WT**a** and WTα cells were studied alongside WTα cells for comparison. *RAD14* is an essential NER protein, which when deleted confers a highly UV sensitive phenotype (Appendix II).

The presence of the TAM plasmid failed to affect the UV sensitivity and survival of the PSY316 strains transformed.

3.4 Discussion

The TAM plasmid was successfully constructed, and contained *MFA2* as a model gene to study NER in a chromatin context. The TRP1-R1 yeast plasmid vector was selected for use due to multiple factors. Firstly, TRP1-R1 is a yeast multiple copy number plasmid, allowing experiments to be undertaken using smaller volumes of

culture, and eliminating the need to extract the plasmid from the genomic DNA to analyse the repair of the plasmid borne *MFA2* gene. The multiple copy number properties can be attributed to the presence of the ARS1 sequence, allowing extra-chromosomal maintenance of the plasmid DNA. TRP1-R1 also contains the *TRP1* gene, allowing for selection in a tryptophan negative background.

Many plasmid models, including TRP1-R1 and its already documented derivative plasmids, have thus far been utilised for the study of chromatin biology, and shown to contain discretely positioned nucleosomes. With this in mind, it was expected that the TAM plasmid will be organised into nucleosomes, and with the current literature on the mcm1 binding site and α2 regulated operator sequence, it would be assumed that the *MFA2* region of the plasmid will contain positioned nucleosomes regardless of the organisation of the TRP1R1 circle.

Having successfully transformed the TAM plasmid into PSY316 cells, confirmed by viewing the discrete plasmid bands on an agarose gel after genomic DNA prep, PCR analysis, and sequencing, the plasmid could then be tested for its suitability in repair analysis. Firstly, upon determination of plasmid copy number, it would appear that the plasmid exists in 27-29 copies per cell. Although this was not as high as originally expected, the incorporation of such a large (1.5Kb) fragment may go some way to explain this copy number level. The plasmid stability was analysed at various stages of growth, and the variation in copy number remained low.

One of the attractive qualities of the *MFA2* gene is the fact the transcriptional regulation of the gene is understood. As *MFA2* is an **a**-mating type specific gene, it is transcriptional active in yeast mating type **a** cells, and repressed in α cells. Not only will this provide a model in which transcriptional activity can be examined with respect to repair, but it is known that an active gene exists in a more open chromatin conformation, than a repressed gene with a repressive chromatin structure. It was therefore necessary to find out whether the TAM borne *MFA2* gene was under the same transcriptional control as seen at the endogenous *MFA2*. In this system, *MFA2* is transcribed in wild type **a** cells, and transcriptionally repressed in α cells, as shown by northern blotting. This confirms that the TAM borne *MFA2* can be used for analysis of repair in two different transcriptional states.

Nucleotide excision repair is responsible for the correction of multiple types of unrelated, bulky lesions. With an increase in UV induced skin cancers in the general

population, and defects in the NER pathway exemplified by the UV-sensitive Xeroderma Pigmentosum disorder, UV light provides an ideal damage induction tool. UV light can be experimentally obtained from germicidal lamps, and induces characteristic structural DNA lesions. As described in Chapter 1, mutants for factors indispensible for NER display a high degree of UV sensitivity, with wild type cells generally able to repair DNA damage, and show no UV sensitive phenotype. On transformation of the TAM plasmid into WT cells, the UV survival was monitored to ensure the presence of the plasmid did not affect the cells ability to deal with UV damage. As very little difference was detected between the strains I concluded that the UV survival was not altered due to the incorporation of the plasmid into PSY316 cells.

The construction of the TAM plasmid creates a chromatinised vector with potential for *in vivo* and *in vitro* studies into NER. The employment of a characterised gene in a reconstituted repair system will prove advantageous for the progression of the field. TAM replicates along with the yeast genome, maintaining a multiple copy phenotype. TAM borne *MFA2* displays the same transcriptional regulation as displayed in the genomic copy of *MFA2*, an essential factor for the use of TAM as a model plasmid. Finally, it has been shown that the presence of TAM does not have an adverse effect on the UV survival of the strains studied, providing a system which can be used for the investigation of UV-induced damage repair.

Chapter 4

Nucleotide Excision Repair and chromatin structure of the TAM plasmid

4.1 Introduction

As considered in Chapter 1, the rate of NER is heterogeneous throughout the genome and can be divided into two pathways TC-NER and GG-NER. Previous studies into repair, including global studies, and at the level of individual genes has seen the distinct modulation of repair across the genome. The discovery of two sub-pathways in NER has shed light not only on the role transcription plays in promoting efficient NER, but has also implicated chromatin as a cellular mediator of the repair mechanism. As repair is to be analysed in the TAM borne *MFA2* gene, this chapter will focus on the properties which afford repair at the endogenous *MFA2* and will uncover the repair profiles of *MFA2* within a plasmid context. This complex repair analysis can then be coupled with nucleosome positioning data to provide a detailed overview of the role the chromatin plays in the NER of *MFA2*.

Repair of the endogenous MFA2

Investigations into repair at the level of the gene in *S. cerevisiae* showed that the *RPB2* gene borne on a centromeric plasmid was repaired preferentially in the TS than the NTS, as well as at its chromosomal location. The faster repair in the TS was shown to be dependant on transcription. This early study validated the use of plasmids to study NER and transcription (Sweder and Hanawalt 1992). The strand specific repair was confirmed in the *GAL7* gene, where active transcription was necessary for faster repair; when the gene is inactive no preferential or strand-selective repair was observed (Leadon and Lawrence 1992). NER has also been shown to have an inducible component, with a pre-irradiation step aiding the repair of both the MATα

and the HMLα loci (Waters et al. 1993), and this inducible repair is confined to the G1 phase of the mitotic cell cycle (Scott and Waters 1997).

These studies at the level of the gene into *RBP2* and *GAL7* both show a difference in repair between the transcriptionally active strand versus the non-transcribed strand, however, control of transcription at these genes does not involve changes in chromatin structure associated with the transcriptional status of the mating type loci (Jones et al. 1992).

To study the effects of chromatin-mediated transcriptional regulation on NER, the *MFA2* gene was employed, as a gene regulated by the presence of an upstream α2 operator sequence. The concerted actions of Mcm1, α2, the general repressor proteins Ssn6-Tup1 and histone deacetylaces provide a repressed gene in α mating-type cells. *MFA2* is transcriptionally active in mating-type **a** cells, displaying a de-repressed chromatin structure (reviewed in Chapter 3).

RNA polymerase II transcribed genes appear to have a stereotypic region of transcription enhanced NER. The work carried out by (Teng et al. 1997) showed the boundaries for this enhancement of repair at the *MFA2* gene. Not only is the actual transcribed region repaired quicker than the non-transcribed region, but the promoter region of the active gene appears to be repaired at a faster rate also (Figure 4.1). This would suggest that the chromatin environment afforded by the presence of transcriptional machinery provides a DNA structure which is more accessible to NER factors.

Not only can *MFA2* be studied with respect to transcriptional status, but it is also possible to look at the effects of the rate of transcription. It has been shown that enhanced transcription of *MFA2* can be induced in **a** cells by the addition of α mating factor. This stimulates the binding of Ste12 protein to pheromone response elements in the upstream promoter region of *MFA2* (Dolan et al. 1989). It is possible that repair in a chromatin-regulated transcription region does not simply exist as an 'open' or 'closed' chromatin conformation, but a variety of chromatin species in between. These would be dependant on whether the gene has been primed for transcription and the relative level of transcription.

As described in Chapter 1, most NER proteins are shared by the GG-NER and TC-NER pathways. In mammalian cells, Cockayne syndrome (CS) group A (CSA) and B (CSB) proteins have been shown to be specifically required for TC-NER, but not for GG-NER (van Hoffen et al. 1993). A gene homologous to human CSB has

been designated *RAD26* in yeast and its absence results in impaired repair of the TS of the active *RPB2* gene (van Gool et al. 1994). Rad26 was shown to be required for efficient repair of the elongation stage of RNA polymerase II transcription (Tijsterman et al. 1997) and in the efficient repair of the transcription initiation region of *MFA2* (Teng and Waters 2000). These results for the *MFA2* gene support the hypothesis that Rad26 is required for the interchange between holo-TFIIH and a putative repairosome containing TFIIH and NER factors. There appears to be further sub-pathways within TC-NER, one requires Rad26, and the other requires the nonessential subunit of RNA polymerase II, Rbp9. Whereas the Rad26 subpathway initiates upstream of the transcription initiation site, and throughout the coding region, the Rbp9 subpathway appears to act more efficiently in the coding region (Li and Smerdon 2002). Thus simultaneous deletion of the *RBP9* and *RAD26* genes completely abolishes TC-NER in both the coding and upstream regions.

TC-NER is therefore mediated by either Rad26 or Rpb9 subpathways, and when deleted, repair in RNA polymerase II genes is dependant on the GG-NER pathway. In *S. cerevisiae*, Rad7 and Rad16 proteins, which form the GG-NER complex along with the essential Abf1 protein, have been shown to be essential for repairing non-transcribed regions of the genome, but dispensable for TC-NER (Reed et al. 1999; Terleth et al. 1990; Verhage et al. 1994). Rad16 is a member of the Swi2/Snf2 superfamily of chromatin remodelers, and in its heterotrimeric complex with Rad7 and Abf1 has been shown to generate superhelicial torsion required for the excision stage of the NER mechanism (Yu et al. 2004). Rad7 and Rad16 are also components of an E3 ubiquitin ligase complex (Ramsey et al. 2004), acting to regulate the general activity of repair factors by controlling the cellular levels of Rad4 (Gillette et al. 2006). Rad16 also has a novel function in mediating the UV-dependant histone H3 acetylation at *MFA2* (Teng et al. 2008) by controlling the occupancy of the histone acetyltranferase Gcn5 (Teng, unpublished data). It can be speculated that Rad16s inherent ATPase activity may result in UV-induced chromatin rearrangement which favours the binding of Gcn5, and subsequent acetylation. TC-NER mediated by Rad26 and Rbp9, and GG-NER mediated by Rad16 appear to be the only NER pathways which exist, at least at the *GAL1-10* region studied (Li and Smerdon 2004).

The *MFA2* gene has been fundamental in developing the relationships between various NER factors in both TC-NER and GG-NER. *MFA2* displays the characteristic repair profile of enhanced repair in the upstream promoter and coding region of the

actively transcribed gene, and slower repair in the NTS of the active gene, along with the repressed gene (displayed in Figure 4.1). The chromatin structure of the vector I have employed and that of the endogenous *MFA2* are explored below.

4.1.1 Chromatin structure and repair

Nucleosome mapping in TRP1RI

Originally identified as a DNA sequence which could form a recombinant plasmid, the TRP1 RI circle was shown to replicate along with chromosomal DNA. Using micrococcal nuclease digestion assays, nucleosome size and spacing within the plasmid were shown to be indistinguishable from that of nucleosomes in bulk yeast chromatin (Zakian and Scott 1982). The chromatin structure of the plasmid was shown to be stable between multiple copies, and after purification as chromatin (Pederson et al. 1986). Seven nucleosomes were shown to present across the plasmid, with an alternative model dismissed (Long et al. 1985), confirmed by micrococcal nuclease mapping data using indirect-end labelling, direct morphological observations of purified plasmid and analysis of linking-number change (Pederson et al. 1986; Thoma et al. 1984). The TRP1 RI plasmid was utilised as a model to investigate the role of α2 operator sequences, and it was shown that α2 causes a positioning of nucleosomes over sequences proximal to its operator in TRP1/ARS1 chromatin (Roth et al. 1990). The active *URA3* gene has also been incorporated into the TRP1 RI circle, creating the TRURAP plasmid. In this system, containing 14 nucleosomes, modulation of repair was seen, which correlated with both gene expression and nucleosome stability (Smerdon and Thoma 1990). This plasmid was also shown to contain sufficient chromatin structure *in vivo* to reflect the repair of genomic chromatin, of both WT and *rad* mutants (Smerdon et al. 1990).

The mapping of nucleosomes in the TRP1 RI plasmid, and the subsequent use of this plasmid to study active genes with respect to chromatin structure and repair suggest that the incorporation of *MFA2* should not alter the chromatin structure of the α2 regulated *MFA2* gene promoter. Previous studies, however, have suggested that the incorporation of additional DNA and therefore chromatin structure may act to alter the nucleosome positions found within the parental TRP1 RI circle (Thoma 1986). It is thought that nuclease sensitive sites act as boundaries to position

nucleosomes, with the positioning of nucleosomes across *TRP1* gene seen to alter in different plasmid constructs (Thoma 1986). The size, sequence and subsequent chromatin folding of the plasmid may also prove to regulate the positioning of nucleosomes (Thoma and Zatchej 1988).

Nucleosome mapping in *MFA2*

Nucleosomes are placed in an ordered array covering the promoter region and extending into the structural gene within **a**-specific genes in α cells (Shimizu et al. 1991). This positioning of nucleosomes is thought to prevent the formation of a pre-initiation complex, a pre-requisite for transcription (Roth et al. 1992). The location of the TATA box within a nucleosome region was thought to aid repression of *MFA2*, however it was shown that this repression was independent of where the TATA box resided, even in the linker region, suggesting that nucleosomal organisation is not dictated by promoter sequence (Patterton and Simpson 1994). The placement of nucleosomes is not the only level of chromatin repression; non-covalent histone modifications also play a substantial role. The de-repression of transcription in certain **a**-specific genes has been shown as a result of deleting histone H4 N-terminal tails (Roth et al. 1992; Shimizu et al. 1991).

A high resolution approach to mapping of nucleosomes across the *MFA2* gene was developed (Teng et al. 2001), positioning four nucleosomes across *MFA2* and its upstream control region when transcription is repressed, in α cells (Figure 4.1). These nucleosomes lose their positioning when the gene is active, in **a** cells. MNase hypersensitive sites were also reported in the α2 operator region of *MFA2* in α cells but not **a** cells, presumed to occur as a result of change in local chromatin conformation, possibly due to protein binding.

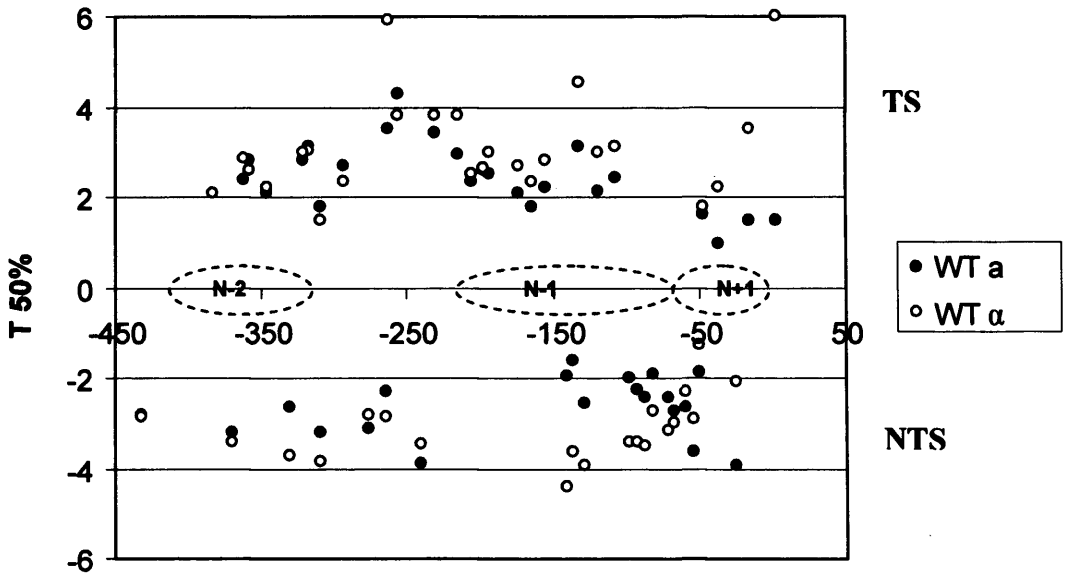

Figure 4.1: Repair profile of endogenous *MFA2*, when transcriptionally active (a cells) and repressed (α cells). The data is displayed as the time it takes to repair 50% of CPDs at a specific nucleotide position. The transcribed strand (TS) and non-transcribed strands (NTS) are displayed above and below the x-axis respectively. Dashed eclipses represent positioned nucleosomes. Adapted from (Liu 2005; Teng et al. 2001) (Appendix III).

4.2 Materials and methods

Any methods which are not detailed below can be found in Chapter 2.

4.2.1 Yeast Strains

PSY316 *(MATα ade2-101 ura 3-52 leu 2-3, 112 Δhis 3-200 lys2 trp1)*

PSY316 *(MATa ade2-101 ura 3-52 leu 2-3 112 Δhis 3-200 lys2 trp1)*

4.2.2 High resolution repair analysis of CPDs

To determine the relative rate of repair in the TAM borne *MFA2* promoter region, high resolution repair analysis was carried out, revealing the repair characteristics at nucleotide resolution. The high resolution method developed was based on that reported by (Li and Waters 1996), but modified so that the reference

sequences were obtained via Sanger as opposed to Maxam & Gilbert sequencing (Teng et al. 1997). Whereas previous global studies have provided generalised repair phenotypes of NER-related factor mutants, the employment of high resolution analysis has revolutionised the repair field, generating much data in terms of chromatin structure, DNA-binding proteins, and effects of DNA rotation.

As described in Chapter 2, the high resolution repair analysis briefly comprises UV irradiation of cells, ensuring a sample is retained for an untreated control. After UV cells are allowed to repair for various time points. The cell walls are then removed, and the total DNA extracted from the spheroplasts. Upon digestion with a specific restriction endonuclease, a fragment containing the region of interest is generated. Damage is detected and cut using the CPD specific enzyme *ML endonuclease*, and the resulting fragments are subject to an end-labelling procedure using Dynabead technology and a radiolabelled dATP-based sequencing reaction (Teng et al. 1997).

Primers for high resolution probe construction

HaeIII1*: BIOTIN-GATAGCTTTTTTCCCTCATCTATTTTCTCGGAAAACT TGGTG

HaeIII2*: BIOTIN-GATAGCTTTTTTCCCTTGATTATATAGATTGTCTTTCT TTTCAGAGGAT

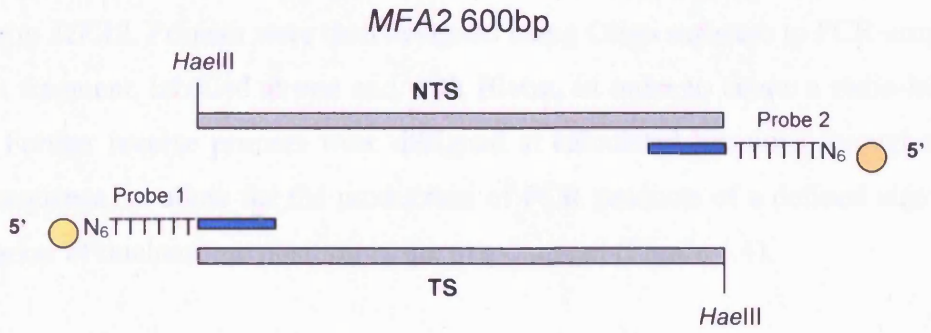

Figure 4.2: Probes 1 and 2 are complementary to the 3' ends of the TS and NTS respectively of the *MFA2* containing *Hae*III-*Hae*III fragment. This restriction fragment contains the *MFA2* promoter region. Each probe has an overhang of a hexad T, then a 5' biotin (●) -hexad N with no 3' dT. *Hae*III restricted DNA is denatured and annealed to probe 1 or 2 to isolate *MFA2* TS or NTS. These fragments can then be separated using Streptavidin coated Dynabeads which bind the biotin.

The beads, and consequently the bound sequences are retained in an eppendorf by placing a magnet alongside the tube whilst non-bound DNA is washed away. The *MFA2* fragments are then end-labelled with exactly six radiolabelled dATP molecules using DNA polymerase. These labelled fragments are eluted from the beads and separated on a DNA sequencing gel (see Chapter 2.11).

4.2.3 Nucleosome mapping

i) Low resolution nucleosome mapping

To map nucleosomes across the TAM plasmid, a MNase-directed assay was chosen. MNase preferentially cuts the linker regions between nucleosomes, to provide information on position and stability of nucleosomes. It is presumed that by employing a limited MNase digestion, that the partial accessibility to MNase accurately reflects the DNA accessibility.

Firstly, a restriction enzyme was chosen, unique within the TAM plasmid sequence, and when employed, would cut the plasmid once, linearising the DNA. This unique restriction site was chosen to be at least 500bp upstream from the *MFA2* operator region of the plasmid, to ensure that the *MFA2* region could be visualised on

the final gel. *Bgl*II restriction endonuclease was chosen, displayed in Figure 4.3 in relation to *MFA2*. Primers were then designed using Oligo software to PCR-amplify a dsDNA fragment, labelled at one end with Biotin, in order to create a radio-labelled probe. Further reverse primers were designed at calculated locations throughout the TAM sequence, to allow for the production of PCR products of a defined size to act as a marker of nucleosome position in the mapping gel (Figure 4.4).

Low resolution nucleosome mapping probe design:

BglMap_For AATGCTAAATCATTTGGCTTTTTGATTG

BglMap_Rev* BIOTIN-CAAGAAAATGATTACGAGGATACGGAGA

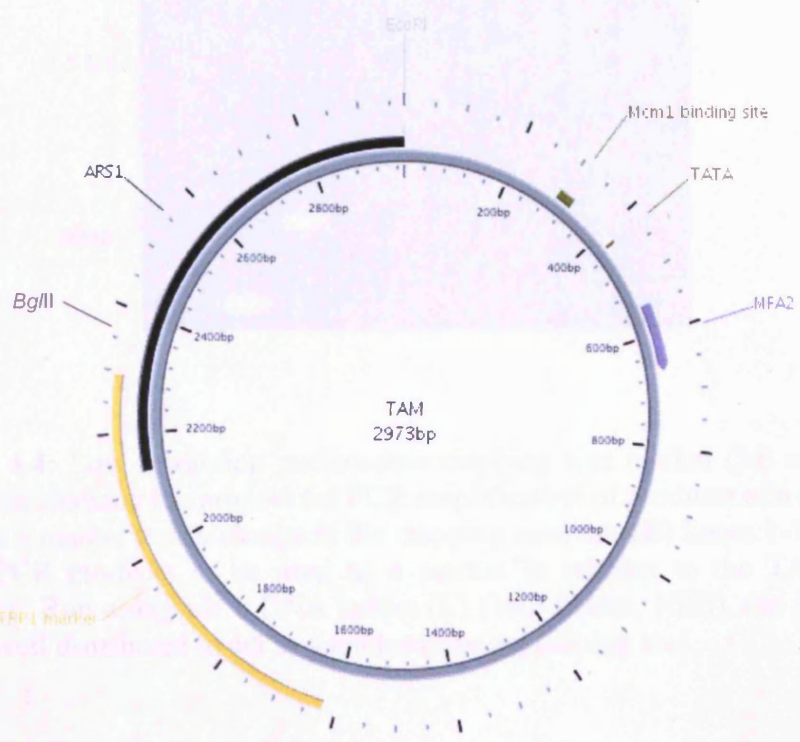

Figure 4.3: Schematic of the TAM plasmid, with the unique *Bgl*II restriction site designated position 1. *Bgl*II was chosen as the restriction endonuclease to linearise the plasmid due to its recognition sequence proximity to the *MFA2* region of interest.

(A)

Primer	Sequence	Resulting PCR product (bp)
BglMap_For	AATGCTAAATCATTTGGCTTTTTGATTG	
Lad_Rev1	CAAGAAAATGATTACGAGGATACGGAGA	240
Lad_Rev2	TGTTAAAATAGTGAAGGAGCATGTTCGG	555
Lad_Rev3	TGAACGACAGAAGAAGTGGATGGAAATA	1038
Lad_Rev4	CTGGCTCAAAACTTTTTCACTTTTACGA	1569
Lad_Rev5	ACGATGCTAATTACGAAGAGGATGATGA	2045
Lad_Rev6	CTTTTAATAACTGGCAAACCGAGGAACT	2538
Lad_Rev7	GCAGGCAAGTGCACAAACAATACTTAAA	2906

(B)

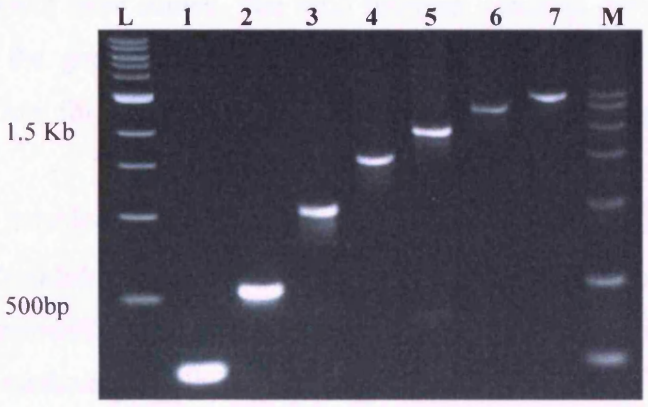

Figure 4.4: Low resolution nucleosome mapping size marker (M) construction. **(A)** Table showing the primers for PCR amplification of products of a defined size to act as a marker to run alongside the mapping samples. **(B)** Lanes 1-7 display the seven PCR products to be used as a marker in relation to the TAM plasmid sequence. Run alongside a DNA ladder (L) (1Kb ladder, NEB), the final marker (M) is well distributed to act as a nucleosome positioning tool.

ii) High resolution nucleosome mapping

Mapping nucleosomes at nucleotide resolution uses the same technology as the high resolution CPD analysis. The previously MNase treated chromatin samples are extracted following the protocol described in Chapter 2.12, then subject to restriction enzyme digestion. The *Hae*III restriction endonuclease was once again chosen to allow the same region of the plasmid to be analysed in terms of both repair

and nucleosome position. Following digestion, the fragments are collected using the probe procedure, end-labelled and run on a sequencing gel.

4.3 Results

4.3.1 Utilising TAM for NER analysis

The elegant high resolution DNA damage repair technology developed by (Teng et al. 1997) will be the main technology used throughout this study. Due to the multiple copy number properties of the TAM plasmid, the aim was to perform total DNA preparations with the appropriate strains, from a smaller number of yeast cells to obtain sufficient gene copies. The ratio between genomic *MFA2* and TAM borne *MFA2* allows the genomic copy to be statistically discarded. The multiple copy number will allow for a reduction in culture volumes required, saving both time and consumables.

Having established that the UV survival rates of the plasmid containing strains are significantly similar to the WT strains (see Chapter 3), it was decided to proceed with UV experiments, treating cells with 254nm UV light at a dose of $100J/m^2$. Following the methods described by (Teng et al. 1997), 2×10^{10} exponential phase yeast cells are grown in appropriate media and subsequently resuspended at 2×10^7 cells/ml in chilled PBS for the UV irradiation step. Following this method 4×10^8 cells are used per sample, resulting in 30μg of DNA isolated for each sample and used for analysis. As the TAM plasmid exists in multiple copies within the cell, it was decided to reduce the volume of starting culture and begin with 2×10^7 exponential phase yeast cells. Using only a fifth of the starting cell number, the cell amount is again reduced in subsequent steps, resulting in 2.4×10^7 cells used per sample. The steps employed result in a 16.67 times reduction in cell number and therefore in cellular DNA (See Chapter 2.11 for details).

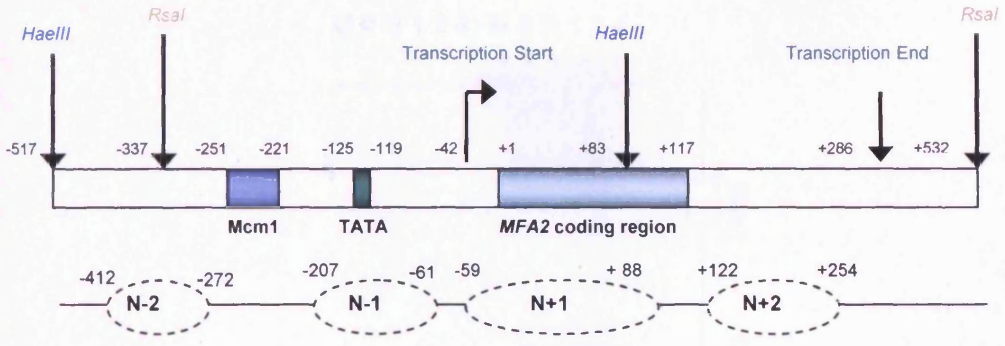

Figure 4.5: Map of the *MFA2* region, including the *Hae*III restriction sites utilised here in high resolution repair and mapping analysis. Displayed below are the nucleosome positions as mapped in the repressed endogenous *MFA2* by (Teng et al. 2001).

The *Hae*III restriction fragment of *MFA2* was initially chosen to study NER in the TAM borne *MFA2* gene. This restriction fragment encompasses the promoter region of *MFA2*, as shown in Figure 4.5. As previously mentioned, the TC-NER and GG-NER mediated repair have clearly been seen in this region of the endogenous *MFA2*.

In order to confirm the viability of a multiple copy number plasmid in high resolution studies, the repair protocol was carried out using cells with and without the presence of the TAM plasmid (Figure 4.6).

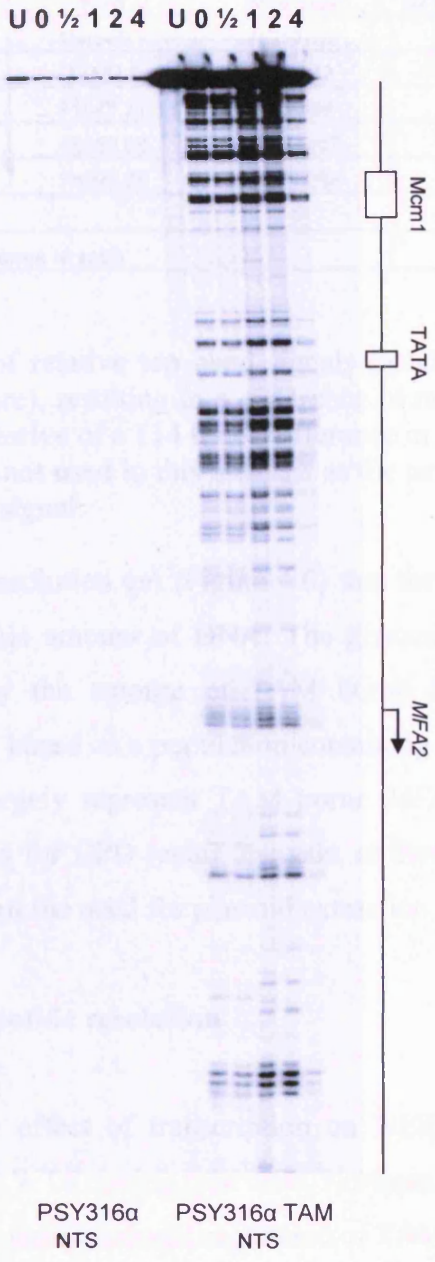

Figure 4.6: A typical high resolution CPD repair analysis of PSY316α (WT) and PSY316α TAM strains. Using ~1.8μg DNA per sample, DNA was loaded onto the gel for repair analysis. Due to the large reduction in DNA amount in the WT strain, very little signal is detected. The presence of TAM allows significant amount of signal to be seen.

	WTα	WTα TAM	WTαTAM / WTα
U	194345.1	10327025	53.13755
0	72462.9	5560942	76.74192
0.5	71047.71	5404499	76.06859
1	48259.88	10017407	207.5721
2	75299.25	11938268	158.5443
Average difference in ratio			**114.4129**

Table 4.1: Table of relative top band signals (band intensity obtained using Imagequant software), resulting in a difference in ratio between WT and WT TAM of 114, suggestive of a 114 times difference in *MFA2* DNA amount. The 4 hours repair was not used in this analysis as the neighbouring band intensity interfered with the signal.

It is clear from the high resolution gel (Figure 4.6) that the genomic *MFA2* signal is hardly detected loading this amount of DNA. The genomic copy of *MFA2* can be significantly overcome by the amount of TAM borne *MFA2*, and although the resulting CPD data will be based on a population containing endogenous *MFA2*, it can be said that these data largely represent TAM borne *MFA2*. This verifies that the TAM plasmid can be used for CPD repair analysis, at these levels of DNA amount (1.8μg/sample), and without the need for plasmid extraction from the cell.

4.3.2 CPD repair at nucleotide resolution

To investigate the effect of transcription on NER, the TAM plasmid was transformed into WTa and WTα mating type cells. Northern blotting of *MFA2* mRNA (Chapter 3) shows that the transcriptional regulation of TAM borne *MFA2* is the same as found in the endogenous gene. *MFA2* is highly transcribed in the plasmid context in WTa cells. Repair in the *MFA2* promoter region of TAM, using the *Hae*III restriction endonuclease fragment is displayed in a high resolution gel below. The *Hae*III fragment encompasses the promoter region of *MFA2*, including the upstream Mcm1p binding site and TATA box, and the positions of these regions are indicated alongside the gel.

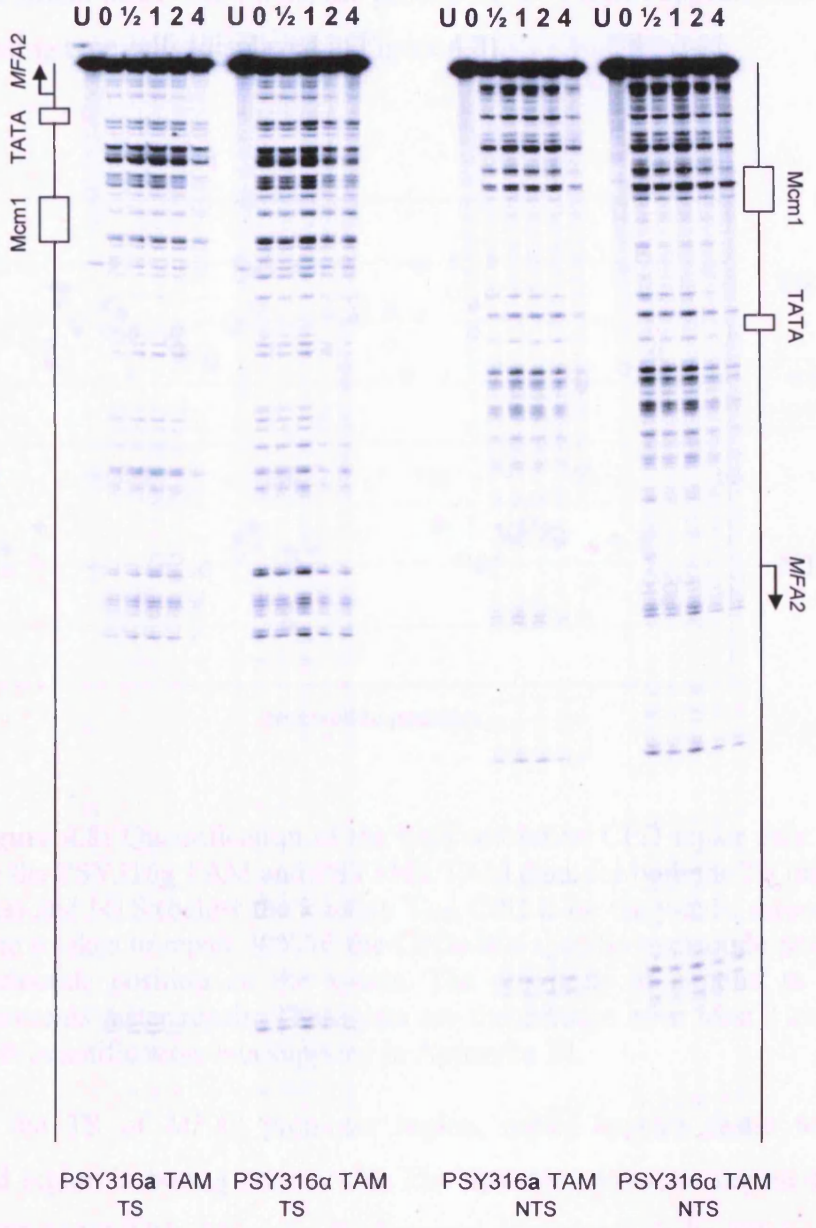

Figure 4.7: A typical gel image of high resolution CPD repair in PSY316a TAM and PSY316α TAM cells. The cells were subjected to 100J/m^2 UV light and allowed to repair for various time points (U: untreated, 0, 0.5, 1, 2, 4 hours repair) in YPD at 30°C. DNA was isolated and digested with *Hae*III, and cleaved specifically at CPD sites using *ML endo*. The purified DNA fragments were end-labelled with [α-^{32}P]dATP and resolved by electrophoresis on a polyacrylamide gel. Displayed are the gels showing the transcribed strand (TS) on the left and non-transcribed strand (NTS) on the right.

The band intensities were quantified using Imagequant software, and the time it takes to repair 50% of CPDs at a specific dinucleotide ($T_{50\%}$ CPD) was subsequently

calculated. With the transcribed strand represented above the x-axis and the non-transcribed strand below the x-axis, the general trend of repair appears similar in both **a** and α mating type cells (displayed in Figure 4.8).

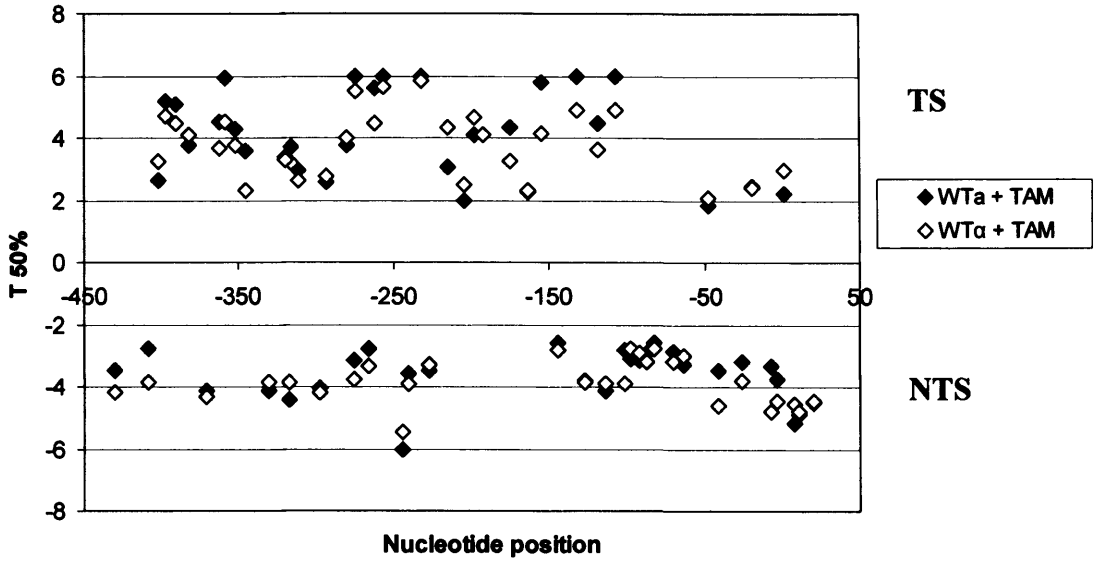

Figure 4.8: Quantification of the high resolution CPD repair gels. Displayed are the PSY316**a** TAM and PSY316α TAM data, for both the TS (above the x-axis) and NTS (below the x-axis). $T_{50\%}$ CPD is on the y-axis, representing the time it takes to repair 50% of the CPDs at a specific nucleotide position, with nucleotide position on the x-axis. The proximity of a point to the x-axis represents faster repair. These data are the average of at least 3 experiments, with quantification data supplied in Appendix III.

In the TS of *MFA2* promoter region, repair appears faster towards the transcribed region in both **a** and α cells. The upstream promoter region displays no great difference ($p>0.01$, Appendix III) between repair rates in the two mating types, suggesting that the transcriptional activity of the *MFA2* gene does not appear to have a great effect on the repair of CPDs in the region studied. Of particular interest, repair in the NTS is generally the same in both mating types. These results are suggestive of a difference between the plasmid borne *MFA2* and genomic *MFA2*, where a distinct difference between TC-NER and GG-NER can be distinguished (see Figure 4.1), resulting in a relative change in the repair phenotype.

4.3.3 Nucleosome mapping in *MFA2*^{TAM}

To link repair with chromatin structure, nucleosome mapping was carried out. The mapping technique involves the use of MNase enzyme, which cuts preferentially at nucleosome linker regions. Protected regions of 140-200bp are assumed to represent positioned nucleosomes.

As the transcriptional status of the TAM borne *MFA2* gene resembles that of endogenous *MFA2*, but the repair does not echo that seen in endogenous *MFA2* in the different mating types, it may be assumed that the chromatin environment of the plasmid borne gene is different from the endogenous gene situation. By analysing the nucleosome positions it may shed light onto this unexpected repair phenotype.

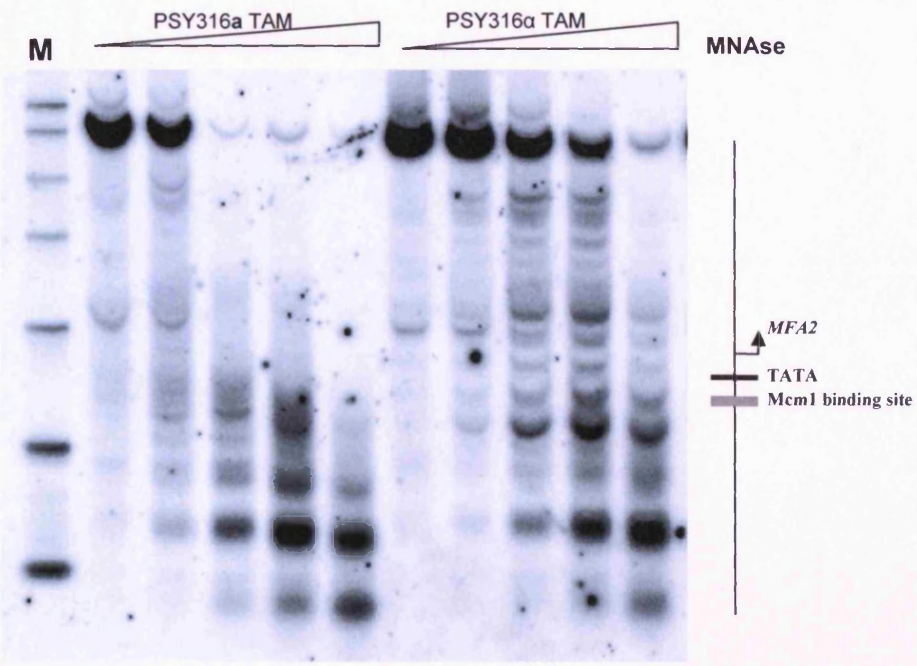

Figure 4.9: Low resolution nucleosome mapping in TAM in **a** and α cells. Limited digestion with MNase, combined with radiolabelled probe hybridisation allows for a nucleosomal ladder to be produced. A size marker (M) allows for the location of the *MFA2* coding region and upstream operator regions to be determined.

In Figure 4.9, it is shown that there is a loss of positioned nucleosomes across the TAM-borne *MFA2* promoter region in active cells compared with repressed *MFA2* (in WTα cells). The loss of nucleosome positioning can be seen upstream of the Mcm1 binding site, and also throughout the *MFA2* coding region. It also appears that the nucleosomes within the ARS1 region of the plasmid (represented by the farthest migrating bands) are subtly different between **a** and α cells.

These patterns in nucleosome positioning are as expected from the studies into endogenous *MFA2*. However, the previously noted differences in repair suggest there may be a further difference in the chromatin environment contributing to the result, and subtle differences in nucleosome position may not have been detected via the low resolution approach. To investigate nucleosome positioning further, a high resolution approach was undertaken. The high resolution CPD repair analysis can be modified to accommodate nucleosome mapping, to create nucleotide resolution MNase footprinting of nucleosomes (Figure 4.10).

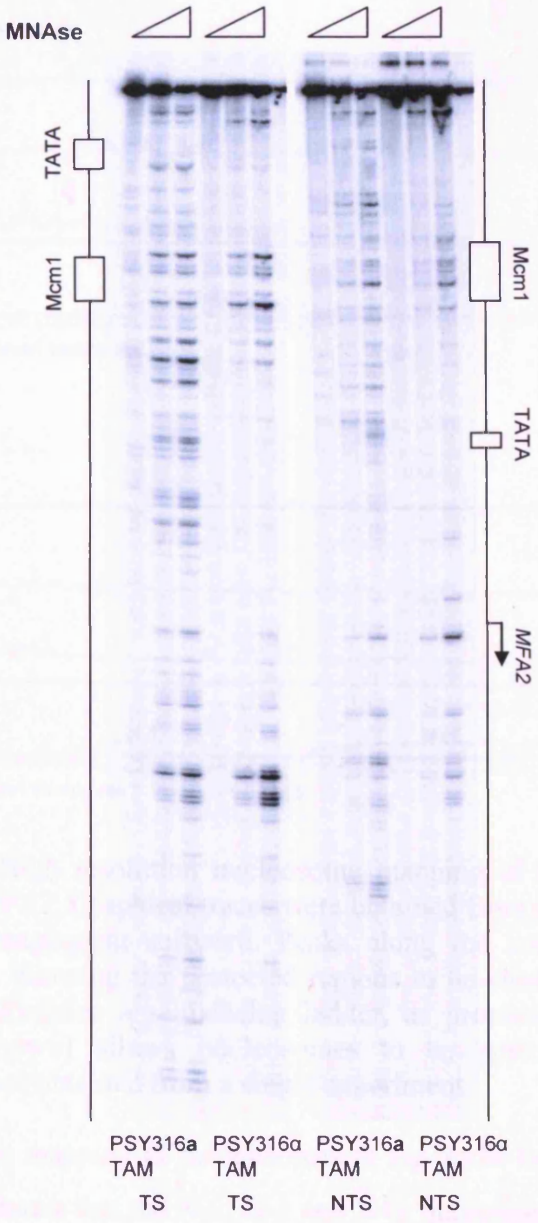

Figure 4.10: A typical high resolution mapping gel. Increasing amounts of MNase were utilised to produce a limited digestion. Bands are representative of MNase sensitive sites and nucleosomes can be positioned to regions of 140-200bp which are protected from MNase digestion in α cells with respect to the band distribution in **a** cells.

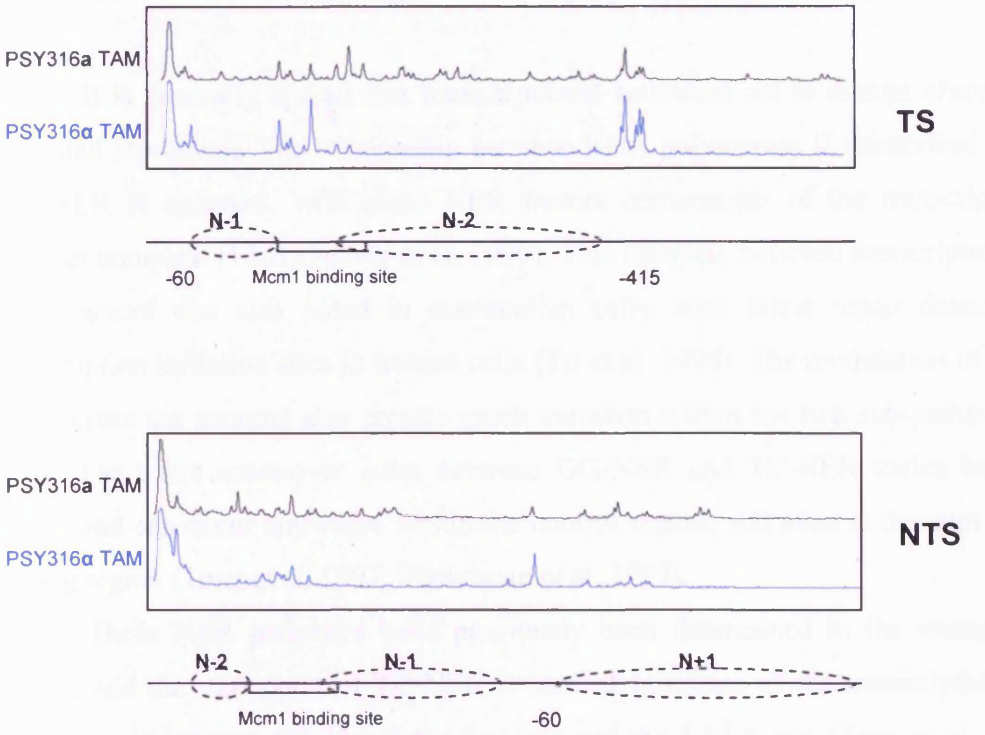

Figure 4.11: High resolution nucleosome mapping of the HaeIII region of TAM borne *MFA2*. Graphical traces were obtained from the gel image (Figure 4.10) using Imagequant software. Peaks along the trace represent MNase sensitive sites, allowing the protected regions to be clearly defined. Running the samples alongside a sequencing ladder, as previously used to position CPDs (not shown) allows nucleosomes to be positioned to nucleotide resolution. Trace obtained from a single experiment.

High resolution mapping of nucleosomes in the TAM borne *MFA2* promoter region (Figure 4.10) shows that the N-2, N-1 and N+1 nucleosomes are positioned in the same location as found at endogenous *MFA2* (N-2 (-412 to -272), N-1 (-207 to -61) and N+1 (-59 to +88)). MNase sensitive regions are found at the Mcm1 binding site, in both WT**a** and WTα cells, and also before nucleosome N-2 (-415) and between nucleosomes N-1 and N+1 (-60). Although this was expected from the literature, with α2 regulating nucleosome positioning, it remains surprising in the light of the difference in repair phenotype between genomic and plasmid *MFA2*.

4.4 Discussion

It is generally agreed that transcriptional activators act to disrupt chromatin-mediated repression. The relationship between RNA polymerase II transcribed genes and NER is apparent, with some NER factors components of the transcriptional initiator complex TFIIH (Feaver et al. 1999). This interplay between transcription and NER factors was also noted in mammalian cells, with faster repair detected at transcription initiation sites in human cells (Tu et al. 1996). The modulation of repair seen across the genome also creates much variation within the two sub-pathways of NER. The exact cross-over point between GG-NER and TC-NER varies between genes, and can occur anywhere within the control region, and even at the start of the coding region (Teng et al. 1997; Tijsterman et al. 1997).

These NER pathways have previously been determined in the endogenous *MFA2*, and the start point of TC-NER is located upstream of the transcription start site, lying in-between the Mcm1 binding site and the TATA box (Teng et al. 1997). With *MFA2* now incorporated into the TAM plasmid, analysis of the repair profile and nucleosome mapping is required to characterise the plasmid for use in repair studies.

Firstly, the plasmid's suitability within PSY316α for high resolution analysis of CPD repair was confirmed. By resolving nearly seventeen times less DNA on the polyacrylamide gels than previously carried out for WT strains, the signal displayed from the PSY316α WT strain was nearly undetectable. The CPD bands could hardly be seen, and this prevented any analysis to be carried out. The PSY316α WT strain containing TAM on the other hand displayed the CPD bands clearly. This reduction in yeast culture volume, and the subsequent amount of DNA used for each sample in the analysis allows the genomic copy of *MFA2* to be discarded. Although the genomic copy of *MFA2* is still present within the population of *MFA2 Hae*III fragments purified, it can be considered that all future high resolution analyses of *MFA2* are primarily of the TAM borne *MFA2*.

Having employed the high resolution technology to study the effect of transcriptional activity on the repair of the *MFA2* promoter region, it appears that in this system there is no significant difference between the rate of repair when *MFA2* is

active or repressed. CPD repair was expected to occur at a faster rate in the TS of the active gene, however it can be seen that in the plasmid context, the repair in the TS is very similar between that seen in **a** and α cells. Repair in both mating types appears to be enhanced at CPDs located in the TS near the *MFA2* coding region, suggestive of a more accessible chromatin structure. The NTS of both the active and inactive *MFA2* gene appear to be repaired again at a similar rate (Figure 4.12).

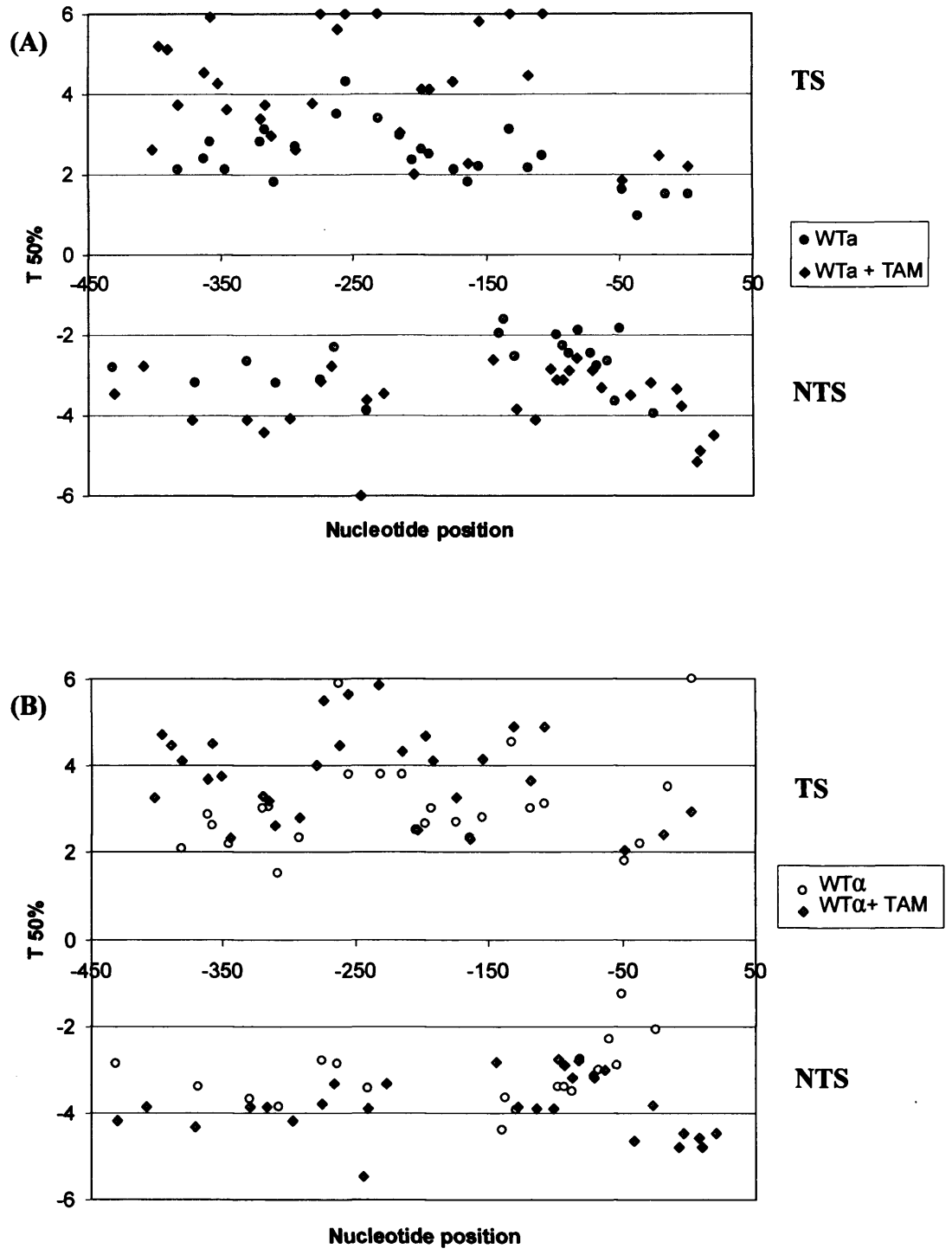

Figure 4.12: High resolution CPD repair analysis to show how repair in the endogenous *MFA2* gene equates to that seen in plasmid. **(A)** and **(B)** refer to the repair seen in WT**a** cells and WTα cells respectively. Data for the endogenous gene extracted from (Liu 2005)(Appendix II & III).

The nucleosome positioning across the plasmid was determined at low resolution, and combined with a high resolution approach, a marked difference between positioning within the *MFA2* promoter region in **a** and α cells was seen. As in the endogenous gene situation, nucleosomes appear to be positioned across the promoter and the gene at specific locations, supposedly dictated by the mcm1/α2 operator sequence. This distinct nucleosome positioning is lost when the gene is active, in **a** cells.

It appears that nucleosomes upstream of the *MFA2* gene, encroaching into the Trp1R1 circle region of TAM, are also in a different location compared to that recorded for the parental TRP1 RI circle. This has previously been displayed (Thoma 1986), and is thought to be dependant on multiple factors, including the proximity to MNase sensitive sites. As the determination of nucleosome position across the *MFA2* gene is regulated by the mcm1 operator sequence, it may influence the nucleosome positions of flanking regions, extending into the TRP1 RI. It has previously been shown that the ARS1 region contains a MNase hypersensitive region, and this is thought to be required for its role as an origin of replication, conferring maintenance of the multiple copy number plasmid. As the low resolution nucleosome mapping assay of the entire TAM plasmid utilised the *Bgl*II restriction enzyme, this produced a cut within the ARS1 region. Unfortunately, this results in the inability to accurately map nucleosomes and sensitive regions at the ARS1 location. Repeating the experiment using a different unique restriction enzyme, and subsequent primers at least 500bp upstream of this region would enable chromatin structure to be visualised for the ARS1 sequence. It is assumed, however, that the chromatin structure is retained in this region, as the plasmid is stable in multiple copy number. The region containing the ARS1 sequence does appear to have a slightly altered nucleosome positioning between **a** and α cells. This could be due to the difference encountered in the *MFA2* gene, having an upstream effect on the spatial arrangement of the nucleosomes. The *TRP1* gene must still be able to function, undisturbed by the change in plasmid conformation, as the strain shows no growth defect in selective media. Further analysis could be carried out to determine whether the *TRP1* gene is affected. High resolution mapping analysis of the entire plasmid may provide some insights.

It is becoming more apparent that the interactions of DNA and histone proteins alone are not the sole factors governing the 'chromatin environment'. The

exact positioning of nucleosomes in the promoter region of *MFA2* is not the principal factor in NER operating in this system. If this were the case, then the fact that nucleosomes are located at the same nucleotide positions in both chromosomal and plasmid DNA, would suggest that the repair profiles would be the same at both loci. Observations within the TAM system, however, prove otherwise, with an uncharacteristic repair profile seen in the TAM borne *MFA2* promoter. This suggests in its simplest form that differences must be apparent in the *MFA2* gene within the plasmid context compared with the gene within its genomic environment. There are multiple possibilities for these differences, with the most prominent outlined below.

a) Although nucleosomes are positioned in the repressed gene in the TAM plasmid, the nature of circular DNA provides a novel chromatin conformation, providing different challenges for the NER machinery as compared with those encountered at endogenous *MFA2*
b) The superhelicity of plasmid DNA provides, in this instance an unconventional DNA substrate, suggesting that the NER mechanism is affected at the level of DNA conformation rather than chromatin conformation
c) TAM chromatin is subject to different post-translational modifications, perhaps due to the requirements of the active *TRP1* gene, or the essential ARS1 sequence for plasmid maintenance, and these modifications present an epigenetic code favourable of the observed repair phenotype.

With repair at the repressed *MFA2* promoter region documented in this plasmid system, a model has been created to pursue repair analysis of *rad* mutants *in vivo* and *in vitro* to discover the effects of the chromatin environment on the NER mechanism.

Chapter 5

NER in a de-repressed chromatin environment, the effects of a Tup1p mutation

5.1 Introduction

Due to the highly ordered structure of chromatin, it is often seen to act as a repressive barrier to cellular processes, such as transcription and repair. To overcome this cellular hurdle multi-protein regulators such as RSC and Swi-Snf chromatin remodelling complexes act through multiple protein interactions. In terms of transcription, little is known about the exact interactions between the RNA polymerase holoenzyme, transcription factors, remodelling complexes and chromatin. Chromatin remodelling complexes can be shown to remodel nucleosomes *in vitro* to allow for transcriptional activation; however nucleosomes are not the only repressive component of the chromatin environment. In order to gain access to DNA multimeric corepressors often have to be overcome. Chromatin-mediated repressors include the Sir and Tup1 proteins, which not only mediate nucleosome position, but alter the local epigenetic code to favour a 'closed' heterochromatic-like structure. The chromatin environment throughout the eukaryotic genome is highly dynamic, with repressors acting antagonistically alongside transcriptional activators and chromatin remodelling complexes. Of particular interest is how NER factors are able to afford access to repair DNA lesions within higher order chromatin structures.

Tup1p as a general repressor

Ssn6p and Tup1p are associated in a large complex (Redd et al. 1997; Varanasi et al. 1996; Williams et al. 1991) of approximately 440kDa, and can act to repress transcription *in vitro* (Redd et al. 1997). The complex is required for the repression of a large subset of genes (Keleher et al. 1992) and microarray analysis has

shown that about 3% of yeast genes are derepressed in *Tup1* mutants (DeRisi et al. 1997).

Tup1p is a WD repeat containing phosphoprotein consisting of a C-terminal and N-terminal repression domain, with the N-terminal domain also being essential for the association of Tup1p with Ssn6p and for oligomerization of Tup1p (Zhang et al. 2002). The Ssn6-Tup1 complex has been shown to comprise four Tup1p molecules and one Ssn6p molecule (Varanasi et al. 1996; Williams et al. 1991). As both Tup1p and Ssn6p have repeated motifs, and form an elongated structure as a complex they have the potential for a diverse set of protein-protein interactions (Smith and Johnson 2000). The repeats also provide flexibility in the complex allowing for different conformations of Ssn6-Tup1 at different promoters to accommodate different DNA architectures. Deletion mutants within the C and N-terminal repression domains of the *TUP1* coding region showed that the C-terminal repression domain, located near the first WD repeat plays a dominant role in repression, with the N-terminal domain sufficient for partial repression (Zhang et al. 2002).

Neither Ssn6p nor Tup1p have DNA binding ability, and repression is therefore mediated by the recruitment of the Ssn6-Tup1 complex to target promoters via sequence specific DNA binding proteins (Keleher et al. 1992; Tzamarias and Struhl 1995). Distinct motifs within the Ssn6-Tup1 complex may regulate their recruitment via the DNA binding proteins to one or more operator sites in the regulatory regions upstream of the genes to bring about transcriptional repression (Tzamarias and Struhl 1995).

Ssn6-Tup1 repressed genes can be divided into different groups according to the cellular processes in which the genes function. The genes investigated to date include those involved in glucose repression (Trumbly 1992), mating-type regulated genes (Keleher et al. 1992), DNA damage inducible genes (Zhou and Elledge 1992), oxygen related genes (Zitomer and Lowry 1992), osmostress inducible genes (Marquez et al. 1998), flocculation genes (Teunissen et al. 1995), sporulation genes (Friesen et al. 1997) and meiosis related genes (Mizuno et al. 1998). These can be found in Table 5.1 alongside the related DNA binding protein.

Gene Sets repressed by the actions of the Ssn6-Tup1 complex	
Function	**DNA binding protein**
a-specific genes	α2/Mcm1
Haploid-specific genes	**a**1/α2
Glucose-repressible genes	Mig1
DNA-damage-inducible genes	Crt1
Oxygen utilisation genes	Rox1
Starch-degrading enzymes	Nrg1
Osmotic stress-inducible genes	Sko1
Sporulation-specific genes	Unknown
Meiosis-specific genes	Unknown
Flocculation genes	Unknown

Table 5.1: Displayed are the various gene families repressed by the actions of the Ssn6-Tup1p complex, along with the sequence specific DNA binding protein which mediates Ssn6-Tup1p association with the target promoter, adapted from (Smith and Johnson 2000).

Various models for the Ssn6-Tup1p complex's role in repression have been proposed, and can be generalised into two groups. Firstly, Tup1p may inhibit transcription by the organisation of a repressive chromatin structure (Cooper et al. 1994) through the direct interaction with histones (Edmondson et al. 1996). Positioned nucleosomes are seen upstream of some **a**-specific genes, occluding binding proteins to DNA around the TATA box and transcription initiation site (Patterton and Simpson 1994; Shimizu et al. 1991). It is thought that the alteration of chromatin structure acts to mask DNA targets for activators or transcription factors. Ssn6p and Tup1p are responsible for the positioning of nucleosomes, but the more severe effects on chromatin structure are seen in the Tup1p mutant compared with Ssn6p mutations (Cooper et al. 1994). Tup1p interacts *in vitro* with the N-terminal tails of histones H3 and H4 (Edmondson et al. 1996). If the histone tails are deleted or mutated, it has been shown to partially relieve Ssn6-Tup1 mediated repression *in vivo* (Edmondson et al. 1996; Huang et al. 1997). Repression by Tup1 is also accompanied by local histone deacetylation (Bone and Roth 2001), with mutations in the histone tails or deacetylases decreasing the association of Tup1p with its target genes, as determined by chromatin immunoprecipitation (Davie et al. 2002). Interestingly, hyperacetylation at lysine 18 of histone H3 generated by a deletion of *HDA1* (a class I histone deacetylase) does not cause derepression of the target gene, indicating that

deacetylation alone is not sufficient to repress most Tup1-controlled genes (Green and Johnson 2004). However, in yeast strains containing three specific histone deacetylase gene mutations, the Ssn6-Tup1 repression is abolished (Watson et al. 2000). Two of these three deacetylases physically interacts with Ssn6-Tup1, suggesting Tup1p actively recruits HDACs to deacetylate adjacent nucleosomes and to promote Tup1p-histone interactions and an organised chromatin structure.

The second mode of repression is postulated to be that Ssn6-Tup1 interacts with the general transcriptional machinery (Herschbach et al. 1994; Redd et al. 1996). This model suggests that the transcriptional machinery is able to assemble at the promoter; however the association with Ssn6-Tup1 prevents the initiation of transcription. This was suggested when Ssn6-Tup1 mediated repression was seen on naked DNA *in vitro* (Redd et al. 1997), however, using crude extracts provided the possibility that additional factors contributed to the repression. Tup1p was also shown to inhibit the ability of mcm1 to activate the expression of **a**-specific genes (Gavin et al. 2000). Multiple genetic screens have shown that there are additional proteins which effect the repression by Ssn6-Tup1 *in vivo*, which are biochemically linked with the RNA polymerase II transcriptional machinery within the RNA polymerase II Srb/Med complex (Lee et al. 2000). Tup1p has been shown to directly interact with some subunits of the Srb/Med complex, for example Srb7p. Mutations in Srb7p result in the Tup1p-dependant derepression of several Tup1p target genes, confirming that the Tup1p interaction with transcriptional machinery is an important pathway (Gromoller and Lehming 2000b). Interestingly, the Srb7p also interacts with the Med6p, and this interaction is required for the activation of transcription by different activators, suggesting Med6p and Tup1p compete for interaction with Srb7p (Gromoller and Lehming 2000a). Genome wide analysis also provides evidence that Srb10 (a cyclin-dependant kinase associated with the Mediator complex) is implicated in Tup1p-mediated repression (Green and Johnson 2004).

Other groups have implied that the complex may block the activation domain of pathway-specific DNA-binding proteins (Tzamarias and Struhl 1995) or directly interfere with the activator (Gavin et al. 2000). At the *GAL4* gene promoter, the activator is still able to bind to the UAS, however, repression takes place (Redd et al. 1996), suggesting that the Ssn6-Tup1 complex could contact the activator once bound to DNA and compromise its ability to activate transcription. Through multiple investigations it would seem more likely that Tup1p exerts its repressive role via a

combination of routes, each perhaps of more significance at specific target genes. The degree of chromatin organization differs at different promoters, and it is likely that there is no general repressional role of Tup1p.

As Ssn6-Tup1 is responsible for the repression of multiple genes, many of which are involved in cell survival in times of stress, the repression must be able to be relieved when required by the cell. No individual factor has been shown to relieve all Ssn6-Tup1 repressed genes, rather it appears that the specific DNA binding proteins which associate Ssn6-Tup1 with the DNA are affected. This tends to occur by a down-regulation of the specific proteins, combined with efficient removal of proteins, for example via the ubiquitin proteosome pathway, reviewed in (Smith and Johnson 2000).

The DNA damage response gene *RNR3* is transcriptionally regulated by the repressive actions of Ssn6-Tup1, and mediated by the DNA binding protein Crt1p (Zhou and Elledge 1992), which recognises DNA damage response elements (DREs) in the URS. Activation of the DNA damage response pathways causes the release of Crt1p from the promoter leading to derepression and chromatin remodelling (Li and Reese 2001). If *CRT1*, *TUP1* or *SSN6* are deleted, *RNR3* is derepressed, with a characteristic loss of positioned nucleosomes, and an increased DNase I hypersensitivity. If Crt1p binds to the promoter, in the absence of Ssn6p or Tup1p, repression is unable to take place. Therefore *RNR3* is regulated by changes in nucleosome positioning and chromatin structure that are mediated by Ssn6p, Tup1p and Crt1p (Li and Reese 2001). Tup1p recruitment is restricted to the URS of the *RNR3* promoter (Davie et al. 2002).

Ssn6-Tup1 requires the *ISW2* chromatin remodelling complex to establish nucleosome positioning *in vivo*, therefore deletion of *ISW2* results in a disruption of chromatin structure without effecting Tup1p repression functions (Zhang and Reese 2004a). Tup1p spreading along the promoter region and into the coding region is seen in a set of Tup1p mediated genes, however, many genes only see Tup1p localisation at the promoter region, suggesting Tup1p spreading can not fully account for its repression and nucleosome positioning activities (Davie et al. 2002). The organised chromatin domain of the repressed *STE6* gene contains two molecules of Tup1p per nucleosome (Ducker and Simpson 2000).

Deletion of *ISW1*, *HDA1* (histone deacetylase) or genes encoding mediator subunits resulted in slight or no derepression of certain genes. However double

deletions or triple mutations resulted in increased transcription of the target genes. Tup1p therefore uses multiple redundant mechanisms to repress transcription of native genes (Zhang and Reese 2004b). The Tup1-Ssn6 complex has been shown to rearrange and also order an extensive array of 32 nucleosomes on the promoter and over 5kb of upstream intergenic region of the *FLO1* gene (Fleming and Pennings 2001), with the complex acting antagonistically with Swi/Snf complexes.

It has also been suggested that Tup1p plays an essential role in the SWR1-C mediated Htz1p deposition at promoters, with deposition of Htz1p at the *GAL1* gene enabling rapid activation of the gene. Following transcriptional repression the histone variant Htz1p is rapidly deposited across the promoter nucleosome covering the transcription start site in a tup1-dependant manner. Tup1p cooperates with SWR1-C, with Htz1p deposition at *GAL1* required for efficient mediator recruitment and subsequent transcription (Gligoris et al. 2007).

The Tup1p mediated repression of **a**-specific genes has been extensively studied, along with the role of the DNA binding protein α2. As detailed in Chapter 4, yeast mating type **a** genes are transcriptionally active in **a** cells, and repressed in α cells by the concerted actions of mcm1/α2 and Ssn6-Tup1. The involvement of Ssn6-Tup1 at mcm1/α2 regulated genes was shown to organise repressive regions of chromatin (Cooper et al. 1994). Through a series of plasmids containing the **a**-specific *STE6* gene promoter in various locations, it was shown that the α2 operator positions the neighbouring nucleosome, and this is not mediated by the local DNA sequence (Patterton and Simpson 1994). In **a**-specific gene *BAR1*, it was shown that nucleosome positioning was required for full repression, however loss of nucleosome positioning is not sufficient to relieve repression completely (Morohashi et al. 2006), and mcm1/α2 positioned nucleosomes limit the binding of transcription factors, such as Hap1p activator *in vivo* (Morohashi et al. 2007). Direct interactions between α2 and Ssn6-Tup1 act to position nucleosomes adjacent to the operator, where Tup1p directly interacts with the core histones H3 and H4 (Cooper et al. 1994; Edmondson et al. 1996). Mutations in the amino terminus of the H4 and truncations of the H3 amino terminus result in a decrease of repression, indicating a central role for histones in α2 mediated repression (Huang et al. 1997). The N-terminus region of α2 interacts directly with Tup1p, and a turn in the α2 homeodomain (located towards the C terminus of α2 between helices 2 and 3 of the homeodomain) interacts directly with Ssn6p (Smith and Johnson 2000), as displayed in Figure 5.1.

The WD40 repeat of Tup1p and the TPR (tetratricopeptide repeat) of Ssn6p are domains which interact with α2, and these are the most evolutionary conserved regions of the proteins, suggesting that the contact with α2 is important.

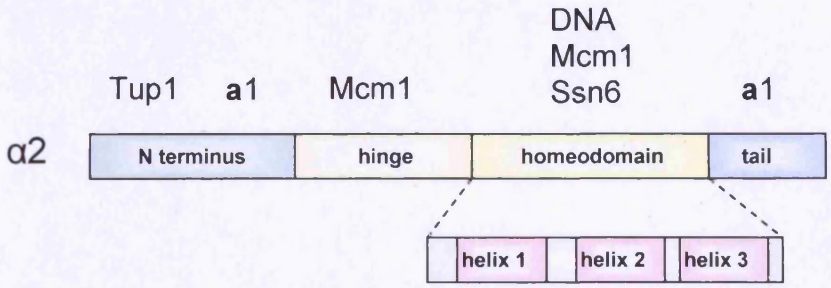

Figure 5.1: Schematic diagram of the structural regions of the α2 mating-type regulator, showing the sites of interaction with other factors, including Ssn6p and Tup1p. Adapted from (Smith and Johnson 2000).

The role of Tup1p in NER at *MFA2*

The **a**-specific *MFA2* gene contains an upstream mcm1/α2 binding site, which regulates the recruitment of the Ssn6-Tup1 repressor complex. Interestingly biochemical studies have shown that association of Tup1p and not of Ssn6p is required for the repression of *MFA2* (Zhang et al. 2002).

The deletion of *TUP1* derepresses *MFA2* transcription in α cells to a level similar to that seen in wild-type **a** cells. Along with a derepression of gene transcription, a loss of positioned nucleosomes is seen across the promoter region, as determined by MNase digestion, an increase in DNase I hypersensitivity and restriction enzyme accessibility. Histone acetylation is intimately linked with transcriptional activity, and the H3 acetylation levels at endogenous *MFA2* show an elevated acetylation level in **a** cells compared with α cells, reflecting the transcriptional status. When *TUP1* is deleted in α cells, a ten-fold increase in constitutive levels of H3Ac is seen. If a TATA box mutation is introduced into the *MFA2* gene promoter, transcription is unable to take place, even when TUP1 is deleted. Interestingly the high level of H3Ac is maintained in the TATA box mutated *tup1* α cells, in the absence of gene transcription. These H3Ac levels are detected in

the absence of UV light, and suggest that deletion of the Tup1p repressor results in constitutively higher levels of H3Ac in the *MFA2* promoter, even when transcription is inhibited (Teng et al. 2008).

NER in *tup1* cells is enhanced for all detectable CPDs in both the TS and NTS. To ensure that this faster repair was not an artefact of increased transcription, repair was studied in the TATA box mutant. Here, repair was not significantly different from that in *tup1* delete cells, showing that *tup1* cells show enhanced lesion removal by GG-NER in the *MFA2* promoter (Teng et al. 2008). This follows previous data suggesting that naked DNA and nucleosome free regions are repaired faster than repressed chromatin regions (Smerdon 1991), and when an 'open' chromatin environment is created by deletion of *TUP1*, NER can be carried out more efficiently.

This chapter will investigate the transcription and NER of the repressed TAM borne *MFA2* gene within a mutant where Tup1p is absent.

5.2 Materials and Methods

Any methods which are not detailed below can be found in Chapter 2.

5.2.1 Yeast strains

The haploid yeast strains used in this Chapter are:

PSY316 *(MATα ade2-101 ura 3-52 leu 2-3, 112 Δhis 3-200 lys2 trp1)*

Δtup1 (MATα ade2-101 ura 3-52 leu 2-3, 112 HIS::TUP1 lys2 trp1)

PSY316 *(MAT**a** ade2-101 ura 3-52 leu 2-3 112 Δhis 3-200 lys2 trp1)*

5.2.2 CPD repair analysis

NER of CPDs was carried out for the *Hae*III-*Hae*III restriction fragment, covering the *MFA2* promoter region, as described in Chapter 4.2.1. Repair data were collected and analysed using Imagequant software for the TAM borne *MFA2* region.

5.2.3 Nucleosome mapping

Both low and high resolution nucleosome mapping was carried out to determine the nucleosome structure within *tup1* cells. The protocols followed are as described in Chapter 4.2.2.

5.2.4 Analysis of histone H3 acetylation levels in the TAM plasmid by Chromatin Immunoprecipitation (ChIP)

ChIP was carried out as described (Kuo and Allis 1999), with the *in vivo* formaldehyde cross-linking of intact cells followed by the selective immunprecipitation of protein-DNA complexes with specific antibodies. In brief, 100ml of exponential phase yeast cells were cross-linked by formaldehyde. Washed cells were lysed by vortexing with glass beads. The lysate was sonicated to generate DNA fragments ranging from 200 to 500bp in size. Histone H3 acetyl antibody (at Lys 9 and Lys14; Upstate Biotechnology, Millipore, MA, USA) was used to immunoprecipitate sheared chromatin and input samples were used as controls. Quantitative PCR was carried out in real time to analyse the enrichment of DNA fragments following immunoprecipitation.

5.2.4.1 Preparation of chromatin samples

1) 100ml of yeast cells were grown to 2 x 10^7 cell/ml from an overnight culture
2) The following morning, cells were fixed by the addition of 3ml 37% formaldehyde, with shaking at room temperature for 10 minutes
3) The cross-linking was stopped with the addition of 5.5ml 2.5M glycine, with shaking for 5 minutes
4) Cells were collected via centrifugation in an Eppendorf benchtop centrifuge for 5 minutes at 4000rpm, washed in cold PBS, then in cold FA/SDS containing PMSF inhibitor. The cells were transferred to a 2ml Eppendorf during the washes
5) The cells were then resuspended in 500µl of FA/SDS (+PMSF) buffer

6) 0.5ml glass beads were added to the sample, vortexed with a 2ml turbomixer at 4°C for 10 minutes
7) After vortexing, a hole was punctured in the bottom of the Eppedorf with a red-hot needle, and the 2ml tube sat on top of a 15ml Corning tube. The tubes were then spun at 2000rpm for 2 minutes in a Eppendorf benchtop centrifuge to collect the lysate without the glass beads. The beads were then washed twice with 250µl FA/SDS (+PMSF) buffer, collecting the lysate in the same Corning tube each time.
8) The sample in the Corning tube was then gently pipetted to ensure a homogenous sample, and used directly for sonication. The cell lysate was sonicated with a Biorupter: power H, 30 seconds on, 30 seconds off for 6 cycles
9) After sonication the cell lysate was then spun at 4000rpm in an Eppendorf bench top centrifuge for 10 minutes. The supernatant was transferred to a fresh Eppendorf, and spun again at 4°C for 20 minutes at top speed. The supernatant was again collected, transferred to a fresh Eppendorf and flash frozen with liquid nitrogen for storage.

5.2.4.2 Preparation of Dynabeads

1) 50µl per sample of Dynabeads (M280 Sheep anti-rabbit IgG H3Ac) were washed 3 times in 500µl PBS BSA 0.1% (4°C). Each wash was mixed with a vortex and spun quickly before placing in an MPC
2) The beads were resuspended in 100µl PBS BSA 0.1% per sample
3) 2.5µl antibody (anti-acetyl hitone H3 K9+K14) was added per sample
4) The beads and antibody were then incubated at 30°C for 30 minutes at 1300rpm in a Eppendorf Thermomixer
5) The beads were then washed 3 times with PBS BSA 0.1%, and resuspended in 50µl PBS BSA 0.1% per sample.

5.2.4.3 Immunoprecipitation (IP)

1) The chromatin samples were defrosted on ice, and 100µl of each sample was transferred to a new tube for an IP sample. 50µl of each sample was also transferred to a new tube, and kept on ice as an input sample (IN).

2) To the 100µl IP sample, 30µl 10 x PBS BSA, 120µl PBS and 48µl of the washed beads were added. This mixture was incubated for at least 2 hours at 1300rpm at 21°C in an Eppendorf Thermomixer
3) The beads were then washed with 500ul FA/SDS, then 3 times with 1ml FA/SDS + NaCl (the NaCl concentration adjusted to 500mM)
4) The beads were then washed in 500µl Li solution, and a final wash with 500µl cold TE buffer, pipetting out the solution
5) The DNA was eluted from the beads with the addition of 125µl Pronase buffer and incubation at 65°C at 900rpm for 20 minutes in an Eppendorf Thermomixer
6) The supernatant was transferred to a new tube, and 6.25µl Pronase (20mg/ml, H_2O) added. The samples were incubated at 37°C for 1 hour, then at 65°C in a water bath overnight
7) To the input samples (50µl), 50µl of TE buffer was added, along with 25µl 5 x Pronase buffer and 6.25µl Pronase (20mg/ml), then incubated as in step (6).
8) 1µl of 10mg/ml DNase-free RNase was added to the IP and IN samples, and incubated at 37°C for 1 hour
9) All samples were then purified using Qiagen PCR purification kit, eluting in 50µl (30µl and 20µl) volume elution buffer
10) 5µl of the IN samples were taken to check the sonication products on an agarose gel
11) The samples could then be diluted appropriately and used for rtPCR

5.2.4.4 Quantitative real-time PCR analysis

The direct detection of PCR product was enabled by measurement of fluorescence, emitted proportionally during the PCR reaction, due to the binding of the SYBR®Green dye to dsDNA. The fluorescence data were collected by a camera, then processed and analysed using the iCycler software (Bio-Rad). Real-time detection enables fluorescence to be monitored during each PCR cycle, allowing data to be collected during the most exponential phase of PCR amplification, the threshold cycle (C_t), which is more sensitive than the collection of data from the end-point accumulation of PCR product alone. The C_t is inversely proportional to the copy number of the target template.

1) The iCycler iQ real-time PCR detection system (Bio-Rad) apparatus was set up and switched on according to the manufacturer's instructions.

2) The following components were mixed to prepare the PCR reaction mixture to a total volume of 25µl:

iQTM SYBR®Green Supermix (Bio-Rad)	10µl
IP/IN sample	10µl
Forward Primer (100mM)	0.1µl
Reverse Primer (100mM)	0.1µl
H_2O	4.8µl

For each IP and IN sample, including the set of standards, the above PCR mix was prepared in triplicate, and two sets were made, one using primers for the unique TAM join site (IP1 and IP2), and the second using primers for the *MFA2* coding region (N1a and N1b).

3) The samples were carefully loaded into the wells of a 96-well plate (Bio-Rad) and a sheet of sealing plastic (Bio-Rad) was secured on top, taking care not to touch the surface of the plastic. A vortex was used to mix the samples and the plate was spun briefly to ensure the samples were at the bottom of the plate and placed into the iCycler.

4) The parameters for the qPCR reaction were as follows:

    1. 95°C for 3min
    2. 95°C for 15sec
    3. 55°C for 20sec
    4. 55°C for 10sec*
    5. Steps 2-4 repeated 45 times
    6. 95°C for 1min
    7. 60°C for 30sec
    8. 60°C for 10secs*
    9. Step 8 repeated 31 times

*Fluorescence data were collected during step 4 and after step 8.

5) When the reaction was complete, the plate was removed and analysis could be undertaken immediately. The iCycler software (Bio-Rad) deduced the threshold cycle (C_t), an arbitrary number of PCR cycles in which all of the amplification graphs in the comparison are in the linear range, although this could be overridden and selected manually. As the C_t is inversely proportional to the copy number of the target template, a low C_t value represents a high template concentration and *vice versa*. The software also calculated the mean value (of the triplicate reactions) and standard deviation for each sample. The inclusion of a standard curve in addition enabled eventual calculation of the amount of mRNA originally present in each sample. The overall turnover time for the experimental and analytical acquisition of data was just a few hours.

Primers

For amplification of unique TAM plasmid:

IP1 FOR: TTAGCATCGTCTTCGTCTTCG

IP2 REV: GCCTTTGTGTGCTTAATCACG

For amplification of *MFA2* coding region:

N1a: GCAACCGATCACCACTGCTTCC

N1b: GGCGGGATCCCAGAAGAGGC

For amplification of *MFA2* promoter region:

N2a: AAAGCAGCATGTTTTCATTTGAAA

N2b: TATGGGCGTCCTATGCATGCAC

5.3 Results

5.3.1 UV Survival

The UV survival phenotype of mutant strains can be a good indicator of the requisite of certain factors in the repair process. Many *rad* mutants confer a moderate

to high UV sensitivity, with limited UV survival, as shown by the deletion of RAD14, an essential NER gene. The UV survival of the various strains may not be due to the protein's direct effect on the NER mechanism, but it may also implicate the protein in general UV stress response pathways, or other DNA repair mechanisms.

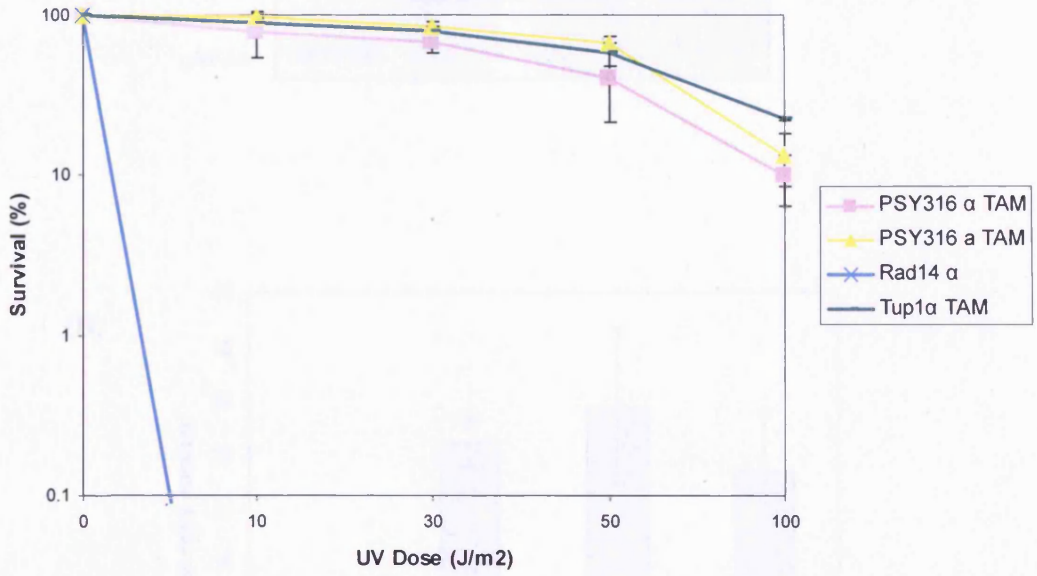

Figure 5.2: UV survival (%) of the *tup1*α TAM strain shows a similar UV sensitivity as the WT strains (Appendix IV).

The UV survival of the *tup1*α TAM strain shows no significant deviation in UV survival from the WT TAM strains, suggesting that Tup1p has no major role in survival after UV. It should be borne in mind that survival is measured by colony forming ability three days after UV, and depends on a spectrum of events such as cell cycle arrest, tolerance of damage, DNA damage response and removal of damage. Therefore one should not always expect correlation between NER and survival immediately after UV.

5.3.2 Copy number determination

The determination of TAM copy number by Southern blot analysis was carried out as outlined in Chapter 3, with the blotting procedure detailed in Chapter 2. The *MFA2* radio-labelled probe was allowed to hybridise to a membrane to detect the

relative levels of TAM borne *MFA2* compared to genomic *MFA2*. The ratio between the two *MFA2* species indicates the copy number of the plasmid, and has been quantified in Figure 5.3 (B).

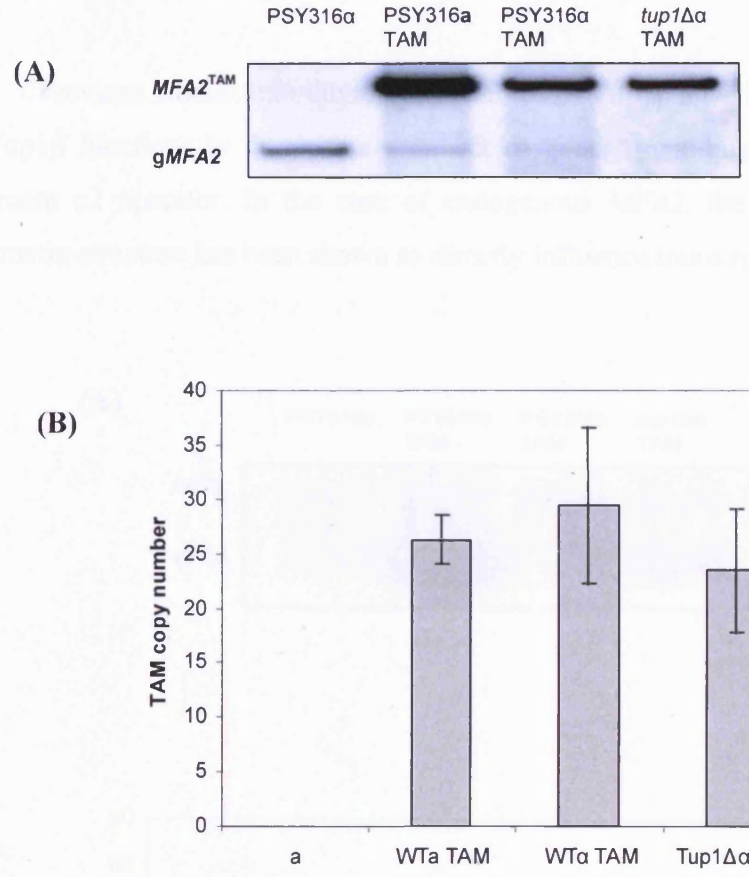

Figure 5.3: Southern blot analysis shows that the copy number is not significantly reduced, in a *tup1* mutant, with sufficient copies to use this strain in CPD repair analysis. (A) Southern blot, probed for *MFA2*. (B) Graphical representation of multiple blots, displaying the copy number of the TAM plasmid, including y-axis standard deviation error bars (Appendix IV).

The number of plasmid borne *MFA2* copies per cell does appear to be marginally lower in the *tup1* mutant when compared to the TAM levels seen in the WT TAM strains, however this figure is not statistically significant ($p>0.01$, Appendix IV). The copy number was not expected to differ between strains, however, Tup1p has many complex repressive roles within yeast, and the slight reduction in copy number may be a result of many indirect factors. Of particular importance to this study is the fact that the copy number within the *tup1* mutant has not been reduced to

levels whereby the analysis of CPD repair can not take place. The multiple copy number (average 23.4 copies) is still sufficient to overcome the single genomic *MFA2* copy.

5.3.3 *MFA2* mRNA analysis

Previous studies into the repressive roles of Tup1p have indicated that the loss of Tup1p functions to de-repress a subset of genes, including those containing an upstream α2 operator. In the case of endogenous *MFA2*, the de-repression of the chromatin structure has been shown to directly influence transcription.

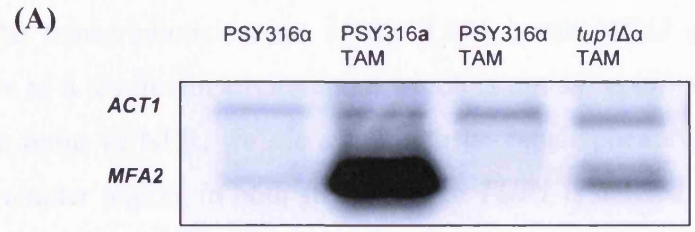

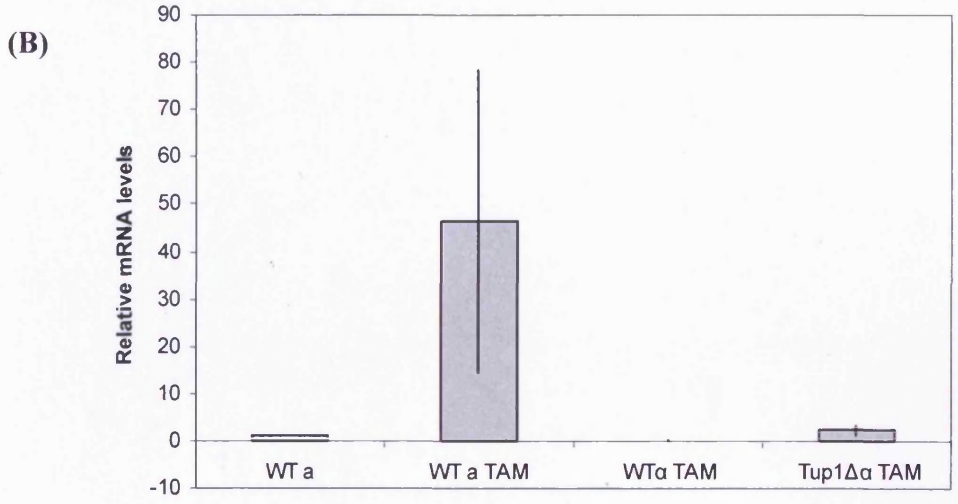

Figure 5.4: Northern blot analysis of relative *MFA2* mRNA levels. A de-repression of *MFA2* is seen, however, not to the expected levels seen in WT **a** cells (Appendix IV).

Detection of the relative levels of *MFA2* mRNA in the TAM containing *tup1* strain has shown that there is a slight de-repression of transcription. At endogenous *MFA2*, a de-repression has been recorded in *tup1α* cells, with transcription levels analogous to those in the active gene. In this plasmid system however, it appears that transcript levels do not reach those seen in WT**a** TAM cells when *TUP1* is deleted, but there is still an increase compared with WT**a** cells, without the plasmid. This could be due to multiple reasons, including a difference in plasmid chromatin structure in the *tup1α* TAM cells versus the WT**a** cells.

5.3.4 Effect of the *TUP1* mutation on CPD repair

The transcriptional status of the TAM borne *MFA2* gene in *tup1* cells is suggestive of a chromatin environment which is not as 'open' as seen at endogenous *MFA2*. In terms of NER, we see a much faster repair phenotype in the endogenous *MFA2* promoter region, in both strands when *TUP1* is deleted. Repair was therefore investigated in $MFA2^{TAM}$ in the absence of *TUP1* (Figure 5.5).

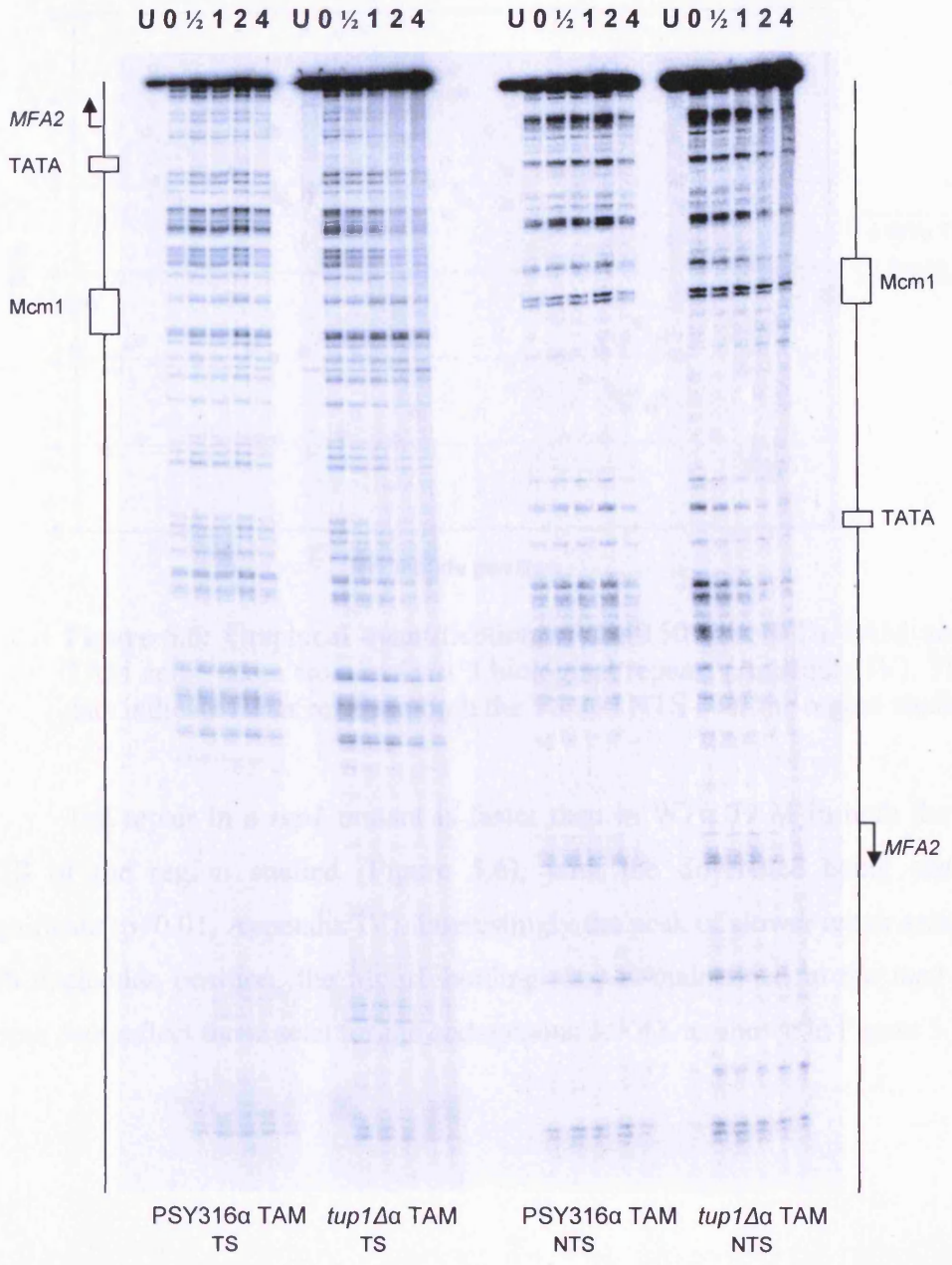

Figure 5.5: A typical high resolution gel image displaying the CPD profiles in WTα TAM and *tup1Δα* TAM cells. Cells were subjected to 100J/m^2 UV light and allowed to repair for various time points (U,0,0.5,1,2,4 hours) in YPD at 30°C. Following digestion with *Hae*III and ML *endo*, samples were end-labelled and resolved on a polyacrylamide gel. TS and NTS displayed.

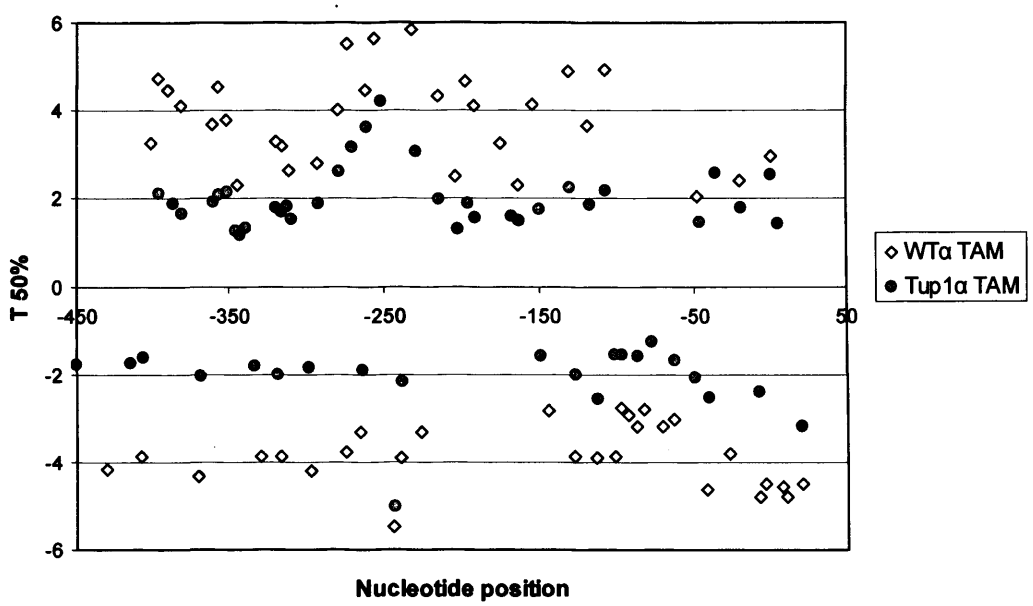

Figure 5.6: Graphical quantification of the T50% in WTα TAM and *tup1α* TAM cells, taken from at least 3 biological repeats (Appendix IV). The Tup1 data indicate faster repair in both the TS and NTS over the region studied.

The repair in a *tup1* mutant is faster than in WTα TAM in both the TS and NTS of the region studied (Figure 5.6), with the difference being statistically significant ($p<0.01$, Appendix IV). Interestingly the peak of slower repair around the -250 nucleotide position, the Mcm1 binding site, is maintained in the *tup1* mutant. These data reflect those seen for the endogenous *MFA2*, as shown in Figure 5.7.

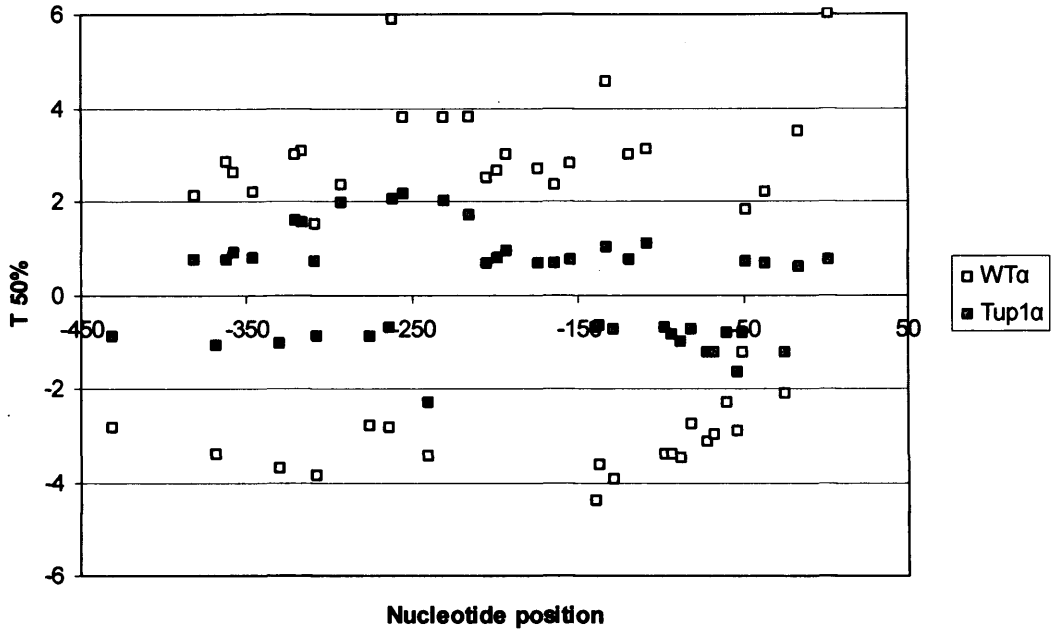

Figure 5.7: Repair profile for the endogenous *MFA2* region of interest in WTα and *tup1α* cells (Appendix IV).

5.3.5 Nucleosome disruption in the *TUP1* mutant

As Tup1p repression is primarily thought to be a chromatin-mediated event, it would seem plausible that a TUP1 deletion disrupts the chromatin organisation. This has been seen previously at the endogenous *MFA2* and other **a**-specific genes with a loss of positioned nucleosomes, and a MNase digestion pattern similar to that seen in naked DNA, suggesting an even more 'open' conformation than seen at the active gene. There has been much speculation on the degree of chromatin unravelling caused by the loss of Tup1p, with an eviction of nucleosomes at least in the promoter region seeming possible. To investigate the nucleosome positioning in the TAM plasmid, both low and high resolution mapping was carried out as previously described in Chapter 4, and data is shown for the active and repressed gene (WT**a** and WTα respectively) as well as for the *tup1α* mutant.

i) Low resolution mapping

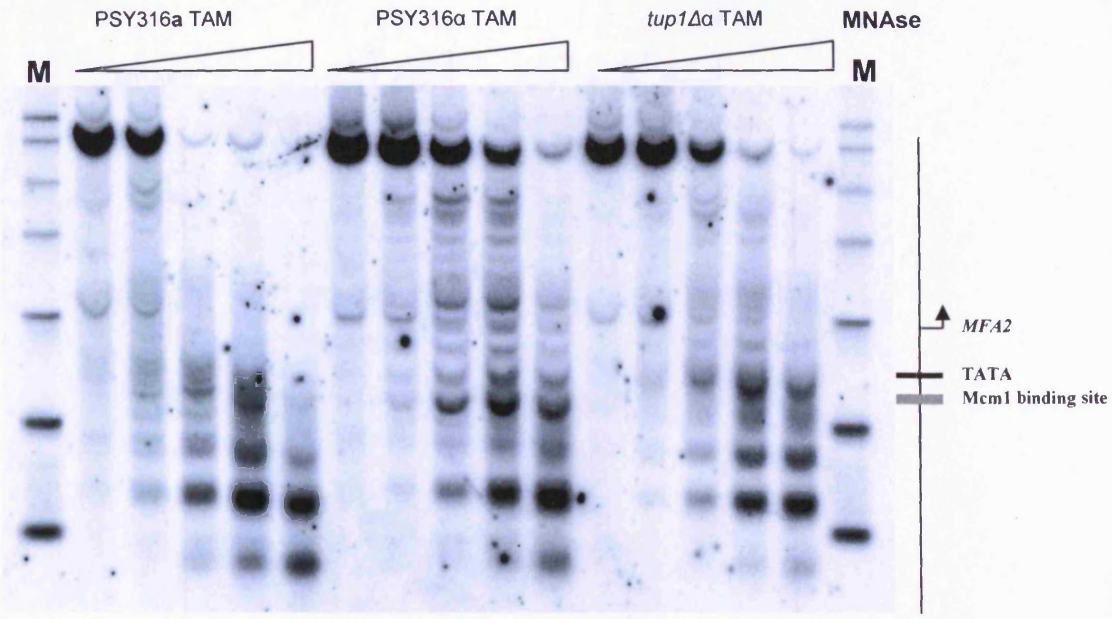

Figure 5.8: Low resolution mapping gel, displaying highly positioned MNase sensitive sites in the repressed *MFA2* region of TAM within α cells (centre), and a loss of positioned nucleosomes in the active *MFA2* gene and in the de-repressed gene, in WT**a** TAM and *tup1*α TAM cells respectively.

The highly positioned nucleosomes, as shown by the distinct MNase sensitive bands in the repressed *MFA2* gene (WTα TAM) are clearly absent from the *tup1* TAM samples. Much like the WT**a** TAM active gene situation, there is a loss of positioned nucleosomes across *MFA2* in the TAM plasmid when *TUP1* is deleted. It may be noted at this point that the MNase pattern is not the same in the active gene as in the *tup1* mutant, with an MNase sensitive site positioned around the TATA box in *tup1* cells. For further confirmation, high resolution analysis was employed (Figure 5.9).

ii) High resolution mapping

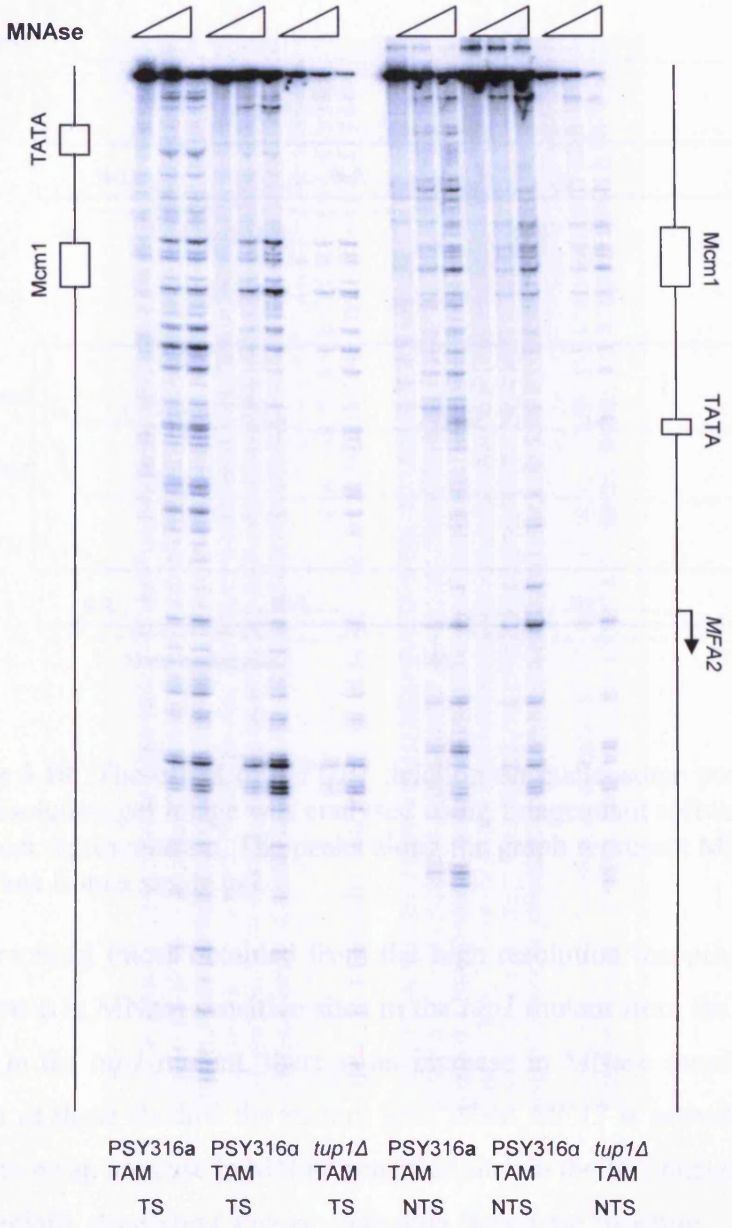

Figure 5.9: A typical high resolution nucleosome mapping gel, displaying WT**a** TAM, WTα TAM and *tup1*α TAM strains, treated with increasing amounts of MNase. The gel shows the *Hae*III restriction fragment, representing the *MFA2* promoter region.

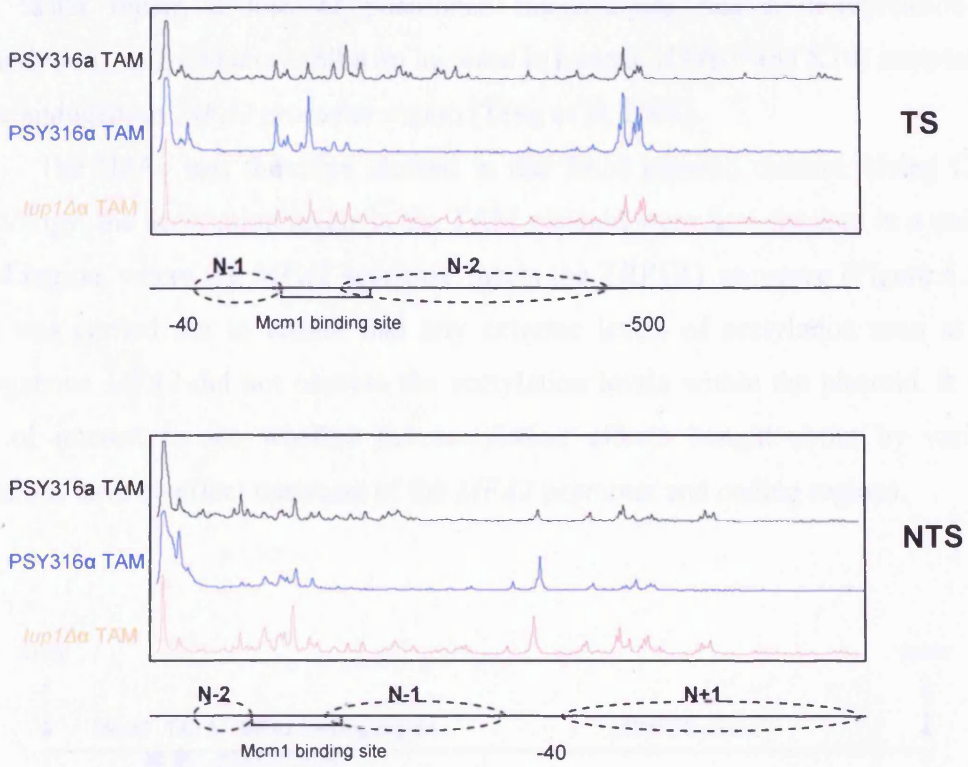

Figure 5.10: The effect of a *TUP1* deletion on nucleosome positioning. The high resolution gel image was analysed using Imagequant software to obtain a graphical representation. The peaks along the graph represent MNase sensitive sites, data from a single gel.

The graphical traces obtained from the high resolution mapping gels show a distinct difference in MNase sensitive sites in the *tup1* mutant from the WTα and the WT**a** results. In the *tup1* mutant, there is an increase in MNase sensitive sites, and although most of these shadow the pattern seen when *MFA2* is actively transcribed, there appears to be an increase in MNase sensitive sites in the N-1 nucleosomal region (-50 to -200 region), suggesting a more accessible chromatin structure.

5.3.6 Histone H3 acetylation

The association of histone acetylation and transcription is a well documented theme, with hyperacetylation intimately linked with enhanced transcriptional activity, and hypoacetylated regions usually associated with the recruitment of histone deacetylases, often indicative of repressed or non-coding regions of the genome. Enhanced histone H3 and H4 acetylation is not necessarily a pre-requisite of

transcription, but a contributory factor to an accessible chromatin structure. Along with faster repair, a loss of positioned nucleosomes and a de-repression of transcription, *tup1* mutants exhibit an increase in histone H3 (K9 and K14) acetylation in the endogenous *MFA2* promoter region (Teng et al. 2008).

The H3Ac was therefore studied in the TAM plasmid context. Using ChIP technology, the acetylation levels in the TAM plasmid were first checked in a unique TAM region, where the *MFA2* sequence meets the TRP1R1 sequence (Figure 5.11). This was carried out to ensure that any extreme levels of acetylation seen at the endogenous *MFA2* did not obscure the acetylation levels within the plasmid. It was also of interest to see whether the acetylation effects bought about by various mutations have an effect upstream of the *MFA2* promoter and coding regions.

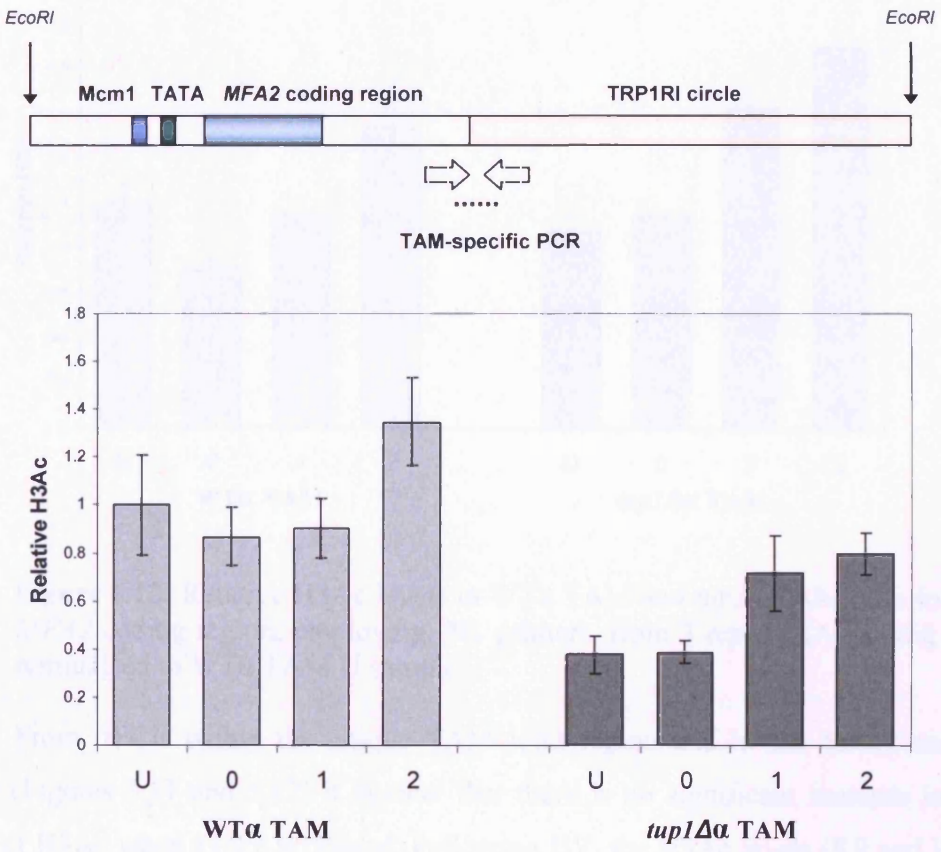

Figure 5.11: RtPCR employing the IP1 and IP2 primers, showing the relative H3Ac levels in the TAM plasmid unique join region, downstream of the *MFA2* gene. Samples were taken from untreated cells, and cells treated with 100Jm^2 UV, and allowed to repair for 0, 1 and 2 hours. WTα TAM and *tup1α* TAM data shown from 3 repeats (Appendix IV), normalised to WTα TAM U sample.

The H3Ac levels could then be determined for the *MFA2* coding region (Figure 5.12). It is known that at the endogenous *MFA2*, the transcriptionally active gene is associated with an increase in acetylation. As a derepression of transcription is seen in TAM borne *MFA2* in cells lacking Tup1p, it would be presumed that an increase in acetylation would be seen.

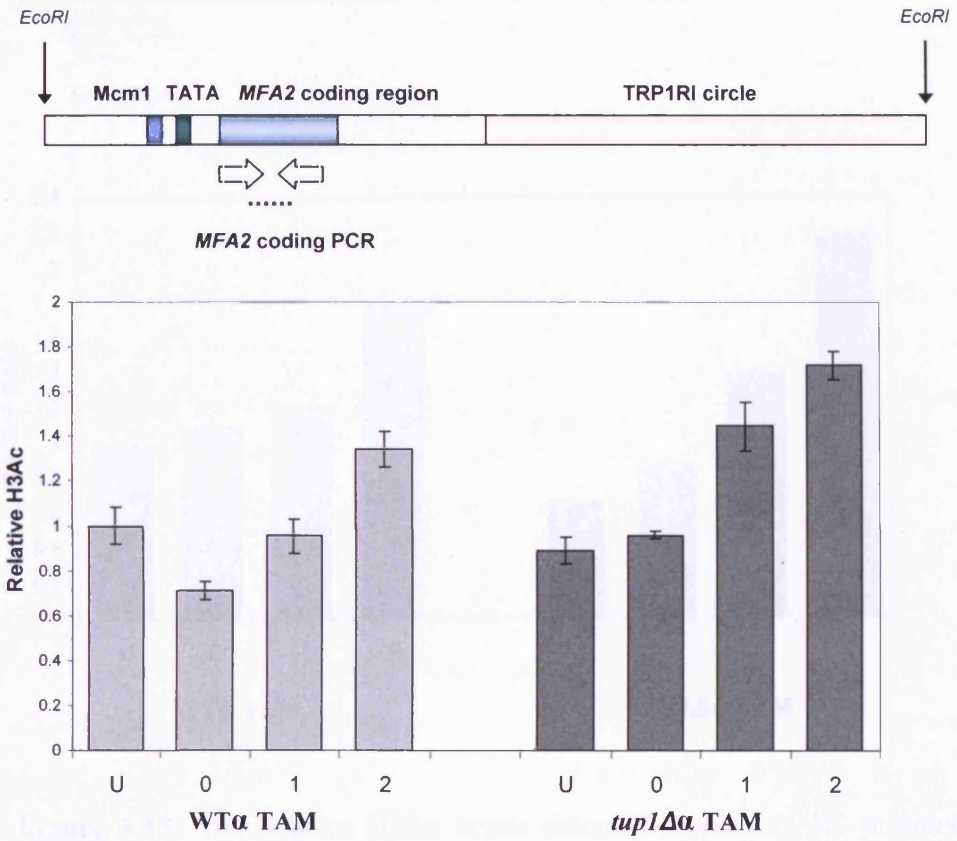

Figure 5.12: Relative H3Ac levels in WTα TAM and *tup1*α TAM cells for the *MFA2* coding region, employing N1 primers, from 3 repeats (Appendix IV), normailsed to WTα TAM U sample.

From rtPCR within the unique TAM joint region and in the *MFA2* coding region (Figures 5.11 and 5.12) it is clear that there is no significant increase in the levels of H3Ac when *TUP1* is deleted. Following UV, the H3Ac levels (K9 and K14) in WTα TAM appear to decrease slightly, followed by a gradual increase in acetylation with hours after repair. When *TUP1* is absent, the same general trend is seen with an increase in acetylation seen 2 hours after UV compared with the untreated samples. It may be noted that the acetylation levels detected within the

MFA2 coding region in *tup1* TAM cells compared with WTα TAM cells are higher than detected within the upstream TAM specific sequence. This may be a direct effect of the transcriptional derepression status of TAM borne *MFA2*.

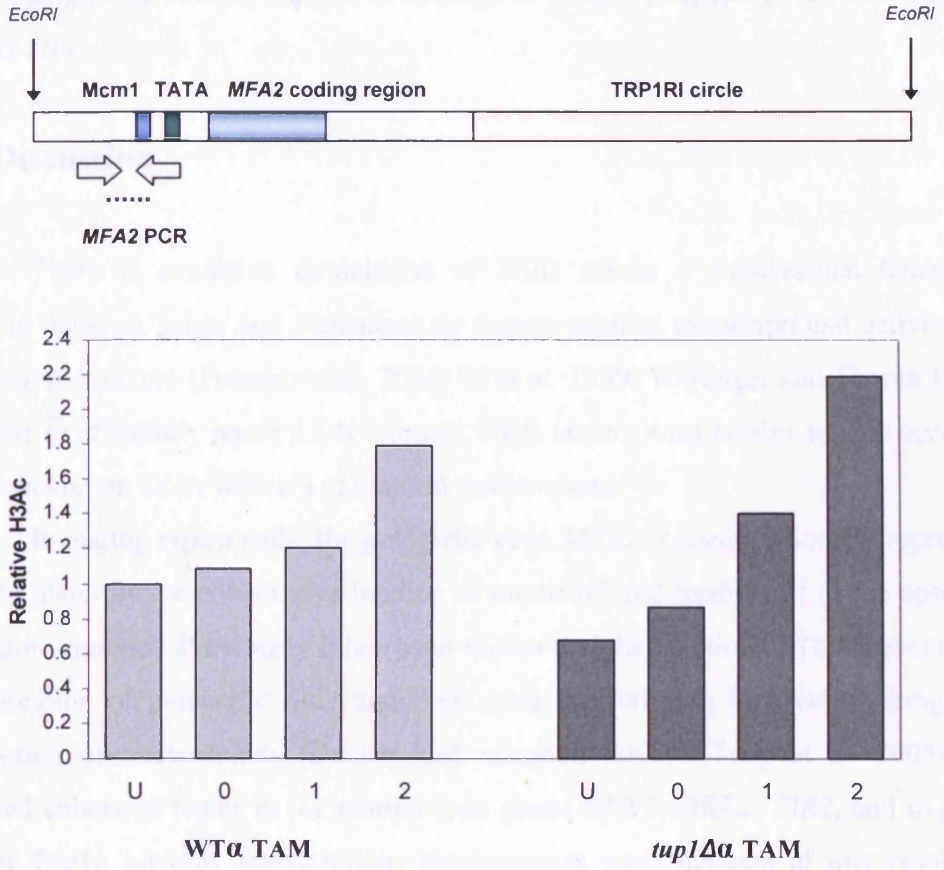

Figure 5.13: The relative H3Ac levels detected employing N2 primers, to amplify the *MFA2* promoter region. Data taken from a single experiment (Appendix IV), normalised to WTα TAM U sample.

Having established the H3Ac level pattern in WTα TAM and *tup1*α TAM cells within the TAM plasmid, and within the *MFA2* coding region, I also checked the acetylation levels within the *MFA2* promoter region, as this is the region studied with respect to high resolution CPD analysis and mapping. It is established from genome-wide data (personal communication, Y Teng) that acetylation levels are modulated throughout a gene sequence, however it was of interest to see local effects at *MFA2*. As displayed in Figure 5.13, there is no increase in the H3Ac levels at the *MFA2* promoter when *TUP1* is deleted, compared to the WT (untreated samples). There does appear to be a more significant difference between the untreated (U) and 2 hours

repair samples for both strains, but especially in *tup1* cells. The change in acetylation is expected to show a marked difference within the promoter region, but these results show that there is no substantial difference between WT acetylation levels at either *MFA2* region studied. It should also be stated that the results shown in Figure 5.13 are from a single experiment, and not an average of at least 3 repeats as for the other two primer sets.

5.4 Discussion

There is extensive modulation of NER across a nucleosomal landscape, varying between genes and dependant on factors such as transcriptional activity and chromatin structure (Ferreiro et al. 2004; Li et al. 1999; Wellinger and Thoma 1997). In order to efficiently repair a DNA lesion, NER factors must be able to gain access to and function on DNA within a chromatin environment.

In mating type α cells, the **a**-specific gene *MFA2* is transcriptionally repressed, bought about by the cooperative binding of mcm1/α2 and Ssn6-Tup1 to the upstream operator sequence. Previously it has been shown that the deletion of *TUP1* results in a derepression of **a**-specific Ste2 and Ste6 gene transcription in α cells, along with disruption of nucleosomes (Ducker and Simpson 2000). (Teng et al. 2005) also showed enhanced repair in the mating type genes *RNR3*, *DRK2*, *TIR2*, and in genes where Tup1p governs transcription. Nucleosomes were mapped at low resolution across these genes in *tup1* cells, displaying a looser chromatin structure, which was confirmed by restriction enzyme accessibility assays.

In terms of NER, deletion of *TUP1* results in faster repair of the endogenous *MFA2* promoter in both DNA strands, irrespective of active transcription. Although deletion of *TUP1* results in a derepression of *MFA2* transcription, mutation of the TATA box reveals that CPDs are still repaired at a faster rate than seen in WTα cells, when transcription is absent. The repair seen in $tup1^{TATA}$ cells is marginally slower than in *tup1* cells. Hence active transcription is not the sole cause of faster repair, which can also help to explain the faster GG-NER detected in the NTS within a *tup1* mutant. The related chromatin structure of these mutants agrees with the theory that positioned nucleosomes reduce NER efficiency. In *tup1*α cells the *MFA2* region studied is more sensitive to MNase digestion than WTα cells, and shows a loss of

positioned nucleosomes. When the TATA box is mutated, the region is less sensitive to MNase digestion, correlating to the repair data. These studies into the endogenous *MFA2* show that chromatin structure modulates NER, and *TUP1* plays a central role not only in the repression of transcription, but also in the reduction of NER efficiency at this gene (Hairong Yu, thesis).

Tup1p mediated repression occurs via multiple mechanisms, which can be placed in two distinct groups, and these different mechanisms predominate at different promoters (Green and Johnson 2004). Firstly, Tup1p acts to repress a subset of genes by altering the local chromatin environment, including the positioning of nucleosomes across the promoter regions of genes, and the hypoacetylation of histone tails via the recruitment of HDACs. Second, Tup1p is thought to directly interact with components of the transcriptional machinery, to prevent transcription initiation. Importantly multiple investigations have shown that the repression of the target gene is a direct consequence of Ssn6-Tup1, and not an indirect effect of Ssn6-Tup1 down regulating activator proteins required for target gene control.

With respect to the endogenous *MFA2*, it is clear that Tup1p has a role in both nucleosome positioning and in mediating the histone acetylation levels. The combination of hyperacetylation of histone H3 and an open chromatin conformation provides an environment whereby enhanced lesion removal is detected. When TAM is incorporated into a *tup1*α strain, there is no significant change in the UV survival of the strain, compared with WTα TAM, suggesting that Tup1p is not essential for NER genome-wide. As the deletion of *TUP1* is known to cause derepression of multiple genes, northern blotting was carried out to determine the relative *MFA2* mRNA levels in a *tup1*α TAM background. It was shown that there was a slight de-repression of *MFA2* transcription, however the level of transcription did not reach the levels detected in WT**a** TAM strain (see Chapter 3), suggesting a complete de-repression of transcription within the plasmid copies did not occur. The level of *MFA2* mRNA was however higher than that seen in WT**a** cells lacking TAM, and therefore this increased level can be attributed to a derepression in TAM. The slight reduction of TAM copy number in the *tup1* background does not account for the reduction in mRNA levels compared with that found in WT**a** TAM. Although it remains unknown why the copy number is slightly reduced in the *tup1* cells, it is likely that a number of factors attributed to the lack of Tup1p may be responsible. Of importance, the copy number is still sufficient to analyse CPD repair in the TAM borne *MFA2* gene.

Repair of CPDs in the *MFA2* promoter region of TAM was shown to be faster in both the TS and NTS in *tup1*α TAM cells. This result is analogous to that seen at endogenous *MFA2*, however a surprising result in light of the transcriptional status of the TAM borne *MFA2* gene in this mutant. With regards to WT transcription levels, it could be assumed that transcriptional activity correlates with faster repair, with TC-NER notably faster than GG-NER in the endogenous *MFA2* promoter. Within the plasmid context however, a high degree of transcription is detected in WT**a** TAM cells, but there is no increase in lesion removal rate in the TS (see Chapter 4). As transcription is detected to a lesser degree in *tup1*α TAM, it would be thought that repair would be slower than found in WT**a** TAM cells. This is not the case, and confirms that Tup1 regulates chromatin structure irrespective of transcriptional status, suggested by results seen in a strain harbouring a TATA box mutation.

The faster repair observed correlated well with a loss of positioned nucleosomes detected by low and high resolution MNase mapping. When *TUP1* is deleted, more MNase sensitive sites are shown across the *MFA2* region of TAM, and specifically in the *MFA2* promoter region. The pattern is similar to that found when *MFA2* is actively transcribed; however, a difference in chromatin environment beyond nucleosomes must exist to provide more efficient repair in the *tup1*α TAM cells.

To further investigate, histone acetylation was studied within the TAM plasmid. Histone hyperacetylation is associated with actively transcribed regions of the genome, and 'open' chromatin structures. UV-induced H3Ac (Lys 9 and Lys 14) was found to be required for efficient NER, and functional NER is not required to observe this H3Ac following UV (Yu and Waters 2005). It has recently been shown that the GG-NER specific Rad16 protein mediates UV-dependant histone H3 acetylation required for efficient GG-NER at *MFA2* (Teng et al. 2008). These previous studies showed that H3 Ac levels at *MFA2* in WTα cells decreased slightly following UV, with a great increase after 1 and 2 hours repair, eventually decreasing back to pre-UV levels. This pattern was echoed in the genome overall (Teng et al. 2008).

Chromatin immunoprecipitation for H3Ac and subsequent rtPCR of various regions within the TAM plasmid showed that H3Ac does increase after 1 and 2 hours post UV in α-cells, as detected in previous studies. Surprisingly, no significant

increase in acetylation levels were detected when *TUP1* was deleted pre-UV, as would be expected from data shown by (Teng et al. 2008). Instead, the acetylation pattern seen in *tup1*α TAM resembled that seen in WTα TAM. When acetylation was looked at specifically in the TAM plasmid, using primers to amplify the TRP1R1/*MFA2* joint region of TAM, downstream of *MFA2*, it was shown that H3Ac was lower in cells lacking *TUP1*. When compared to the results detected for the *MFA2* coding region, and promoter region, it could be assumed that Tup1p does not act to mediate histone acetylation downstream of the *MFA2* sequence in the TAM plasmid.

It may also be suggested that deletion of *TUP1* results in a loss of nucleosomes completely from the *MFA2* promoter region, an aspect which could be investigated using ChIP for histone protein occupancy. This may account for the lack of increase in acetylation, as many nucleosomes within the TAM population are simply evicted. A preliminary assay to determine nucleosome presence in the absence of *TUP1* is described in Appendix IV.6.

It is clear from the literature that Tup1p repression is not mediated by a sole mechanism, but by a combination of factors which interact differently at individual promoters. Multiple conclusions can be drawn from the data obtained from cells lacking *TUP1*. Firstly absence of Tup1p does not derepress *MFA2* transcription fully in the plasmid context, suggesting that the derepressed chromatin environment of the plasmid is not sufficient for full transcriptional activity. The reduction in transcription (compared with fully active *MFA2* with WT**a** TAM cells) could also be related to the DNA structure created by the change in chromatin structure. Due to the supercoiled nature of plasmid DNA, a relaxation of chromatin structure may create a new structure which reduces the ability of the transcription factors and machinery to gain access. The spatial organisation may not favour transcription, however it is also possible that the lack of histone H3 hyperacetylation in the *MFA2* region within *tup1*α TAM cells prevents active recruitment of transcription factors (Reinke and Horz 2003).

It may also be concluded that the relaxation of chromatin structure, defined by the loss of positioned nucleosomes in *tup1*α TAM acts to produce faster lesion removal in both strands of the *MFA2* promoter. This faster repair is independent of transcription, as shown by enhanced GG-NER in the NTS. Therefore, over and above the loss of positioned nucleosomes, the chromatin structure produced when the *TUP1*

repressor gene is deleted is conducive to efficient NER in the TAM borne *MFA2* promoter.

Chapter 6

The role of histone acetylation in NER of the TAM plasmid

6.1 Introduction

As described in Chapter 1, to enable transcriptional, replication and repair machinery to gain access to cellular DNA packaged as condensed chromatin, chromatin modifying agents are employed. These modifying complexes can be broadly divided into two classes, namely (i) histone modifying complexes, such as acetylases and deacetylases, and (ii) ATP-dependant chromatin remodelling complexes. This chapter will focus on the role of histone acetylation in NER operating at the *MFA2* gene.

The N-terminal protruding tails of histone proteins can be subject to multiple modifications including lysine acetylation, methylation and ubiquitination, arginine methylation and serine phophorylation (Berger 2002; Escargueil et al. 2008). The epigenetic information carried on modified histone amino tails may mediate transient changes in transcription, through modification of promoter-proximal nucleosomes, disrupting DNA-chromatin contacts. This code may be read by the actions of non-histone protein recruitment, such as transcriptional activators or by a structural change in the chromatin environment (Escargueil et al. 2008; Turner 2000). The presence of these histone modifications may therefore dictate the higher order chromatin structure along with interactions of enzyme complexes with DNA. The modification of histones may influence many cellular processes, and these epigenetic patterns can be inherited, so introducing an additional level of genetic complexity (Kouzarides 2007).

The hypothesis of a histone code first emerged in 2000 (Strahl and Allis 2000; Turner 2000); it detailed the variety of histone modifications, mainly in the amino terminal tail, which can mediate cellular processes as well as the overall chromatin structure (Jenuwein and Allis 2001). Multiple combinations of histone modifications

may exist on the same histone particle tail, or across a local domain to generate many interdependent codes. The regulation of higher order chromatin structures such as euchromatin and heterochromatin are also thought to be dependant on the local combination and concentration of the histone modifications. It was thought that a change in the relative charge of the histone proteins altered the association with DNA, acting to create an open chromatin structure (Davie and Chadee 1998). However, this is now known to be a complex system with multiple modifications having been discovered to date. The functional landscape of chromatin can be altered by the histone modifications, modulating DNA accessibility and chromatin stability, providing a variety of alternative interaction surfaces for trans-acting factors (Krebs 2007). Modifications may also act differentially depending on the residue affected and the exact modification. For example, both hyperacetylation (H3K9/18/27) and hypoacetylation (H4K16 and H2BK11/16) of specific lysine residues can correlate with transcriptional activity (Kurdistani et al. 2004).

Most histone modifications have been shown to associate with non-histone proteins, usually with a specific protein domain. For example, methylated K9 of histone H3 is recognised by the chromodomain of the heterochromatin protein 1 (HP1) (Lachner et al. 2001). Many chromatin remodelling complexes, and chromatin related proteins contain bromodomains, which link acetylation with transcriptional activity (Hassan et al. 2006; Hassan et al. 2007). Bromodomains bind acetylated lysine residues, and these domains are found in many transcription factors including Gcn5, and chromatin remodelling complexes such as Snf2 (Hassan et al. 2002), acting to anchor chromatin-modifying complexes to promoter nucleosomes. Bromodomains also act in transcription, with acetylated histones bringing bromodomains of transcription factors, such as TFIID to the promoter (Martinez-Campa et al. 2004).

In general HAT mediated histone hyperacetylation is associated with increased transcription (de la Cruz et al. 2005; Hebbes et al. 1988; Myers et al. 2001) and HDAC mediated histone hypoacetylation along with methylation is associated with transcriptional repression (Kouzarides 2007; Pikaart et al. 1998; Vogelauer et al. 2000; Wu and Grunstein 2000). HATs and HDACs are independent chromatin remodelers, they may modulate the structure of chromatin, or the modified residues may provide specific binding surfaces for the recruitment of activators and repressors (Kurdistani et al. 2004). The *in vivo* regulation of gene transcription is highly regulated by the acetylation of histone proteins (Gregory et al. 2001), with the HATs

Gcn5p and Esa1p both recruited to promoters of active protein coding genes (Robert et al. 2004).

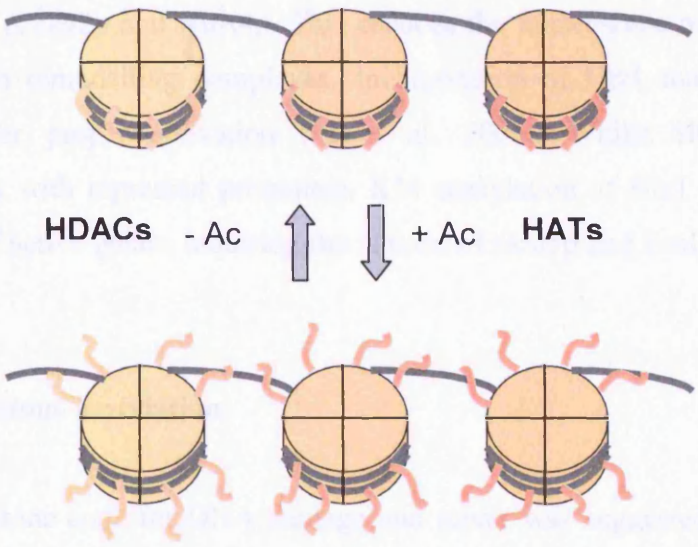

Figure 6.1: HATs transfer an acetyl group to a lysine chain within a core histones basic N-terminal tail region. Lysine acetylation is thought to weaken interactions between the histone particle and DNA, creating a more accessible chromatin environment. HDACs act antagonistically with HATs, removing acetylation groups, and providing a repressive chromatin structure.

HATs and HDACs are both targeted to the transcribed regions of active genes by phosphorylated RNA polymerase II. The majority of HDACs within the human genome function to reset chromatin by removing acetylation at active genes, as discovered by genome wide mapping (Wang et al. 2009).

Unlike canonical histones, histone variants are deposited independently of DNA replication and it has been shown that histone variants including the H2A variant H2A.Z (Htz1 in yeast), play an important role in DNA replication, damage repair, recombination and gene expression (Altaf et al. 2009; Li and Liu 2006). Htz1 is preferentially present in promoter regions of euchromatic genes, required for the activation of the genes, upon which Htz1 is evicted (Li et al. 2005; Zhang et al. 2005). The yeast histone variant H2AZ (Htz1) has been implicated in transcription activation, prevention of the ectopic spread of heterochromatin and genome integrity. In a genome wide localization analysis (Li et al. 2005) it was found that Htz1 is widely and non-randomly distributed throughout the genome in a SWR1-dependant

manner. Htz1 is enriched in intergenic regions compared with coding regions, with the deposition partially reliant on Gcn5p and Bdf1p (a SWR1 complex member that binds acetylated histones) (Zhang et al. 2005). Incorporation of Htz1 into nucleosomes inhibits activities of histone modifiers associated with transcription, namely Dot1p, Set2p and NuA4p. This reduces the nucleosome mobilization driven by chromatin remodelling complexes. Incorporation of Htz1 may mark quiescent promoters for proper activation (Li et al. 2005). Whilst Htz1 is associated preferentially with repressed promoters, K14 acetylation of Htz1 is enriched at the promoters of active genes, requiring the actions of Gcn5p and Esa1p HATs (Millar et al. 2006).

NER and histone acetylation

A histone code for DNA damage and repair was suggested by (Moore et al. 2007) who showed multiple histone H2A modifications in response to DSBs, UV irradiation and oxidative damage. It has been shown that histone acetylation stimulates the initial rate of NER *in vivo* by increasing the chromatin accessibility (Smerdon and Lieberman 1978) and that hyperacetylated mononucleosomes significantly enhance DNA repair synthesis occurring early after UV irradiation (Ramanathan and Smerdon 1989). *In vitro* studies have shown NER is less efficient in reconstituted nucleosomes than in naked DNA (Ura et al. 2001; Wang et al. 1991). NER requires both global and local changes in chromatin structure, allowing the NER machinery to access the damaged DNA, with the degree of silencing directly modulating NER efficiency of the *URA3* gene (Livingstone-Zatchej et al. 2003). Also, CPDs are repaired more readily in transcriptionally active regions of the genome, compared with repressed regions (Bohr et al. 1985). The levels of transcription directly relate to the rate of removal of CPDs in the yeast genome (Ferreiro et al. 2006), and it is likely that the histone modifications are shared by transcription and TC-NER.

UV-DDB, found to be deficient in some XP-E patients, has been found to co-immunoprecipitate with HATs hGcn5 and CBP/p300 (Brand et al. 2001; Datta et al. 2001). In mouse embryonic fibrolasts (MEFs), it has been shown that HMGN1, a nucleosome binding protein which reduces the compaction of the chromatin fibre forms a cellular regulator in the repair of UV-induced damage. HMGN proteins

enhance the rate of transcription initiation and the rate of repair of UV damaged DNA in chromatin. Loss of HMGN1 results in an increased UV sensitivity, suggesting HMGN1 is a chromatin architectural protein involved in the repair of UV damage (Birger et al. 2003). HMGN1 enhances the level of Lys 14 acetylation at histone H3 (Lim et al. 2005).

In mammalian cells, a model involving the tumour suppressor gene p53 has been suggested. UV-induced chromatin relaxation spreads out throughout the entire nucleus in a p53-dependant manner. Interestingly, blockage of an elongating polymerase II also induces a similar chromatin relaxation dependant on p53. This suggests that the UV-induced stalling of RNA polymerase II may be involved in TC-NER and GG-NER, indirectly by increasing the global chromatin accessibility, with p53 as an effector (Rubbi and Milner 2003). Interestingly, not only are H3 and H4 basal acetylation levels increased, but a dramatic change in nuclear distribution in response to p53 is observed, with staining changing from bright punctate spots of transcriptional activity to diffuse staining, representative of global relaxation (Allison and Milner 2003; Rubbi and Milner 2003). The ING family of tumour suppressors also interact with HATs and HDACs to mediate the degree of chromatin relaxation (Kuo et al. 2007; Wang et al. 2006b). ING1 and ING2 act to increase the H4 acetylation levels, and aid in the retention of XPA at the lesion site, but do not colocalise with the repair factors (Kuo et al. 2007; Wang et al. 2006b) suggesting they regulate the chromatin structure rather than directly being involved in the NER mechanism. In yeast H3 and H4 acetylation changes are independent of functional NER, indicating that acetylation occurs prior to repair (Yu et al. 2005). The overall relaxation of the genome may help in the damage detection stage of the NER pathway, with more specific local histone modifications allowing for efficient NER at that locus. The epigenetic landscape is also of importance following NER repair synthesis, as nucleosomes which are deposited in the repaired region contain ubiquitinated H2A (Zhu et al. 2009).

The role of Gcn5p at *MFA2*

Gcn5p acts as a catalytic subunit in the ADA and SAGA HAT complexes specific for histones H3/H2B (Clements et al. 2003; Grant et al. 1997; Trievel et al. 1999). Gcn5p is also a member of the SAGA-like complex (SLIK) (Pray-Grant et al.

2002). Gcn5p is recruited to promoters by activators such as Gcn4p or Swi5p, stimulating histone acetylation, and subsequent transcription (Cosma et al. 1999; Krebs et al. 1999; Kuo et al. 2000). Gcn5p HAT is required for Gcn4p-mediated transcriptional activation and for activation of the *PHO8* promoter (Teng et al. 2002).

Gcn5p regulates the expression of 5% of the yeast genome (Holstege et al. 1998), however other HATs may complement Gcn5p. Deletion of *GCN5* has no effect on the repression of endogenous *MFA2*, with no active transcription detected in *gcn5*Δα cells (Liu 2005). However, deletion of *GCN5* in mating type **a** cells severely impairs the transcription of *MFA2* (Liu 2005; Teng et al. 2002). Gcn5p has clearly been implicated in the transcription of *MFA2*, allowing for the efficient recruitment of the transcription machinery, however the precise role of Gcn5p in NER is not fully understood.

A deletion of *GCN5* confers a moderate UV sensitivity phenotype, suggestive of a role in UV survival. In both **a** and α mating type cells lacking the HAT Gcn5p, a marked reduction in CPD removal is detected in both the TS and NTS of the *MFA2* promoter. Deletion of *GCN5* impairs but does not prevent the NER of CPDs at the repressed *MFA2* promoter, therefore this role of Gcn5p is independant of its role in transcription (Yu et al. 2005). Although the reduction in repair in the TS of **a** cells may be accounted for by the four-fold reduction in functional transcription, Gcn5p has a clear role in GG-NER. A general down regulation of NER genes was disregarded as NER is unchanged at loci such as *RPB2* (Teng et al. 2002).

(Yu and Waters 2005) found a *GCN5*-dependant ten-fold hyperacetylation of histone H3 in WTα cells at the repressed *MFA2* promoter following UV. The acetylation levels decreased with repair, eventually returning to pre-UV levels. This change in acetylation shadows the chromatin accessibility data, confirming that hyperacetylation and a more accessible chromatin environment result in faster lesion removal at *MFA2*.

6.2 Materials and methods

All materials and methods are as described in Chapters 2 and 4.

6.2.1 Yeast strains

PSY316 *(MATα ade2-101 ura 3-52 leu 2-3, 112 Δhis 3-200 lys2 trp1)*

Δgcn5 (MATα ade2-101 ura 3-52 leu2-3, 112 Δhis 3-200 lys2 trp1)

6.3 Results

6.3.1 UV survival

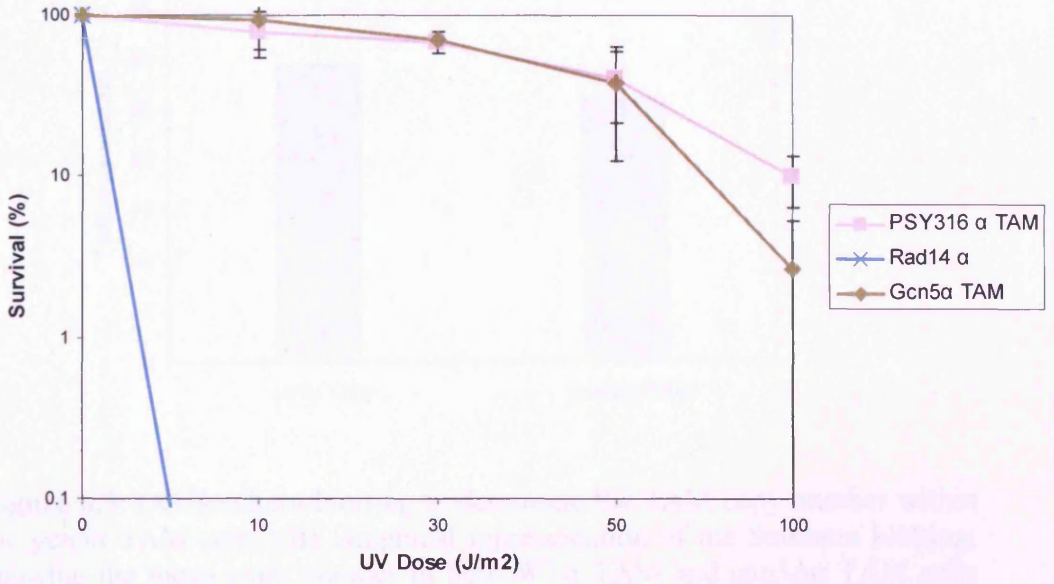

Figure 6.2: UV survival curves displaying the slightly reduced UV survival (%) of the *gcn5α* TAM strain (Appendix V).

It appears that the UV survival is only minimally affected when *GCN5* is deleted (Figure 6.2). Previous studies have shown that *gcn5* cells show a slight UV sensitivity, and these results agree with the previous conclusions.

6.3.2 Copy number determination

As performed for previous TAM-containing strains, the relative plasmid copy number was determined to ensure that the TAM borne *MFA2* gene was represented for experimental procedures.

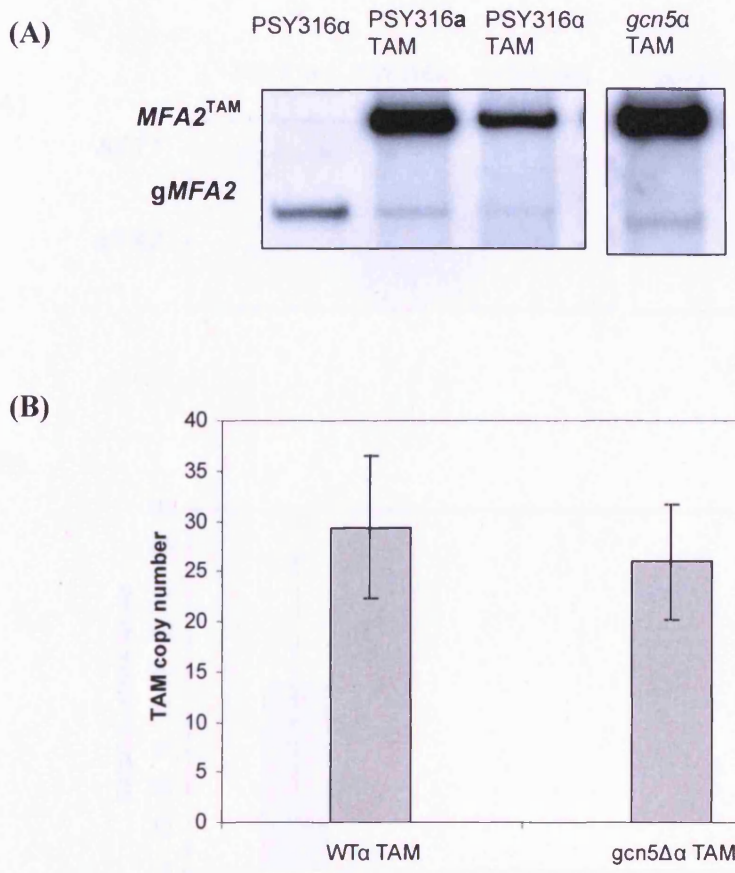

Figure 6.3: (A) Southern blotting to determine the TAM copy number within the *gcn5α* TAM cells. **(B)** Graphical representation of the Southern blotting, showing the mean copy number in both WTα TAM and gcn5Δα TAM cells (Appendix V).

There is no effect of deleting the HAT *GCN5* on the retention of the TAM plasmid within this strain, as shown in Figure 6.3. There is no significant difference ($p>0.01$, Appendix V) in the copy number of TAM in the strain studied, with an average of 26 copies per cell. The multiple copy number properties are sufficient for high resolution analysis.

6.3.3 The effect of *GCN5* deletion on *MFA2* mRNA levels

As Gcn5p has a role in transcription-related histone acetylation at the *MFA2* locus, the *MFA2* mRNA levels were determined for the *gcn5*Δα strain. As the strain was constructed within WTα mating type cells, *MFA2* is assumed to be transcriptionally repressed.

(A)

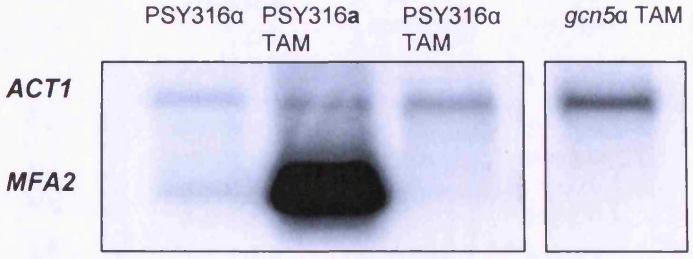

(B)

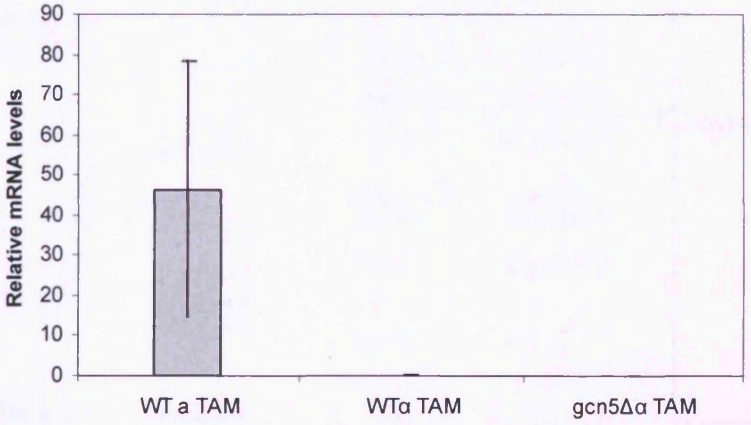

Figure 6.4: (A) and **(B)** Northern blotting analysis for *MFA2* mRNA level determination indicates there is no visible mRNA production when *GCN5* is deleted (Appendix V).

As can be shown in Figure 6.4, the deletion of *GCN5* does not affect *MFA2* transcription. The gene remains transcriptionally repressed in an α cell background, even within the plasmid context. This is unlike the role of Gcn5p in **a** cells where its absence automatically reduces transcription of *MFA2* (Teng et al. 2002).

6.3.4 CPD repair

The repair of CPDs in a *gcn5*Δ mutant was studied to determine the role H3 acetylation plays in NER of the *MFA2* region studied.

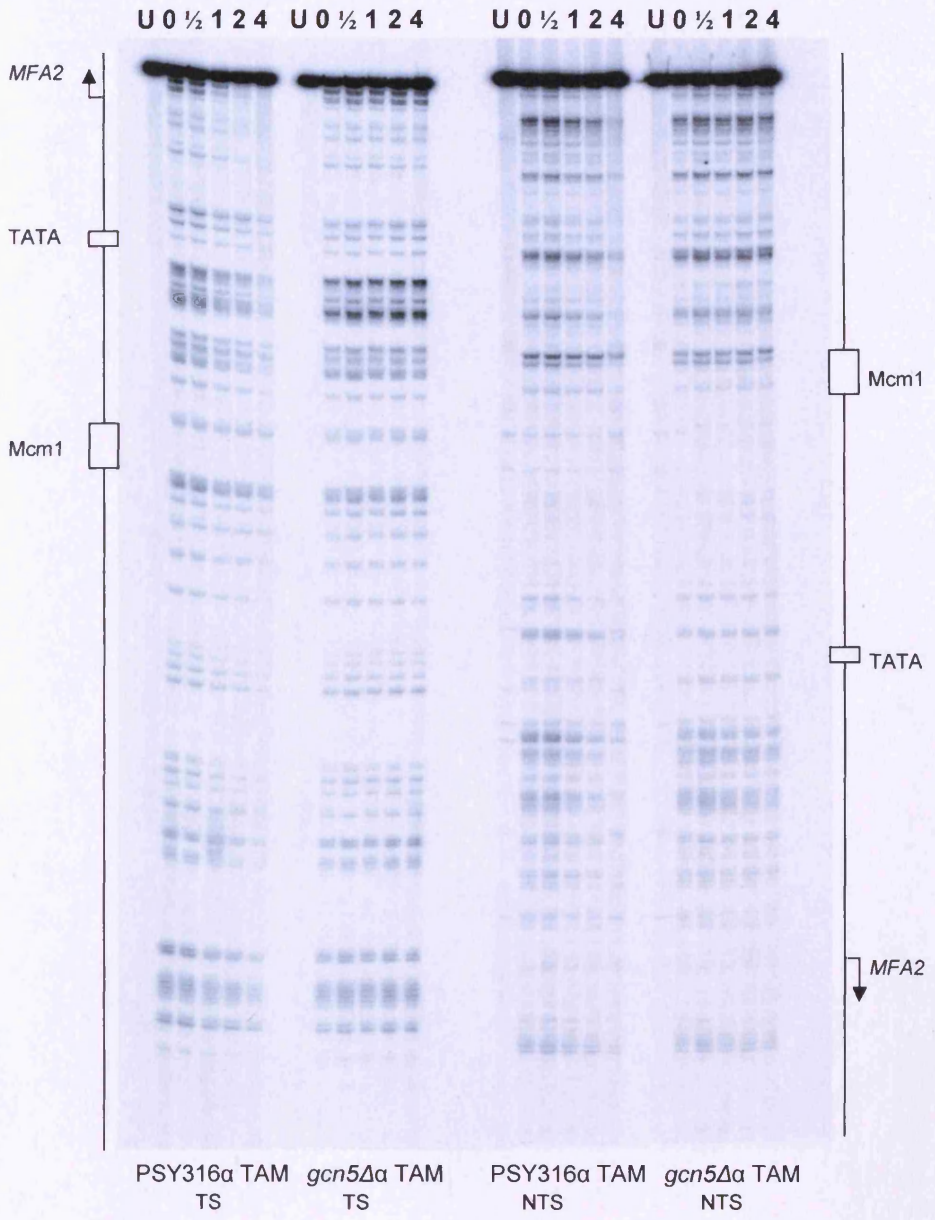

Figure 6.5: A typical high resolution gel, depicting the removal of specific CPDs from WTα TAM and *gcn5*Δα TAM strains with time after UV (U,0,0.5,1,2,4 hours). Following *Hae*III and ML *endo* digestion, samples were end-labelled and resolved on a polyacrylamide gel. TS and NTS displayed.

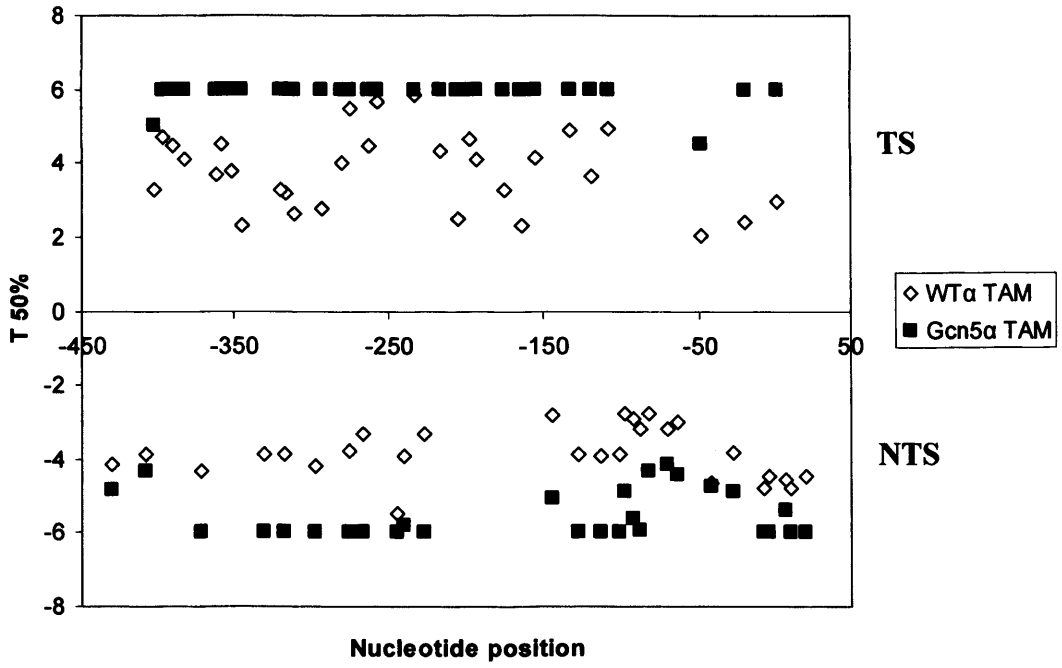

Figure 6.6: Graphical quantification of the T50% in WTα TAM and *gcn5*Δα cells, taken from 3 biological repeats (Appendix V). Little or no repair is seen in both strands of the *MFA2* promoter region after 6 hours when *GCN5* is absent.

CPD removal analysis shows that NER is compromised when the gene for the acetyltransferase Gcn5p is deleted (Figures 6.5 and 6.6). Little or no repair is seen across the *MFA2* promoter region studied, in both the TS and NTS in *gcn5* TAM cells. Repair is significantly slower when *GCN5* is absent ($p<0.01$, Appendix V). This shows that Gcn5p is required for efficient lesion removal in the *MFA2* promoter of the TAM plasmid.

6.3.5 Nucleosome mapping

The positioning of nucleosomes was examined for the *gcn5* strain, expected to resemble that of WTα TAM cells.

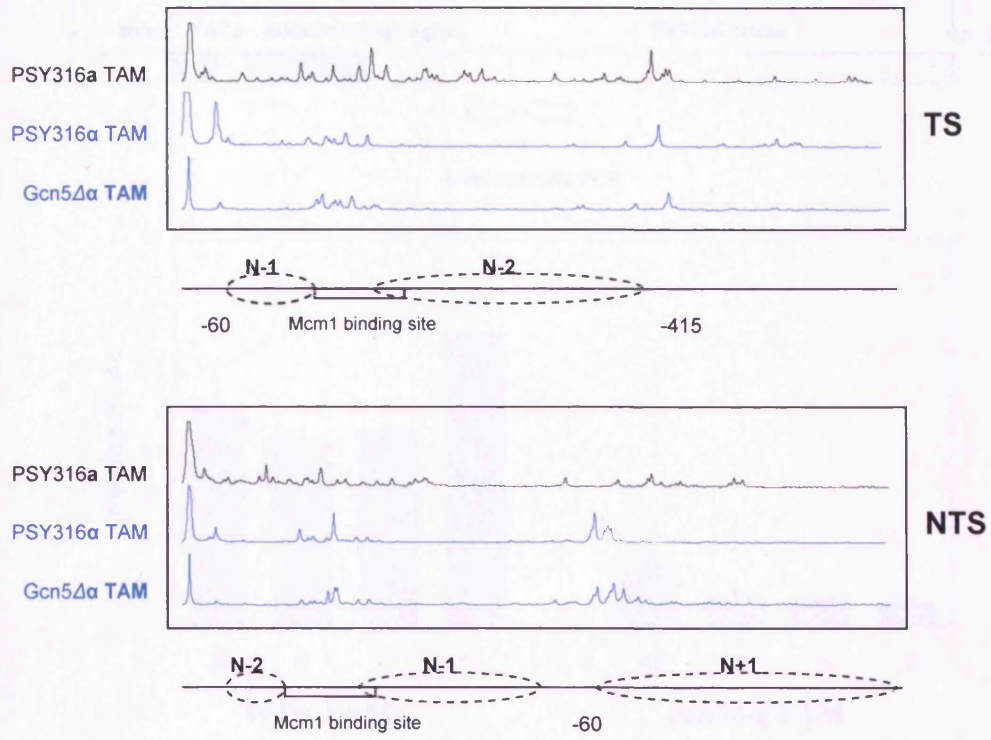

Figure 6.7: High resolution nucleosome mapping within the *MFA2* promoter region. The trace obtained in *gcn5*α TAM cells resembles that seen in WTα TAM cells, showing positioned nucleosomes in the repressed gene, obtained from a single gel (Appendix V.6).

Nucleosomes appear to be positioned in the *gcn5*Δα strain, in the same manner as detected in WTα cells, confirmed by low and high resolution mapping (Appendix V.6). This positioning correlates with the transcription data, showing that the *MFA2* gene is repressed.

6.3.6 H3 acetylation

As Gcn5p has been implicated as the HAT involved in the transcriptional activation of *MFA2*, as well as roles in NER at this gene, H3 acetylation levels were

studied both specifically within the TAM plasmid (Figure 6.8), and at *MFA2* (Figure 6.9).

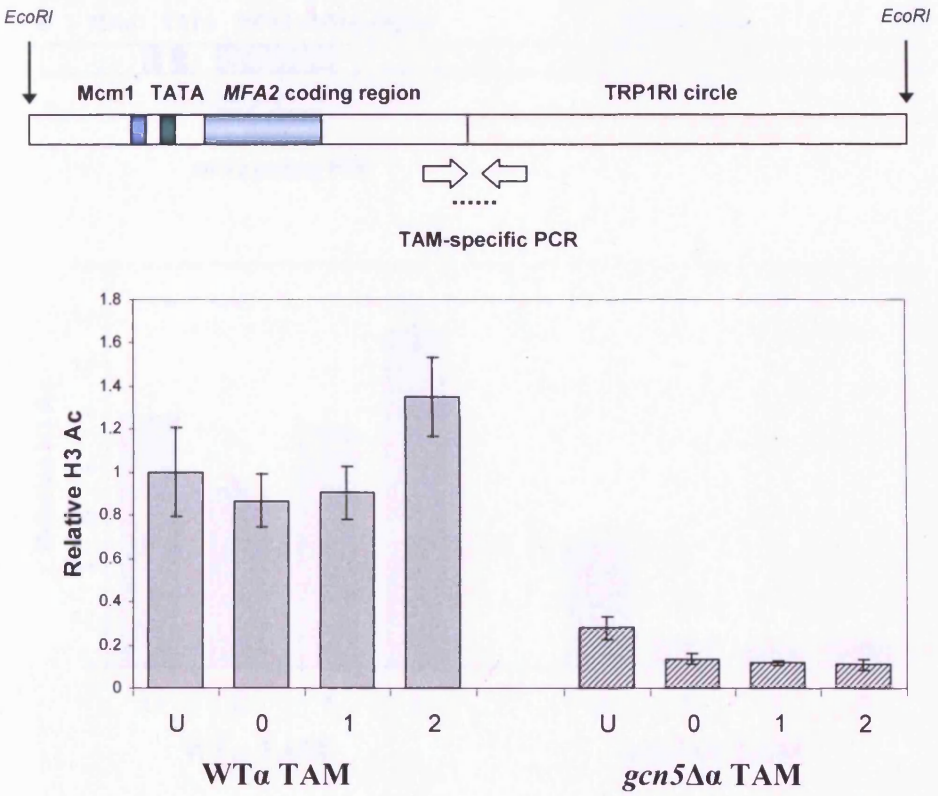

Figure 6.8: RtPCR employing the IP1 and IP2 primers, showing the relative H3Ac levels in the TAM plasmid unique join region, downstream of the *MFA2* gene. Samples were taken from untreated cells, and cells treated with 100Jm^2 UV, and allowed to repair for 0, 1 and 2 hours. WTα TAM and *gcn5*α TAM data shown from 3 repeats (Appendix V).

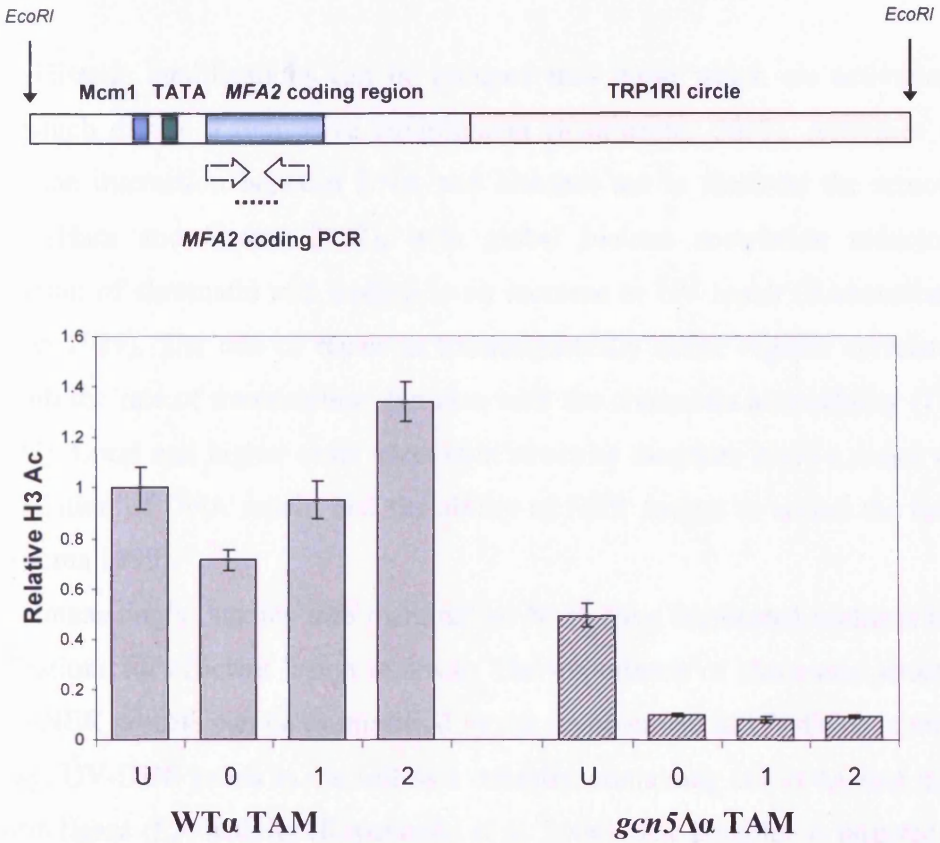

Figure 6.9: Relative H3Ac levels in WTα TAM and *gcn5*α TAM cells for the *MFA2* coding region I untreated and UV irradiated cells allowed to repair for 0,1 and 2 hours, employing N1 primers, from 3 repeats (Appendix V).

As displayed in both Figure 6.8 and 6.9, H3 acetylation at both locations is reduced in a *gcn5* mutant when compared with the WT. The dramatic reduction in acetylation levels in the untreated samples are further reduced after UV treatment, with no signs of recovery after 2 hours repair. These results suggest that Gcn5p is required for the H3 acetylation at the *MFA2* gene, and within the TAM plasmid. The residual H3 acetylation levels detected may be due to the actions of an alterative HAT acting on the plasmid. There is a hint of such activity at the endogenous *MFA2* gene as H3 acetylation is modestly increased at time points following UV in the absence of Gcn5 (Yu et al. 2005).

6.4 Discussion

Histone modifications can be grouped into those which are activating and those which dictate a repressive environment (Kouzarides 2007). Activities which disrupt the interaction between DNA and histones act to facilitate the removal of lesions (Hara and Sancar 2002), with global histone acetylation reducing the compaction of chromatin and leading to an increase in UV repair (Ramanathan and Smerdon 1989). The rate of repair in transcriptionally active regions correlates not only with the rate of transcription, but also with the chromatin accessibility (Teng et al. 1997). Local and higher order chromatin structure therefore plays a major role in the regulation of DNA repair, and the ability of NER factors to access the lesion is key (Thoma 1999).

Interestingly, studies into mammalian NER have implicated multiple histone modifications for efficient lesion removal. The importance of chromatin structure in the GG-NER process can be exemplified by the involvement of UV-DDB in the NER pathway. UV-DDB exists in the cell as a complex containing cullin 4A that displays ubiquitin ligase (E3) activity (Kapetanaki et al. 2006). The complex is targeted to the UV-induced lesion via DDB2 while DDB1 acts to bring about the ubiquitin ligase activity. The DDB1-CUL4A aids in the ubiquitylation of both DDB2 and XPC, along with histones H2A, H3 and H4 (Kapetanaki et al. 2006; Sugasawa et al. 2005; Wang et al. 2006a). The ubiquitylation may act to destabilise nucleosomes on the DNA, or could act to recruit NER factors. The DNA repair protein hHR23B (part of the DNA damage recognition complex along with XPC) contains ubiquitin-associated domains. It is likely that DDB1-CUL4a^{DDB2} E3 stabilises the repair complex and destabilises the nucleosomes, providing an efficient platform for GG-NER (Zhou et al. 2008).

Human disease can be associated with changes in the epigenetic landscape and the disregulation of histone modification effector proteins such as histone acetylases (Hirst and Marra 2008). Many HAT genes are altered in human cancers leading to a loss of H3 acetylation at tumour suppressor genes (Gibbons 2005).

The importance of the interplay between HATs and HDACs can be exemplified in transcriptional studies, where the activation or repression of a gene or subset of genes occurs. At the Tup1p-regulated *MFA2* gene, HDACs play a role in

transcriptional repression, with Tup1p known to interact with at least 3 different HDACs (Watson et al. 2000; Wu et al. 2001). When histone tails or deacetylases are mutated it can result in the derepression of Tup1p-regulated genes including *MFA2*. The transcriptional activation of *MFA2* however is associated with hyperacetylation of residues within core histone tails, a reaction catalysed by the HAT Gcn5p. The data accrued within this chapter sheds light on the role of Gcn5p, and therefore histone acetylation in NER of the TAM borne *MFA2* gene.

This study has shown that yeast cells lacking the HAT Gcn5p confer a mild UV sensitivity, being slightly more sensitive than WT cells. It can also be seen that there is no significant difference in TAM copy number within this strain, and the deletion of *GCN5* does not affect the repression of the TAM borne *MFA2* gene.

The defective lesion removal across the *MFA2* promoter region within *gcn5* cells confirms Gcn5p has a role in the GG-NER of this region. Repair of CPDs is shown to be very slow in both the TS and NTS of the repressed *MFA2* promoter, a result similar to that seen in the endogenous gene. The deletion of *GCN5* does not alter the nucleosome positioning across the *MFA2* promoter region, with the nucleosomes residing in the same position as found in WTα cells.

The rtPCR results show that deletion of *GCN5* causes a significant reduction of acetylation levels both specifically within the TAM plasmid and in the *MFA2* coding region, suggesting Gcn5p is responsible for the majority of the H3 acetylation at this locus required for efficient repair. As the change in histone code appears to be the driving force behind the slower rate of CPD repair, without a change in nucleosome positioning, it is clear that subtle changes in the epigenetic landscape act to affect the cellular processes. This may be by directly affecting the local chromatin environment, or by altering the ability or affinity of non-histone proteins being recruited to the region. Taken together, the repressed TAM borne *MFA2* gene contains positioned nucleosomes, and no active transcription is seen. By deleting *GCN5*, repair becomes slower across the *MFA2* promoter region, suggesting that a more 'closed' chromatin environment is created when histone H3 acetylation is unable to take place efficiently.

As the histone code may act in a highly specific manner depending on the loci, it may be suggested that the histone code alone does not regulate the efficiency of a particular cellular process, for example NER, at a specific gene promoter. It is highly likely that the DNA sequence and structure also play a role in providing a platform for

DNA-binding proteins and an efficient environment for factor recruitment. The links between histone acetylation and NER will be discussed in greater detail in the general discussion.

Chapter 7

A role for Rad16p in NER of the TAM plasmid

7.1 Introduction

In order to facilitate the access of transcription factors to DNA, changes must take place within the repressive chromatin structure. These changes are mediated by chromatin remodelling complexes such as Swi/Snf or the acetylation of histones by histone acetyltransferases (Berger 2002). NER requires at least 30 proteins to remove damage from a naked DNA template (de Laat et al. 1999), and, like transcription, these proteins must be able to afford access in a chromatin template for efficient NER to take place. The interface between an open and a repressive chromatin structure in terms of NER can vary greatly between genes, where the TC-NER/GG-NER border can be found either upstream or downstream of the transcription start site (Tijsterman et al. 1996). This chapter focuses on the *RAD16* gene product, a protein implicated in the GG-NER pathway, required for lesion removal from the repressive chromatin structures encountered throughout transcriptionally inactive regions of the genome and the NTS of transcriptionally active genes.

The heterogeneous rates of lesion removal within the genome have been well documented, and exemplified in 1989 utilising the mating type loci genes MATα and HMLα (Terleth et al. 1989). These loci contain the same DNA sequence, however MATα is transcriptionally active and HMLα is inactive, allowing repair to be determined in terms of transcriptional activity and chromatin structure. UV induced CPDs were shown to be removed preferentially from the active MATα locus when compared with the inactive HMLα locus (Terleth et al. 1989). This removal of CPDs from both strands of the inactive HMLα locus was later found to be dependant on the *RAD7* and *RAD16* gene products (Terleth et al. 1990). Further investigations uncovered that *RAD16* and *RAD7* deletion mutants confer the same repair phenotype and moderate UV sensitivity (Verhage et al. 1994), confirming roles in the same

repair pathway; and the proteins were designated as a GG-NER specific complex (Terleth et al. 1990; Verhage et al. 1994).

As well as Rad16p's role in the removal of CPDs from repressed genes such as HMLα, there is also a requisite for the protein in the removal of CPDs from the NTS of active genes such as *GAL7* and the constitutively expressed *RBP2* and *MFA2* genes (Jones et al. 1992; Sweder and Hanawalt 1992; Teng et al. 1997; Tijsterman et al. 1996). The involvement of *RAD16* in the differential repair within *S. cerevisiae* was confirmed following the cloning of the gene (Bang et al. 1992).

Due to the role of Rad16p in repair at inactive loci and silenced genes, it was suggested that it may function to provide access for the excision repair enzymes (Bang et al. 1992). This idea was supported when it was discovered that Rad16p was a member of the snf2/swi2 family of chromatin remodelers (Eisen et al. 1995), with inherent DNA dependant ATPase activity (Guzder et al. 1997). With many Snf2 family proteins able to remodel chromatin (Vignali et al. 2000) it was suggested that Rad16p may function to unravel the chromatin environment ahead of NER protein recruitment (Prakash and Prakash 2000; Thoma 1999).

Further roles for Rad16p arose when structural protein analysis showed that the protein contains a zinc binding domain, within its ATPase domain along with a RING finger motif (Eisen et al. 1995). The presence of the RING finger motif suggested the potential of Rad16p to function as an ubiquitin protein ligase (E3), with the ability to interact with ubiquitin conjugating enzymes (E2) (Aravind et al. 2003; Lorick et al. 1999). Further investigations showed Elc1, a homologue of the mammalian E3 ligase has also been associated with the Rad16p-7p complex (Ho et al. 2002; Ramsey et al. 2004). The GG-NER complex is known to interact with the Rad4p-23p complex (Wang et al. 1997), and the association with Elc1 is thought to regulate the levels of intracellular Rad4p, and therefore the NER protein response to UV light (Gillette et al. 2006; Ramsey et al. 2004).

The complex role of Rad16p in GG-NER is confounded by a series of *in vitro* studies, which suggest Rad16p is not absolutely required for the initial pre-access stages of the repair mechanism. In contrast to the defective incision of damaged DNA observed in most extracts of NER mutant strains, *RAD7* and *RAD16* mutants are fully proficient in the incision step of damaged DNA *in vitro* and at HMLα and MATα, but defective in the oligonucleotide excision stage and repair synthesis, supporting a role after damage recognition (Reed et al. 1998; Wang et al. 1997).

The essential protein Abf1p has also been found to be a component of the GG-NER complex (Reed et al. 1999). Rad16p has more recently been shown to be required for the generation of superhelical torsion *in vitro* necessary for the excision of the damage containing oligonucleotide (Yu et al. 2004). The superhelical torsion generated along with the translocase activity of the GG-NER complex was found to be insufficient to slide nucleosomes in an *in vitro* assay (Yu et al. 2008), a possible mechanism for the prevention of spurious transcription. However, the effect on the local chromatin environment appears sufficient to allow access to the histone acetyltransferase Gcn5p.

As discussed in Chapter 6, Gcn5p-mediated H3 acetylation modulates NER at *MFA2* (Teng et al. 2002). In the repressed *MFA2* gene following UV, H3 hyperacetylation results in chromatin remodelling required for efficient lesion removal. The alterations in chromatin structure were found to be independent of the DNA damage recognition factors Rad4p or Rad14p (Yu et al. 2005). The H3 hyperacetylation was shown to facilitate efficient lesion removal, and subsequently the response to UV was attributed to Rad16p (Teng et al. 2008).

Following chromatin immunoprecipitation studies it was shown that UV-dependant H3 acetylation is mediated by Rad16p at the *MFA2* promoter and throughout the genome. A model can therefore be suggested for the GG-NER complex, outlined in Figure 7.1. It is speculated that Rad16p aids in preparing the local chromatin structure in such a way which allows further chromatin modifying proteins, such as Gcn5p, to efficiently bind to and alter the chromatin environment.

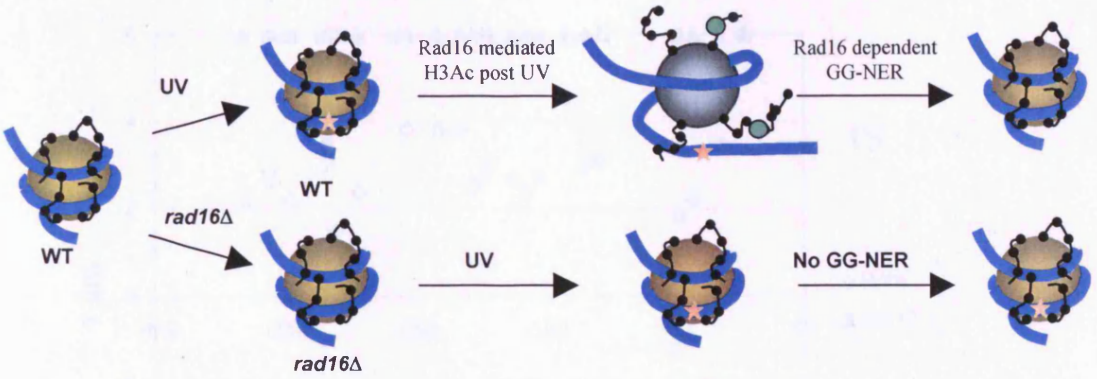

Figure 7.1: UV irradiation can induce DNA damage, such as CPDs ( ), which induce a Rad16p mediated H3Ac event ( ) to alter the DNA-histone interactions, allowing for Rad16p dependant GG-NER. When *RAD16* is deleted, no H3Ac event takes place following UV and GG-NER fails to remove the CPDs. Adapted from Y. Teng.

At the endogenous *MFA2* gene, Rad16p is required for the repair of the NTS in **a** and α cells, but only a partial requisite is seen for Rad16p in repairing the control region (Teng et al. 1997). As Rad16p is thought to activate the Gcn5p-mediated H3 acetylation required for efficient NER, it seems plausible that a hyperacetylated chromatin environment would not need Rad16p for this initial NER process. Utilising a *tup1* mutant (as discussed in Chapter 5) which is constitutively transcriptionally activated and therefore hyperacetylated it was shown that the requisite for Rad16p could be overcome at the *MFA2* promoter. However, it should be noted that although the Tup1p regulated *STE2* and *BAR1* genes follow the trend seen at *MFA2*, repair at *RNR3* still depends on Rad16p, perhaps due to the difference in regulatory regions (*RNR3* does not contain an upstream mcm1 binding site) ((Teng et al. 2008) and Y Teng, personal communication).

Following high resolution CPD repair analysis, it was shown that Rad16p is absolutely required for the repair of CPDs in the inactive endogenous *MFA2* gene within WTα cells. The deletion of *RAD16* results in no repair detected across the region studied (Liu 2005) (Figure 7.2). These data confirm that Rad16p plays a vital role in the GG-NER pathway at this gene.

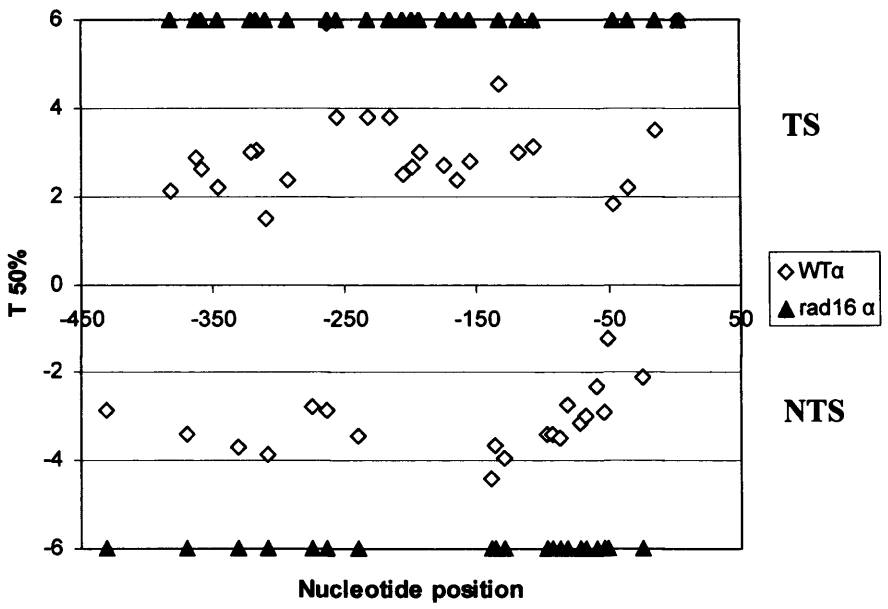

Figure 7.2: The repair profiles for the endogenous *MFA2* promoter region in both WTα and *rad16α* mutant strains. The CPDs within this region fail to be repaired within 6 hours when *RAD16* is absent (Liu 2005).Also trend seen in (Teng et al. 2008) (Appendix VI).

Much of the work regarding the role of Rad16p in NER has been carried out at *MFA2*, and subsequently it is essential to compare the previously recorded data with the responses seen in the plasmid context. This will then provide a clear picture of GG-NER in the plasmid context when compared to the above events at the endogenous locus.

7.2 Materials and Methods

All materials and methods were carried out as previously described.

7.2.1 Yeast strains

PSY316 *(MATα ade2-101 ura 3-52 leu 2-3, 112 Δhis 3-200 lys2 trp1)*

Δrad16 (MATα ade2-101 ura 3-52 leu2-3, 112 Δhis 3-200 lys2 trp1)

7.3 Results

7.3.1 UV survival

As previously described, *RAD16* deletion confers a moderate UV sensitive phenotype (Prakash et al. 1993), consistent with a role for the gene in the removal of UV induced damage. UV survival data were collected for the TAM containing *RAD16* mutant strain.

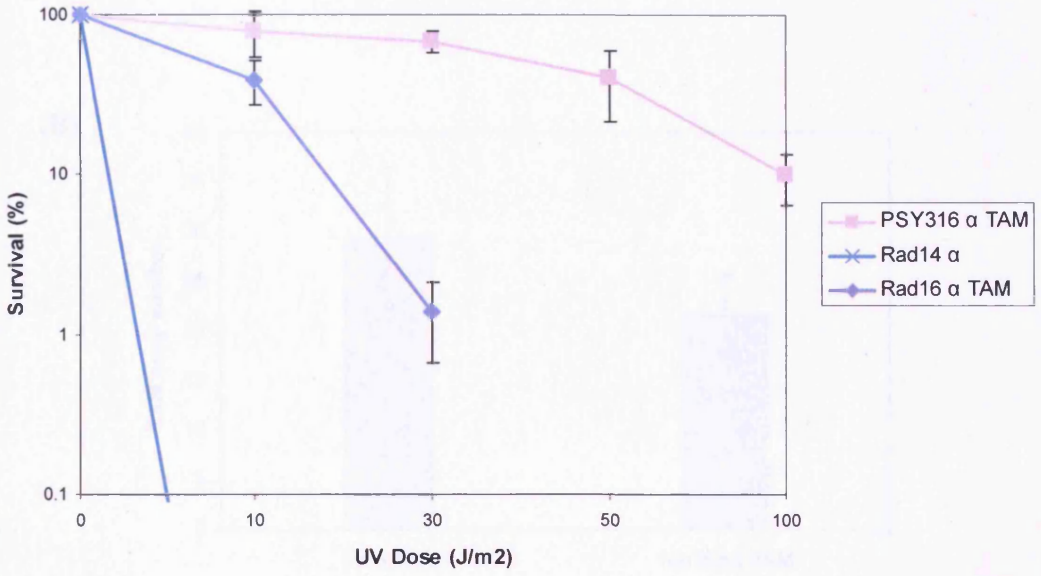

Figure 7.3: The UV survival was calculated for the *rad16α* TAM strain. Also shown is the WTα TAM strain, and the UV sensitive The *rad14α* strain for comparison. Rad14 is an essential NER factor, conferring considerable UV sensitivity (Appendix VI).

Having introduced the TAM plasmid into a *rad16α* strain, the UV survival was calculated. As shown in Figure 7.3, cells are moderately UV sensitive when *RAD16* is deleted, so following the phenotype previously described for *rad16* cells. This suggests that incorporation of the plasmid does not alter the cell's ability to repair UV-induced lesions globally.

7.3.2 Copy number determination

Having transformed TAM into a *rad16α* background, the copy number was determined for the resulting strain.

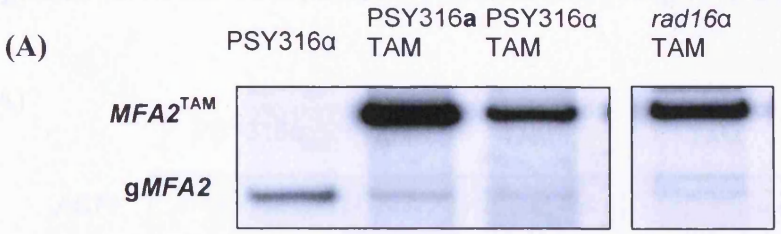

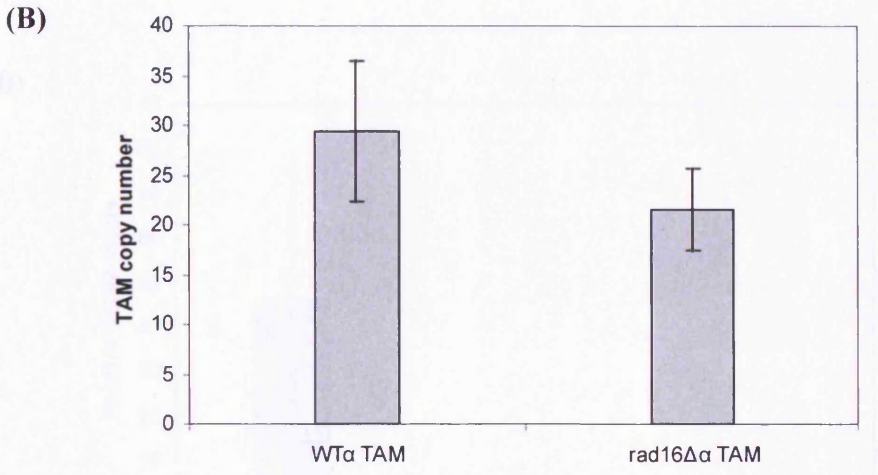

Figure 7.4: (A) Southern blot analysis, using a probe for *MFA2*, to determine the relative copy number of the TAM plasmid within the various strains. (B) Graphical representation of the mean copy number in WTα TAM and *rad16* α cells (Appendix VI).

The copy number of TAM within the *rad16α* TAM cells is reduced compared to that seen in WTα TAM cells, but this is not a significant decrease ($p>0.01$, Appendix VI). A sufficient number of copies persist per cell for accurate high resolution damage analysis, employing at least 10-fold less cells than for the analysis of the endogenous gene.

7.3.3 mRNA analysis in a Rad16 mutant

As previously described, *MFA2* is not transcriptionally active in WTα mating type cells. When *RAD16* is deleted, no change in the transcriptional status of endogenous *MFA2* has been previously documented (Teng et al. 2008).

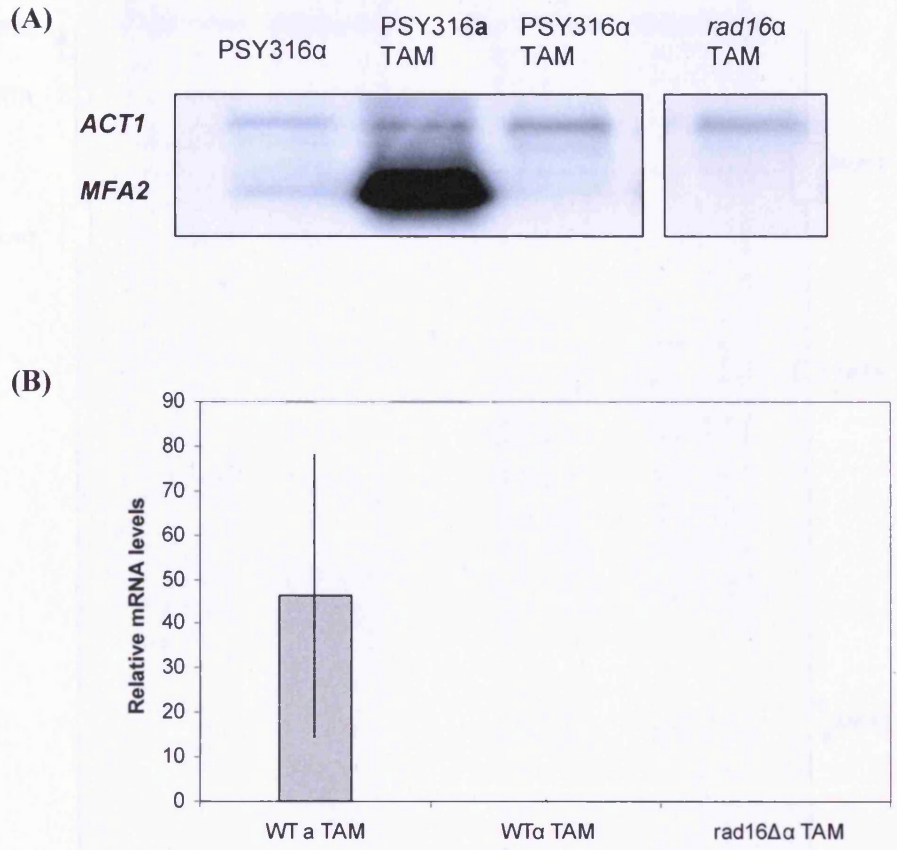

Figure 7.5: (A) Northern blot analysis to determine whether any active transcription is taking place in the *rad16*α TAM strain. Displayed graphically beneath (B), it is clear that *MFA2* is not transcribed in this strain (Appendix VI).

As expected in mating type α cells, *MFA2* is not transcribed within the TAM strain, even when *RAD16* is deleted. There is no detection of *MFA2* mRNA levels, suggestive of a repressed gene.

7.3.4 CPD repair

The repair of CPDs in a *rad16*Δα TAM mutant was studied to determine the role of *RAD16* in NER of the *MFA2* region studied.

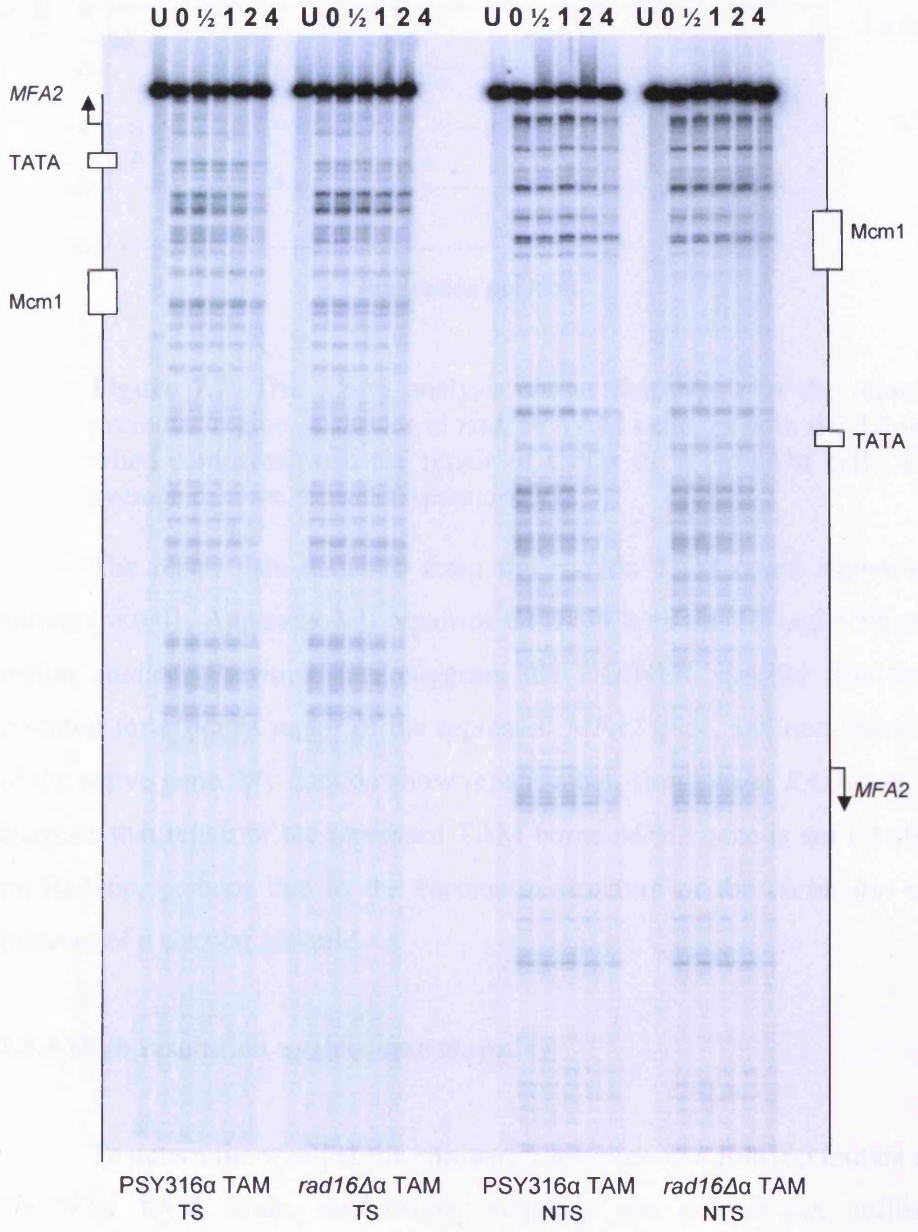

Figure 7.6: A typical high resolution gel to detect CPD repair in WTα TAM and *rad16*α TAM cells. A decrease in signal across a specific CPD-indicating band is representative of repair at that lesion. However, precise extents of repair are only arrived at following quantification of bands, and these images should not be used as indications of repair extents. TS and NTS displayed.

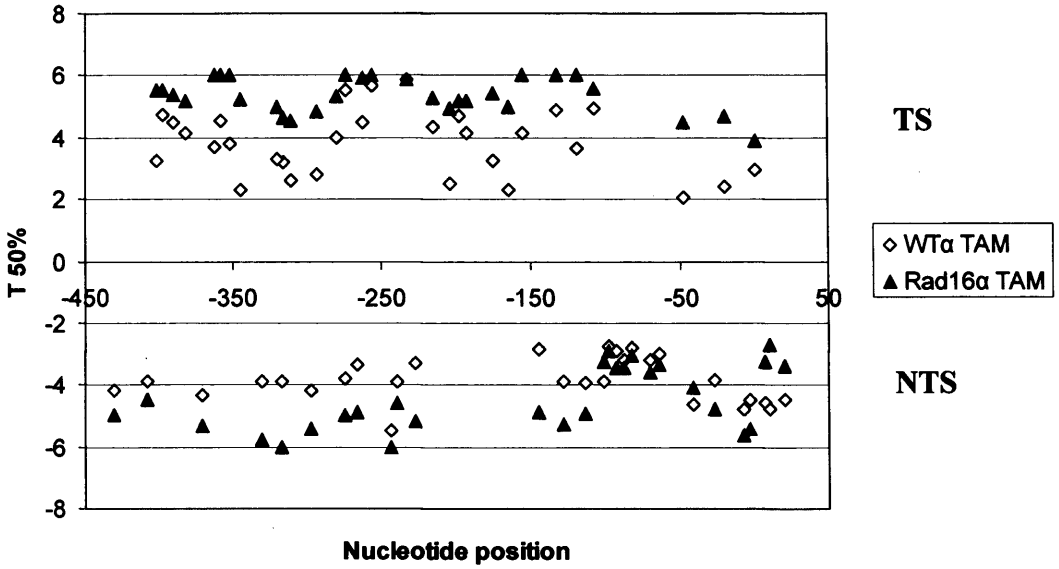

Figure 7.7: The T50% analysis shows that repair of the repressed *MFA2* promoter region is slower in *rad16α* TAM cells, in both the TS and the NTS when compared with the repair of CPDs in WTα TAM cells. Data are the average of three repeats (Appendix VI).

The repair data acquired from the *rad16α* TAM strain shows significantly slower ($p<0.01$, Appendix VI) repair of CPDs in both the TS and NTS of the *MFA2* region studied. Previous data suggests the GG-NER specific Rad16p protein is essential for efficient repair of the repressed *MFA2* gene, and non-transcribed strand of the active gene. My data do show repair, albeit slow, when *RAD16* is absent. This suggests that repair of the repressed TAM borne *MFA2* gene is not totally dependant on Rad16p, perhaps due to the chromatin structure or the chromatin environment inherent of a circular plasmid.

7.3.5 High resolution nucleosome mapping

To determine whether the chromatin structure in a Rad16p mutant differs from the WTα TAM strain, nucleosome mapping was carried out, utilising MNase digestion to position nucleosomes across the *MFA2* region of interest.

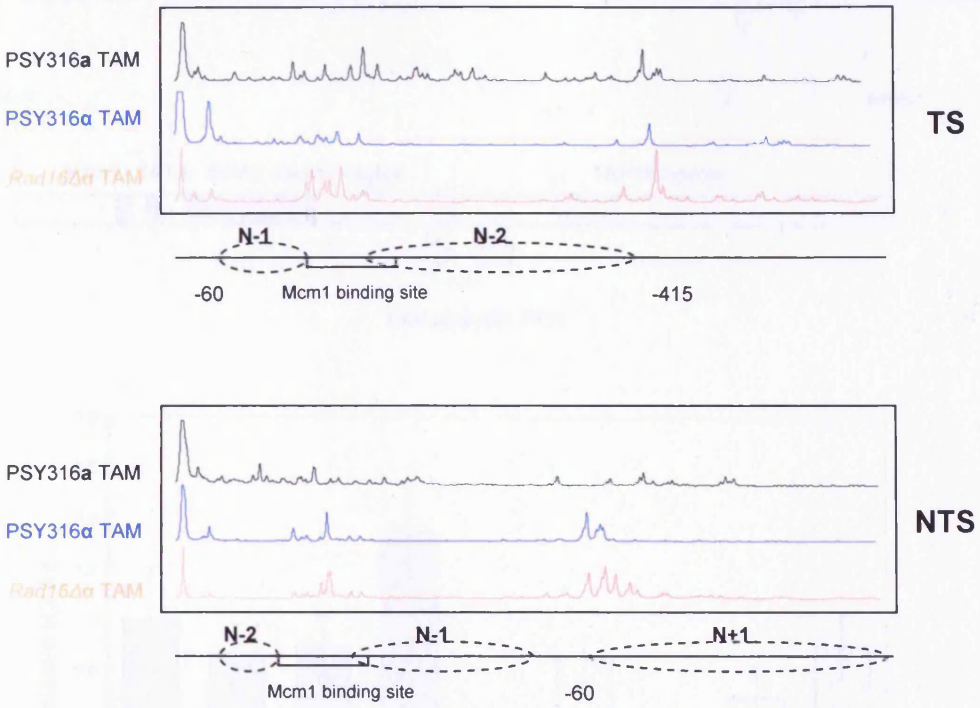

Figure 7.8: A typical densitometric scan of MNase sensitivity sites of the *MFA2* promoter region. This figure shows that nucleosomes are positioned in Rad16α TAM cells, the same as in WTα TAM cells, in both the TS and NTS.

The transcriptionally repressed *MFA2* gene in *rad16*α TAM contains positioned nucleosomes as found in WTα TAM cells, as confirmed by both low and high resolution nucleosome mapping (Appendix V.6 and VI.6).

7.3.6 Histone acetylation

Due to the recent involvement of Rad16p in the UV-dependant histone acetylation required for efficient GG-NER, the H3 acetylation levels were investigated for the TAM system (Figure 7.9) and at the *MFA2* promoter (Figure 7.10).

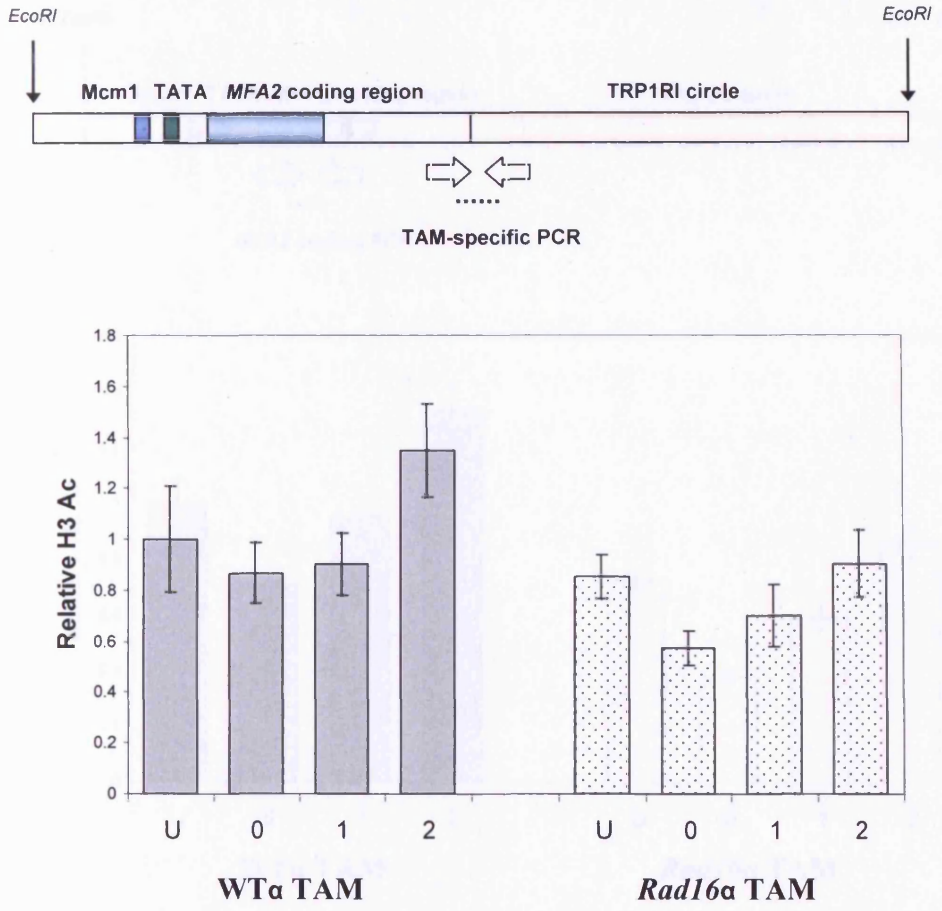

Figure 7.9: RtPCR employing the IP1 and IP2 primers, showing the relative H3Ac levels in the TAM plasmid unique join region, downstream of the *MFA2* gene. Samples were taken from untreated cells, and cells treated with 100Jm^2 UV, and allowed to repair for 0, 1 and 2 hours. WTα TAM and *rad16α* TAM data shown from 3 repeats (Appendix VI).

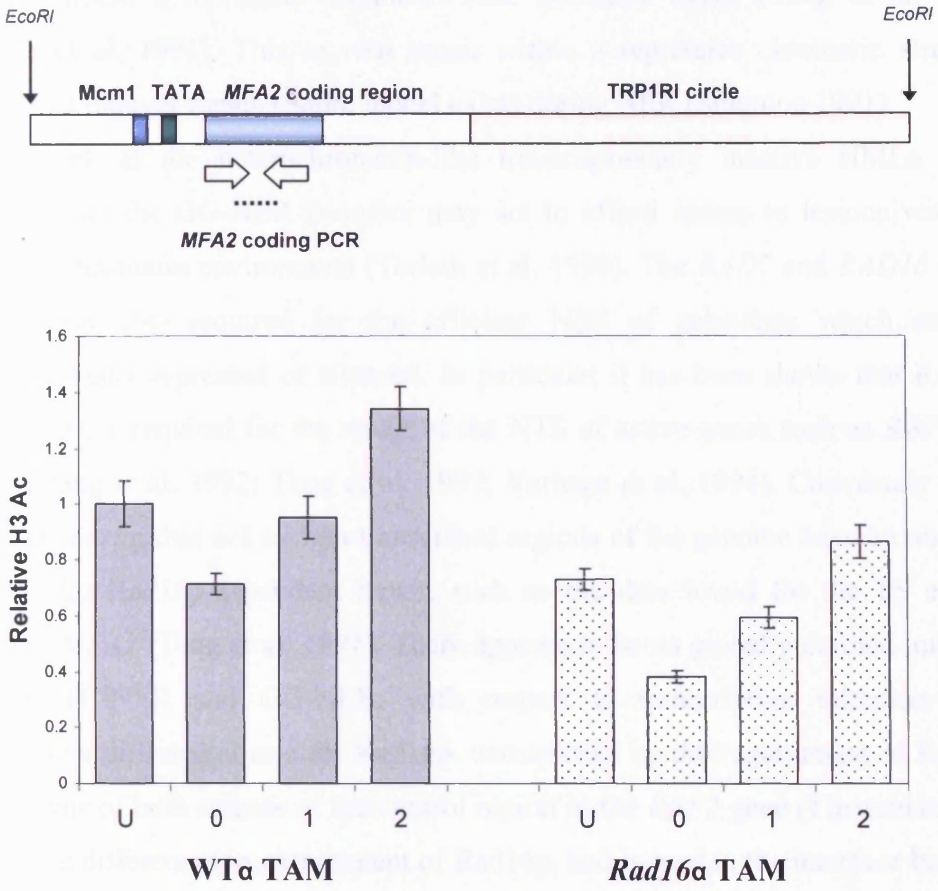

Figure 7.10: Relative H3Ac levels in WTα TAM and *rad16α* TAM cells for the *MFA2* coding region, employing N1 primers, from 3 repeats (Appendix VI).

The H3 acetylation levels detected were lower when *RAD16* is absent in both regions studied. Interestingly, the reduction in H3 acetylation levels is marginal and still follows the same pattern after UV.

7.4 Discussion

The Rad16p protein has been implicated in many aspects of the NER mechanism, however the primary functions are still unclear. The Rad7p-Rad16p-containing GG-NER complex is not essential for all NER, exemplified by an intermediate UV sensitivity (Prakash et al. 1993). *In vitro* studies indicated that NER is slow at the nucleosomal surface (Thoma 1999), however, *in vivo* studies have seen

the NER of multiple types of DNA damage in transcriptionally inactive regions of the genome, where a repressed chromatin state generally exists (Teng et al. 1997; Verhage et al. 1994). This *in vivo* repair within a repressive chromatin structure suggests an unravel-repair-restore model exists during NER (Smerdon 1991).

Work at the heterochromatin-like transcriptionally inactive HMLα locus proposed that the GG-NER complex may act to afford access to lesions within a repressed chromatin environment (Terleth et al. 1990). The *RAD7* and *RAD16* genes are however also required for the efficient NER of substrates which are not transcriptionally repressed or silenced. In particular it has been shown that Rad16p and Rad7p are required for the repair of the NTS of active genes such as *RBP2* and *MFA2* (Bang et al. 1992; Teng et al. 1997; Verhage et al. 1994). Conversely it has also been shown that not all non-transcribed regions of the genome have an absolute requisite for Rad16p-dependant repair, such as the data found for the TS control region of *MFA2* (Teng et al. 1997). There appears to be no globally defined interface between TC-NER and GG-NER, with respect to transcription initiation sites, suggesting a differential role for Rad16p, exemplified by the requirement of Rad16p in the repair of both strands of the control region in the *RBP2* gene (Tijsterman et al. 1996). The differences in requirement of Rad16p, and indeed in the interface between TC-NER and GG-NER are most likely attributed to the relationship between transcription and chromatin structure at these genes. It is therefore suggested that the NER repair sub-pathway responsible for the repair of CPDs depends not only on the gene being studied, but also on the mode of regulation at that gene site. It is thought that Rad16p dependant repair occurs globally, even to a degree in actively transcribed strands of DNA, however the rate of transcription and localisation of transcriptional machinery may well determine the degree of TC-NER (Verhage et al. 1994). Further to this it has also been shown that Rad16p-independent repair takes places in the TS of *RPB2* when TC-NER is abolished (Rad26p mutant), and this could be linked directly to the degree of transcription taking place (van Gool et al. 1994).

The heterogeneity of NER repair rates in yeast largely reflects the structural hierarchy of the chromatin environment, with nucleosome free regions (NFRs) and linker DNA repaired more readily than nucleosomal DNA. Recent work has implicated the Rad7p-Rad16p complex in the efficient NER of UV lesions in NFRs (Lettieri et al. 2008), placing the proteins role beyond chromatin remodelling. It is postulated that in this environment Rad16p primarily acts to create DNA torsion

required for the excision of the damage containing oligonucleotide, rather than induction of Gcn5p-mediated histone acetylation.

Interestingly Rad16p appears to have a central role in the NER mechanism, both directly, with associations identified between various protein complexes such as Rad4-23, Abf1, Elc1, and indirectly with the mediation of intracellular Gcn5p occupancy (Gillette et al. 2006; Prakash and Prakash 2000; Ramsey et al. 2004; Teng et al. 2008).

Hyperacetylation of histones has historically been associated with increased transcription, and has been linked to the increase in repair synthesis of lesions by NER. This was exemplified in human cells by the inhibition of histone deacetylases leading to more efficient NER (Ramanathan and Smerdon 1989). As discussed in Chapter 6, UV irradiation results in hyperacetylation of histone H3 within the *MFA2* promoter region, which reaches an elevated peak at 30 minutes post-UV (Yu et al. 2005). Residual levels of CPD lesion removal still occurs in the absence of Gcn5p and associated H3 hyperacetylation at the *MFA2* promoter, considerably reducing the efficiency of NER. The deletion of *GCN5* does not however affect the chromatin accessibility in terms of speed and extent of restriction enzyme cutting. It should be noted that a *rad16gcn5* double mutant has abolished H3Ac and in this instance one does see a reduction in restriction enzyme cutting (unpublished data, S Yu, 2010). It is possible that the histone acetylation levels provide a suitable epigenetic environment for efficient NER without inducing transcription, as TBP, a transcriptional factor is still excluded from the *MFA2* promoter region (Jenuwein and Allis 2001; Yu et al. 2005).

UV-induced histone H3 acetylation mediated by Gcn5p requires the presence of Rad16p for efficient repair at *MFA2* and throughout the genome. However it has also to be borne in mind that Rad16p governs most UV induced H3 acetylation, and some of this is mediated by HATs other than Gcn5p. It is likely that the combined effect in the *rad16gcn5* double mutant is due to changes in H3 acetylation both pre- and post-UV.

Interestingly in this study, it has been shown that the absolute requisite of Rad16p in the GG-NER of the *MFA2* promoter region is overcome when *MFA2* resides in the plasmid context of TAM. The deletion of *RAD16* does not alter the transcriptional regulation of the *MFA2* gene, as previously shown for endogenous *MFA2*, and the nucleosome positions across *MFA2* remain unaltered in the absence of

Rad16p. Previous studies carried out by (Teng et al. 2008) show that relative H3 acetylation levels at the endogenous *MFA2* promoter are reduced in a *RAD16* mutant following UV, when compared with WT. This reduction is thought to be bought about in part by the inability to recruit Gcn5p to the appropriate sites in a Rad16p deficient background. When the occupancy of Gcn5p is compromised it is thought that the epigenetic landscape becomes less accommodating for the repair machinery. The acetylation levels in the TAM plasmid are reduced in the absence of *RAD16*, however not to the extent seen for the endogenous gene.

Taken together, it can be suggested that the TAM plasmid context is such that GG-NER is not absolutely mediated by Rad16p at *MFA2*, and this could be due to the differences in the chromatin structure or the inherent chromatin environment.

Chapter 8

General Discussion

The field of DNA repair continues to provide an exciting avenue of research, unveiling unique insights into the complex chromatin biology associated with cellular metabolic processes. The mechanistic stages of NER have largely been elucidated, along with the major genes involved, however how this operates in a chromatin environment is of increasing interest. This study aimed to gain and characterise a tool within the simple eukaryote *S. cerevisiae* to further knowledge regarding the accessibility of the NER machinery within a chromatin context.

The experiments presented in this study encompass the construction and employment of a yeast minichromosome containing *MFA2* as a model gene (Chapter 3). Subsequent repair profiles alongside nucleosome mapping data were then presented in Chapter 4, to characterise the use of the plasmid model in UV-induced NER studies. To ensure the TAM borne *MFA2* was under the same transcriptional regulation as found in the endogenous gene mRNA levels were detected within WT**a** and WTα cells, where *MFA2* is active and repressed respectively, as well as within a *tup1α* strain, where *MFA2* is released from its transcription repression. The *tup1α* strain also provided useful information regarding the DNA repair profiles and chromatin environment including nucleosome mapping and H3 acetylation (K9 and K14) in relation to NER (Chapter 5).

As emerging research is gaining momentum in the direction of chromatin remodelling and repair, I also utilised the TAM plasmid to investigate two contributing factors to chromatin remodelling. Firstly in Chapter 6, I investigated the HAT Gcn5p, which when absent results in a decrease in H3 acetylation and corresponds to a decrease in NER. Secondly the Rad16p protein, which has been implicated in multiple roles in GG-NER, was of particular interest due to the chromatin remodelling properties implicated largely by the inherent Snf2-like ATP dependant activity of the protein and the fact that it governs UV-induced histone acetylation. Chapter 7 described the repair profile and chromatin properties of

MFA2^{TAM} in cells with or without *RAD16*. Having explored these experiments within the relevant chapters, this chapter will focus on the outcomes and routes for further investigation involving NER and the TAM plasmid.

Construction of a tool to study NER in a chromatin context

Previously substrates have been constructed in which to investigate chromatin dynamics, as well as NER intricacies (Lettieri et al. 2008; Reed et al. 1998; Smerdon and Thoma 1990). This project has seen the construction of a yeast minichromosome to enable NER to be studied within a chromatin environment. The use of *MFA2* as a model gene provided a template in which NER can be explored independently of transcription, in WTα cells, where *MFA2* is repressed. The gene is also of a size which lends itself to well characterised high resolution technologies (Teng et al. 1997; Teng et al. 2001).

Having gained much insight into NER at this gene in its endogenous cellular context (Yu et al. 2005; Yu and Waters 2005), *MFA2* was successfully incorporated via a fusion PCR method into the TRP1-R1 circle. The resulting TAM plasmid was then studied in terms of transcriptional regulation, nucleosome positioning and correlated with the NER of UV-induced CPDs at nucleotide resolution. Having created a defined yeast minichromosome, the potential for dual studies *in vivo* and *in vitro* utilising the same substrate can be realised.

Repair profile and nucleosome positioning in TAM

The primary focus of this study was to establish a tool for studying NER. This study has investigated the roles of various mutants which have been implicated in chromatin modification associated with efficient repair, as well as characterising these NER-related data for the plasmid model.

It was shown in Chapter 4 that nucleosomes are positioned across the *MFA2*^{TAM} promoter in WTα cells at the precise positions found at endogenous *MFA2* (Teng et al. 2001), using both low and high resolution mapping techniques. The loss of positioned nucleosomes in actively transcribed *MFA2*^{TAM} does correlate with the pattern displayed in endogenous *MFA2*. Interestingly a subtle difference in nucleosome positioning has been noted in the ARS1 region of the TAM plasmid in

WT**a** and WTα cells, and this may go some way to further explaining the differences in chromatin environment. It would be of interest to map the remainder of the plasmid utilising the high resolution technology developed by (Teng et al. 2001).

Regardless of the precise positioning of nucleosomes across $MFA2^{TAM}$ there was no obvious interface between the TC-NER and GG-NER pathways identified at the $MFA2^{TAM}$ promoter region studied. Further investigations into the repair within the coding region of $MFA2^{TAM}$ would determine whether TC-NER occurs at a relatively faster rate than GG-NER (Hanawalt 2001) in the plasmid context. The lack of a pronounced faster rate of repair in the TS of the active $MFA2^{TAM}$ promoter is not however a hindrance to the study, as all constructed mutant strains studied have been so in a PSY316α background providing a relative reference for comparison, and importantly the focus of my study has been on GG-NER.

In *tup1p* deleted cells a marked derepression of transcription is seen. However *MFA2* mRNA levels are not elevated to the levels seen in WT**a** TAM cells, regardless of the loss of positioned nucleosomes. There is however an increase in the relative *MFA2* mRNA levels compared to those seen in WT**a** cells lacking the plasmid, suggesting that a population of plasmid copies are transcriptionally derepressed. There are two suggestions as to why this may occur (i) the chromatin conformation, or the DNA conformation within the plasmid context does not allow for constitutive transcription in the absence of the Tup1p repressor protein due to steric hindrance of the transcriptional machinery (ii) cellular protein levels of relevant transcription factors may not be sufficient to attend multiple plasmid copies. In *tup1* cells, the endogenous *MFA2* gene shows a nucleosome positioning map analogous to naked DNA (personal communication Y Teng). It should be noted that there is a visible difference between the MNAse sensitive sites in *tup1*α TAM compared to WT**a** TAM, suggesting that the degree of chromatin 'opening' for transcription is different from that induced in a derepressed gene.

A further question which has been raised in this study is why there is not a substantial increase in H3 Ac levels at the $MFA2^{TAM}$ regions studied in the absence of *TUP1*? Previously it has been shown that a *TUP1* deletion results in a constitutively elevated level of H3 acetylation, even in a transcription-inhibited TATA box mutated strain, all in the absence of UV (Teng et al. 2008). Previous studies have also shown a modified chromatin structure at the *MFA2* promoter when either component of the Ssn6-Tup1 repressor complex is absent (Bone and Roth 2001). As we know that

repair is faster in a *TUP1* deleted system without increased transcription, it agrees with the data in this study, where although transcription is not seen to the levels expected, the chromatin environment promotes efficient repair; however this repair was previously attributed to the remaining elevated acetylation levels which are not seen in the plasmid system. Therefore, it is possible that there is a loss of nucleosomes in a population of TAM, resulting in the reduced acetylation level, simply as the histone proteins are not present. This would go some way to explaining the difference seen at the endogenous gene and within TAM. This brings about the further question, why would there be no nucleosomes in *tup1p* cells, but present in the genome as highly mobile hyperacetylated particles as suggested by (Teng et al. 2008)? A major factor may be the circular nature of the plasmid, and although nucleosome positioning is dictated by the mcm1/alpha2 binding site in previous models, the plasmid chromatin environment (including PTMs) may be subtly different to that of the endogenous gene. Further investigations should encompass DNA accessibility assays, to determine whether the changes in MNase sensitive sites and CPD repair rates correlate with a more accessible DNA substrate. Following a preliminary experiment to determine nucleosome presence (Appendix VI.6), it would also be of interest to determine whether the nucleosome particles remain at the *MFA2* promoter in the absence of Tup1p, or whether they dissociate completely to allow the repair machinery to access. This could be determined using ChIP studies, and antibodies against the individual histone proteins would indicate if partial dissociation of the histone takes place, as it has previously been shown that H2A-H2B exchange occurs more rapidly that that of H3-H4 (Kimura and Cook 2001). A direct comparison of the epigenetic histone modifications would be of great interest, and enhance understanding of the chromatin environment inherent in TAM.

Gcn5-mediated histone acetylation is required for efficient repair of MFA2^{TAM} promoter region

Chromatin has an impact on cellular metabolic processes, mediating not only the accessibility of protein complexes but also functional interactions between proteins and DNA sequences required for survival (Ataian and Krebs 2006). To overcome the repressive nature of chromatin two mechanisms have evolved, histone modification and ATP-dependant chromatin remodelling complexes, both of which

have been implicated with roles in NER (Gong et al. 2006; Teng et al. 2008). It was shown in Chapter 6 that the deletion of the HAT gene *GCN5* results in a significant reduction in H3 acetylation (K9 and K14) levels in untreated cells, with a further reduction following UV. The maintenance of a repressed chromatin environment as displayed by nucleosome mapping, along with the reduction in H3 acetylation results in a substrate which is not efficiently repaired by GG-NER. The H3 acetylation levels also reduce with time after UV, going against the trend seen for the WT acetylation levels.

It has been shown that increased histone acetylation levels throughout the genome, induced by the general inhibition of histone deacetylase enzymes results in the enhanced repair of lesions within hyperacetylated nucleosomes (Ramanathan and Smerdon 1989). Conversely, the deletion of *GCN5* results in a defective NER phenotype at *MET16* (Ferreiro et al. 2006) and within the hypoacetylated nucleosomes of the endogenous *MFA2* promoter. The effects of *GCN5* deletion were shown to occur locally, with no global NER defect (Teng et al. 2002). It is thought that the requisite for Gcn5p in repair of *MFA2* is a result of the proteins role in transcription activation of *MFA2*. However, how the protein is able to function independently in the two processes (Yu et al. 2005) without spurious induction of the other is not understood. As Gcn5p is not required for GG-NER in all regions of the genome, a redundancy of HATs for NER within the genome is presumed. A compensatory HAT mechanism has also been suggested following studies at endogenous *MFA2*, where a *tup1gcn5* double mutant still shows elevated H3 levels (unpublished data, S Yu, 2010).

Multiple questions arise from H3 acetylation data: Is acetylation the predominant factor for efficient NER in a chromatin environment? Is there a factor which can lead to efficient NER in the absence of hyperacetylation? What is the mechanistic pathway mediating acetylation in genomic chromatin and how are the various HATs recruited? The UV mediated H3 acetylation by Gcn5p at *MFA2* is dependant on Rad16p, although the mechanistic link is not understood (Teng et al. 2008). Does hyperactylation at these particular epigenetic sites increase nucleosome mobility to allow for efficient repair or is the subsequent recruitment of chromatin remodelling complexes the key factor? Furthermore, if different HATs can have roles perhaps there is a division of labour throughout the genome. The recruitment patterns and locality of various HATs could be followed in real time analysis by employing

microscopy studies involving the tagging of the proteins with fluorescent markers such as GFP. Genome wide studies employing a new micro-array-based technology developed within the group (unpublished data, Y Teng, 2010) can also address this.

The absolute requisite for Rad16 in GG-NER is overcome in the $MFA2^{TAM}$ promoter region

The hypothesis that ATP-dependant chromatin remodelling complexes aid in the repair process has been identified for many years (Thoma 1999). The GG-NER specific Rad7-Rad16 containing complex has been of recent interest following functional characterisation of the Rad16 protein. Firstly Rad16p has been shown to contain an ATPase domain, placing the protein in the SWI/SNF superfamily of chromatin remodelling factors (Bang et al. 1992), which have been shown to generate superhelical torsion via a DNA translocase activity (Havas et al. 2000). Rad16p however, despite having DNA translocase activity, does not catalyse the sliding of nucleosomes in the substrates examined to date (Yu et al. 2008). Therefore, although it is assumed that Rad16p is involved in chromatin remodelling, no direct evidence is currently available.

Recent data implicating Rad16p with a role in Gcn5p-mediated H3 acetylation required for efficient NER has provided an additional chromatin related role for Rad16p, again implicating the protein in early stages of the NER mechanism (Teng et al. 2008). This UV-induced H3 Ac does not require functional NER, but does require the presence of Rad16p. It is suggested that Rad7p and Rad16p regulate chromatin structure in response to UV during GG-NER by controlling the occupancy of Gcn5p and therefore the Gcn5p-mediated H3 acetylation levels. The absolute requisite for the Rad16 and Rad7 proteins is abrogated in a hyperacetylated open chromatin confirmation when *TUP1* is deleted (Teng et al. 2008).

In the plasmid context, GG-NER requires the presence, and following acetylation data, the activity of the HAT Gcn5p. As Rad16p is proposed to mediate this Gcn5p occupancy required for its function, it would stand to reason that a Rad16p mutant would have a repair phenotype similar to that seen in a Gcn5p mutant. At the endogenous *MFA2* this is the case, with defective GG-NER at the gene, however $MFA2^{TAM}$ promoter sees a reduced CPD repair rate in *rad16* cells, but not to the extent of the repair defect seen in *gcn5* cells.

The chromatin structure of the TAM borne *MFA2* promoter as determined by mapping of MNase sensitive sites appears the same in *rad16* cells as found in WTα and *gcn5* cells. Interestingly a reduction in H3 acetylation is noted, however not to the extent seen in *gcn5* cells. Taken together, it could be presumed that a reduction in histone acetylation compared to that seen in WTα cells would produce a more closed chromatin environment. Although not confirmed with accessibility assays, this does appear to be the case, as H3Ac is reduced to background levels in *gcn5* cells, with almost no repair, and a lesser reduction in acetylation levels is observed in *rad16* cells resulting in the absolute requisite for Rad16p in the GG-NER of $MFA2^{TAM}$ promoter being overcome. Employment of chromatin accessibility studies as described by (Yu et al. 2005) could provide data on whether the relative levels of H3 Ac determine the relative level of DNA accessibility and whether this is a more direct predictor of repair rate.

The results presented in this study imply the importance of acetylation levels either directly or indirectly for NER, and suggest that a further HAT may be responsible in part for the acetylation levels required for efficient GG-NER at TAM. These may be associated with the plasmid due to the *TRP1* gene or ARS1 sequence, such as Esa1p. Intriguingly, a triple *rad16gcn5tup1* mutant abolishes H3 acetylation at the endogenous *MFA2* promoter, suggesting that any alternative HAT activity is also dependant on Rad16p (unpublished data, S Yu, 2010).

It must be noted that this study investigates the repair of CPDs over time following UV in a population of TAM-containing cells, and does not provide information of which stage of the NER mechanism is affected. Due to Rad16ps multiple proposed roles in the NER pathway, other possibilities should be borne in mind. Rad7p/16p/Abf1p has been shown to generate superhelical torsion in a naked DNA substrate, which is required for the excision step of the NER mechanism (Yu et al. 2004). In this study, the requirement for superhelical tension may be overcome in a significant proportion of plasmids due to the helical nature, and employment of an assay to determine whether the incision and excision stages are functional would provide important information.

Recently, mutation of the two catalytic subunits of Rad16p, the ATPase domain and the RING domain with associated E3 ligase activity resulted in an intermediate UV sensitivity. However, deletion of both these domains results in an UV sensitivity analogous to that seen when RAD16 is deleted. This implies Rad16p

has at least 2 independent roles in UV survival. It was found that both domains were required for the Gcn5p occupancy and H3 acetylation, which were shown to both contribute to efficient repair. Functional similarities exist between Rad7p/16p and the DDB1/DDB2 human proteins, both with roles in the ubiquitination of Rad4p/XPC, in yeast and humans respectively, as well as the role in the repair of non-transcribed regions of the genome, GG-NER. It is surprising that the evolutionarily conserved pathway has not given rise to structural homologues, which may be attributed to differences in chromatin hierarchy and organisation of the genomes. If the Rad7p/16p complex acts to scan along DNA, recruiting Gcn5p in response to damage to initiate H3 acetylation, when does the E3 ligase activity of Rad16p function to mediate intracellular Rad4p? And how do these seemingly independent activities impinge on H3 acetylation?

Further investigations

The construction of a plasmid system provides many beneficial aspects in terms of repair analysis. The plasmid can be easily manipulated, with the ability to introduce point mutations in regions such as the mcm1 binding site, or TATA box; or the insertion of alternative model genes. Large preparations of the plasmid can also be achieved, and plasmid purification for either *in vivo* or *in vitro* work is relatively straight forward. TAM provides a chromosomal template which can be mapped in terms of MNAse sensitive sites, and subjected to high resolution repair analyses. The unique join region between the TRP1R1 circle and *MFA2* regions of the plasmid provide a means of selecting the plasmid for ChIP work.

As these studies have highlighted, subtle differences have arisen between the plasmid borne *MFA2* gene and the endogenous gene. This may be considered as a drawback of this model, however with further work to gain understanding into the plasmid model, it will provide a characterised substrate in which to investigate NER. This study has highlighted the importance of *in vivo* studies with a plasmid model before employing potential *in vitro* techniques.

The main focus of any future *in vivo* work should lie in determining the DNA accessibility of the plasmid within the various strains. This can be achieved by employing a variety of assays including the previously documented assay utilising restriction enzymes (Yu et al. 2005).

Nucleosome disruption in the early stages of NER is suggested as the histone chaperone chromatin assembly factor 1 (CAF-1) is implicated in the chromatin assembly post DNA synthesis in the last step of NER (Gaillard et al. 1996; Martini et al. 1998; Moggs et al. 2000). As previously mentioned it would be of interest to determine whether the histone particles become more mobile, or whether they partially or totally dissociate in some cases to allow for repair. The determination of the possible alterative HATs involved in efficient repair would also be interesting, as well as determining the HAT occupancy at $MFA2^{TAM}$. Employing ChIP, histones have been shown to be hyperacetylated before losing contact with the *PHO5* promoter region, displaying the need for strict monitoring of ChIP experiments involving chromatin remodelling (Reinke and Horz 2003). A way of combating this would be to employ an additional ChIP to determine nucleosome presence. To enable these studies, specific high-grade antibodies would be required, many of which are as yet unavailable to ChIP standards. Alternative assays to determine nucleosome presence may be beneficial in compiling repair data, with such an approach outlined in Appendix VI.6.

Chromatin rearrangement occurs during NER, and a modulation of repair is seen so that repair occurs slower within the internal protected regions of nucleosomes (Wellinger and Thoma 1997). In this study a distinct modulation of repair was especially seen for one region within TAM, at the site of mcm1 binding, where it appeared that repair was slower in the TS, a trend previously established in genomic *MFA2* studies. A ChIP for bound proteins at this site would shed light on the basis of this modulation.

Further routes of investigation include alternative histone modifications, such as methylation (Chaudhuri et al. 2009) and ubiquitination. Of particular interest within the Waters' group is the histone variant Htz1, the homologue of the human H2A.Z. Htz1 deposition has been implicated with a role in relieving promoter regions from their repressive structures, such as seen in at the *SUC2* and *GAL1* promoters. Tup1p mediated Htz1 deposition, along with cooperative actions of SWR1-C promotes mediator recruitment and transcriptional activation (Gligoris et al. 2007). We now know that NER at the Htz1 bearing nucleosome in the *MFA2* promoter is more rapid than at regions where Htz1 is absent, for example, HMRa (unpublished data, Y Yu, 2010). It may well be that NER accessibility and functionality is enhanced at Htz1 located nucleosomes versus other regions, and again only a genome

wide study will resolve this possibility. Finally, Htz1 can be acetylated by the HAT NuA4 (Krogan et al. 2004). However as yet we do not know whether this event impinges on NER efficiency.

SWI/SNF-independent (Sin) mutations, generated by the disruption of the H3 and H4 histone-DNA contacts provide a more accessible DNA substrate, without altering the histone octamer stoichiometry. The importance of histone modifications and repair can be exemplified by the finding that Sin H4 mutants are more resistant to UV induced cell death, have an increased nucleosomal accessibility and increased repair of CPDs at specific regions (Nag et al. 2008). This, along with data provided in this study suggests that nucleosome accessibility is paramount for efficient repair, whether this is achieved via hyperacetylation of histones, or the concerted actions of acetyltransferases and chromatin remodelling complexes.

The use of computational programs to determine *in silico* links between the NER factors and transcriptional processes is also progressing (Tran et al. 2009), which should shed light on further avenues of investigation, and may provide some crucial links between the chromatin modification factors and NER.

In vitro applications

Previous *in vitro* studies have led to the development of cell free extracts which can support efficient NER of naked DNA substrates (Wood et al. 1988), however functional repair of chromatin substrates has been found at a diminished rate in these systems (Sugasawa et al. 1993; Wang et al. 1991). Nucleosomal templates which contain specifically placed 6-4 photoproducts have further indicated that the human NER factors RPA, XPA, XPC-hHR23B, XPG, ERCC1-XPF and TFIIH are not sufficient to allow for efficient NER in nucleosomal DNA (Araki et al. 2000; Hara et al. 2000; Ura et al. 2001).

The specific placement of a UV adduct within a synthetic substrate allowed conformation of slower repair in nucleosomal DNA (Hara et al. 2000), in agreement with *in vivo* data in yeast using a reconstituted minichromosome with defined nucleosomes (Smerdon and Thoma 1990).

Using a dinucleosome system, previously constructed for transcriptional studies (Ura et al. 1997), it was shown that the kink induced by the presence of a 6-4 PP did not alter the nucleosome positioning, although the histone-DNA contacts were

altered, as shown by enzymatic assays. The repair of 6-4 PPs and CPDs in a mononucleosome substrate using the DNA photolyase and T4 endonuclease repair enzymes showed a modulation of repair, suggesting chromatin alters the repair efficiency (Schieferstein and Thoma 1998).

Using cell free systems such as that developed by (Wang et al. 1993), the NER mechanism can be supported independently of RNAPII transcription to enable the GG-NER pathway to be examined. Utilising TAM, a chromatin substrate more representative of genomic chromatin than a mono- or di-nucleosome substrate can be employed. *In vitro* work to date has gathered much information for the NER of naked DNA, however very little repair has been identified in a chromatin environment using these *in vitro* systems. A fraction within cell extracts which was previously discarded for *in vitro* studies has been identified (unpublished data, S Reed) which enables the repair of chromatin. Therefore examination of this fraction to determine the nature of the factors is crucial. However genome wide studies *in vivo* suggest that different modifications are needed for different domains of chromosomes. It is therefore likely that there are multiple factors which facilitate NER of chromatin and these can vary for different parts of the genome. Hence once these factors are identified different combinations can be examined *in vitro* to unravel the biochemistry behind the events.

Conclusions

Efficient repair of DNA damage is essential for the maintenance of genomic integrity (Friedberg 2001). With CPD formation being a key initiator in the development of skin cancer (Jhappan et al. 2003), and defective tumour suppressor genes, such as specific homozygous mutations in p53 (Ford and Hanawalt 1995) giving rise to UV induced skin tumours (Adimoolam and Ford 2003), NER continues to be an advancing area of research. Interestingly Li-Fraumeni cells (homozygous mutations in p53) are defective in GG-NER, but not for TC-NER (Ford and Hanawalt 1995). Progressive research has led to novel treatments being established for patients with the inherited cancer prone condition XP, such as T4N5 topical lotion, which contains T4 endonuclease to aid reduce the development of solar keratoses (Yarosh et al. 2001).

Although chromatin has been shown to be repressive in terms of efficient NER, chromatin does provide a binding platform for a multitude of proteins (Osley et

al. 2007), as well as accommodating the dynamic epigenetic landscape often referred to as the histone code (de la Cruz et al. 2005; Escargueil et al. 2008; Jenuwein and Allis 2001). Chromatin is therefore a vital molecular entity, enabling efficient metabolic processes thereby promoting genetic stability, which we are just beginning to unravel.

In summary, my research has provided a tool in the shape of the TAM plasmid. This circular DNA molecule provides a chromatin substrate representative of genomic DNA, for use both *in vivo* and *in vitro*.

References

Aboussekhra, A. and Thoma, F. 1999. TATA-binding protein promotes the selective formation of UV-induced (6-4)-photoproducts and modulates DNA repair in the TATA box. *EMBO J* 18(2), pp. 433-443.

Abraham, R. T. 2001. Cell cycle checkpoint signaling through the ATM and ATR kinases. *Genes Dev* 15(17), pp. 2177-2196.

Adimoolam, S. and Ford, J. M. 2003. p53 and regulation of DNA damage recognition during nucleotide excision repair. *DNA Repair (Amst)* 2(9), pp. 947-954.

Adkins, M. W. and Williams, S. K. and Linger, J. and Tyler, J. K. 2007. Chromatin disassembly from the PHO5 promoter is essential for the recruitment of the general transcription machinery and coactivators. *Mol Cell Biol* 27(18), pp. 6372-6382.

Alberts, B. and Johnson, A. and Lewis, J. and Raff, M. and Roberts, K. and Walter, P. 2002. *Molecular Biology of the Cell.* 4 ed. London: Garland Science, Taylor & Francis Group.

Allison, S. J. and Milner, J. 2003. Loss of p53 has site-specific effects on histone H3 modification, including serine 10 phosphorylation important for maintenance of ploidy. *Cancer Res* 63(20), pp. 6674-6679.

Almeida, K. H. and Sobol, R. W. 2007. A unified view of base excision repair: lesion-dependent protein complexes regulated by post-translational modification. *DNA Repair (Amst)* 6(6), pp. 695-711.

Altaf, M. and Auger, A. and Covic, M. and Cote, J. 2009. Connection between histone H2A variants and chromatin remodeling complexes. *Biochem Cell Biol* 87(1), pp. 35-50.

Araki, M. and Masutani, C. and Maekawa, T. and Watanabe, Y. and Yamada, A. and Kusumoto, R. and Sakai, D. and Sugasawa, K. and Ohkuma, Y. and Hanaoka, F. 2000. Reconstitution of damage DNA excision reaction from SV40 minichromosomes with purified nucleotide excision repair proteins. *Mutat Res* 459(2), pp. 147-160.

Araujo, S. J. and Wood, R. D. 1999. Protein complexes in nucleotide excision repair. *Mutat Res* 435(1), pp. 23-33.

Aravind, L. and Iyer, L. M. and Koonin, E. V. 2003. Scores of RINGS but no PHDs in ubiquitin signaling. *Cell Cycle* 2(2), pp. 123-126.

Ataian, Y. and Krebs, J. E. 2006. Five repair pathways in one context: chromatin modification during DNA repair. *Biochem Cell Biol* 84(4), pp. 490-504.

Bang, D. D. and Verhage, R. and Goosen, N. and Brouwer, J. and van de Putte, P. 1992. Molecular cloning of RAD16, a gene involved in differential repair in *Saccharomyces cerevisiae*. *Nucleic Acids Res* 20(15), pp. 3925-3931.

Batty, D. P. and Wood, R. D. 2000. Damage recognition in nucleotide excision repair of DNA. *Gene* 241(2), pp. 193-204.

Bazett-Jones, D. P. and Cote, J. and Landel, C. C. and Peterson, C. L. and Workman, J. L. 1999. The SWI/SNF complex creates loop domains in DNA and polynucleosome arrays and can disrupt DNA-histone contacts within these domains. *Mol Cell Biol* 19(2), pp. 1470-1478.

Berger, S. L. 2002. Histone modifications in transcriptional regulation. *Curr Opin Genet Dev* 12(2), pp. 142-148.

Bhatia, P. K. and Verhage, R. A. and Brouwer, J. and Friedberg, E. C. 1996. Molecular cloning and characterization of *Saccharomyces cerevisiae* RAD28, the yeast homolog of the human Cockayne syndrome A (CSA) gene. *J Bacteriol* 178(20), pp. 5977-5988.

Birger, Y. and West, K. L. and Postnikov, Y. V. and Lim, J. H. and Furusawa, T. and Wagner, J. P. and Laufer, C. S. and Kraemer, K. H. and Bustin, M. 2003. Chromosomal protein HMGN1 enhances the rate of DNA repair in chromatin. *EMBO J* 22(7), pp. 1665-1675.

Bohr, V. A. and Smith, C. A. and Okumoto, D. S. and Hanawalt, P. C. 1985. DNA repair in an active gene: removal of pyrimidine dimers from the DHFR gene of CHO cells is much more efficient than in the genome overall. *Cell* 40(2), pp. 359-369.

Bone, J. R. and Roth, S. Y. 2001. Recruitment of the yeast Tup1p-Ssn6p repressor is associated with localized decreases in histone acetylation. *J Biol Chem* 276(3), pp. 1808-1813.

Brand, M. and Moggs, J. G. and Oulad-Abdelghani, M. and Lejeune, F. and Dilworth, F. J. and Stevenin, J. and Almouzni, G. and Tora, L. 2001. UV-damaged DNA-binding protein in the TFTC complex links DNA damage recognition to nucleosome acetylation. *EMBO J* 20(12), pp. 3187-3196.

Brooks, P. J. 2007. The case for 8,5'-cyclopurine-2'-deoxynucleosides as endogenous DNA lesions that cause neurodegeneration in xeroderma pigmentosum. *Neuroscience* 145(4), pp. 1407-1417.

Brush, G. S. and Kelly, T. J. 2000. Phosphorylation of the replication protein A large subunit in the *Saccharomyces cerevisiae* checkpoint response. *Nucleic Acids Res* 28(19), pp. 3725-3732.

Bucceri, A. and Kapitza, K. and Thoma, F. 2006. Rapid accessibility of nucleosomal DNA in yeast on a second time scale. *EMBO J* 25(13), pp. 3123-3132.

Bucheli, M. and Sweder, K. 2004. In UV-irradiated *Saccharomyces cerevisiae*, overexpression of Swi2/Snf2 family member Rad26 increases transcription-coupled repair and repair of the non-transcribed strand. *Mol Microbiol* 52(6), pp. 1653-1663.

Budd, M. E. and Campbell, J. L. 1995. DNA polymerases required for repair of UV-induced damage in *Saccharomyces cerevisiae*. *Mol Cell Biol* 15(4), pp. 2173-2179.

Buratowski, S. 2003. The CTD code. *Nat Struct Biol* 10(9), pp. 679-680.

Carey, M. and Li, B. and Workman, J. L. 2006. RSC exploits histone acetylation to abrogate the nucleosomal block to RNA polymerase II elongation. *Mol Cell* 24(3), pp. 481-487.

Chandrasekhar, D. and Van Houten, B. 2000. In vivo formation and repair of cyclobutane pyrimidine dimers and 6-4 photoproducts measured at the gene and nucleotide level in *Escherichia coli*. *Mutat Res* 450(1-2), pp. 19-40.

Chaudhuri, S. and Wyrick, J. J. and Smerdon, M. J. 2009. Histone H3 Lys79 methylation is required for efficient nucleotide excision repair in a silenced locus of *Saccharomyces cerevisiae*. *Nucleic Acids Res* 37(5), pp. 1690-1700.

Chen-Cleland, T. A. and Smith, M. M. and Le, S. and Sternglanz, R. and Allfrey, V. G. 1993. Nucleosome structural changes during derepression of silent mating-type loci in yeast. *J Biol Chem* 268(2), pp. 1118-1124.

Chen, L. and Madura, K. 2002. Rad23 promotes the targeting of proteolytic substrates to the proteasome. *Mol Cell Biol* 22(13), pp. 4902-4913.

Chen, P. and Sapperstein, S. K. and Choi, J. D. and Michaelis, S. 1997. Biogenesis of the *Saccharomyces cerevisiae* mating pheromone a-factor. *J Cell Biol* 136(2), pp. 251-269.

Chiba, H. and Muramatsu, M. and Nomoto, A. and Kato, H. 1994. Two human homologues of *Saccharomyces cerevisiae* SWI2/SNF2 and Drosophila brahma are transcriptional coactivators cooperating with the estrogen receptor and the retinoic acid receptor. *Nucleic Acids Res* 22(10), pp. 1815-1820.

Clements, A. and Poux, A. N. and Lo, W. S. and Pillus, L. and Berger, S. L. and Marmorstein, R. 2003. Structural basis for histone and phosphohistone binding by the GCN5 histone acetyltransferase. *Mol Cell* 12(2), pp. 461-473.

Cooper, J. P. and Roth, S. Y. and Simpson, R. T. 1994. The global transcriptional regulators, SSN6 and TUP1, play distinct roles in the establishment of a repressive chromatin structure. *Genes Dev* 8(12), pp. 1400-1410.

Cosma, M. P. and Tanaka, T. and Nasmyth, K. 1999. Ordered recruitment of transcription and chromatin remodeling factors to a cell cycle- and developmentally regulated promoter. *Cell* 97(3), pp. 299-311.

Cote, J. and Peterson, C. L. and Workman, J. L. 1998. Perturbation of nucleosome core structure by the SWI/SNF complex persists after its detachment, enhancing subsequent transcription factor binding. *Proc Natl Acad Sci U S A* 95(9), pp. 4947-4952.

Croteau, D. L. and DellaVecchia, M. J. and Perera, L. and Van Houten, B. 2008. Cooperative damage recognition by UvrA and UvrB: identification of UvrA residues that mediate DNA binding. *DNA Repair (Amst)* 7(3), pp. 392-404.

Crowley, D. J. and Hanawalt, P. C. 1998. Induction of the SOS response increases the efficiency of global nucleotide excision repair of cyclobutane pyrimidine dimers, but not 6-4 photoproducts, in UV-irradiated *Escherichia coli*. *J Bacteriol* 180(13), pp. 3345-3352.

Datta, A. and Bagchi, S. and Nag, A. and Shiyanov, P. and Adami, G. R. and Yoon, T. and Raychaudhuri, P. 2001. The p48 subunit of the damaged-DNA binding protein DDB associates with the CBP/p300 family of histone acetyltransferase. *Mutat Res* 486(2), pp. 89-97.

Davie, J. K. and Trumbly, R. J. and Dent, S. Y. 2002. Histone-dependent association of Tup1-Ssn6 with repressed genes *in vivo*. *Mol Cell Biol* 22(3), pp. 693-703.

Davie, J. R. and Chadee, D. N. 1998. Regulation and regulatory parameters of histone modifications. *J Cell Biochem Suppl* 30-31, pp. 203-213.

de Boer, J. and Hoeijmakers, J. H. 2000. Nucleotide excision repair and human syndromes. *Carcinogenesis* 21(3), pp. 453-460.

de la Cruz, X. and Lois, S. and Sanchez-Molina, S. and Martinez-Balbas, M. A. 2005. Do protein motifs read the histone code? *Bioessays* 27(2), pp. 164-175.

de Laat, W. L. and Jaspers, N. G. and Hoeijmakers, J. H. 1999. Molecular mechanism of nucleotide excision repair. *Genes Dev* 13(7), pp. 768-785.

Deaconescu, A. M. and Savery, N. and Darst, S. A. 2007. The bacterial transcription repair coupling factor. *Curr Opin Struct Biol* 17(1), pp. 96-102.

DellaVecchia, M. J. and Croteau, D. L. and Skorvaga, M. and Dezhurov, S. V. and Lavrik, O. I. and Van Houten, B. 2004. Analyzing the handoff of DNA from UvrA to UvrB utilizing DNA-protein photoaffinity labeling. *J Biol Chem* 279(43), pp. 45245-45256.

den Dulk, B. and Sun, S. M. and de Ruijter, M. and Brandsma, J. A. and Brouwer, J. 2006. Rad33, a new factor involved in nucleotide excision repair in *Saccharomyces cerevisiae*. *DNA Repair (Amst)* 5(6), pp. 683-692.

DeRisi, J. L. and Iyer, V. R. and Brown, P. O. 1997. Exploring the metabolic and genetic control of gene expression on a genomic scale. *Science* 278(5338), pp. 680-686.

Dolan, J. W. and Kirkman, C. and Fields, S. 1989. The yeast STE12 protein binds to the DNA sequence mediating pheromone induction. *Proc Natl Acad Sci U S A* 86(15), pp. 5703-5707.

Ducker, C. E. and Simpson, R. T. 2000. The organized chromatin domain of the repressed yeast a cell-specific gene STE6 contains two molecules of the corepressor Tup1p per nucleosome. *EMBO J* 19(3), pp. 400-409.

Dulbecco, R. 1949. Reactivation of ultra-violet-inactivated bacteriophage by visible light. *Nature* 163(4155), p. 949.

Edmondson, D. G. and Smith, M. M. and Roth, S. Y. 1996. Repression domain of the yeast global repressor Tup1 interacts directly with histones H3 and H4. *Genes Dev* 10(10), pp. 1247-1259.

Eisen, J. A. and Sweder, K. S. and Hanawalt, P. C. 1995. Evolution of the SNF2 family of proteins: subfamilies with distinct sequences and functions. *Nucleic Acids Res* 23(14), pp. 2715-2723.

Eker, A. P. and Kooiman, P. and Hessels, J. K. and Yasui, A. 1990. DNA photoreactivating enzyme from the cyanobacterium Anacystis nidulans. *J Biol Chem* 265(14), pp. 8009-8015.

Escargueil, A. E. and Soares, D. G. and Salvador, M. and Larsen, A. K. and Henriques, J. A. 2008. What histone code for DNA repair? *Mutat Res* 658(3), pp. 259-270.

Feaver, W. J. and Huang, W. and Friedberg, E. C. 1999. The TFB4 subunit of yeast TFIIH is required for both nucleotide excision repair and RNA polymerase II transcription. *J Biol Chem* 274(41), pp. 29564-29567.

Ferreiro, J. A. and Powell, N. G. and Karabetsou, N. and Kent, N. A. and Mellor, J. and Waters, R. 2004. Cbf1p modulates chromatin structure, transcription and repair at the *Saccharomyces cerevisiae* MET16 locus. *Nucleic Acids Res* 32(5), pp. 1617-1626.

Ferreiro, J. A. and Powell, N. G. and Karabetsou, N. and Mellor, J. and Waters, R. 2006. Roles for Gcn5p and Ada2p in transcription and nucleotide excision repair at the *Saccharomyces cerevisiae* MET16 gene. *Nucleic Acids Res* 34(3), pp. 976-985.

Fleming, A. B. and Pennings, S. 2001. Antagonistic remodelling by Swi-Snf and Tup1-Ssn6 of an extensive chromatin region forms the background for FLO1 gene regulation. *EMBO J* 20(18), pp. 5219-5231.

Ford, J. M. and Hanawalt, P. C. 1995. Li-Fraumeni syndrome fibroblasts homozygous for p53 mutations are deficient in global DNA repair but exhibit normal transcription-coupled repair and enhanced UV resistance. *Proc Natl Acad Sci U S A* 92(19), pp. 8876-8880.

Fousteri, M. and Vermeulen, W. and van Zeeland, A. A. and Mullenders, L. H. 2006. Cockayne syndrome A and B proteins differentially regulate recruitment of chromatin

remodeling and repair factors to stalled RNA polymerase II in vivo. *Mol Cell* 23(4), pp. 471-482.

Friedberg, E. C. 1996. Relationships between DNA repair and transcription. *Annu Rev Biochem* 65, pp. 15-42.

Friedberg, E. C. 2001. How nucleotide excision repair protects against cancer. *Nat Rev Cancer* 1(1), pp. 22-33.

Friedberg, E. C. 2003. DNA damage and repair. *Nature* 421(6921), pp. 436-440.

Friedberg, E. C. and McDaniel, L. D. and Schultz, R. A. 2004. The role of endogenous and exogenous DNA damage and mutagenesis. *Curr Opin Genet Dev* 14(1), pp. 5-10.

Friedberg, E. C. 2005. Suffering in silence: the tolerance of DNA damage. *Nat Rev Mol Cell Biol* 6(12), pp. 943-953.

Friedberg, E. C. and Walker, G. C. and Siede, W. and Wood, R. D. and Schultz, R. A. and Ellenberger, T. 2006. *DNA Repair and Mutagenesis*. 2nd Edition ed. Washington DC: ASM Press.

Friesen, H. and Hepworth, S. R. and Segall, J. 1997. An Ssn6-Tup1-dependent negative regulatory element controls sporulation-specific expression of DIT1 and DIT2 in *Saccharomyces cerevisiae*. *Mol Cell Biol* 17(1), pp. 123-134.

Fu, Y. and Pastushok, L. and Xiao, W. 2008. DNA damage-induced gene expression in *Saccharomyces cerevisiae*. *FEMS Microbiol Rev* 32(6), pp. 908-926.

Gaillard, H. and Fitzgerald, D. J. and Smith, C. L. and Peterson, C. L. and Richmond, T. J. and Thoma, F. 2003. Chromatin remodeling activities act on UV-damaged nucleosomes and modulate DNA damage accessibility to photolyase. *J Biol Chem* 278(20), pp. 17655-17663.

Gaillard, P. H. and Martini, E. M. and Kaufman, P. D. and Stillman, B. and Moustacchi, E. and Almouzni, G. 1996. Chromatin assembly coupled to DNA repair: a new role for chromatin assembly factor I. *Cell* 86(6), pp. 887-896.

Gale, J. M. and Nissen, K. A. and Smerdon, M. J. 1987. UV-induced formation of pyrimidine dimers in nucleosome core DNA is strongly modulated with a period of 10.3 bases. *Proc Natl Acad Sci U S A* 84(19), pp. 6644-6648.

Gale, J. M. and Smerdon, M. J. 1990. UV induced (6-4) photoproducts are distributed differently than cyclobutane dimers in nucleosomes. *Photochem Photobiol* 51(4), pp. 411-417.

Gao, S. and Drouin, R. and Holmquist, G. P. 1994. DNA repair rates mapped along the human PGK1 gene at nucleotide resolution. *Science* 263(5152), pp. 1438-1440.

Gaspari, A. A. and Fleisher, T. A. and Kraemer, K. H. 1993. Impaired interferon production and natural killer cell activation in patients with the skin cancer-prone disorder, xeroderma pigmentosum. *J Clin Invest* 92(3), pp. 1135-1142.

Gavin, I. M. and Kladde, M. P. and Simpson, R. T. 2000. Tup1p represses Mcm1p transcriptional activation and chromatin remodeling of an a-cell-specific gene. *EMBO J* 19(21), pp. 5875-5883.

Gibbons, R. J. 2005. Histone modifying and chromatin remodelling enzymes in cancer and dysplastic syndromes. *Hum Mol Genet* 14 Spec No 1, pp. R85-92.

Gillette, T. G. and Yu, S. and Zhou, Z. and Waters, R. and Johnston, S. A. and Reed, S. H. 2006. Distinct functions of the ubiquitin-proteasome pathway influence nucleotide excision repair. *EMBO J* 25(11), pp. 2529-2538.

Gligoris, T. and Thireos, G. and Tzamarias, D. 2007. The Tup1 corepressor directs Htz1 deposition at a specific promoter nucleosome marking the GAL1 gene for rapid activation. *Mol Cell Biol* 27(11), pp. 4198-4205.

Gong, F. and Kwon, Y. and Smerdon, M. J. 2005. Nucleotide excision repair in chromatin and the right of entry. *DNA Repair (Amst)* 4(8), pp. 884-896.

Gong, F. and Fahy, D. and Smerdon, M. J. 2006. Rad4-Rad23 interaction with SWI/SNF links ATP-dependent chromatin remodeling with nucleotide excision repair. *Nat Struct Mol Biol* 13(10), pp. 902-907.

Gontijo, A. M. and Green, C. M. and Almouzni, G. 2003. Repairing DNA damage in chromatin. *Biochimie* 85(11), pp. 1133-1147.

Goosen, N. and Moolenaar, G. F. 2008. Repair of UV damage in bacteria. *DNA Repair (Amst)* 7(3), pp. 353-379.

Grant, P. A. and Duggan, L. and Cote, J. and Roberts, S. M. and Brownell, J. E. and Candau, R. and Ohba, R. and Owen-Hughes, T. and Allis, C. D. and Winston, F. and Berger, S. L. and Workman, J. L. 1997. Yeast Gcn5 functions in two multisubunit complexes to acetylate nucleosomal histones: characterization of an Ada complex and the SAGA (Spt/Ada) complex. *Genes Dev* 11(13), pp. 1640-1650.

Green, C. M. and Almouzni, G. 2003. Local action of the chromatin assembly factor CAF-1 at sites of nucleotide excision repair in vivo. *EMBO J* 22(19), pp. 5163-5174.

Green, S. R. and Johnson, A. D. 2004. Promoter-dependent roles for the Srb10 cyclin-dependent kinase and the Hda1 deacetylase in Tup1-mediated repression in *Saccharomyces cerevisiae*. *Mol Biol Cell* 15(9), pp. 4191-4202.

Gregory, P. D. and Wagner, K. and Horz, W. 2001. Histone acetylation and chromatin remodeling. *Exp Cell Res* 265(2), pp. 195-202.

Gregory, S. M. and Sweder, K. S. 2001. Deletion of the CSB homolog, RAD26, yields Spt(-) strains with proficient transcription-coupled repair. *Nucleic Acids Res* 29(14), pp. 3080-3086.

Gromoller, A. and Lehming, N. 2000a. Srb7p is essential for the activation of a subset of genes. *FEBS Lett* 484(1), pp. 48-54.

Gromoller, A. and Lehming, N. 2000b. Srb7p is a physical and physiological target of Tup1p. *EMBO J* 19(24), pp. 6845-6852.

Groth, A. and Rocha, W. and Verreault, A. and Almouzni, G. 2007. Chromatin challenges during DNA replication and repair. *Cell* 128(4), pp. 721-733.

Guzder, S. N. and Sung, P. and Prakash, L. and Prakash, S. 1993. Yeast DNA-repair gene RAD14 encodes a zinc metalloprotein with affinity for ultraviolet-damaged DNA. *Proc Natl Acad Sci U S A* 90(12), pp. 5433-5437.

Guzder, S. N. and Sung, P. and Bailly, V. and Prakash, L. and Prakash, S. 1994. RAD25 is a DNA helicase required for DNA repair and RNA polymerase II transcription. *Nature* 369(6481), pp. 578-581.

Guzder, S. N. and Habraken, Y. and Sung, P. and Prakash, L. and Prakash, S. 1995. Reconstitution of yeast nucleotide excision repair with purified Rad proteins, replication protein A, and transcription factor TFIIH. *J Biol Chem* 270(22), pp. 12973-12976.

Guzder, S. N. and Habraken, Y. and Sung, P. and Prakash, L. and Prakash, S. 1996a. RAD26, the yeast homolog of human Cockayne's syndrome group B gene, encodes a DNA-dependent ATPase. *J Biol Chem* 271(31), pp. 18314-18317.

Guzder, S. N. and Sung, P. and Prakash, L. and Prakash, S. 1996b. Nucleotide excision repair in yeast is mediated by sequential assembly of repair factors and not by a pre-assembled repairosome. *J Biol Chem* 271(15), pp. 8903-8910.

Guzder, S. N. and Sung, P. and Prakash, L. and Prakash, S. 1997. Yeast Rad7-Rad16 complex, specific for the nucleotide excision repair of the nontranscribed DNA strand, is an ATP-dependent DNA damage sensor. *J Biol Chem* 272(35), pp. 21665-21668.

Guzder, S. N. and Sung, P. and Prakash, L. and Prakash, S. 1998a. Affinity of yeast nucleotide excision repair factor 2, consisting of the Rad4 and Rad23 proteins, for ultraviolet damaged DNA. *J Biol Chem* 273(47), pp. 31541-31546.

Guzder, S. N. and Sung, P. and Prakash, L. and Prakash, S. 1998b. The DNA-dependent ATPase activity of yeast nucleotide excision repair factor 4 and its role in DNA damage recognition. *J Biol Chem* 273(11), pp. 6292-6296.

Haber, J. E. 1998. Mating-type gene switching in *Saccharomyces cerevisiae*. *Annu Rev Genet* 32, pp. 561-599.

Habraken, Y. and Sung, P. and Prakash, L. and Prakash, S. 1995. Structure-specific nuclease activity in yeast nucleotide excision repair protein Rad2. *J Biol Chem* 270(50), pp. 30194-30198.

Habraken, Y. and Sung, P. and Prakash, S. and Prakash, L. 1996. Transcription factor TFIIH and DNA endonuclease Rad2 constitute yeast nucleotide excision repair factor 3: implications for nucleotide excision repair and Cockayne syndrome. *Proc Natl Acad Sci U S A* 93(20), pp. 10718-10722.

Halliday, G. M. and Bock, V. L. and Moloney, F. J. and Lyons, J. G. 2009. SWI/SNF: a chromatin-remodelling complex with a role in carcinogenesis. *Int J Biochem Cell Biol* 41(4), pp. 725-728.

Hanawalt, P. C. 1994. Transcription-coupled repair and human disease. *Science* 266(5193), pp. 1957-1958.

Hanawalt, P. C. 2001. Controlling the efficiency of excision repair. *Mutat Res* 485(1), pp. 3-13.

Hanawalt, P. C. and Ford, J. M. and Lloyd, D. R. 2003. Functional characterization of global genomic DNA repair and its implications for cancer. *Mutat Res* 544(2-3), pp. 107-114.

Hanawalt, P. C. and Spivak, G. 2008. Transcription-coupled DNA repair: two decades of progress and surprises. *Nat Rev Mol Cell Biol* 9(12), pp. 958-970.

Hara, R. and Mo, J. and Sancar, A. 2000. DNA damage in the nucleosome core is refractory to repair by human excision nuclease. *Mol Cell Biol* 20(24), pp. 9173-9181.

Hara, R. and Sancar, A. 2002. The SWI/SNF chromatin-remodeling factor stimulates repair by human excision nuclease in the mononucleosome core particle. *Mol Cell Biol* 22(19), pp. 6779-6787.

Hara, R. and Sancar, A. 2003. Effect of damage type on stimulation of human excision nuclease by SWI/SNF chromatin remodeling factor. *Mol Cell Biol* 23(12), pp. 4121-4125.

Harrison, J. C. and Haber, J. E. 2006. Surviving the breakup: the DNA damage checkpoint. *Annu Rev Genet* 40, pp. 209-235.

Hassan, A. H. and Prochasson, P. and Neely, K. E. and Galasinski, S. C. and Chandy, M. and Carrozza, M. J. and Workman, J. L. 2002. Function and selectivity of bromodomains in anchoring chromatin-modifying complexes to promoter nucleosomes. *Cell* 111(3), pp. 369-379.

Hassan, A. H. and Awad, S. and Prochasson, P. 2006. The Swi2/Snf2 bromodomain is required for the displacement of SAGA and the octamer transfer of SAGA-acetylated nucleosomes. *J Biol Chem* 281(26), pp. 18126-18134.

Hassan, A. H. and Awad, S. and Al-Natour, Z. and Othman, S. and Mustafa, F. and Rizvi, T. A. 2007. Selective recognition of acetylated histones by bromodomains in transcriptional co-activators. *Biochem J* 402(1), pp. 125-133.

Havas, K. and Flaus, A. and Phelan, M. and Kingston, R. and Wade, P. A. and Lilley, D. M. and Owen-Hughes, T. 2000. Generation of superhelical torsion by ATP-dependent chromatin remodeling activities. *Cell* 103(7), pp. 1133-1142.

He, Z. and Henricksen, L. A. and Wold, M. S. and Ingles, C. J. 1995. RPA involvement in the damage-recognition and incision steps of nucleotide excision repair. *Nature* 374(6522), pp. 566-569.

Hebbes, T. R. and Thorne, A. W. and Crane-Robinson, C. 1988. A direct link between core histone acetylation and transcriptionally active chromatin. *EMBO J* 7(5), pp. 1395-1402.

Henning, K. A. and Li, L. and Iyer, N. and McDaniel, L. D. and Reagan, M. S. and Legerski, R. and Schultz, R. A. and Stefanini, M. and Lehmann, A. R. and Mayne, L. V. and Friedberg, E. C. 1995. The Cockayne syndrome group A gene encodes a WD repeat protein that interacts with CSB protein and a subunit of RNA polymerase II TFIIH. *Cell* 82(4), pp. 555-564.

Herschbach, B. M. and Arnaud, M. B. and Johnson, A. D. 1994. Transcriptional repression directed by the yeast α2 protein *in vitro*. *Nature* 370, pp. 309-311.

Hirst, M. and Marra, M. A. 2008. Epigenetics and human disease. *Int J Biochem Cell Biol.*

Ho, Y. and Gruhler, A. and Heilbut, A. and Bader, G. D. and Moore, L. and Adams, S. L. and Millar, A. and Taylor, P. and Bennett, K. and Boutilier, K. and Yang, L. and Wolting, C. and Donaldson, I. and Schandorff, S. and Shewnarane, J. and Vo, M. and Taggart, J. and Goudreault, M. and Muskat, B. and Alfarano, C. and Dewar, D. and Lin, Z. and Michalickova, K. and Willems, A. R. and Sassi, H. and Nielsen, P. A. and Rasmussen, K. J. and Andersen, J. R. and Johansen, L. E. and Hansen, L. H. and Jespersen, H. and Podtelejnikov, A. and Nielsen, E. and Crawford, J. and Poulsen, V. and Sorensen, B. D. and Matthiesen, J. and Hendrickson, R. C. and Gleeson, F. and Pawson, T. and Moran, M. F. and Durocher, D. and Mann, M. and Hogue, C. W. and Figeys, D. and Tyers, M. 2002. Systematic identification of protein complexes in *Saccharomyces cerevisiae* by mass spectrometry. *Nature* 415(6868), pp. 180-183.

Holstege, F. C. and van der Vliet, P. C. and Timmers, H. T. 1996. Opening of an RNA polymerase II promoter occurs in two distinct steps and requires the basal transcription factors IIE and IIH. *EMBO J* 15(7), pp. 1666-1677.

Holstege, F. C. and Jennings, E. G. and Wyrick, J. J. and Lee, T. I. and Hengartner, C. J. and Green, M. R. and Golub, T. R. and Lander, E. S. and Young, R. A. 1998. Dissecting the regulatory circuitry of a eukaryotic genome. *Cell* 95(5), pp. 717-728.

Hoogstraten, D. and Bergink, S. and Ng, J. M. and Verbiest, V. H. and Luijsterburg, M. S. and Geverts, B. and Raams, A. and Dinant, C. and Hoeijmakers, J. H. and

Vermeulen, W. and Houtsmuller, A. B. 2008. Versatile DNA damage detection by the global genome nucleotide excision repair protein XPC. *J Cell Sci* 121(Pt 17), pp. 2850-2859.

Huang, L. and Zhang, W. and Roth, S. Y. 1997. Amino termini of histones H3 and H4 are required for a1-alpha2 repression in yeast. *Mol Cell Biol* 17(11), pp. 6555-6562.

Janion, C. 2001. Some aspects of the SOS response system--a critical survey. *Acta Biochim Pol* 48(3), pp. 599-610.

Jansen, L. E. and Verhage, R. A. and Brouwer, J. 1998. Preferential binding of yeast Rad4.Rad23 complex to damaged DNA. *J Biol Chem* 273(50), pp. 33111-33114.

Jenuwein, T. and Allis, C. D. 2001. Translating the histone code. *Science* 293(5532), pp. 1074-1080.

Jhappan, C. and Noonan, F. P. and Merlino, G. 2003. Ultraviolet radiation and cutaneous malignant melanoma. *Oncogene* 22(20), pp. 3099-3112.

Johnson, A. D. 1995. Molecular mechanisms of cell-type determination in budding yeast. *Curr Opin Genet Dev* 5(5), pp. 552-558.

Jones, C. J. and Wood, R. D. 1993. Preferential binding of the xeroderma pigmentosum group A complementing protein to damaged DNA. *Biochemistry* 32(45), pp. 12096-12104.

Jones, E. W. and Pringle, J. R. and Broach, J. R. 1992. *The Molecular and Cellular Biology of the yeast Saccharomyces*. Cold Spring Harbor, NY: Cold Spring Harbor Press.

Jun, S. H. and Kim, T. G. and Ban, C. 2006. DNA mismatch repair system. Classical and fresh roles. *FEBS J* 273(8), pp. 1609-1619.

Kapetanaki, M. G. and Guerrero-Santoro, J. and Bisi, D. C. and Hsieh, C. L. and Rapic-Otrin, V. and Levine, A. S. 2006. The DDB1-CUL4ADDB2 ubiquitin ligase is deficient in xeroderma pigmentosum group E and targets histone H2A at UV-damaged DNA sites. *Proc Natl Acad Sci U S A* 103(8), pp. 2588-2593.

Keleher, C. A. and Redd, M. J. and Schultz, J. and Carlson, M. and Johnson, A. D. 1992. Ssn6-Tup1 is a general repressor of transcription in yeast. *Cell* 68(4), pp. 709-719.

Kelner, A. 1949a. Effect of visible light on the recovery of *Streptomyces griseus* conidia from ultraviolet irradiation injury. *Proc Natl Acad Sci U S A* 35(2), pp. 73-79.

Kelner, A. 1949b. Photoreactivation of ultraviolet-irradiated *Escherichia coli*, with special reference to the dose-reduction principle and to ultraviolet-induced mutation. *J Bacteriol* 58(4), pp. 511-522.

Kent, N. A. and Karabetsou, N. and Politis, P. K. and Mellor, J. 2001. *In vivo* chromatin remodeling by yeast ISWI homologs Isw1p and Isw2p. *Genes Dev* 15(5), pp. 619-626.

Kim, J. K. and Patel, D. and Choi, B. S. 1995. Contrasting structural impacts induced by cis-syn cyclobutane dimer and (6-4) adduct in DNA duplex decamers: implication in mutagenesis and repair activity. *Photochem Photobiol* 62(1), pp. 44-50.

Kimura, H. and Cook, P. R. 2001. Kinetics of core histones in living human cells: little exchange of H3 and H4 and some rapid exchange of H2B. *J Cell Biol* 153(7), pp. 1341-1353.

Kireeva, M. L. and Hancock, B. and Cremona, G. H. and Walter, W. and Studitsky, V. M. and Kashlev, M. 2005. Nature of the nucleosomal barrier to RNA polymerase II. *Mol Cell* 18(1), pp. 97-108.

Kleibl, K. 2002. Molecular mechanisms of adaptive response to alkylating agents in Escherichia coli and some remarks on O(6)-methylguanine DNA-methyltransferase in other organisms. *Mutat Res* 512(1), pp. 67-84.

Kouzarides, T. 2007. Chromatin modifications and their function. *Cell* 128(4), pp. 693-705.

Kraemer, K. H. and Patronas, N. J. and Schiffmann, R. and Brooks, B. P. and Tamura, D. and DiGiovanna, J. J. 2007. Xeroderma pigmentosum, trichothiodystrophy and Cockayne syndrome: a complex genotype-phenotype relationship. *Neuroscience* 145(4), pp. 1388-1396.

Krebs, J. E. and Kuo, M. H. and Allis, C. D. and Peterson, C. L. 1999. Cell cycle-regulated histone acetylation required for expression of the yeast HO gene. *Genes Dev* 13(11), pp. 1412-1421.

Krebs, J. E. 2007. Moving marks: dynamic histone modifications in yeast. *Mol Biosyst* 3(9), pp. 590-597.

Krogan, N. J. and Baetz, K. and Keogh, M. C. and Datta, N. and Sawa, C. and Kwok, T. C. and Thompson, N. J. and Davey, M. G. and Pootoolal, J. and Hughes, T. R. and Emili, A. and Buratowski, S. and Hieter, P. and Greenblatt, J. F. 2004. Regulation of chromosome stability by the histone H2A variant Htz1, the Swr1 chromatin remodeling complex, and the histone acetyltransferase NuA4. *Proc Natl Acad Sci U S A* 101(37), pp. 13513-13518.

Kunkel, T. A. and Erie, D. A. 2005. DNA mismatch repair. *Annu Rev Biochem* 74, pp. 681-710.

Kuo, M. H. and Brownell, J. E. and Sobel, R. E. and Ranalli, T. A. and Cook, R. G. and Edmondson, D. G. and Roth, S. Y. and Allis, C. D. 1996. Transcription-linked acetylation by Gcn5p of histones H3 and H4 at specific lysines. *Nature* 383(6597), pp. 269-272.

Kuo, M. H. and Allis, C. D. 1999. In vivo cross-linking and immunoprecipitation for studying dynamic Protein:DNA associations in a chromatin environment. *Methods* 19(3), pp. 425-433.

Kuo, M. H. and vom Baur, E. and Struhl, K. and Allis, C. D. 2000. Gcn4 activator targets Gcn5 histone acetyltransferase to specific promoters independently of transcription. *Mol Cell* 6(6), pp. 1309-1320.

Kuo, W. H. and Wang, Y. and Wong, R. P. and Campos, E. I. and Li, G. 2007. The ING1b tumor suppressor facilitates nucleotide excision repair by promoting chromatin accessibility to XPA. *Exp Cell Res* 313(8), pp. 1628-1638.

Kurdistani, S. K. and Tavazoie, S. and Grunstein, M. 2004. Mapping global histone acetylation patterns to gene expression. *Cell* 117(6), pp. 721-733.

Lachner, M. and O'Carroll, D. and Rea, S. and Mechtler, K. and Jenuwein, T. 2001. Methylation of histone H3 lysine 9 creates a binding site for HP1 proteins. *Nature* 410(6824), pp. 116-120.

Laine, J. P. and Egly, J. M. 2006. Initiation of DNA repair mediated by a stalled RNA polymerase IIO. *EMBO J* 25(2), pp. 387-397.

Lamers, M. H. and Winterwerp, H. H. and Sixma, T. K. 2003. The alternating ATPase domains of MutS control DNA mismatch repair. *EMBO J* 22(3), pp. 746-756.

Le May, N. and Mota-Fernandes, D. and Velez-Cruz, R. and Iltis, I. and Biard, D. and Egly, J. M. 2010a. NER factors are recruited to active promoters and facilitate chromatin modification for transcription in the absence of exogenous genotoxic attack. *Mol Cell* 38(1), pp. 54-66.

Le May, N. and Egly, J. M. and Coin, F. 2010b. True lies: the double life of the nucleotide excision repair factors in transcription and DNA repair. *J Nucleic Acids* 2010.

Leadon, S. A. and Lawrence, D. A. 1992. Strand-selective repair of DNA damage in the yeast GAL7 gene requires RNA polymerase II. *J Biol Chem* 267(32), pp. 23175-23182.

Lee, K. and Kim, D. R. and Ahn, B. 2004. Chromatin remodeling facilitates DNA incision in UV-damaged nucleosomes. *Mol Cells* 18(1), pp. 100-106.

Lee, M. and Chatterjee, S. and Struhl, K. 2000. Genetic analysis of the role of Pol II holoenzyme components in repression by the Cyc8-Tup1 corepressor in yeast. *Genetics* 155(4), pp. 1535-1542.

Lee, S. K. and Yu, S. L. and Prakash, L. and Prakash, S. 2002. Yeast RAD26, a homolog of the human CSB gene, functions independently of nucleotide excision repair and base excision repair in promoting transcription through damaged bases. *Mol Cell Biol* 22(12), pp. 4383-4389.

Lehmann, A. R. 2003. DNA repair-deficient diseases, xeroderma pigmentosum, Cockayne syndrome and trichothiodystrophy. *Biochimie* 85(11), pp. 1101-1111.

Leibeling, D. and Laspe, P. and Emmert, S. 2006. Nucleotide excision repair and cancer. *J Mol Histol* 37(5-7), pp. 225-238.

Lettieri, T. and Kraehenbuehl, R. and Capiaghi, C. and Livingstone-Zatchej, M. and Thoma, F. 2008. Functionally distinct nucleosome-free regions in yeast require Rad7 and Rad16 for nucleotide excision repair. *DNA Repair (Amst)* 7(5), pp. 734-743.

Li, B. and Reese, J. C. 2001. Ssn6-Tup1 regulates RNR3 by positioning nucleosomes and affecting the chromatin structure at the upstream repression sequence. *J Biol Chem* 276(36), pp. 33788-33797.

Li, B. and Pattenden, S. G. and Lee, D. and Gutierrez, J. and Chen, J. and Seidel, C. and Gerton, J. and Workman, J. L. 2005. Preferential occupancy of histone variant H2AZ at inactive promoters influences local histone modifications and chromatin remodeling. *Proc Natl Acad Sci U S A* 102(51), pp. 18385-18390.

Li, B. and Carey, M. and Workman, J. L. 2007a. The role of chromatin during transcription. *Cell* 128(4), pp. 707-719.

Li, J. and Uchida, T. and Todo, T. and Kitagawa, T. 2006. Similarities and differences between cyclobutane pyrimidine dimer photolyase and (6-4) photolyase as revealed by resonance Raman spectroscopy: Electron transfer from the FAD cofactor to ultraviolet-damaged DNA. *J Biol Chem* 281(35), pp. 25551-25559.

Li, S. and Waters, R. 1996. Nucleotide level detection of cyclobutane pyrimidine dimers using oligonucleotides and magnetic beads to facilitate labelling of DNA fragments incised at the dimers and chemical sequencing reference ladders. *Carcinogenesis* 17(8), pp. 1549-1552.

Li, S. and Livingstone-Zatchej, M. and Gupta, R. and Meijer, M. and Thoma, F. and Smerdon, M. J. 1999. Nucleotide excision repair in a constitutive and inducible gene of a yeast minichromosome in intact cells. *Nucleic Acids Res* 27(17), pp. 3610-3620.

Li, S. and Smerdon, M. J. 2002. Rpb4 and Rpb9 mediate subpathways of transcription-coupled DNA repair in *Saccharomyces cerevisiae*. *EMBO J* 21(21), pp. 5921-5929.

Li, S. and Smerdon, M. J. 2004. Dissecting transcription-coupled and global genomic repair in the chromatin of yeast GAL1-10 genes. *J Biol Chem* 279(14), pp. 14418-14426.

Li, S. and Liu, H. 2006. Functions of histone H2A variants. *Animal Science Journal* 77, pp. 549-555.

Li, S. and Ding, B. and LeJeune, D. and Ruggiero, C. and Chen, X. and Smerdon, M. J. 2007b. The roles of Rad16 and Rad26 in repairing repressed and actively transcribed genes in yeast. *DNA Repair (Amst)* 6(11), pp. 1596-1606.

Lichon, V. and Khachemoune, A. 2007. Xeroderma pigmentosum: beyond skin cancer. *J Drugs Dermatol* 6(3), pp. 281-288.

Lim, J. H. and West, K. L. and Rubinstein, Y. and Bergel, M. and Postnikov, Y. V. and Bustin, M. 2005. Chromosomal protein HMGN1 enhances the acetylation of lysine 14 in histone H3. *EMBO J* 24(17), pp. 3038-3048.

Liu, H. 2005. *DNA repair and transcription of the yeast MFA2 gene: roles of Tup1p, Gcn5p and Rad16p.* Cardiff University.

Livingstone-Zatchej, M. and Marcionelli, R. and Moller, K. and de Pril, R. and Thoma, F. 2003. Repair of UV lesions in silenced chromatin provides *in vivo* evidence for a compact chromatin structure. *J Biol Chem* 278(39), pp. 37471-37479.

Long, C. M. and Brajkovich, C. M. and Scott, J. F. 1985. Alternative model for chromatin organization of the *Saccharomyces cerevisiae* chromosomal DNA plasmid TRP1 RI circle (YARp1). *Mol Cell Biol* 5(11), pp. 3124-3130.

Lorick, K. L. and Jensen, J. P. and Fang, S. and Ong, A. M. and Hatakeyama, S. and Weissman, A. M. 1999. RING fingers mediate ubiquitin-conjugating enzyme (E2)-dependent ubiquitination. *Proc Natl Acad Sci U S A* 96(20), pp. 11364-11369.

Lynch, H. T. and de la Chapelle, A. 1999. Genetic susceptibility to non-polyposis colorectal cancer. *J Med Genet* 36(11), pp. 801-818.

Malhotra, K. and Baer, M. and Li, Y. F. and Sancar, G. B. and Sancar, A. 1992. Identification of chromophore binding domains of yeast DNA photolyase. *J Biol Chem* 267(5), pp. 2909-2914.

Marquez, J. A. and Pascual-Ahuir, A. and Proft, M. and Serrano, R. 1998. The Ssn6-Tup1 repressor complex of *Saccharomyces cerevisiae* is involved in the osmotic induction of HOG-dependent and -independent genes. *EMBO J* 17(9), pp. 2543-2553.

Martinez-Campa, C. and Politis, P. and Moreau, J. L. and Kent, N. and Goodall, J. and Mellor, J. and Goding, C. R. 2004. Precise nucleosome positioning and the TATA box dictate requirements for the histone H4 tail and the bromodomain factor Bdf1. *Mol Cell* 15(1), pp. 69-81.

Martini, E. and Roche, D. M. and Marheineke, K. and Verreault, A. and Almouzni, G. 1998. Recruitment of phosphorylated chromatin assembly factor 1 to chromatin after UV irradiation of human cells. *J Cell Biol* 143(3), pp. 563-575.

Mayne, L. V. and Lehmann, A. R. 1982. Failure of RNA synthesis to recover after UV irradiation: an early defect in cells from individuals with Cockayne's syndrome and xeroderma pigmentosum. *Cancer Res* 42(4), pp. 1473-1478.

Meijer, M. and Smerdon, M. J. 1999. Accessing DNA damage in chromatin: insights from transcription. *Bioessays* 21(7), pp. 596-603.

Mellon, I. and Bohr, V. A. and Smith, C. A. and Hanawalt, P. C. 1986. Preferential DNA repair of an active gene in human cells. *Proc Natl Acad Sci U S A* 83(23), pp. 8878-8882.

Mellon, I. and Hanawalt, P. C. 1989. Induction of the *Escherichia coli* lactose operon selectively increases repair of its transcribed DNA strand. *Nature* 342(6245), pp. 95-98.

Michaelis, S. and Herskowitz, I. 1988. The a-factor pheromone of *Saccharomyces cerevisiae* is essential for mating. *Mol Cell Biol* 8(3), pp. 1309-1318.

Millar, C. B. and Xu, F. and Zhang, K. and Grunstein, M. 2006. Acetylation of H2AZ Lys 14 is associated with genome-wide gene activity in yeast. *Genes Dev* 20(6), pp. 711-722.

Mills, K. D. and Sinclair, D. A. and Guarente, L. 1999. MEC1-dependent redistribution of the Sir3 silencing protein from telomeres to DNA double-strand breaks. *Cell* 97(5), pp. 609-620.

Mitchell, D. L. and Nguyen, T. D. and Cleaver, J. E. 1990. Nonrandom induction of pyrimidine-pyrimidone (6-4) photoproducts in ultraviolet-irradiated human chromatin. *J Biol Chem* 265(10), pp. 5353-5356.

Mitchell, D. L. and Jen, J. and Cleaver, J. E. 1992. Sequence specificity of cyclobutane pyrimidine dimers in DNA treated with solar (ultraviolet B) radiation. *Nucleic Acids Res* 20(2), pp. 225-229.

Mizuno, T. and Nakazawa, N. and Remgsamrarn, P. and Kunoh, T. and Oshima, Y. and Harashima, S. 1998. The Tup1-Ssn6 general repressor is involved in repression of IME1 encoding a transcriptional activator of meiosis in *Saccharomyces cerevisiae. Curr Genet* 33(4), pp. 239-247.

Moggs, J. G. and Grandi, P. and Quivy, J. P. and Jonsson, Z. O. and Hubscher, U. and Becker, P. B. and Almouzni, G. 2000. A CAF-1-PCNA-mediated chromatin assembly pathway triggered by sensing DNA damage. *Mol Cell Biol* 20(4), pp. 1206-1218.

Moore, J. D. and Yazgan, O. and Ataian, Y. and Krebs, J. E. 2007. Diverse roles for histone H2A modifications in DNA damage response pathways in yeast. *Genetics* 176(1), pp. 15-25.

Morohashi, N. and Yamamoto, Y. and Kuwana, S. and Morita, W. and Shindo, H. and Mitchell, A. P. and Shimizu, M. 2006. Effect of sequence-directed nucleosome disruption on cell-type-specific repression by alpha2/Mcm1 in the yeast genome. *Eukaryot Cell* 5(11), pp. 1925-1933.

Morohashi, N. and Nakajima, K. and Kurihara, D. and Mukai, Y. and Mitchell, A. P. and Shimizu, M. 2007. A nucleosome positioned by alpha2/Mcm1 prevents Hap1 activator binding *in vivo. Biochem Biophys Res Commun* 364(3), pp. 583-588.

Morrison, A. J. and Shen, X. 2009. Chromatin remodelling beyond transcription: the INO80 and SWR1 complexes. *Nat Rev Mol Cell Biol* 10(6), pp. 373-384.

Mu, D. and Wakasugi, M. and Hsu, D. S. and Sancar, A. 1997. Characterization of reaction intermediates of human excision repair nuclease. *J Biol Chem* 272(46), pp. 28971-28979.

Mueller, J. P. and Smerdon, M. J. 1996. Rad23 is required for transcription-coupled repair and efficient overrall repair in *Saccharomyces cerevisiae*. *Mol Cell Biol* 16(5), pp. 2361-2368.

Myers, F. A. and Evans, D. R. and Clayton, A. L. and Thorne, A. W. and Crane-Robinson, C. 2001. Targeted and extended acetylation of histones H4 and H3 at active and inactive genes in chicken embryo erythrocytes. *J Biol Chem* 276(23), pp. 20197-20205.

Nag, R. and Gong, F. and Fahy, D. and Smerdon, M. J. 2008. A single amino acid change in histone H4 enhances UV survival and DNA repair in yeast. *Nucleic Acids Res* 36(11), pp. 3857-3866.

Natrajan, G. and Lamers, M. H. and Enzlin, J. H. and Winterwerp, H. H. and Perrakis, A. and Sixma, T. K. 2003. Structures of *Escherichia coli* DNA mismatch repair enzyme MutS in complex with different mismatches: a common recognition mode for diverse substrates. *Nucleic Acids Res* 31(16), pp. 4814-4821.

Niedernhofer, L. J. 2008. Tissue-specific accelerated aging in nucleotide excision repair deficiency. *Mech Ageing Dev* 129(7-8), pp. 408-415.

Osley, M. A. and Tsukuda, T. and Nickoloff, J. A. 2007. ATP-dependent chromatin remodeling factors and DNA damage repair. *Mutat Res* 618(1-2), pp. 65-80.

Paetkau, D. W. and Riese, J. A. and MacMorran, W. S. and Woods, R. A. and Gietz, R. D. 1994. Interaction of the yeast RAD7 and SIR3 proteins: implications for DNA repair and chromatin structure. *Genes Dev* 8(17), pp. 2035-2045.

Park, H. and Zhang, K. and Ren, Y. and Nadji, S. and Sinha, N. and Taylor, J. S. and Kang, C. 2002a. Crystal structure of a DNA decamer containing a cis-syn thymine dimer. *Proc Natl Acad Sci U S A* 99(25), pp. 15965-15970.

Park, J. S. and Marr, M. T. and Roberts, J. W. 2002b. *E. coli* Transcription repair coupling factor (Mfd protein) rescues arrested complexes by promoting forward translocation. *Cell* 109(6), pp. 757-767.

Patterton, H. G. and Simpson, R. T. 1994. Nucleosomal location of the STE6 TATA box and Mat alpha 2p-mediated repression. *Mol Cell Biol* 14(6), pp. 4002-4010.

Pederson, D. S. and Venkatesan, M. and Thoma, F. and Simpson, R. T. 1986. Isolation of an episomal yeast gene and replication origin as chromatin. *Proc Natl Acad Sci U S A* 83(19), pp. 7206-7210.

Pehrson, J. R. 1989. Thymine dimer formation as a probe of the path of DNA in and between nucleosomes in intact chromatin. *Proc Natl Acad Sci U S A* 86(23), pp. 9149-9153.

Pehrson, J. R. and Cohen, L. H. 1992. Effects of DNA looping on pyrimidine dimer formation. *Nucleic Acids Res* 20(6), pp. 1321-1324.

Peltomaki, P. 2001. DNA mismatch repair and cancer. *Mutat Res* 488(1), pp. 77-85.

Pikaart, M. J. and Recillas-Targa, F. and Felsenfeld, G. 1998. Loss of transcriptional activity of a transgene is accompanied by DNA methylation and histone deacetylation and is prevented by insulators. *Genes Dev* 12(18), pp. 2852-2862.

Pokholok, D. K. and Harbison, C. T. and Levine, S. and Cole, M. and Hannett, N. M. and Lee, T. I. and Bell, G. W. and Walker, K. and Rolfe, P. A. and Herbolsheimer, E. and Zeitlinger, J. and Lewitter, F. and Gifford, D. K. and Young, R. A. 2005. Genome-wide map of nucleosome acetylation and methylation in yeast. *Cell* 122(4), pp. 517-527.

Polo, S. E. and Roche, D. and Almouzni, G. 2006. New histone incorporation marks sites of UV repair in human cells. *Cell* 127(3), pp. 481-493.

Prakash, S. and Sung, P. and Prakash, L. 1993. DNA repair genes and proteins of *Saccharomyces cerevisiae*. *Annu Rev Genet* 27, pp. 33-70.

Prakash, S. and Prakash, L. 2000. Nucleotide excision repair in yeast. *Mutat Res* 451(1-2), pp. 13-24.

Pray-Grant, M. G. and Schieltz, D. and McMahon, S. J. and Wood, J. M. and Kennedy, E. L. and Cook, R. G. and Workman, J. L. and Yates, J. R., 3rd and Grant, P. A. 2002. The novel SLIK histone acetyltransferase complex functions in the yeast retrograde response pathway. *Mol Cell Biol* 22(24), pp. 8774-8786.

Qiu, H. and Park, E. and Prakash, L. and Prakash, S. 1993. The *Saccharomyces cerevisiae* DNA repair gene RAD25 is required for transcription by RNA polymerase II. *Genes Dev* 7(11), pp. 2161-2171.

Quilliet, X. and Chevallier-Lagente, O. and Zeng, L. and Calvayrac, R. and Mezzina, M. and Sarasin, A. and Vuillaume, M. 1997. Retroviral-mediated correction of DNA repair defect in xeroderma pigmentosum cells is associated with recovery of catalase activity. *Mutat Res* 385(3), pp. 235-242.

Ramanathan, B. and Smerdon, M. J. 1989. Enhanced DNA repair synthesis in hyperacetylated nucleosomes. *J Biol Chem* 264(19), pp. 11026-11034.

Ramsey, K. L. and Smith, J. J. and Dasgupta, A. and Maqani, N. and Grant, P. and Auble, D. T. 2004. The NEF4 complex regulates Rad4 levels and utilizes Snf2/Swi2-related ATPase activity for nucleotide excision repair. *Mol Cell Biol* 24(14), pp. 6362-6378.

Redd, M. J. and Stark, M. R. and Johnson, A. D. 1996. Accessibility of α2-repressed promoters to the activator Gal4. *Molecular and Cellular Biology* 16(6), pp. 2865-2869.

Redd, M. J. and Arnaud, M. B. and Johnson, A. D. 1997. A complex composed of tup1 and ssn6 represses transcription in vitro. *J Biol Chem* 272(17), pp. 11193-11197.

Reed, S. H. and You, Z. and Friedberg, E. C. 1998. The yeast RAD7 and RAD16 genes are required for postincision events during nucleotide excision repair. *In vitro* and *in vivo* studies with rad7 and rad16 mutants and purification of a Rad7/Rad16-containing protein complex. *J Biol Chem* 273(45), pp. 29481-29488.

Reed, S. H. and Akiyama, M. and Stillman, B. and Friedberg, E. C. 1999. Yeast autonomously replicating sequence binding factor is involved in nucleotide excision repair. *Genes Dev* 13(23), pp. 3052-3058.

Reed, S. H. and Gillette, T. G. 2007. Nucleotide excision repair and the ubiquitin proteasome pathway--do all roads lead to Rome? *DNA Repair (Amst)* 6(2), pp. 149-156.

Reinke, H. and Horz, W. 2003. Histones are first hyperacetylated and then lose contact with the activated PHO5 promoter. *Mol Cell* 11(6), pp. 1599-1607.

Robert, F. and Pokholok, D. K. and Hannett, N. M. and Rinaldi, N. J. and Chandy, M. and Rolfe, A. and Workman, J. L. and Gifford, D. K. and Young, R. A. 2004. Global position and recruitment of HATs and HDACs in the yeast genome. *Mol Cell* 16(2), pp. 199-209.

Roth, S. Y. and Dean, A. and Simpson, R. T. 1990. Yeast alpha 2 repressor positions nucleosomes in TRP1/ARS1 chromatin. *Mol Cell Biol* 10(5), pp. 2247-2260.

Roth, S. Y. and Shimizu, M. and Johnson, L. and Grunstein, M. and Simpson, R. T. 1992. Stable nucleosome positioning and complete repression by the yeast alpha 2 repressor are disrupted by amino-terminal mutations in histone H4. *Genes Dev* 6(3), pp. 411-425.

Roth, S. Y. and Denu, J. M. and Allis, C. D. 2001. Histone acetyltransferases. *Annu Rev Biochem* 70, pp. 81-120.

Rouse, J. and Jackson, S. P. 2002. Interfaces between the detection, signaling, and repair of DNA damage. *Science* 297(5581), pp. 547-551.

Rubbi, C. P. and Milner, J. 2003. p53 is a chromatin accessibility factor for nucleotide excision repair of DNA damage. *EMBO J* 22(4), pp. 975-986.

Rupert, C. S. 1960. Photoreactivation of transforming DNA by an enzyme from bakers' yeast. *J Gen Physiol* 43, pp. 573-595.

Russell, S. J. and Reed, S. H. and Huang, W. and Friedberg, E. C. and Johnston, S. A. 1999. The 19S regulatory complex of the proteasome functions independently of proteolysis in nucleotide excision repair. *Mol Cell* 3(6), pp. 687-695.

Saha, A. and Wittmeyer, J. and Cairns, B. R. 2006. Chromatin remodelling: the industrial revolution of DNA around histones. *Nat Rev Mol Cell Biol* 7(6), pp. 437-447.

Sancar, A. and Franklin, K. A. and Sancar, G. B. 1984. *Escherichia coli* DNA photolyase stimulates uvrABC excision nuclease in vitro. *Proc Natl Acad Sci U S A* 81(23), pp. 7397-7401.

Sancar, G. B. 1990. DNA photolyases: physical properties, action mechanism, and roles in dark repair. *Mutat Res* 236(2-3), pp. 147-160.

Sancar, G. B. 2000. Enzymatic photoreactivation: 50 years and counting. *Mutat Res* 451(1-2), pp. 25-37.

Schieferstein, U. and Thoma, F. 1998. Site-specific repair of cyclobutane pyrimidine dimers in a positioned nucleosome by photolyase and T4 endonuclease V in vitro. *EMBO J* 17(1), pp. 306-316.

Schnitzler, G. and Sif, S. and Kingston, R. E. 1998. Human SWI/SNF interconverts a nucleosome between its base state and a stable remodeled state. *Cell* 94(1), pp. 17-27.

Scott, A. D. and Waters, R. 1997. Inducible nucleotide excision repair (NER) of UV-induced cyclobutane pyrimidine dimers in the cell cycle of the budding yeast *Saccharomyces cerevisiae*: evidence that inducible NER is confined to the G1 phase of the mitotic cell cycle. *Mol Gen Genet* 254(1), pp. 43-53.

Sekinger, E. A. and Moqtaderi, Z. and Struhl, K. 2005. Intrinsic histone-DNA interactions and low nucleosome density are important for preferential accessibility of promoter regions in yeast. *Mol Cell* 18(6), pp. 735-748.

Selby, C. P. and Sancar, A. 1990. Transcription preferentially inhibits nucleotide excision repair of the template DNA strand *in vitro*. *J Biol Chem* 265(34), pp. 21330-21336.

Selby, C. P. and Sancar, A. 1994. Mechanisms of transcription-repair coupling and mutation frequency decline. *Microbiol Rev* 58(3), pp. 317-329.

Selby, C. P. and Sancar, A. 1997. Human transcription-repair coupling factor CSB/ERCC6 is a DNA-stimulated ATPase but is not a helicase and does not disrupt the ternary transcription complex of stalled RNA polymerase II. *J Biol Chem* 272(3), pp. 1885-1890.

Shimizu, M. and Roth, S. Y. and Szent-Gyorgyi, C. and Simpson, R. T. 1991. Nucleosomes are positioned with base pair precision adjacent to the alpha 2 operator in *Saccharomyces cerevisiae*. *EMBO J* 10(10), pp. 3033-3041.

Shivji, K. K. and Kenny, M. K. and Wood, R. D. 1992. Proliferating cell nuclear antigen is required for DNA excision repair. *Cell* 69(2), pp. 367-374.

Shogren-Knaak, M. and Ishii, H. and Sun, J. M. and Pazin, M. J. and Davie, J. R. and Peterson, C. L. 2006. Histone H4-K16 acetylation controls chromatin structure and protein interactions. *Science* 311(5762), pp. 844-847.

Skorvaga, M. and DellaVecchia, M. J. and Croteau, D. L. and Theis, K. and Truglio, J. J. and Mandavilli, B. S. and Kisker, C. and Van Houten, B. 2004. Identification of residues within UvrB that are important for efficient DNA binding and damage processing. *J Biol Chem* 279(49), pp. 51574-51580.

Smerdon, M. J. and Lieberman, M. W. 1978. Nucleosome rearrangement in human chromatin during UV-induced DNA- reapir synthesis. *Proc Natl Acad Sci U S A* 75(9), pp. 4238-4241.

Smerdon, M. J. and Bedoyan, J. and Thoma, F. 1990. DNA repair in a small yeast plasmid folded into chromatin. *Nucleic Acids Res* 18(8), pp. 2045-2051.

Smerdon, M. J. and Thoma, F. 1990. Site-specific DNA repair at the nucleosome level in a yeast minichromosome. *Cell* 61(4), pp. 675-684.

Smerdon, M. J. 1991. DNA repair and the role of chromatin structure. *Curr Opin Cell Biol* 3(3), pp. 422-428.

Smith, R. L. and Johnson, A. D. 2000. Turning genes off by Ssn6-Tup1: a conserved system of transcriptional repression in eukaryotes. *Trends Biochem Sci* 25(7), pp. 325-330.

Strahl, B. D. and Allis, C. D. 2000. The language of covalent histone modifications. *Nature* 403(6765), pp. 41-45.

Sugasawa, K. and Masutani, C. and Hanaoka, F. 1993. Cell-free repair of UV-damaged simian virus 40 chromosomes in human cell extracts. I. Development of a cell-free system detecting excision repair of UV-irradiated SV40 chromosomes. *J Biol Chem* 268(12), pp. 9098-9104.

Sugasawa, K. and Ng, J. M. and Masutani, C. and Iwai, S. and van der Spek, P. J. and Eker, A. P. and Hanaoka, F. and Bootsma, D. and Hoeijmakers, J. H. 1998. Xeroderma pigmentosum group C protein complex is the initiator of global genome nucleotide excision repair. *Mol Cell* 2(2), pp. 223-232.

Sugasawa, K. and Okuda, Y. and Saijo, M. and Nishi, R. and Matsuda, N. and Chu, G. and Mori, T. and Iwai, S. and Tanaka, K. and Hanaoka, F. 2005. UV-induced ubiquitylation of XPC protein mediated by UV-DDB-ubiquitin ligase complex. *Cell* 121(3), pp. 387-400.

Sun, Z. W. and Allis, C. D. 2002. Ubiquitination of histone H2B regulates H3 methylation and gene silencing in yeast. *Nature* 418(6893), pp. 104-108.

Sung, P. and Prakash, L. and Matson, S. W. and Prakash, S. 1987. RAD3 protein of *Saccharomyces cerevisiae* is a DNA helicase. *Proc Natl Acad Sci U S A* 84(24), pp. 8951-8955.

Sutherland, B. M. and Harber, L. C. and Kochevar, I. E. 1980. Pyrimidine dimer formation and repair in human skin. *Cancer Res* 40(9), pp. 3181-3185.

Svedruzic, Z. M. and Wang, C. and Kosmoski, J. V. and Smerdon, M. J. 2005. Accommodation and repair of a UV photoproduct in DNA at different rotational settings on the nucleosome surface. *J Biol Chem* 280(48), pp. 40051-40057.

Svejstrup, J. Q. and Wang, Z. and Feaver, W. J. and Wu, X. and Bushnell, D. A. and Donahue, T. F. and Friedberg, E. C. and Kornberg, R. D. 1995. Different forms of TFIIH for transcription and DNA repair: holo-TFIIH and a nucleotide excision repairosome. *Cell* 80(1), pp. 21-28.

Sweder, K. and Madura, K. 2002. Regulation of repair by the 26S proteasome. *J Biomed Biotechnol* 2(2), pp. 94-105.

Sweder, K. S. and Hanawalt, P. C. 1992. Preferential repair of cyclobutane pyrimidine dimers in the transcribed strand of a gene in yeast chromosomes and plasmids is dependent on transcription. *Proc Natl Acad Sci U S A* 89(22), pp. 10696-10700.

Tamburini, B. A. and Tyler, J. K. 2005. Localized histone acetylation and deacetylation triggered by the homologous recombination pathway of double-strand DNA repair. *Mol Cell Biol* 25(12), pp. 4903-4913.

Tamkun, J. W. and Deuring, R. and Scott, M. P. and Kissinger, M. and Pattatucci, A. M. and Kaufman, T. C. and Kennison, J. A. 1992. brahma: a regulator of Drosophila homeotic genes structurally related to the yeast transcriptional activator SNF2/SWI2. *Cell* 68(3), pp. 561-572.

Tang, J. and Chu, G. 2002. Xeroderma pigmentosum complementation group E and UV-damaged DNA-binding protein. *DNA Repair (Amst)* 1(8), pp. 601-616.

Teng, Y. and Li, S. and Waters, R. and Reed, S. H. 1997. Excision repair at the level of the nucleotide in the *Saccharomyces cerevisiae MFA2* gene: mapping of where enhanced repair in the transcribed strand begins or ends and identification of only a partial rad16 requisite for repairing upstream control sequences. *J Mol Biol* 267(2), pp. 324-337.

Teng, Y. and Waters, R. 2000. Excision repair at the level of the nucleotide in the upstream control region, the coding sequence and in the region where transcription terminates of the *Saccharomyces cerevisiae MFA2* gene and the role of RAD26. *Nucleic Acids Res* 28(5), pp. 1114-1119.

Teng, Y. and Yu, S. and Waters, R. 2001. The mapping of nucleosomes and regulatory protein binding sites at the *Saccharomyces cerevisiae MFA2* gene: a high resolution approach. *Nucleic Acids Res* 29(13), pp. E64-64.

Teng, Y. and Yu, Y. and Waters, R. 2002. The *Saccharomyces cerevisiae* histone acetyltransferase Gcn5 has a role in the photoreactivation and nucleotide excision repair of UV-induced cyclobutane pyrimidine dimers in the *MFA2* gene. *J Mol Biol* 316(3), pp. 489-499.

Teng, Y. and Yu, Y. and Ferreiro, J. A. and Waters, R. 2005. Histone acetylation, chromatin remodelling, transcription and nucleotide excision repair in *S. cerevisiae*: studies with two model genes. *DNA Repair (Amst)* 4(8), pp. 870-883.

Teng, Y. and Liu, H. and Gill, H. W. and Yu, Y. and Waters, R. and Reed, S. H. 2008. *Saccharomyces cerevisiae* Rad16 mediates ultraviolet-dependent histone H3 acetylation required for efficient global genome nucleotide-excision repair. *EMBO Rep* 9(1), pp. 97-102.

Terleth, C. and van Sluis, C. A. and van de Putte, P. 1989. Differential repair of UV damage in *Saccharomyces cerevisiae*. *Nucleic Acids Res* 17(12), pp. 4433-4439.

Terleth, C. and Schenk, P. and Poot, R. and Brouwer, J. and van de Putte, P. 1990. Differential repair of UV damage in rad mutants of *Saccharomyces cerevisiae*: a possible function of G2 arrest upon UV irradiation. *Mol Cell Biol* 10(9), pp. 4678-4684.

Teunissen, A. W. and van den Berg, J. A. and Steensma, H. Y. 1995. Transcriptional regulation of flocculation genes in *Saccharomyces cerevisiae*. *Yeast* 11(5), pp. 435-446.

Thoma, F. and Bergman, L. W. and Simpson, R. T. 1984. Nuclease digestion of circular TRP1ARS1 chromatin reveals positioned nucleosomes separated by nuclease-sensitive regions. *J Mol Biol* 177(4), pp. 715-733.

Thoma, F. 1986. Protein-DNA interactions and nuclease-sensitive regions determine nucleosome positions on yeast plasmid chromatin. *J Mol Biol* 190(2), pp. 177-190.

Thoma, F. and Zatchej, M. 1988. Chromatin folding modulates nucleosome positioning in yeast minichromosomes. *Cell* 55(6), pp. 945-953.

Thoma, F. 1996. Mapping of nucleosome positions. *Methods Enzymol* 274, pp. 197-214.

Thoma, F. 1999. Light and dark in chromatin repair: repair of UV-induced DNA lesions by photolyase and nucleotide excision repair. *EMBO J* 18(23), pp. 6585-6598.

Thoma, F. 2005. Repair of UV lesions in nucleosomes--intrinsic properties and remodeling. *DNA Repair (Amst)* 4(8), pp. 855-869.

Tijsterman, M. and Tasseron-de Jong, J. G. and van de Putte, P. and Brouwer, J. 1996. Transcription-coupled and global genome repair in the *Saccharomyces cerevisiae* RPB2 gene at nucleotide resolution. *Nucleic Acids Res* 24(18), pp. 3499-3506.

Tijsterman, M. and Verhage, R. A. and van de Putte, P. and Tasseron-de Jong, J. G. and Brouwer, J. 1997. Transitions in the coupling of transcription and nucleotide excision repair within RNA polymerase II-transcribed genes of *Saccharomyces cerevisiae*. *Proc Natl Acad Sci U S A* 94(15), pp. 8027-8032.

Todo, T. and Takemori, H. and Ryo, H. and Ihara, M. and Matsunaga, T. and Nikaido, O. and Sato, K. and Nomura, T. 1993. A new photoreactivating enzyme that specifically repairs ultraviolet light-induced (6-4)photoproducts. *Nature* 361(6410), pp. 371-374.

Todo, T. and Ryo, H. and Yamamoto, K. and Toh, H. and Inui, T. and Ayaki, H. and Nomura, T. and Ikenaga, M. 1996. Similarity among the Drosophila (6-4)photolyase, a human photolyase homolog, and the DNA photolyase-blue-light photoreceptor family. *Science* 272(5258), pp. 109-112.

Tomkinson, A. E. and Bardwell, A. J. and Bardwell, L. and Tappe, N. J. and Friedberg, E. C. 1993. Yeast DNA repair and recombination proteins Rad1 and Rad10 constitute a single-stranded-DNA endonuclease. *Nature* 362(6423), pp. 860-862.

Tran, N. and Qu, P. P. and Simpson, D. A. and Lindsey-Boltz, L. and Guan, X. and Schmitt, C. P. and Ibrahim, J. G. and Kaufmann, W. K. 2009. *In silico* construction of a protein interaction landscape for nucleotide excision repair. *Cell Biochem Biophys* 53(2), pp. 101-114.

Tremblay, M. and Teng, Y. and Paquette, M. and Waters, R. and Conconi, A. 2008. Complementary roles of yeast Rad4p and Rad34p in nucleotide excision repair of active and inactive rRNA gene chromatin. *Mol Cell Biol* 28(24), pp. 7504-7513.

Trievel, R. C. and Rojas, J. R. and Sterner, D. E. and Venkataramani, R. N. and Wang, L. and Zhou, J. and Allis, C. D. and Berger, S. L. and Marmorstein, R. 1999. Crystal structure and mechanism of histone acetylation of the yeast GCN5 transcriptional coactivator. *Proc Natl Acad Sci U S A* 96(16), pp. 8931-8936.

Troelstra, C. and van Gool, A. and de Wit, J. and Vermeulen, W. and Bootsma, D. and Hoeijmakers, J. H. 1992. ERCC6, a member of a subfamily of putative helicases, is involved in Cockayne's syndrome and preferential repair of active genes. *Cell* 71(6), pp. 939-953.

Truglio, J. J. and Croteau, D. L. and Van Houten, B. and Kisker, C. 2006. Prokaryotic nucleotide excision repair: the UvrABC system. *Chem Rev* 106(2), pp. 233-252.

Trumbly, R. J. 1992. Glucose repression in the yeast *Saccharomyces cerevisiae*. *Mol Microbiol* 6(1), pp. 15-21.

Tu, Y. and Tornaletti, S. and Pfeifer, G. P. 1996. DNA repair domains within a human gene: selective repair of sequences near the transcription initiation site. *EMBO J* 15(3), pp. 675-683.

Turner, B. M. 2000. Histone acetylation and an epigenetic code. *Bioessays* 22(9), pp. 836-845.

Tzamarias, D. and Struhl, K. 1995. Distinct TPR motifs of Cyc8 are involved in recruiting the Cyc8-Tupl corepressor complex to differentially regulated promoters. *Genes Dev* 9(7), pp. 821-831.

Ulrich, H. D. 2007. Conservation of DNA damage tolerance pathways from yeast to humans. *Biochem Soc Trans* 35(Pt 5), pp. 1334-1337.

Ura, K. and Kurumizaka, H. and Dimitrov, S. and Almouzni, G. and Wolffe, A. P. 1997. Histone acetylation: influence on transcription, nucleosome mobility and positioning, and linker histone-dependent transcriptional repression. *EMBO J* 16(8), pp. 2096-2107.

Ura, K. and Araki, M. and Saeki, H. and Masutani, C. and Ito, T. and Iwai, S. and Mizukoshi, T. and Kaneda, Y. and Hanaoka, F. 2001. ATP-dependent chromatin remodeling facilitates nucleotide excision repair of UV-induced DNA lesions in synthetic dinucleosomes. *EMBO J* 20(8), pp. 2004-2014.

Utley, R. T. and Cote, J. and Owen-Hughes, T. and Workman, J. L. 1997. SWI/SNF stimulates the formation of disparate activator-nucleosome complexes but is partially redundant with cooperative binding. *J Biol Chem* 272(19), pp. 12642-12649.

van Gool, A. J. and Verhage, R. and Swagemakers, S. M. and van de Putte, P. and Brouwer, J. and Troelstra, C. and Bootsma, D. and Hoeijmakers, J. H. 1994. RAD26, the functional *S. cerevisiae* homolog of the Cockayne syndrome B gene ERCC6. *EMBO J* 13(22), pp. 5361-5369.

van Gool, A. J. and Citterio, E. and Rademakers, S. and van Os, R. and Vermeulen, W. and Constantinou, A. and Egly, J. M. and Bootsma, D. and Hoeijmakers, J. H. 1997. The Cockayne syndrome B protein, involved in transcription-coupled DNA repair, resides in an RNA polymerase II-containing complex. *EMBO J* 16(19), pp. 5955-5965.

van Hoffen, A. and Natarajan, A. T. and Mayne, L. V. and van Zeeland, A. A. and Mullenders, L. H. and Venema, J. 1993. Deficient repair of the transcribed strand of active genes in Cockayne's syndrome cells. *Nucleic Acids Res* 21(25), pp. 5890-5895.

Varanasi, U. S. and Klis, M. and Mikesell, P. B. and Trumbly, R. J. 1996. The Cyc8 (Ssn6)-Tupl corepressor complex is composed of one Cyc8 and four Tupl subunits. *Mol Cell Biol* 16(12), pp. 6707-6714.

Venema, J. and Mullenders, L. H. and Natarajan, A. T. and van Zeeland, A. A. and Mayne, L. V. 1990a. The genetic defect in Cockayne syndrome is associated with a defect in repair of UV-induced DNA damage in transcriptionally active DNA. *Proc Natl Acad Sci U S A* 87(12), pp. 4707-4711.

Venema, J. and van Hoffen, A. and Natarajan, A. T. and van Zeeland, A. A. and Mullenders, L. H. 1990b. The residual repair capacity of xeroderma pigmentosum complementation group C fibroblasts is highly specific for transcriptionally active DNA. *Nucleic Acids Res* 18(3), pp. 443-448.

Venema, J. and van Hoffen, A. and Karcagi, V. and Natarajan, A. T. and van Zeeland, A. A. and Mullenders, L. H. 1991. Xeroderma pigmentosum complementation group C cells remove pyrimidine dimers selectively from the transcribed strand of active genes. *Mol Cell Biol* 11(8), pp. 4128-4134.

Verhage, R. and Zeeman, A. M. and de Groot, N. and Gleig, F. and Bang, D. D. and van de Putte, P. and Brouwer, J. 1994. The RAD7 and RAD16 genes, which are essential for pyrimidine dimer removal from the silent mating type loci, are also required for repair of the nontranscribed strand of an active gene in *Saccharomyces cerevisiae*. *Mol Cell Biol* 14(9), pp. 6135-6142.

Verhage, R. A. and van Gool, A. J. and de Groot, N. and Hoeijmakers, J. H. and van de Putte, P. and Brouwer, J. 1996. Double mutants of *Saccharomyces cerevisiae* with alterations in global genome and transcription-coupled repair. *Mol Cell Biol* 16(2), pp. 496-502.

Verhage, R. A. and Heyn, J. and van de Putte, P. and Brouwer, J. 1997. Transcription elongation factor S-II is not required for transcription-coupled repair in yeast. *Mol Gen Genet* 254(3), pp. 284-290.

Vignali, M. and Hassan, A. H. and Neely, K. E. and Workman, J. L. 2000. ATP-dependent chromatin-remodeling complexes. *Mol Cell Biol* 20(6), pp. 1899-1910.

Vogelauer, M. and Wu, J. and Suka, N. and Grunstein, M. 2000. Global histone acetylation and deacetylation in yeast. *Nature* 408(6811), pp. 495-498.

Wade, P. A. and Pruss, D. and Wolffe, A. P. 1997. Histone acetylation: chromatin in action. *Trends Biochem Sci* 22(4), pp. 128-132.

Wang, H. and Zhai, L. and Xu, J. and Joo, H. Y. and Jackson, S. and Erdjument-Bromage, H. and Tempst, P. and Xiong, Y. and Zhang, Y. 2006a. Histone H3 and H4 ubiquitylation by the CUL4-DDB-ROC1 ubiquitin ligase facilitates cellular response to DNA damage. *Mol Cell* 22(3), pp. 383-394.

Wang, J. and Chin, M. Y. and Li, G. 2006b. The novel tumor suppressor p33ING2 enhances nucleotide excision repair via inducement of histone H4 acetylation and chromatin relaxation. *Cancer Res* 66(4), pp. 1906-1911.

Wang, Z. and Wu, X. and Friedberg, E. C. 1993. Nucleotide-excision repair of DNA in cell-free extracts of the yeast *Saccharomyces cerevisiae*. *Proc Natl Acad Sci U S A* 90(11), pp. 4907-4911.

Wang, Z. and Wei, S. and Reed, S. H. and Wu, X. and Svejstrup, J. Q. and Feaver, W. J. and Kornberg, R. D. and Friedberg, E. C. 1997. The RAD7, RAD16, and RAD23 genes of *Saccharomyces cerevisiae*: requirement for transcription-independent nucleotide excision repair *in vitro* and interactions between the gene products. *Mol Cell Biol* 17(2), pp. 635-643.

Wang, Z. and Zang, C. and Cui, K. and Schones, D. E. and Barski, A. and Peng, W. and Zhao, K. 2009. Genome-wide mapping of HATs and HDACs reveals distinct functions in active and inactive genes. *Cell* 138(5), pp. 1019-1031.

Wang, Z. G. and Wu, X. H. and Friedberg, E. C. 1991. Nucleotide excision repair of DNA by human cell extracts is suppressed in reconstituted nucleosomes. *J Biol Chem* 266(33), pp. 22472-22478.

Wasielewski, M. and Riaz, M. and Vermeulen, J. and van den Ouweland, A. and Labrijn-Marks, I. and Olmer, R. and van der Spaa, L. and Klijn, J. G. and Meijers-Heijboer, H. and Dooijes, D. and Schutte, M. 2009. Association of rare MSH6 variants with familial breast cancer. *Breast Cancer Res Treat.*

Waters, R. and Zhang, R. and Jones, N. J. 1993. Inducible removal of UV-induced pyrimidine dimers from transcriptionally active and inactive genes of *Saccharomyces cerevisiae*. *Mol Gen Genet* 239(1-2), pp. 28-32.

Waters, R. 2006. Maintaining genome integrity. *EMBO Rep* 7(4), pp. 377-381.

Watkins, J. F. and Sung, P. and Prakash, L. and Prakash, S. 1993. The *Saccharomyces cerevisiae* DNA repair gene RAD23 encodes a nuclear protein containing a ubiquitin-like domain required for biological function. *Mol Cell Biol* 13(12), pp. 7757-7765.

Watson, A. D. and Edmondson, D. G. and Bone, J. R. and Mukai, Y. and Yu, Y. and Du, W. and Stillman, D. J. and Roth, S. Y. 2000. Ssn6-Tup1 interacts with class I histone deacetylases required for repression. *Genes Dev* 14(21), pp. 2737-2744.

Watson, J. D. and Baker, T. A. and Bell, S. P. and Gann, A. and Levine, M. and Losick, R. 2004. *Molecular Biology of the Gene*. Fifth ed. San Francisco: Benjamin Cummings, Pearson. Cold Spring Harbour Laboratory Press.

Weber, S. 2005. Light-driven enzymatic catalysis of DNA repair: a review of recent biophysical studies on photolyase. *Biochim Biophys Acta* 1707(1), pp. 1-23.

Wellinger, R. E. and Thoma, F. 1997. Nucleosome structure and positioning modulate nucleotide excision repair in the non-transcribed strand of an active gene. *EMBO J* 16(16), pp. 5046-5056.

Williams, F. E. and Trumbly, R. J. 1990. Characterization of TUP1, a mediator of glucose repression in *Saccharomyces cerevisiae*. *Mol Cell Biol* 10(12), pp. 6500-6511.

Williams, F. E. and Varanasi, U. and Trumbly, R. J. 1991. The CYC8 and TUP1 proteins involved in glucose repression in *Saccharomyces cerevisiae* are associated in a protein complex. *Mol Cell Biol* 11(6), pp. 3307-3316.

Wood, R. D. and Robins, P. and Lindahl, T. 1988. Complementation of the xeroderma pigmentosum DNA repair defect in cell-free extracts. *Cell* 53(1), pp. 97-106.

Wu, J. and Grunstein, M. 2000. 25 years after the nucleosome model: chromatin modifications. *Trends Biochem Sci* 25(12), pp. 619-623.

Wu, J. and Suka, N. and Carlson, M. and Grunstein, M. 2001. TUP1 utilizes histone H3/H2B-specific HDA1 deacetylase to repress gene activity in yeast. *Mol Cell* 7(1), pp. 117-126.

Xiao, W. and Samson, L. 1992. The *Saccharomyces cerevisiae* MGT1 DNA repair methyltransferase gene: its promoter and entire coding sequence, regulation and in vivo biological functions. *Nucleic Acids Res* 20(14), pp. 3599-3606.

Yarosh, D. and Klein, J. and O'Connor, A. and Hawk, J. and Rafal, E. and Wolf, P. 2001. Effect of topically applied T4 endonuclease V in liposomes on skin cancer in xeroderma pigmentosum: a randomised study. Xeroderma Pigmentosum Study Group. *Lancet* 357(9260), pp. 926-929.

You, Z. and Feaver, W. J. and Friedberg, E. C. 1998. Yeast RNA polymerase II transcription in vitro is inhibited in the presence of nucleotide excision repair: complementation of inhibition by Holo-TFIIH and requirement for RAD26. *Mol Cell Biol* 18(5), pp. 2668-2676.

Yu, S. and Owen-Hughes, T. and Friedberg, E. C. and Waters, R. and Reed, S. H. 2004. The yeast Rad7/Rad16/Abf1 complex generates superhelical torsion in DNA that is required for nucleotide excision repair. *DNA Repair (Amst)* 3(3), pp. 277-287.

Yu, S. and Smirnova, J. B. and Friedberg, E. C. and Stillman, B. and Akiyama, M. and Owen-Hughes, T. and Waters, R. and Reed, S. H. 2008. ABF1 binding sites promote efficient global genome nucleotide excision repair. *J Biol Chem.*

Yu, Y. and Teng, Y. and Liu, H. and Reed, S. H. and Waters, R. 2005. UV irradiation stimulates histone acetylation and chromatin remodeling at a repressed yeast locus. *Proc Natl Acad Sci U S A* 102(24), pp. 8650-8655.

Yu, Y. and Waters, R. 2005. Histone acetylation, chromatin remodelling and nucleotide excision repair: hint from the study on MFA2 in *Saccharomyces cerevisiae*. *Cell Cycle* 4(8), pp. 1043-1045.

Yuan, G. C. and Liu, Y. J. and Dion, M. F. and Slack, M. D. and Wu, L. F. and Altschuler, S. J. and Rando, O. J. 2005. Genome-scale identification of nucleosome positions in *S. cerevisiae*. *Science* 309(5734), pp. 626-630.

Zakian, V. A. and Scott, J. F. 1982. Construction, Replication, and chromatin structure of TRP1 R1 circle, a multiple-copy synthetic plasmid derived from *Saccharomyces cerevisiae* chromosomal DNA. *Molecular and Cellular Biology* 2(3), pp. 221-232.

Zanton, S. J. and Pugh, B. F. 2006. Full and partial genome-wide assembly and disassembly of the yeast transcription machinery in response to heat shock. *Genes Dev* 20(16), pp. 2250-2265.

Zhang, H. and Roberts, D. N. and Cairns, B. R. 2005. Genome-wide dynamics of Htz1, a histone H2A variant that poises repressed/basal promoters for activation through histone loss. *Cell* 123(2), pp. 219-231.

Zhang, Z. and Varanasi, U. and Trumbly, R. J. 2002. Functional dissection of the global repressor Tup1 in yeast: dominant role of the C-terminal repression domain. *Genetics* 161(3), pp. 957-969.

Zhang, Z. and Reese, J. C. 2004a. Ssn6-Tup1 requires the ISW2 complex to position nucleosomes in *Saccharomyces cerevisiae*. *EMBO J* 23(11), pp. 2246-2257.

Zhang, Z. and Reese, J. C. 2004b. Redundant mechanisms are used by Ssn6-Tup1 in repressing chromosomal gene transcription in *Saccharomyces cerevisiae*. *J Biol Chem* 279(38), pp. 39240-39250.

Zhou, W. and Wang, X. and Rosenfeld, M. G. 2008. Histone H2A ubiquitination in transcriptional regulation and DNA damage repair. *Int J Biochem Cell Biol.*

Zhou, Z. and Elledge, S. J. 1992. Isolation of crt mutants constitutive for transcription of the DNA damage inducible gene RNR3 in *Saccharomyces cerevisiae*. *Genetics* 131(4), pp. 851-866.

Zhu, Q. and Wani, G. and Arab, H. H. and El-Mahdy, M. A. and Ray, A. and Wani, A. A. 2009. Chromatin restoration following nucleotide excision repair involves the incorporation of ubiquitinated H2A at damaged genomic sites. *DNA Repair (Amst)* 8(2), pp. 262-273.

Zitomer, R. S. and Lowry, C. V. 1992. Regulation of gene expression by oxygen in *Saccharomyces cerevisiae*. *Microbiol Rev* 56(1), pp. 1-11.

Appendix I

Growth media, solutions and buffers

1. Growth media

YPD (400 ml)
4 g Bacto Yeast Extract
8 g Bacto Peptone
8 g Glucose
Made up to 400 ml with H_2O.
YPD plates were obtained by supplementing this medium with 8 g Bacto-Agar.

LB (400 ml)
4g Bacto Tryptone Peptone
2 g Bacto Yeast Extract
2 g NaCl
Made up to 400 ml with H_2O.
LB plates were obtained by supplementing above medium with 6 g Bacto Agar.

MM (400 ml)
2.68 g Yeast Nitrogen Base w/o Amino Acids
8 g Glucose
Made up to 400 ml with H_2O.
For plates, supplemented with 2 % Bacto Agar.

Dosage of Amino Acids Added (According to demand):

Adenine	40 µg/ml	Tryptophan	40 µg/ml
Leucine	60 µg/ml	Lysine	40 µg/ml
Uracil	20 µg/ml	Histidine	40 µg/ml

2. Stock Solutions

0.5 M EDTA (pH 8.0)

$EDTA \cdot Na_2 \cdot 2H_2O$	186.1 g
H_2O	800 ml

Stir on a magnetic stirrer. Adjust the pH to 8.0 with NaOH (~ 22 g of NaOH pellets).
Add H_2O to make 1 litre and sterilize by autoclaving.

1 M Tris

Tris base	121.1 g
H_2O	800 ml

Adjust the pH to the desired value by adding concentrated HCl. Add H_2O to make 1 litre.

pH	HCl
7.6	~ 60 ml
8.0	~ 42 ml

10 ×TE Buffer (400 ml)

40 ml 1 M Tris-HCl, pH 7.5
8 ml 0.5M EDTA, pH 8.0
352 ml of H_2O

3 M Sodium acetate (pH 5.2) (400 ml)

Sodium acetate·$3H_2O$	163.24 g
H_2O	300 ml

Adjust the pH to 5.2 with acetic acid. Adjust the volume to 400 ml with H_2O. Filter to sterilize.

1 M Phosphate Buffer (1 L)

71 g Na_2HPO_4 or 89 g $Na_2HPO_4 \cdot 2\ H_2O$ or 134 g $Na_2HPO_4 \cdot 7\ H_2O$
4 ml 85 % H_3PO_4.
Add H_2O to make up 1 L.

5 M NaCl (400 ml)

Dissolve 116.9 g of NaCl in 350 ml of H_2O. Adjust the volume to 400 ml with H_2O. Sterilize by autoclaving.

10% SDS (Sodium dodecyl sulfate) (1 L)

Dissolve 100 g of SDS in 800 ml of distilled H_2O. Add distilled H_2O to make a total volume of 1 litre.

20% SDS (Sodium dodecyl sulfate) (500 ml)

Dissolve 100 g of SDS in 350 ml of distilled H_2O. Add distilled H_2O to make a total volume of 500 ml.

20×SSC (1 L)

NaCl	175.3 g
Sodium citrate dihydrate	88.2 g
H_2O	800 ml

Adjust the pH to 7.0. Make up the volume to 1 litre with H_2O.

PBS (1 L)

NaCl			8 g
KCl			0.2 g
Na_2HPO_4	1.44 g or	$Na_2HPO_4 \cdot 2H_2O$	1.8g
KH_2PO_4			0.24 g
H_2O			800 ml

Adjust the pH to 7.4 . Add H_2O to 1 litre. Sterilize by autoclaving.

Sorbitol TE (1L) (Kept in cold room)

Sorbitol	165g
Tris·HCl (pH 8.0)	100 ml
EDTA	200 ml

Add 500 ml H_2O to dissolve the sorbitol completely. Adjust the final volume to 1 L.

DNA Lysis Buffer (1 L)

Urea	240 g
NaCl	11.69 g
CDTA	5 g
SDS	5 g
1 M Tris-HCl (pH 8.0)	100 ml

Add 700 ml of H_2O to dissolve the chemicals, and then adjust the final volume to 1 L with H_2O.

RNA lysis buffer

Tris-HCl (pH 7.5)	10mM
EDTA (pH 8.0)	10mM
SDS	0.5%

10 N NaOH (400 ml)

Add 160 g of NaOH pellets to 350 ml of H_2O, stirring until the pellets have completely dissolved, adjust the final volume to 400 ml. (Sterilization is not required)

1M DTT (Dithiothreitol)

DTT	3.09g

Dissolved in 20ml of 0.01M sodium acetate (pH 5.2)
Sterilise by filtration. Do not autoclave DTT or solutions containing DTT.

3. Solutions for electrophoresis

50× TAE (Tris-acetate, 1 litre)

Tris base	242 g
Sodium Acetate·$3H_2O$	136 g
0.5 M EDTA	200ml

Adjust to pH7.2 with acetic acid. Add H_2O to make 1 litre.

10× TBE (1 L)

Tris base	108 g
Boric acid	~55 g
EDTA	8.3 g

Add H_2O to 1 litre.

Denaturing Running Buffer

NaOH	36mM
EDTA	1mM

Non-denaturing loading Buffer (10ml)

Ficoll	10%	1g
SDS	0.5%	0.5ml of 10% solution
Bromophenol Blue	0.06%	6mg

Made up in 1 x TAE

Denaturing loading buffer (10ml)

NaOH	50mM	166ul of 3M stock
EDTA	1mM	20ul of 0.5M stock
Ficoll	2.5%	0.25g
Bromophenol Blue	0.025%	2.5mg

Sequencing gel loading buffer

Deionised formamide	95%
EDTA (pH 8.0)	20mM
Xylene cyanol FF	0.05%
Bromophenol Blue	0.05%

Fixative solution for sequencing gel

Methanol (15%)	600ml
Acetic acid (5%)	200ml

Add H2O to make 4 litres.

4. Solutions for Southern and Northern Blotting

10× FA gel buffer (Using RNase free H_2O) (500 ml)

3-[N-Morpholino]propanesulfonic acid (MOPS) (free acid)	20.9 g
3 M Sodium acetete	8.2 ml
0.5 M EDTA	10 ml

Adjust pH to 7.0 with NaOH.

1 x FA gel running buffer

10 x FA gel buffer	100ml
37% (12.3) Formaldehyde	20ml
RNase-free water	880ml

5 x RNA loading buffer	10ml
Saturated aqueous bromophenol blue	16ul
0.5M EDTA, pH 8.0	80ul
37% (12.3) formaldehyde	720ul
Formamide	3ml
10 x FA gel buffer	4ml

Add RNase-free water to 10ml.

Hybridisation Solution (10ml)	
SDS (1%)	1ml (10%)
Dextran sulphate (10%)	1g
NaCl (1M)	0.58g

Add H2O to 10ml. Heat to 65oC for 10 mins before adding NaCl and heating again to 65oC before use.

Probe Stripping solution	
SSC (20 x)	2.5ml
SDS (10%)	50ml
H2O	to 500ml

2 x Dynabead Washing and Binding Buffer (2 x BW)	
NaCl	2M
Tris-HCl (pH 8.0)	10mM
EDTA	1mM

5. Solutions for Transformation

Each solution needs to be filter sterilised

Solution A	10ml
10 x LiAc (10mM)	1ml
10 x TE buffer (10, 1mM)	1ml
H2O	8ml

Solution B	10ml
10 x LiAc (10mM)	1ml
10 x TE buffer (10, 1mM)	1ml
PEG 50% (40%)	8ml

Appendix II

Data from experiments presented in Chapter 3

A.II.1 Southern blotting data

The data represent the band intensities obtained using ImageQuant software, and the average ratios between *MFA2*^{TAM} and g*MFA2* which provides an average copy number estimation.

Strain	*MFA2*^{TAM}	g*MFA2*	Ratio
WTa	0.0	49249835.7	0.0
	0.0	8559619.3	0.0
Average			**0.0**
Standard deviation			0.0
WTa TAM	304387645.9	10617149.8	28.7
	49494237.6	2034778.9	24.3
	87029640.3	3399059.1	25.6
Average			**26.2**
Standard deviation			2.2
WTα TAM	146086508.8	4240615.8	34.4
	36618517.3	1503769.8	24.4
	42433160.1	594276.4	
Average			**29.4**
Standard deviation			7.1

Statistical analysis: Students t-test assuming equal variances (alpha value = 0.01).

	WT a TAM	WTα TAM
Mean	26.19920183	29.40025382
Variance	4.986062276	50.98698863
Observations	3	2
Pooled Variance	20.3197044	
Hypothesized Mean Difference	0	
df	3	
t Stat	-0.777901587	
P(T<=t) one-tail	0.246670309	
t Critical one-tail	4.540702858	
P(T<=t) two-tail	0.493340619	
t Critical two-tail	5.840909309	

A.II.2 Northern blotting

The data represent the relative band intensities quantified using ImageQuant software. Using *ACT1* as an internal control, relative *MFA2* mRNA levels were obtained. These figures were then normalised against mRNA levels in WTa cells to provide an average mRNA level.

Strain	*ACT1*	*MFA2*
WTa	2664257	3083012
	161929.4	115161
	26352799	40949631
WTa TAM	4074131	3.56E+08
	372555.7	21251.35
	57246695	1.08E+09
WTα TAM	8123853	3757399
	358809.2	599904
	70356755	

	WTa	WTa TAM	WTα TAM
	1.000	75.438	0.400
	1.000	12.166	0.000
	1.000	51.659	0.080
AVERAGE	1.000	46.421	0.160
ST DEV	0.000	31.960	0.211

A.II.3 Cell survival following UV treatment

PSY316 (wild type), 200 cells/100µl dilution

UV dose (J/m2)	0	10	30	50	100
WTα	281	271	122	99	14
	269	255	161	122	17
	268	228	159	92	15
Average	272.67	251.33	147.33	104.33	15.33
Standard deviation	7.23	21.73	21.96	15.70	1.53
% Survival	**100**	**92.17604**	**54.03423**	**38.26406**	**5.623472**
WTα TAM	609	577	484	364	69
	570	590	522	422	56
	588	552	494	394	112
Average	589.00	573.00	500.00	393.33	79.00
Standard deviation	19.52	19.31	19.70	29.01	29.31
% Survival	**100**	**97.28353**	**84.88964**	**66.77985**	**13.41256**
WTα TAM	341	210	195	136	20
	233	202	170	159	23
	410	173	243	58	26
	846	785	631	291	107
	720	776	607	417	104
	826	819	571	360	99
Average	562.67	494.17	402.83	236.83	63.17
Standard deviation	266.65	328.27	221.35	140.55	44.12
% Survival	**100**	**79.47477**	**68.70785**	**40.26141**	**9.986031**
Rad14α	342	0	0	0	0
	336	0	0	0	0
	343	0	0	0	0
Average	340.33	0.00	0.00	0.00	0.00
Standard deviation	3.79	0.00	0.00	0.00	0.00
% Survival	**100**	**0**	**0**	**0**	**0**

A.II.4 TAM species

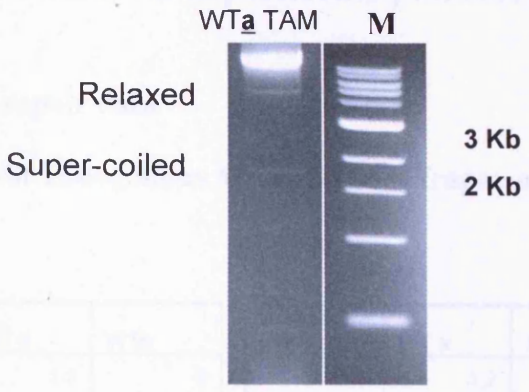

A crude genomic prep of a TAM-containing strain allows visualisation of the different plasmid species. The highly concentrated high molecular weight band represents total genomic DNA. M = NEB 1Kb marker.

Appendix III

Data from experiments presented in Chapter 4

A.III.1 CPD repair data

CPD repair for endogenous *MFA2*, *Hae*III fragment (Lui, 2005).

TS

Nucleotide position	WT a	WTα
2	1.5	6
-16	1.5	3.5
-37	0.95	2.2
-48	1.6	1.8
-108	2.45	3.1
-119	2.15	3
-133	3.1	4.55
-155	2.2	2.8
-164	1.8	2.35
-174	2.1	2.7
-193	2.5	3
-198	2.6	2.65
-205	2.35	2.5
-215	2.95	3.8
-231	3.4	3.8
-255	4.3	3.8
-262	3.5	5.9
-293	2.7	2.35
-309	1.8	1.5
-316	3.1	3.05
-320	2.8	3
-346	2.1	2.2
-358	2.8	2.6
-362	2.4	2.85
-382	2.1	2.1
-431	2.8	2.85

NTS

Nucleotide position	WT a	WTα
-369	3.2	3.4
-330	2.65	3.7
-308	3.2	3.85
-275	3.1	2.8
-264	2.3	2.85
-240	3.9	3.45
-140	1.95	4.4
-137	1.6	3.65
-129	2.55	3.95
-98	2	3.4
-93	2.25	3.4
-88	2.45	3.5
-82	1.9	2.75
-72	2.45	3.15
-68	2.75	3
-60	2.65	2.3
-54	3.65	2.9
-51	1.85	1.25
-25	3.95	2.1

A.III.1.1 WTaTAM TS
i) Band density values (peak areas)

CPD	Expt 1					CPD	Expt 2				
Position	0	0.5	1	2	4	Position	0	0.5	1	2	4
Top bands	1570676	1611857	1719048	1784598	2021774	Top bands	12094156	13565954	16214443	15234725	13620983
1	10360	12509	9403	5316	4096	1	41259	40748	50226	28874	12898
-20	10201	9536	10136	6752	5006	-20	50881	61289	65018	40133	11285
-48	28969	22154	18604	10627	6533	-48	111755	99916	125516	62001	18963
-108	34935	37552	35957	30229	30564	-108	178334	213306	222053	223828	116717
-119	18926	19925	19614	16878	19260	-119	108879	124279	113808	109101	73641
-132	10099	11161	10968	10312	14678	-132	46726	47079	57475	127931	51992
-155	121456	131234	125669	116089	113942	-155	495395	542959	666610	682244	439973
-164	17536	18341	17282	11281	8446	-164	59156	48343	52780	43584	17150
-175	159169	166975	153798	124186	108603	-175	588421	647713	817506	593711	331491
-192	30787	32228	34064	24632	17949	-192	135801	153028	172486	152011	63383
-198	14951	13073	12847	8898	7152	-198	34398	36872	39344	28739	10766
-204	50891	50847	42635	23353	15812	-204	191039	201993	201294	105566	33757
-215	16616	18354	15975	11257	8817	-215	79159	88651	104488	74319	24022
-232	35008	39885	43223	33365	33906	-232	154002	192822	239455	209099	109828
-256	77662	88711	92594	73316	73340	-256	355203	454115	549551	485028	258955
-262	17753	18197	16079	13603	17186	-262	60999	70137	87696	85439	42529
-274	11364	16443	16192	11644	11791	-274	59207	67884	83719	72238	42237
-280	18837	21578	22243	14587	10617	-280	75574	90340	110799	91720	39501
-293	18963	18939	14753	9633	7133	-293	54633	56612	77541	46629	15438
-311	10892	12394	10748	5851	4230	-311	30663	36603	41499	35084	10158
-316	11744	12553	12526	7460	5331	-316	51051	69205	93040	62810	18971
-320	25002	30359	29944	20546	15179	-320	120540	150236	164978	148180	49820
-345	33260	35064	35032	22413	19648	-345	154181	193083	226187	193622	90711
-352	15996	16859	18248	13253	11781	-352	61354	66218	71934	60374	35962
-358	62007	71382	74004	59598	50705	-358	76638	98210	114864	86687	50307
-362	39138	42956	41602	29295	30505	-362	56960	79130	87416	66718	50071
-382	18669	16634	17367	9915	8484	-382	96078	134863	178380	122006	48266
-390	26578	30494	29970	18067	15370	-390	185206	237186	299468	249100	104656
-397	19637	20941	21237	14831	13480	-397	105744	137165	181353	153697	63086
-402	7588	9138	6634	3864	3198	-402	45932	52621	53545	23476	13095
Total	2545671	2658273	2728393	2545649	2714518	Total	15959322	18058563	21564472	19698672	15870612
Ratio	1.00	1.04	1.07	1.00	1.07	Ratio	1.00	1.13	1.35	1.23	0.99

ii) Adjusted band density values

CPD	Expt 1					CPD	Expt 2				
Position	0	0.5	1	2	4	Position	0	0.5	1	2	4
1	10360	11979	8773	5316	3841	1	41259	36012	37171	23393	12970
-20	10201	9132	9457	6752	4695	-20	50881	54164	48118	32515	11348
-48	28969	21215	17358	10628	6126	-48	111755	88302	92891	50232	19069
-108	34935	35961	33549	30229	28663	-108	178334	188510	164336	181339	117369
-119	18926	19081	18301	16879	18062	-119	108879	109832	84226	88390	74053
-132	10099	10688	10233	10312	13765	-132	46726	41606	42536	103646	52282
-155	121456	125675	117253	116090	106854	-155	495395	479842	493341	552735	442433
-164	17536	17564	16125	11281	7921	-164	59156	42724	39061	35311	17246
-175	159169	159902	143498	124188	101847	-175	588421	572419	605016	481008	333343
-192	30787	30863	31783	24632	16833	-192	135801	135239	127652	123155	63737
-198	14951	12519	11987	8898	6707	-198	34398	32586	29118	23283	10826
-204	50891	48693	39780	23353	14829	-204	191039	178512	148973	85527	33946
-215	16616	17576	14905	11257	8268	-215	79159	78346	77329	60211	24156
-232	35008	38195	40328	33366	31797	-232	154002	170408	177215	169407	110442
-256	77662	84953	86393	73317	68778	-256	355203	401326	406709	392957	260403
-262	17753	17426	15002	13603	16117	-262	60999	61984	64901	69221	42767
-274	11364	15746	15108	11644	11058	-274	59207	59993	61959	58525	42473
-280	18837	20664	20753	14587	9956	-280	75574	79839	81999	74309	39722
-293	18963	18137	13765	9633	6690	-293	54633	50031	57386	37777	15524
-311	10892	11869	10028	5851	3967	-311	30663	32348	30712	28424	10215
-316	11744	12021	11687	7460	4999	-316	51051	61160	68856	50887	19077
-320	25002	29073	27939	20546	14235	-320	120540	132771	122096	120051	50099
-345	33260	33578	32686	22413	18426	-345	154181	170638	167395	156867	91218
-352	15996	16145	17026	13253	11048	-352	61354	58520	53237	48913	36163
-358	62007	68359	69048	59598	47552	-358	76638	86794	85008	70231	50588
-362	39138	41136	38815	29295	28607	-362	56960	69932	64694	54053	50351
-382	18669	15929	16204	9915	7956	-382	96078	119186	132014	98846	48536
-390	26578	29202	27963	18067	14414	-390	185206	209614	221629	201814	105241
-397	19637	20054	19814	14831	12642	-397	105744	121220	134215	124521	63439
-402	7588	8751	6189	3864	3000	-402	45932	46504	39628	19019	13168

iii) Signal remaining (%)

CPD	Expt 1						CPD	Expt 2					
Position	0	0.5	1	2	4	t50%	Position	0	0.5	1	2	4	t50%
1	100	116	85	51	37	3	1	100	87	90	57	31	2.8
-20	100	90	93	66	46	3.6	-20	100	106	95	64	22	2.75
-48	100	73	60	37	21	2	-48	100	79	83	45	17	2.15
-108	100	103	96	87	82	6	-108	100	106	92	102	66	6
-119	100	101	97	89	95	6	-119	100	101	77	81	68	6
-132	100	106	101	102	136	6	-132	100	89	91	222	112	6
-155	100	103	97	96	88	6	-155	100	97	100	112	89	6
-164	100	100	92	64	45	3.5	-164	100	72	66	60	29	2.5
-175	100	100	90	78	64	5.4	-175	100	97	103	82	57	4.75
-192	100	100	103	80	55	4.5	-192	100	100	94	91	47	4.2
-198	100	84	80	60	45	3.3	-198	100	95	85	68	31	3
-204	100	96	78	46	29	2.6	-204	100	93	78	45	18	2.2
-215	100	106	90	68	50	3.8	-215	100	99	98	76	31	3.15
-232	100	109	115	95	91	6	-232	100	111	115	110	72	6
-256	100	109	111	94	89	6	-256	100	113	115	111	73	6
-262	100	98	85	77	91	6	-262	100	102	106	113	70	6
-274	100	139	133	102	97	6	-274	100	101	105	99	72	6
-280	100	110	110	77	53	4.3	-280	100	106	109	98	53	4.8
-293	100	96	73	51	35	2.8	-293	100	92	105	69	28	3
-311	100	109	92	54	36	3	-311	100	105	100	93	33	3.5
-316	100	102	100	64	43	3.4	-316	100	120	135	100	37	4
-320	100	116	112	82	57	4.6	-320	100	110	101	100	42	4
-345	100	101	98	67	55	4.2	-345	100	111	109	102	59	5.4
-352	100	101	106	83	69	6	-352	100	95	87	80	59	4.8
-358	100	110	111	96	77	6	-358	100	113	111	92	66	5.8
-362	100	105	99	75	73	6	-362	100	123	114	95	88	6
-382	100	85	87	53	43	3.1	-382	100	124	137	103	51	4.75
-390	100	110	105	68	54	4.1	-390	100	113	120	109	57	5.4
-397	100	102	101	76	64	5.2	-397	100	115	127	118	60	6
-402	100	115	82	51	40	3	-402	100	101	86	41	29	2.5
Average	100	103	96	73	62	4.513	Average	100	103	101	91	52	4.515

A.III.1.2 WTa TAM NTS
i) Band density values (peak area)

CPD Position	Expt 1					CPD position	Expt 2				
	0	0.5	1	2	4		0	0.5	1	2	4
Top bands	3544601	4857900	4888144	5715384	4944354		1490303	1614475	1621002	1729515	2198442
-430	167664.4	248023.6	279664.7	233853.2	65702.58	-430	126328.1	138001.9	94442.73	67826.59	40181.17
-408	9440.544	21715.31	18457.85	8900.845	1893.187	-408	8160.448	8987.131	5281.462	2516.884	1716.134
-371	73194.75	112850.8	119116.6	105981.1	38669.35	-371	57465.12	54349.51	48274.01	40164.14	25897.81
-330	13872.54	25000.26	21643.76	22209.43	9224.767	-330	11705.77	12044.29	8012.024	7480.129	5583.089
-317	17459.44	26595.77	27897.42	25739.84	11013.55	-317	9549.837	10343.63	7097.687	7259.835	5582.484
-297	149190.8	223918.7	236748	212665.4	86778.1	-297	82782.26	97709.84	72253.47	57568.07	46014.27
-275	7103.339	10475.76	9379.095	11238.72	2846.209	-275	5142.866	4109.536	2433.878	1063.845	1323.558
-266	59477.59	79863.91	57068.35	58489.35	7986.91	-266	44201.22	46435.94	30182.71	18361.41	12382.25
-244	20511.49	31938.28	34797.7	38663.29	20126.41	-244	10851.93	9059.898	9264.245	7917.449	9035.813
-240	10965.09	20816.01	20770.22	18573.47	5419.744	-240	7697.261	7112.392	4249.685	3370.649	2234.258
-227	6949.156	10672.33	10221.96	7943.729	3040.754	-227	4910.122	5138.174	3567.089	2011.278	1558.865
-145	26218.46	38162.9	36090.4	26056.56	8840.82	-145	15400.34	14147.88	10346.97	6240.614	3917.081
-128	49003.48	70040.33	74650.94	72120.06	29982.16	-128	28807.88	30604.19	23618.27	20170.3	16121.8
-114	18360.88	27227.61	28031.44	25966.64	9678.626	-114	11270.98	13298.9	9577.711	8507.587	6302.21
-102	69754.59	93517.99	88573.12	76520.48	25802.5	-102	31057.94	31198.57	22439.61	16180.46	11134.29
-98	19837.19	28229.72	24317.06	22336.71	8738.887	-98	12096.73	11515.39	7641.105	6801.558	5288.476
-93	4768.524	7011.367	5070.128	5237.21	1286.993	-93	1330.391	1690.537	1092.721	398.697	480.416
-88	6411.231	10147.78	7198.241	6935.008	1995.722	-88	4225.994	4136.903	2662.171	1902.055	1245.073
-83	25751.76	32532.62	28196.62	20612.14	6735.436	-83	16505.38	14516.88	8712.813	6689.883	5083.688
-71	26913.53	37952.59	33040.08	22804.2	5709.195	-71	25278.26	25609.76	16994.15	10877.18	6805.698
-64	23177.58	42321.63	41258.79	32534.4	8343.743	-64	22736.24	21498.82	14817.39	9280.724	6749.719
-42	3833.946	5474.183	4631.465	3358.911	1604.946	-42	3056.362	3504.342	2366.184	1049.415	1063.601
-27	51191.86	71136.15	63062.07	31745.46	12662.89	-27	13589.65	12941.86	8459.691	5337.951	3499.702
-8	3866.277	5616.299	5089.239	3631.267	1381.156	-8	2883.837	2795.915	2131.844	1100.864	833.42
-4	46323.31	56930.23	42857.75	36204.41	14696.61	-4	15096.61	15850.98	11267.57	8495.962	5888.396
7	6592.331	10684.97	11428.56	8611.841	2423.099	7	1973.381	2071.572	1492.683	1811.362	1625.659
10	3510.653	6068.015	6519.26	5400.723	1590.701	10	2907.086	2685.976	2310.701	1999.719	2000.252
20	75504.4	104640.9	112489.9	102073.5	37813.49	20	27631.87	32229.76	22698.96	18765.32	14852.99
Total	4541451	6317466	6336414	6961792	5376343	Total	2094947	2248065	2074692	2070665	2442844
Ratio	1	1.391068	1.39524	1.532945	1.183838	Ratio	1	1.073089	0.990331	0.988409	1.166065

ii) Adjusted band density values

CPD Position	Expt 1					CPD position	Expt 2				
	0	0.5	1	2	4		0	0.5	1	2	4
-430	167664.4	178297.2	200442	152551.6	55499.62	-430	126328.1	128602.5	95364.77	68621.98	34458.78
-408	9440.544	15610.53	13229.16	5806.371	1599.194	-408	8160.448	8375.007	5333.025	2546.395	1471.731
-371	73194.75	81125.34	85373.56	69135.63	32664.39	-371	57465.12	50647.69	48745.31	40635.14	22209.58
-330	13872.54	17971.99	15512.57	14488.08	7792.253	-330	11705.77	11223.93	8090.245	7567.838	4787.975
-317	17459.44	19118.96	19994.71	16791.11	9303.252	-317	9549.837	9639.117	7166.982	7344.972	4787.456
-297	149190.8	160968.9	169682.6	138730	73302.33	-297	82782.26	91054.71	72958.88	58243.16	39461.16
-275	7103.339	7530.729	6722.208	7331.457	2404.221	-275	5142.866	3829.631	2457.641	1076.326	1135.064
-266	59477.59	57411.94	40902.17	38154.97	6746.623	-266	44201.22	43273.14	30477.37	18576.73	10618.84
-244	20511.49	22959.54	24940.29	25221.58	17000.98	-244	10851.93	8442.818	9354.695	8010.296	7748.982
-240	10965.09	14964.05	14886.48	12116.21	4578.112	-240	7697.261	6627.959	4291.175	3410.176	1916.067
-227	6949.156	7672.039	7326.309	5182.007	2568.555	-227	4910.122	4788.209	3601.918	2034.867	1336.867
-145	26218.46	27434.25	25866.82	16997.72	7467.929	-145	15400.34	13184.25	10447.97	6313.797	3359.231
-128	49003.48	50350.04	53504.01	47046.75	25326.23	-128	28807.88	28519.76	23848.86	20406.83	13825.82
-114	18360.88	19573.17	20090.76	16939.06	8175.632	-114	11270.98	12393.11	9671.218	8607.358	5404.683
-102	69754.59	67227.48	63482.36	49917.31	21795.63	-102	31057.94	29073.66	22658.68	16370.21	9548.603
-98	19837.19	20293.56	17428.56	14571.11	7381.825	-98	12096.73	10731.06	7715.705	6881.319	4535.319
-93	4768.524	5040.277	3633.875	3416.438	1087.136	-93	1330.391	1575.393	1103.389	403.3724	411.9977
-88	6411.231	7294.955	5159.141	4523.978	1685.806	-88	4225.994	3855.134	2688.161	1924.366	1067.756
-83	25751.76	23386.79	20209.15	13446.11	5689.49	-83	16505.38	13528.12	8797.877	6768.338	4359.696
-71	26913.53	27283.06	23680.57	14876.08	4822.614	-71	25278.26	23865.45	17160.07	11004.73	5836.467
-64	23177.58	30423.84	29571.17	21223.47	7048.043	-64	22736.24	20034.51	14962.07	9389.557	5788.467
-42	3833.946	3935.238	3319.478	2191.158	1355.714	-42	3056.362	3265.657	2389.287	1061.726	912.1286
-27	51191.86	51137.88	45198.1	20708.81	10696.47	-27	13589.65	12060.38	8542.287	5400.548	3001.293
-8	3866.277	4037.401	3647.572	2368.818	1166.676	-8	2883.837	2605.482	2152.653	1113.778	714.7287
-4	46323.31	40925.56	30717.16	23617.56	12414.38	-4	15096.61	14771.36	11377.58	8595.597	5049.807
7	6592.331	7681.127	8191.107	5617.846	2046.816	7	1973.381	1930.475	1507.256	1832.607	1394.147
10	3510.653	4362.127	4672.54	3523.104	1343.681	10	2907.086	2503.031	2333.269	2023.169	1715.387
20	75504.4	75223.45	80624.05	66586.55	31941.44	20	27631.87	30034.55	22920.57	18985.37	12737.71

iii) Signal remaining (%)

CPD Position	Expt 1					t50%	CPD position	Expt 2					t50%
	0	0.5	1	2	4			0	0.5	1	2	4	
	10	106.34	119.54	90.986	33.101			10	101.80	75.489	54.320	27.277	
-430	0	18	95	31	62	3.6	-430	0	04	77	45	22	2.6
	10	165.35	140.13	61.504	16.939			10	102.62	65.352	31.204	18.034	
-408	0	63	13	62	64	3	-408	0	93	11	11	93	2.1
	10	110.83	116.63	94.454	44.626			10	88.136	84.825	70.712	38.648	
-371	0	49	89	36	69	4.1	-371	0	4	9	7	8	3.3
	10	129.55	111.82	104.43	56.170			10	95.883	69.113	64.650	40.902	
-330	0	08	21	72	35	5	-330	0	8	32	5	7	3.2
	10	109.50	114.52	96.172	53.284			10	100.93	75.048	76.911	50.131	
-317	0	5	09	1	94	4.7	-317	0	49	21	99	29	4
	10	107.89	113.73	92.988	49.133			10	109.99	88.133	70.357	47.668	
-297	0	46	53	31	27	4.5	-297	0	3	48	06	62	3.7
	10	106.01	94.634	103.21	33.846			10	74.464	47.787	20.928	22.070	
-275	0	68	48	14	35	3.75	-275	0	91	36	42	65	1.7
	10	96.527	68.769	64.150	11.343			10	97.900	68.951	42.027	24.023	
-266	0	02	04	05	13	2.3	-266	0	32	42	64	86	2.4
	10	111.93	121.59	122.96	82.885			10	77.800	86.203	73.814	71.406	
-244	0	5	18	32	14	6	-244	0	14	01	47	47	6
	10	136.46	135.76	110.49	41.751			10	86.108	55.749	44.303	24.892	
-240	0	99	25	8	69	4.3	-240	0	02	37	76	84	2.2
	10	110.40	105.42	74.570	36.962			10	97.517	73.356	41.442	27.226	
-227	0	25	73	3	12	3.4	-227	0	07	92	23	61	2.4
	10	104.63	98.658	64.831	28.483			10	85.610	67.842	40.997	21.812	
-145	0	72	74	12	48	3	-145	0	15	55	78	71	2.2
	10	102.74	109.18	96.006	51.682			10	98.999	82.785	70.837	47.993	
-128	0	79	41	95	52	4.7	-128	0	66	89	68	2	2.8
	10	106.60	109.42	92.256	44.527			10	109.95	85.806	76.367	47.952	
-114	0	26	16	24	45	4.1	-114	0	58	37	4	2	3.9
	10	96.377	91.008	71.561	31.246			10	93.610	72.956	52.708	30.744	
-102	0	14	12	33	15	3.1	-102	0	83	17	61	48	2.6
	10	102.30	87.858	73.453	37.212			10	88.710	63.783	56.885	37.492	
-98	0	06	13	5	05	3.3	-98	0	45	42	79	12	2.8
	10	105.69	76.205	71.645	22.798			10	118.41	82.937	30.319	30.968	
-93	0	89	44	6	16	2.8	-93	0	58	21	84	17	2.6
	10	113.78	80.470	70.563	26.294			10	91.224	63.610	45.536	25.266	
-88	0	4	37	33	58	2.9	-88	0	31	16	27	39	2.4
	10	90.816	78.476	52.214	22.093			10	81.961	53.303	41.006	26.413	
-83	0	3	78	35	6	2.4	-83	0	87	06	83	78	2.1
	10	101.37	87.987	55.273	17.918			10	94.410	67.884	43.534	23.088	
-71	0	3	6	61	92	2.5	-71	0	98	68	37	88	2.3
	10	131.26	127.58	91.568	30.408			10	88.117	65.807	41.297	25.459	
-64	0	41	49	95	88	3.6	-64	0	1	06	77	18	2.3
	10	102.64	86.581	57.151	35.360			10	106.84	78.174	34.738	29.843	
-42	0	2	16	29	8	3	-42	0	79	15	07	6	2.5
	10	99.894	88.291	40.453	20.894			10	88.746	62.858	39.740	22.085	
-27	0	41	4	33	86	2.4	-27	0	8	75	16	14	2.1
	10	104.42	94.343	61.268	30.175			10	90.347	74.645	38.621	24.783	
-8	0	61	26	71	7	2.9	-8	0	76	45	24	95	2.3
	10	88.347	66.310	50.984	26.799			10	97.845	75.365	56.937	33.449	
-4	0	66	27	17	42	2.4	-4	0	54	14	26	92	2.9
	10	116.51	124.25	85.217	31.048			10	97.825	76.379	92.866	70.647	
7	0	61	21	84	44	3.5	7	0	75	37	18	34	6
	10	124.25	133.09	100.35	38.274			10	86.101	80.261	69.594	59.007	
10	0	4	49	47	39	4	10	0	03	14	41	08	4.7
	10	99.627	106.78	88.188	42.304			10	108.69	82.949	68.708	46.097	
20	0	91	06	97	08	3.9	20	0	53	74	25	88	3.6
	10	110.07	103.18	79.961	35.627	3.5410		10	95.021	72.405	53.263	35.549	2.9892
Average	0	66	19	78	44	71	Average	0	26	76	26	64	86

A.III.1.3 WTα TAM TS

i) Band density values (peak areas)

CPD Position	Expt 1 0	0.5	1	2	4	CPD Position	Expt 2 0	0.5	1	2	4
Top bands	211382 65	181020 20	262721 22	198612 27	330396 75	Top bands	197868 6	197808 7	217540 0	228523 2	208550 2
1	71621.2 9	35557.7 5	80272.5 4	17809.2 8	24614.7 7	1	13691.0 1	15697.8 2	7190.31 6	5847.40 2	1684.05 4
-20	82797.6 5	55089.8 4	96173.7 1	27575.2 2	26559	-20	19568.3 1	21928.6 9	15626.4 7	5645.65 2	3495.40 1
-48	226062. 8	143438. 7	160571. 4	68235.2 3	21432.1 1	-48	47084.8 1	45438.7 3	33442.7 4	9545.63 8	6212.72 1
-108	344560. 2	321607. 4	509084. 7	270626. 1	233335. 8	-108	76939.4 1	102098. 5	107023	76262.8 7	47037.3
-119	154539	139934. 4	207782. 7	72092.4 5	52799.6 6	-119	39045.3 3	48925.0 4	45937.3 1	29581.9 1	13156.7 8
-132	81669.6	72687.6 8	116516. 9	60547.7 9	48676.3 7	-132	16087.0 3	20573.4 6	23863.5	19172.1 2	9134.32 6
-155	709754	495044. 4	931271. 1	413651. 8	314256. 8	-155	154973. 6	191069. 4	215049. 2	141219. 5	62144.1
-164	73851.3 3	52386.7 5	89755.4 7	15771.1 3	12946.9 8	-164	20080.0 7	18850.4 1	24131.8	6950.42 5	3326.15 5
-175	846978. 4	680683. 6	105399 2	413553. 4	310369. 2	-175	189359. 7	213370. 4	223643. 5	126159. 5	66648.6 2
-192	130274. 2	142241. 3	221009. 9	81354.9 6	54217.3	-192	29874.7 2	40495.3 7	40389.2 5	27361.4	13650.9 9
-198	103009. 4	107386. 1	174582. 7	63843.7 5	50170.3 2	-198	29403.6 4	41386.1 1	43410.7 6	29092.3 2	15429.0 6
-204	271761. 7	221574. 7	279043	57245.0 8	44418.2 3	-204	64111.1 6	79983.9 8	69907.7 1	32359.1 7	15736.3 7
-215	143780. 7	152430. 7	230104. 9	99306.9 6	65860.5 4	-215	30817.3 5	41479.5 2	43257.8 8	27495.1 9	13570.2 6
-232	387694. 6	312863. 5	517335. 3	280290. 5	296705. 9	-232	76169.2 7	106256. 5	102463	79681.9 9	56923.1
-256	823152	712007. 3	108793 4	551793. 1	471236. 9	-256	151046. 2	211288. 1	215864	147858. 8	86348.3 2
-262	92799.3 7	68143.0 7	93864.6 9	34028.6	39010.9 6	-262	22530.8 3	27174.8 6	26024.1 9	16631.5 5	9764.03 9
-274	165904. 4	111539. 1	185706. 9	80812.1 3	78545.0 8	-274	22638.2 4	33715.1 8	28017.8 5	26416.9 5	13951.9
-280	241913. 1	176218	270657. 8	95820.8 8	73325.2	-280	41896.5 7	55382.0 4	53722.8 2	25716.3	12319.1 4
-293	171802. 6	111105. 2	163920. 1	58670.2 7	43049.7 6	-293	40349.1 3	47219.2 5	42047.9 3	23772.9 1	11092.5 1
-311	76402.8 5	67522.6 1	99736.1 3	31244.0 1	23059.1 8	-311	18198.2 2	22807.6 6	21269.1 6	9491.09 1	4618.70 1
-316	116724	104703. 2	141189	48427.0 9	39691.9 9	-316	19471.6 8	25925.6 2	25961.4 2	13321.3 3	6880.5
-320	150397. 3	117687. 1	194002. 3	75693.0 9	49159.4 7	-320	26689.4 3	35920.5 5	35644.6	20270.8 4	6561.31 9
-345	383849. 9	292457. 2	376752. 7	129493. 9	106093. 3	-345	53162.1 4	65301.9 9	60357.4 5	28418.1 3	11980.4 7
-352	163385. 4	152423. 6	204510. 4	83943.4 5	75148.9 6	-352	41053.0 4	48174.5 8	45794.1 8	27097.8 6	10840.9 1
-358	85507.2 1	152071. 1	131056. 3	63597.2 1	70700.8	-358	70792.0 5	79423.3 2	81796.2 6	51584.5 3	26175.6 9
-362	106131. 8	100615. 4	139708. 3	59573.4	49577.5 6	-362	49924.9 5	73992.9 9	71352.3 8	37764.3 5	17610.4 5
-382	265687. 3	185727	324584. 1	135800. 4	111193. 5	-382	30885.3 9	42697.2 3	46053.4 7	25809.1 3	14809.1 9
-390	335644. 7	241199. 6	347603. 1	169238. 3	145276. 2	-390	30675.6 6	50603.1 4	48672.1 7	33987.9	18771.3 9
-397	297023. 3	232018. 7	402993	196380. 6	195961. 9	-397	35327.4 7	48420.3 6	54610.9 1	38987.7	25124.4 3
-402	98117.3	73332.0 8	100613. 9	38574.9 2	38597.2 6	-402	14187.0 7	16091.4 2	15202.2 1	7203.87	5950.13 6
Total	283410 63	239337 17	352044 51	236562 22	362056 66	Total	345471 9	384977 9	404312 7	343594 1	269645 0
Ratio	1	0.84448 9	1.24217 1	0.83469 8	1.27749 9	Ratio	1	1.11435 4	1.17032	0.99456 4	0.78051 2

ii) Adjusted band density values

CPD Position	Expt 1					CPD Position	Expt 2				
	0	0.5	1	2	4		0	0.5	1	2	4
	71621.2	42105.6	64622.7		19267.9		13691.0	14086.9	6143.88		2157.62
1	9	4	7	21336.2	4	1	1	3	8	5879.36	7
	82797.6	65234.5	77423.8	33036.1	20789.8		19568.3		13352.3	5676.50	4478.34
-20	5	2	8	8	4	-20	1	19678.4	1	7	3
	226062.	169852.	129266.	81748.4	16776.6		47084.8	40775.8	28575.7	9597.80	7959.80
-48	8	7	8	3	2	-48	1	6	2	7	1
	344560.	380830.	409834.	324220.	182650.		76939.4	91621.2	91447.6	76679.6	60264.6
-108	2	8	6	5	6	-108	1	3	7	7	6
			167273.	86369.5	41330.5		39045.3		39251.9	29743.5	
-119	154539	165703	8	2	1	-119	3	43904.4	1	8	16856.6
		86072.9		72538.5	38102.8		16087.0	18462.2	20390.5		11702.9
-132	81669.6	7	93801	8	8	-132	3	3	7	19276.9	9
		586205.	749712.	495570.	245993.		154973.	171462.	183752.	141991.	79619.6
-155	709754	8	4	8	8	-155	6	1	4	3	5
	73851.3	62033.6	72256.9	18894.4	10134.6		20080.0		20619.8	6988.41	4261.50
-164	3	7	2	2	3	-164	7	16916	3	1	3
	846978.	806030.	848508.	495452.	242950.		189359.	191474.		126848.	85390.8
-175	4	1	2	9	7	-175	7	5	191096	9	8
	130274.	168434.	177922.	97466.3	42440.2		29874.7	36339.7	34511.2	27510.9	17489.7
-192	2	8	3	7	1	-192	2	8	8	4	9
	103009.	127161.	140546.	76487.2	39272.3		29403.6	37139.1	37093.0	29251.3	19767.8
-198	4	1	4	7	1	-198	4	2	6	2	6
	271761.	262377.	224641.	68581.8	34769.6		64111.1	71776.1	59733.8	32536.0	20161.5
-204	7	2	3	1	9	-204	6	2	3	2	9
	143780.	180500.	185244.	118973.			30817.3	37222.9	36962.4	27645.4	17386.3
-215	7	5	2	6	51554.3	-215	5	4	3	5	6
	387694.	370476.	416476.	335798.	232255.		76169.2	95352.6	87551.2	80117.4	72930.4
-232	6	6	7	8	4	-232	7	1	4	7	4
			875832.	661069.	368874.		151046.	189605.	184448.	148666.	110630.
-256	823152	843122	9	3	7	-256	2	9	7	9	3
	92799.3	80691.4	75565.0	40767.5	30536.9		22530.8		22236.8	16722.4	12509.7
-262	7	8	2	7	9	-262	3	24386.2	1	5	9
	165904.	132078.	149501.	96816.0			22638.2	30255.3	23940.3	26561.3	17875.3
-274	4	8	8	3	61483.5	-274	4	6	3	2	1
	241913.	208668.	217890.	114797.	57397.4		41896.5		45904.3	25856.8	15783.4
-280	1	2	9	1	8	-280	7	49698.8	8	4	1
	171802.		131962.	70289.2	33698.4		40349.1	42373.6	35928.5	23902.8	14211.8
-293	6	131565	5	4	8	-293	3	2	9	5	4
	76402.8	79956.7	80291.7	37431.5	18050.2		18198.2	20467.1		9542.96	5917.52
-311	5	6	7	3	6	-311	2	6	18173.8	2	6
		123984.		58017.5	31070.0		19471.6	23265.1	22183.1	13394.1	8815.36
-316	116724	1	113663	1	9	-316	8	7	7	3	6
	150397.			90683.2	38481.0		26689.4	32234.4	30457.1	20381.6	8406.42
-320	3	139359	156180	3	4	-320	3	2	4	2	8
	383849.	346312.	303301.	155138.			53162.1	58600.7	51573.4	28573.4	
-345	9	6	7	6	83047.7	-345	4	8	5	4	15349.5
	163385.	180492.	164639.	100567.	58825.0		41053.0	43230.9	39129.6	27245.9	13889.4
-352	4	1	4	5	8	-352	4	6	2	5	8
	85507.2	180074.	105505.		55343.1		70792.0	71272.9		51866.4	33536.5
-358	1	7	8	76191.9	6	-358	5	9	69892.2	5	6
	106131.	119143.	112471.	71371.2	38808.3		49924.9	66399.9	60968.2	37970.7	22562.6
-362	8	5	1	2	1	-362	5	1	6	4	8
	265687.	219928.	261303.	162694.	87040.0		30885.3	38315.6	39351.1	25950.1	18973.6
-382	3	2	8	1	3	-382	9	9	7	8	8
	335644.		279835.		113719.		30675.6	45410.3	41588.7	34173.6	24050.0
-390	7	285616	1	202754	3	-390	6	1	6	6	9
	297023.	274744.	324426.	235271.			35327.4	43451.5	46663.2	39200.7	32189.6
-397	3	5	3	5	153395	-397	7	2	2	8	8
		86836.0		46214.2	30213.1		14187.0	14440.1	12989.7	7243.24	7623.37
-402	98117.3	3	80998.4	3	5	-402	7	3	8	1	4

iii) Signal remaining (%)

CPD Position	Expt 1 0	0.5	1	2	4	t50 %	CPD Position	Expt 2 0	0.5	1	2	4	t50%
	10	58.789	90.228	29.790	26.902	2.1		10	102.89	44.875	42.943	15.759	
1	0	28	43	3	53	5	1	0	18	33	2	44	2
	10	78.787	93.509	39.899	25.109			10	100.56	68.234	29.008	22.885	
-20	0	89	76	9	22	2.4	-20	0	26	33	67	69	2.2
	10	75.135	57.181	36.161	7.4212	1.7		10	86.600	60.689	20.384	16.905	
-48	0	18	8	83	24	5	-48	0	88	9	09	24	1.8
	10	110.52	118.94	94.096	53.009	4.7		10	119.08	118.85	99.662	78.327	
-108	0	66	43	91	77	5	-108	0	23	67	41	43	6
	10	107.22	108.24	55.888	26.744			10	112.44	100.52	76.177	43.171	
-119	0	41	05	51	39	2.4	-119	0	47	91	04	87	3.7
	10	105.39	114.85	88.819	46.654			10	114.76	126.75	119.82	72.748	
-132	0	17	42	56	91	4.2	-132	0	47	17	89	01	6
	10	82.592	105.62	69.822	34.659			10	110.63	118.57	91.622	51.376	
-155	0	81	99	89	03	3.2	-155	0	95	01	9	26	4.6
	10	83.998	97.841	25.584	13.723	2.1		10	84.242	102.68	34.802	21.222	
-164	0	04	06	4	02	5	-164	0	72	8	71	55	2.4
	10	95.165	100.18	58.496	28.684			10	101.11	100.91	66.988	45.094	
-175	0	36	06	52	4	2.9	-175	0	68	69	36	54	3.6
	10	129.29	136.57	74.816	32.577			10	121.64		92.087	58.543	
-192	0	25	52	3	59	3.4	-192	0	06	115.52	69	78	5
	10	123.44	136.44	74.252	38.124			10	126.30	126.15	99.481	67.229	
-198	0	6	03	68	97	3.6	-198	0	79	13	95	3	6
	10	96.546	82.661	25.236	12.794			10	111.95	93.172	50.749	31.447	
-204	0	8	15	01	18	2.1	-204	0	57	28	39	87	2.9
	10	125.53	128.83	82.746	35.856			10	120.78	119.94	89.707	56.417	
-215	0	87	8	53	2	3.6	-215	0	57	03	44	44	4.8
	10	95.558	107.42	86.614	59.906			10	125.18	114.94	105.18	95.747	
-232	0	88	39	25	78	5.1	-232	0	51	3	35	85	6
	10	102.42	106.39	80.309	44.812			10	125.52	122.11	98.424	73.242	
-256	0	6	99	52	47	3.9	-256	0	84	41	8	71	6
	10	86.952	81.428	43.930	32.906			10	108.23	98.695	74.220	55.522	
-262	0	61	38	87	46	2.6	-262	0	48	04	3	97	4.4
	10	79.611	90.113	58.356	37.059			10	133.64	105.75	117.32	78.960	
-274	0	37	23	5	59	3	-274	0	72	17	94	69	6
	10	86.257	90.069	47.453	23.726			10	118.62	109.56	61.715	37.672	
-280	0	5	88	85	48	2.4	-280	0	26	6	9	31	3.3
	10	76.579	76.810	40.912	19.614			10	105.01	89.044	59.240	35.222	
-293	0	18	57	8	66	2.2	-293	0	74	27	07	16	3
	10	104.65		48.992	23.625			10	112.46	99.865	52.438	32.517	
-311	0	15	105.09	32	11	2.4	-311	0	79	81	99	06	3
	10	106.21	97.377	49.704	26.618			10	119.48	113.92	68.787	45.272	
-316	0	99	58	86	42	2.6	-316	0	21	53	75	76	3.8
	10	92.660	103.84	60.295	25.586			10	120.77	114.11	76.365	31.497	
-320	0	58	5	79	26	2.8	-320	0	6	68	89	22	3.4
	10	90.220	79.015	40.416	21.635			10	110.23	97.011	53.747	28.872	
-345	0	85	71	49	46	2.3	-345	0	03	61	72	98	2.8
	10	110.47	100.76	61.552	36.003			10	105.30	95.314	66.367	33.833	
-352	0	01	75	31	89	3.2	-352	0	51	78	68	01	3.1
	10	210.59	123.38	89.105	64.723			10	100.67	98.728	73.265	47.373	
-358	0	59	82	81	38	4.6	-358	0	94	89	93	35	3.9
	10		105.97	67.247	36.566			10	132.99	122.11	76.055	45.193	
-362	0	112.26	31	75	16	3.3	-362	0	94	98	64	2	3.9
	10	82.777	98.350	61.235	32.760			10	124.05	127.41	84.020	61.432	
-382	0	1	14	17	33	3	-382	0	76	03	9	54	5
	10	85.094	83.372	60.407	33.880			10	148.03	135.57	111.40	78.401	
-390	0	74	42	33	84	2.9	-390	0	37	58	32	22	6
	10	92.499	109.22	79.209	51.644			10	122.99	132.08	110.96	91.117	
-397	0	31	59	77	09	4.3	-397	0	64	77	4	98	6
	10	88.502	82.552		30.792			10	101.78	91.560	51.055	53.734	
-402	0	26	62	47.101	89	2.6	-402	0	38	73	24	67	3.7
	10	99.192	100.41	59.281	32.804	3.0		10	114.26	105.49	75.134	50.224	4.1433
Average	0	43	1	96	16	6	Average	0	94	09	39	8	33

A.III.1.4 WTα TAM NTS

i) Band density values (peak areas)

CPD Position	Expt 1 0	0.5	1	2	4	CPD Position	Expt 2 0	0.5	1	2	4
	689555	622766	732279	715780	790598		230122	223250	234605	247099	136008
	8	0	0	8	2		2	9	4	5	2
	428972.	375568.	511755.	277962.	128407.		235706.	252267.	284782.	213070.	22791.2
-430	5	9	5	8	1	-430	5	3	5	1	4
	20534.7	19458.1		9438.98	3358.72		11727.6		13669.8	9711.30	1237.59
-408	6	8	17323.2	9	6	-408	1	13138.6	3	9	4
	118816.	100533.	126419.	84510.2	55793.7		73371.3	83212.4		74256.1	11407.5
-371	7	7	5	4	8	-371	5	9	92268.3	5	9
	56139.2	46862.6	50726.4	29100.8	14662.9		31507.7	26566.2	29348.6	21296.3	3140.15
-330	7	2	4	7	5	-330	1	4	9	2	4
	27340.8	22925.2	22084.8	10849.0			14992.2		17102.0	12373.5	1735.56
-317	1	3	5	3	6021.54	-317	2	13686.6	4	8	6
	274367.	222057.	288175.	151250.	99693.4		126437.	148811.	172201.	114202.	21152.2
-297	8	2	7	5	7	-297	6	5	5	9	4
	16659.3	14240.2	18200.6	15160.2	5204.55		6206.64	8771.26	10871.8	8022.73	
-275	7	7	5	7	4	-275	9	3	8	7	1809.95
	129620.	91128.9		44219.2	21271.6			75161.3	81762.6	60434.2	7983.58
-266	8	3	117322	5	8	-266	85331.6	9	4	7	4
	84222.5	73253.3	100011.	76234.7	75230.7		39334.2	47521.4	60276.3	60609.8	17346.5
-244	4	5	2	8	6	-244	5	4	9	5	1
	25107.2	20481.0	23433.7	6860.41	5824.34			16957.8	14597.0	8090.13	1912.92
-240	7	5	4	8	9	-240	13616.9	7	7	8	9
	47793.9	30644.5			17364.3		23085.0	19491.9	23561.3		4036.57
-227	8	9	46850.8	25914.3	8	-227	2	3	5	18600.3	9
	72559.3	50940.1	49199.3	17198.7	4679.80		26793.2	28970.5	23960.0	11851.2	1973.69
-145	4	1	2	7	9	-145	8	5	9	6	2
		92655.1	116810.	61273.6	33405.2		60676.8	65433.7	68327.4	47069.9	11831.0
-128	106905	8	9	3	1	-128	8	5	9	8	4
	30873.4	22282.3	26964.5	16108.7	7411.90		18727.5	14914.0		11399.2	2584.28
-114	7	3	8	7	2	-114	5	2	18642.1	5	4
	130659.	98774.9	121870.	45928.9	26071.6		63789.1	67835.0	65645.5	36384.2	8987.78
-102	5	5	1	2	7	-102	2	9	2	3	7
	62793.0	46335.3	54483.0	22374.5	12920.7		30259.0	27596.1	28709.8	17832.3	4661.82
-98	4	6	5	6	5	-98	5	7	2	6	1
	5927.10	4619.45	5102.22	2551.39	1603.22		1939.59	3249.06	2847.36	1073.54	
-93	4	8	2	9	9	-93	4	4	4	1	228.732
	20983.9	13165.0		8340.79	4707.62		10624.5	10388.4	11177.6	7430.27	1959.35
-88	3	2	15616.2	2	1	-88	2	8	7	9	6
	69224.1		63223.5	24548.9	14353.3			34002.7	37810.2	20671.7	6111.54
-83	8	50149.6	2	9	3	-83	35307.4	9	4	9	1
	62066.0	39163.3	57778.1	20143.4	6235.42		37901.7	41630.7	44324.8	28014.9	6685.44
-71	8	9	2	2	1	-71	5	7	1	7	2
	88946.9			33165.2	15450.5		42207.8	44695.7	48620.1	30238.8	8308.56
-64	3	36622.4	83789.9	9	4	-64	4	1	9	6	6
	11612.3	9267.31	12811.3		4466.45		8065.67	8253.46	9046.76	6271.70	1956.01
-42	6	5	7	5200.09	6	-42	2	2	4	2	5
	127614.		140236.	61706.7			28827.8	28831.1	32356.5	26188.1	8157.08
-27	3	98264.3	5	4	46998.7	-27	9	2	9	6	9
		7190.82		5101.20	3540.55		7131.97	7654.26	8870.37	5682.12	2288.02
-8	6716.35	6	9720.21	5	5	-8	2	5	4	8	3
	104968.	73716.0	114980.	53843.6			28236.9	31862.9	38509.3	27806.4	10792.2
-4	9	8	6	5	46552.1	-4	3	8	1	9	1
	18161.6	13794.3		9283.30	5959.46		5707.98	7297.40	8224.39	5898.72	2753.37
7	4	8	21876.8	9	8	7	4	8	2	7	7
	8714.11	8390.30	11798.0	5225.56	3301.54		7407.18	8586.22	10013.4		3191.63
10	1	9	4	8	1	10	3	1	1	7341.67	7
	234706.	156276.		115309.	108098.		60604.3	67252.5	85084.0	59909.5	21746.2
20	7	9	217286	9	9	20	2	1	1	3	2
	928856	806642	976864	839661	868457		343674	343655	368866	342272	155885
Total	7	2	2	5	2	Total	8	0	6	8	3
		0.86842	1.05168	0.90397	0.93497			0.99994	1.07330	0.99592	0.45358
Ratio	1	5	4	3	4	Ratio	1	2	1	1	4

ii) Adjusted band density values

CPD Position	Expt 1					CPD Position	Expt 2				
	0	0.5	1	2	4		0	0.5	1	2	4
-430	428972.5	432471.4	486605.6	307490.1	137337.6	-430	2301222	2232638	2185830	2481117	2998525
-408	20534.76	22406.29	16471.86	10441.67	3592.319	-408	235706.5	252281.9	265333.3	213942.9	50247.04
-371	118816.7	115765.5	120206.7	93487.56	59674.12	-371	11727.61	13139.35	12736.25	9751.088	2728.48
-330	56139.27	53962.79	48233.51	32192.19	15682.73	-330	73371.35	83217.28	85966.83	74560.32	25149.92
-317	27340.81	26398.64	20999.5	12001.5	6440.326	-317	31507.71	26567.77	27344.32	21383.56	6922.987
-297	274367.8	255701.2	274013.4	167317.5	106626.9	-297	14992.22	13687.39	15934.06	12424.26	3826.341
-275	16659.37	16397.81	17306.19	16770.7	5566.52	-275	126437.6	148820.1	160441	114670.7	46633.59
-266	129620.8	104935.9	111556.3	48916.56	22751.08	-266	6206.649	8771.768	10129.38	8055.599	3990.333
-244	84222.54	84351.97	95096.19	84333.01	80462.91	-244	85331.6	75165.71	76178.65	60681.82	17601.13
-240	25107.27	23584.14	22282.1	7589.184	6229.421	-240	39334.25	47524.17	56159.81	60858.12	38243.23
-227	47793.98	35287.56	44548.34	28667.11	18572.04	-227	13616.9	16958.84	13600.16	8123.277	4217.367
-145	72559.34	58658.05	46781.45	19025.75	5005.28	-145	23085.02	19493.06	21952.23	18676.49	8899.304
-128	106905	106693.4	111070.3	67782.58	35728.48	-128	26793.28	28972.22	22323.73	11899.81	4351.329
-114	30873.47	25658.33	25639.42	17819.96	7927.385	-114	60676.88	65437.52	63661.06	47262.79	26083.48
-102	130659.5	113740.4	115880.9	50807.84	27884.91	-102	18727.55	14914.88	17368.94	11445.95	5697.48
-98	62793.04	53355.64	51805.51	24751.35	13819.36	-98	63789.12	67839	61162.25	36533.26	19815.06
-93	5927.104	5319.353	4851.476	2822.428	1714.73	-93	30259.05	27597.75	26749.08	17905.4	10277.75
-88	20983.93	15159.66	14848.75	9226.814	5035.027	-88	1939.594	3249.255	2652.903	1077.938	504.2774
-83	69224.18	57747.78	60116.43	27156.76	15351.57	-83	10624.52	10389.08	10414.29	7460.715	4319.723
-71	62066.08	45097.04	54938.65	22283.2	6669.082	-71	35307.4	34004.75	35227.99	20756.46	13473.9
-64	88946.93	42171.06	79672.09	36688.36	16525.1	-64	37901.75	41633.16	41297.65	28129.72	14739.16
-42	11612.36	10671.41	12181.76	5752.483	4777.089	-42	42207.84	44698.28	45299.67	30362.72	18317.6
-27	127614.3	113152.3	133344.7	68261.7	50267.37	-27	8065.672	8253.937	8428.915	6297.392	4312.358
-8	6716.35	8280.309	9242.515	5643.094	3786.794	-8	28827.89	28832.78	30146.8	26295.43	17983.65
-4	104968.9	84884.81	109330	59563.33	49789.71	-4	7131.972	7654.705	8264.571	5705.403	5044.324
7	18161.64	15884.36	20801.68	10269.45	6373.937	7	28236.93	31864.81	35879.31	27920.39	23793.2
10	8714.111	9661.526	11218.23	5780.668	3531.157	10	5707.984	7297.828	7662.706	5922.889	6070.274
20	234706.7	179954.4	206607.6	127559	115616.9	20	7407.183	8586.715	9329.544	7371.743	7036.49

iii) Signal remaining (%)

CPD Position	Expt 1					t50%	CPD Position	Expt 2					t50%
	0	0.5	1	2	4			0	0.5	1	2	4	
	10	100.81	113.43	71.680	32.015			10	97.019	94.985	107.81	130.30	
-430	0	56	51	61	47	3.2	-430	0	67	61	74	14	6
	10	109.11	80.214	50.848	17.493			10	107.03	112.56	90.766	21.317	
-408	0	4	53	75	84	2.4	-408	0	22	94	66	63	3.2
	10	97.432	101.16	78.682	50.223			10	112.03	108.60	83.146	23.265	
-371	0	03	98	18	68	4.1	-371	0	77	05	39	43	3.2
	10	96.123	85.917	57.343	27.935			10	113.41	117.16	101.62	34.277	
-330	0	06	6	44	41	2.7	-330	0	93	68	05	57	3.9
	10	96.553	76.806	43.895	23.555			10	84.321	86.786	67.867	21.972	
-317	0	98	43	92	73	2.4	-317	0	48	11	7	36	2.9
	10	93.196	99.870	60.982	38.862			10	91.296	106.28	82.871	25.522	
-297	0	49	85	92	78	3.2	-297	0	64	22	41	18	3.2
	10	98.429	103.88	100.66	33.413			10	117.70	126.89	90.693	36.882	
-275	0	98	26	83	75	3.7	-275	0	24	34	53	69	3.8
	10	80.956	86.063	37.738	17.552			10	141.32	163.20	129.78	64.291	
-266	0	02	51	18	02	2.2	-266	0	86	21	98	27	6
	10	100.15	112.91	100.13	95.536			10	88.086	89.273	71.112	20.626	
-244	0	37	06	12	08	6	-244	0	61	67	96	74	2.8
	10	93.933	88.747	30.227	24.811			10	120.82	142.77	154.72	97.226	
-240	0	51	62	04	23	2.3	-240	0	14	59	04	3	6
	10	73.832	93.209	59.980	38.858			10	124.54	99.877	59.655	30.971	
-227	0	64	1	59	52	3	-227	0	26	05	84	57	3.1
	10	80.841	64.473	26.220	6.8981			10	84.440	95.092	80.903	38.550	
-145	0	49	36	95	89	1.7	-145	0	27	94	06	12	3.6
	10	99.802	103.89	63.404	33.420			10	108.13	83.318	44.413	16.240	
-128	0	09	63	53	79	3.1	-128	0	24	4	4	38	2.4
	10	83.108	83.046	57.719	25.677			10	107.84	104.91	77.892	42.987	
-114	0	02	79	35	01	2.6	-114	0	59	81	58	51	3.8
	10	87.050	88.689	38.885	21.341			10	79.641	92.745	61.118	30.422	
-102	0	96	21	67	66	2.3	-102	0	36	39	22	99	2.9
	10	84.970		39.417	22.007			10	106.34	95.881	57.271	31.063	
-98	0	63	82.502	35	79	2.3	-98	0	88	94	93	38	3
	10	89.746	81.852	47.619	28.930			10	91.204	88.400	59.173	33.965	
-93	0	24	38	01	32	2.5	-93	0	96	26	71	88	3
	10	72.244	70.762	43.970	23.994			10	167.52	136.77	55.575	25.999	
-88	0	13	48	86	68	2.2	-88	0	22	62	47	12	3.1
	10	83.421	86.843	39.230	22.176			10	97.783	98.021	70.221	40.658	
-83	0	4	12	17	6	2.3	-83	0	96	24	65	05	3.5
	10	72.659	88.516	35.902	10.745			10	96.310	99.775	58.787	38.161	
-71	0	72	38	39	13	2	-71	0	56	09	85	69	3.2
	10	47.411	89.572	41.247	18.578			10	109.84	108.95	74.217	38.887	
-64	0	49	62	48	61	2	-64	0	5	97	48	81	3.6
	10	91.896	104.90	49.537	41.137			10	105.90	107.32	71.936	43.398	
-42	0	94	33	57	96	3.1	-42	0	04	53	21	58	3.7
	10	88.667	104.49	53.490	39.390			10	102.33	104.50	78.076	53.465	
-27	0	47	04	65	09	3.1	-27	0	42	36	47	57	4.4
	10	123.28	137.61	84.020	56.381			10	100.01	104.57	91.215	62.382	
-8	0	58	22	25	72	4.6	-8	0	7	51	25	81	5.6
	10	80.866	104.15	56.743	47.432			10	107.32	115.88	79.997	70.728	
-4	0	63	46	78	82	3.5	-4	0	94	06	55	32	6
	10	87.461	114.53	56.544	35.095			10	112.84	127.06	98.878	84.262	
7	0	05	63	74	6	3.1	7	0	8	52	98	71	6
	10	110.87	128.73	66.336	40.522			10	127.85	134.24	103.76	106.34	
10	0	22	64	86	28	3.5	10	0	3	54	5	71	6
	10	76.672		54.348	49.260			10	115.92	125.95	99.521	94.995	
20	0	03	88.028	24	18	3.4	20	0	42	27	54	49	6
	10	89.339	95.172	55.243	32.973	2.9464		10	107.81	109.70	82.251	48.541	4.0678
Average	0	98	99	53	21	29	Average	0	75	89	03	88	57

A.III.1.5 CPD repair statistics

All repair statistics were carried out using a paired t-test for means. The alpha value for the two-tailed test was 0.01.

TS	*WTa TAM*	*Wtalpha TAM*
Mean	4.122778	3.813056
Variance	1.938094	1.104036
Observations	30	30
Pearson Correlation	0.86393	
Hypothesized Mean Difference	0	
df	29	
t Stat	2.364703	
P(T<=t) one-tail	0.012476	
t Critical one-tail	2.462021	
P(T<=t) two-tail	0.024952	
t Critical two-tail	2.756386	

NTS	*WTa TAM*	*Wtalpha TAM*
Mean	3.857024	3.629167
Variance	0.483464	0.690651
Observations	28	28
Pearson Correlation	0.754907	
Hypothesized Mean Difference	0	
df	27	
t Stat	2.195186	
P(T<=t) one-tail	0.018464	
t Critical one-tail	2.47266	
P(T<=t) two-tail	0.036927	
t Critical two-tail	2.770683	

A.III.1.6 High Resolution sequencing ladder

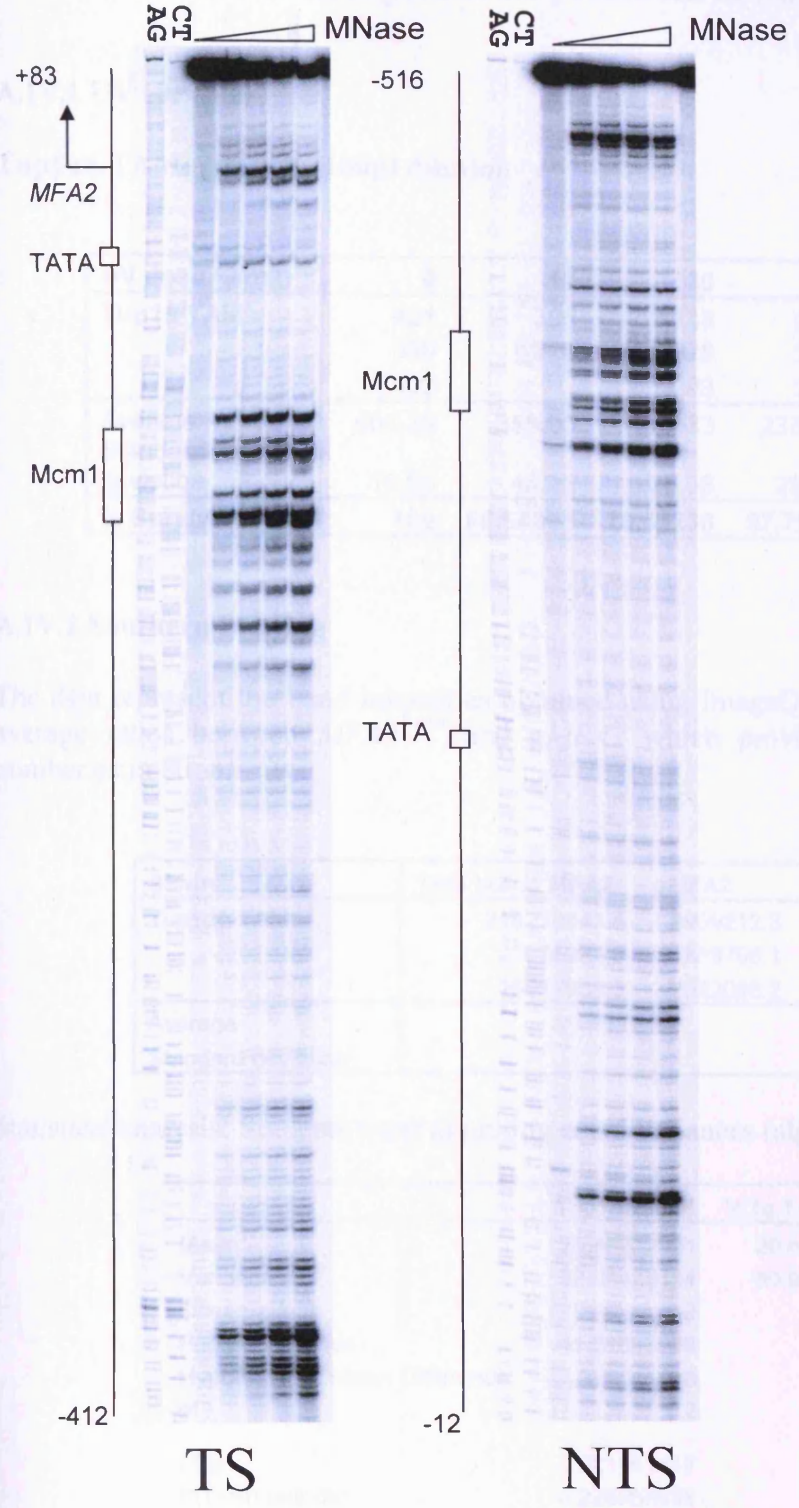

Appendix IV

Data from experiments presented in Chapter 5

A.IV.1 UV survival

Tup1αΔ TAM, 200 cells/100µl dilution

UV dose (J/m2)	0	10	30	50	100
Tup1α TAM	421	390	343	211	94
	390	326	328	267	87
	402		293	223	92
Average	404.33	358.00	321.33	233.67	91.00
Standard deviation	15.63	45.25	25.66	29.48	3.61
% Survival	**100**	**88.54081**	**79.47238**	**57.7906**	**22.50618**

A.IV.2 Southern blotting

The data represent the band intensities obtained using ImageQuant software, and the average ratios between $MFA2^{TAM}$ and g*MFA2* which provides an average copy number estimation.

Strain	TAM borne MFA2	gMFA2	Ratio
Tup1αΔ TAM	218272543.6	8909212.3	24.5
	23035937.8	838796.1	27.5
	19017808.3	2082086.2	
Average			**23.5**
Standard deviation			5.7

Statistical analysis: Students t-test assuming equal variances (alpha value = 0.01).

	Tup1Δα TAM	WTα TAM
Mean	23.46032961	29.40025382
Variance	32.04428154	50.98698863
Observations	2	2
Pooled Variance	41.51563509	
Hypothesized Mean Difference	0	
df	2	
t Stat	-0.921881417	
P(T<=t) one-tail	0.226955838	
t Critical one-tail	6.964556734	
P(T<=t) two-tail	0.453911677	
t Critical two-tail	9.9248432	

A.IV.3 Northern blotting

The data represent the relative band intensities quantified using Imagequant software. Using *ACT1* as an internal control, relative MFA2 mRNA levels were obtained. These figures were then normalised against mRNA levels in WTa cells to provide an average MRNA level.

Strain	ACT1	MFA2
Tup1αΔ TAM	8343030	31839613
	683359.4	6988.885
	51367109	1.1E+08

	WT a	WT a TAM	WTα TAM	Tup1Δα TAM
	1.000	75.438	0.400	3.298
	1.000	12.166	0.000	1.377
	1.000	51.659	0.080	2.351
AVERAGE	1.000	46.421	0.160	2.342
ST DEV	0.000	31.960	0.211	0.960

A.IV.4 CPD repair

A.IV.4.1 Tup1Δα TAM TS

i) Band density values (peak areas)

CPD Position	Expt 1					CPD position	Expt 2				
	0	0.5	1	2	4		0	0.5	1	2	4
	136959	114913	141755	171930	194121		133978	131319	161898	195742	213495
Top bands	5	8	0	3	0	Top bands	6	8	6	1	3
	16971.9	7903.40	3144.65				95793.7	50928.2	42389.3	47491.7	27305.0
5	7	7	1	513.943	660.61	5	2	4	3	3	3
	2524.86	1801.81	1560.87	1006.23				16907.9	14743.6	17650.4	21633.0
1	4	6	3	6	803.645	1	32172.5	2	7	6	1
	7370.24		2687.41				20699.4	11502.3	8692.40	15786.8	9949.14
-19	1	4036.43	9	943.041	299.348	-19	5	6	1	8	7
	2118.69	1031.88					12354.1	5697.88	5044.41	18198.9	14007.5
-36	4	5	392.774	42.33	52.406	-36	9	3	5	4	7
	8821.08	5369.42	2893.85				24002.6		7137.54	8535.16	7668.13
-46	9	8	3	746.61	433.498	-46	4	11777	3	9	2
	17073.4	14010.5	13011.5	7316.14	4072.10		35502.6	21694.3		17697.7	9439.46
-107	8	2	3	1	9	-107	4	8	19752.3	2	6
	10376.8	7992.32	6660.09	2481.62	1786.13		21460.8	12161.1		8734.73	
-118	8	9	1	9	4	-118	3	1	9130.18	5	4480
		3234.55	3649.00	1600.59			10891.4	5373.51	5224.42	10228.1	2320.50
-131	4013.97	3	8	6	683.916	-131	3	4	9	8	8
	32997.1	24115.4	19520.2	9642.40	6048.47		64854.2	35686.0	28500.1	18847.7	11389.5
-150	4	2	3	6	1	-150	1	9	7	5	9
	5891.83	2958.71	2042.54	1185.85	1061.37		19598.7	11861.3		6857.23	4017.87
-163	7	3	5	9	8	-163	5	2	9133.92	2	7
	46903.6		16321.2		6230.09			46741.9	32122.0	20464.0	14259.1
-168	5	24281.9	4	8480.46	7	-168	82134.9	7	2	5	3
	10713.1	7151.84		2720.75			29745.1	15042.5	11161.6		5063.54
-191	5	7	6267.34	2	2080.2	-191	6	6	2	8948.49	4
	8586.33	5716.77		2865.10	1704.15		25358.4		14485.1	8011.84	4411.38
-196	3	6	6201.25	5	9	-196	3	17962.3	1	5	8
	15137.9	6385.22	4765.95	2440.73	2890.29		32494.5	13281.0	8921.54	8351.50	6021.58
-202	8	2	7	9	9	-202	3	5	4	9	5
	10207.2	7142.87	6889.35	4376.75	2944.84		15864.8	11049.5	9866.75		2995.88
-214	2	4	6	9	4	-214	4	4	5	10022.3	1
	15036.4	13182.5	15312.3	14383.0	7021.63			14324.9	16797.8	21141.3	7390.57
-229	3	1	5	3	1	-229	22029.4	3	5	3	7
	41938.4	33578.5	42597.9	43311.4	23550.5		52878.5	42303.3	52196.4	52134.7	26508.6
-252	4	9	7	2	8	-252	3	8	7	2	2
	3587.72	2565.63	2883.99		1775.44		9975.48		5681.34	7855.60	3673.09
-261	6	9	9	2692.19	6	-261	6	6373.61	7	9	1
	7959.37	5105.33	6841.88	5855.66	1955.01		11920.8	6242.09	9692.21	9723.39	3324.92
-270	4	3	1	4	2	-270	4	6	2	3	3
	11442.3	8549.80	9250.32	5837.44	2421.95		17068.1	10915.4	13800.0	8092.71	5197.20
-279	4	7	9	8	8	-279	9	9	1	5	7
	7795.27	5029.72	3565.08	2015.23	1694.68		11002.5	5704.39	4078.33	3475.51	
-292	4	7	2	2	5	-292	5	6	9	1	2651.38
	1871.82						3707.78	2174.70	1751.27	1410.83	
-309	4	898.506	684.266	548.954	340.74	-309	3	3	3	5	848.494
	3771.53	2570.08	1700.76				5162.85	3469.36	2191.46	1476.37	1709.09
-312	5	1	5	639.678	486.47	-312	1	5	7	3	9
	5901.88	3854.07	2787.30		1153.90		9189.40	5068.34	4626.17	2664.10	2263.30
-316	2	3	6	1739.07	1	-316	7	7	4	7	8
	5427.28	3853.27	3250.29	2004.12	1264.52		11528.2	7045.27	5240.91	3337.60	
-320	7	8	4	7	7	-320	2	7	6	2	3489.83
	5629.18	2631.42	1259.80				8933.47	4134.73	2833.03	2272.76	2703.84
-339	4	8	3	831.124	996.777	-339	1	2	4	8	9
	6286.69	2689.39	1868.75	1061.28			10819.9	5352.17	3619.93	2117.29	2234.53
-343	6	1	7	3	820.462	-343	8	3	1	2	4
	3335.40	1359.20	1376.89					7315.23	4560.26	2460.04	3145.54
-346	4	6	7	780.258	422.838	-346	7886.81	6	1	8	6
	5040.36	4311.58	3583.76	1578.52	1469.17		14725.3	18248.8	12049.8	7300.48	3525.22
-351	3	4	9	6	4	-351	4	4	2	1	4
	16152.7	8486.42	7883.58	3901.78	2490.72			15411.1	11166.6	6428.88	4506.31
-357	5	4	5	7	8	-357	21320.9	7	2	9	5
	17496.7	9501.36	7155.38	3887.62	3487.11		21396.8		9307.97	4874.11	4380.74
-361	9	3	9	9	4	-361	3	12362.4	8	1	7
	27881.3	17419.2	14860.0	8406.19	5789.94		31619.5	19500.9	16491.3	9867.01	6760.83
-381	5	7	2	8	2	-381	9	9	7	1	3
	47358.8	32284.7	30482.9	17446.8	9399.86			37342.9	34199.5	19778.7	10611.6
-387	5	6	1	3	8	-387	53901.6	2	5	6	7
	23679.6	15490.2	15915.7		5006.79		31225.9	22542.7	22534.7	13767.5	7917.40
-396	8	3	4	9621.51	1	-396	8	9	5	3	8
	182689	144563	168681	189220	204451		221900	184669	207811	236342	238275
Total	7	2	9	7	0	Total	8	8	0	7	7
		0.79130	0.92332	1.03574	1.11911			0.83221	0.93650	1.06508	1.07379
Ratio	1	5	5	9	6	Ratio	1	8	4	3	4

ii) Adjusted band density values

CPD Position	Expt 1					CPD position	Expt 2				
	0	0.5	1	2	4		0	0.5	1	2	4
	16971.9	9987.81			590.296		95793.7	61195.8	45263.3	44589.7	25428.5
5	7	5	3405.79	496.204	1	5	2	1	6	2	6
	2524.86	2277.01	1690.49	971.505	718.106					16571.9	20146.3
1	4	9	1	3	7	1	32172.5	20316.7	15743.3	2	3
	7370.24	5100.97	2910.58	910.491			20699.4	13821.3	9281.75	14822.2	9265.41
-19	1	9	8	5	267.486	-19	5	4	3	1	6
	2118.69		425.390	40.8689	46.8280		12354.1	6846.62	5386.43	17086.8	13044.9
-36	4	1304.03	8	6	2	-36	9	4	1	8	3
	8821.08	6785.53	3134.16	720.840	387.357		24002.6	14151.3	7621.47	8013.62	7141.15
-46	9	6	5	4	4	-46	4	4	5	2	8
	17073.4	17705.5	14092.0	7063.62	3638.68		35502.6	26068.1	21091.5	16616.2	8790.76
-107	8	9	4	1	2	-107	4	5	3	9	2
	10376.8	10100.1		2395.97	1596.02		21460.8	14612.8	9749.21	8200.99	4172.12
-118	8	9	7213.16	4	2	-118	3	9	4	3	3
		4087.61		1545.35	611.121		10891.4				2161.03
-131	4013.97	9	3952.03	1	4	-131	3	6456.86	5578.65	9603.18	7
	32997.1	30475.5	21141.2	9309.59	5404.68		64854.2	42880.7		17696.0	10606.8
-150	4	1	3	4	5	-150	1	1	30432.5	5	7
	5891.83		2212.16	1144.92	948.407		19598.7	14252.6	9753.20	6438.21	3741.75
-163	7	3739.03	2	9	2	-163	5	6	8	6	8
	46903.6		17676.5	8187.75	5566.97			56165.5	34299.9	19213.5	13279.2
-168	5	30685.9	9	3	9	-168	82134.9	5	2	8	1
	10713.1	9038.04	6787.79	2626.84	1858.78		29745.1	18075.2	11918.3	8401.68	4715.56
-191	5	2	4	4	8	-191	6	6	9	7	4
	8586.33	7224.49	6716.21	2766.21	1522.77		25358.4	21583.6	15467.2	7522.27	4108.22
-196	3	2	6	5	2	-196	3	5	2	6	6
	15137.9	8069.23	5161.73	2356.49	2582.66		32494.5	15958.6	9526.43	7841.18	5607.76
-202	8	1	3	6	2	-202	3	2	2	5	6
	10207.2	9026.70	7461.46	4225.69	2631.40		15864.8	13277.2	10535.7	9409.87	2789.99
-214	2	2	3	3	1	-214	4	2	3	8	6
	15036.4	16659.2	16583.9	13886.5	6274.26			17212.9	17936.7	19849.4	6882.67
-229	3	1	2	9	3	-229	22029.4	6	6	8	8
	41938.4	42434.4			21043.9		52878.5		55735.4		24686.8
-252	4	5	46135.4	41816.5	1	-252	3	50832.1	4	48949	8
	3587.72	3242.28	3123.49	2599.26	1586.47		9975.48	7658.58	6066.54	7375.58	3420.66
-261	6	9	3	8	1	-261	6	4	7	7	7
	7959.37		7410.04	5653.55	1746.92		11920.8	7500.55	10349.3	9129.23	3096.42
-270	4	6451.79	6	3	5	-270	4	5	5	9	6
	11442.3	10804.6		5635.96			17068.1	13116.1	14735.6	7598.20	4840.04
-279	4	9	10018.5	6	2164.17	-279	9	4	6	4	2
	7795.27	6356.24	3861.13	1945.67	1514.30		11002.5		4354.85	3263.13	
-292	4	4	4	5	6	-292	5	6854.45	4	8	2469.17
	1871.82	1135.47		530.006	304.472		3707.78	2613.14	1870.01	1324.62	790.183
-309	4	4	741.089	6	4	-309	3	2	1	5	3
	3771.53	3247.90		617.599	434.691		5162.85	4168.81		1386.15	1591.64
-312	5	2	1842	2	2	-312	1	8	2340.05	8	5
	5901.88	4870.52		1679.04	1031.08		9189.40	6090.16	4939.83	2501.31	2107.76
-316	2	8	3018.77	5	2	-316	7	9	3	5	8
	5427.28	4869.52	3520.20	1934.95	1129.93		11528.2	8465.66	5596.25	3133.65	
-320	7	4	6	4	3	-320	2	4	5	6	3250
	5629.18	3325.42		802.437	890.682		8933.47	4968.32	3025.11	2133.88	2518.03
-339	4	9	1364.42	4	2	-339	1	9	6	9	4
	6286.69	3398.67	2023.94	1024.65	733.133		10819.9	6431.21	3865.36	1987.91	2080.97
-343	6	9	3	2	8	-343	8	6	5	4	1
	3335.40	1717.67	1491.23					8790.04	4869.45	2309.72	2929.37
-346	4	7	8	753.327	377.832	-346	7886.81	9	1	5	6
	5040.36	5448.70	3881.37	1524.04	1312.79		14725.3	21927.9	12866.8		3282.96
-351	3	1	3	2	8	-351	4	6	1	6854.38	2
	16152.7	10724.5	8538.25	3767.11				18518.1	11923.7	6036.04	
-357	5	9	5	5	2225.62	-357	21320.9	9	2	8	4196.63
	17496.7	12007.2	7749.58	3753.44	3115.95		21396.8	14854.7	9939.06	4576.27	4079.69
-361	9	1	8	6	3	-361	3	7	7	5	1
	27881.3	22013.3	16094.0	8116.05	5173.67		31619.5	23432.5	17609.4	9264.08	6296.21
-381	5	5	3	4	3	-381	9	5	9	1	1
	47358.8	40799.3	33014.2	16844.6	8399.36			44871.5	36518.3	18570.1	9882.40
-387	5	9	8	5	6	-387	53901.6	7	1	6	7
	23679.6	19575.5	17237.4	9289.41	4473.87		31225.9	27087.6	24062.6	12926.2	7373.30
-396	8	5	2	9	9	-396	8	1	2	6	3

iii) Signal remaining (%)

	Expt 1							Expt 2						
CPD Position	0	0.5	1	2	4	t50%	CPD position	0	0.5	1	2	4	t50%
5	100	58.84887	20.06714	2.923667	3.478064	0.9	5	100	63.8829	47.25087	46.54765	26.54512	2
1	100	90.18381	66.95376	38.47753	28.4414	2.25	1	100	63.14926	48.93404	51.50957	62.61972	4.2
-19	100	69.21048	39.49109	12.35362	3.629271	1.25	-19	100	66.77151	44.84058	71.60679	44.76165	3.1
-36	100	61.54875	20.07797	1.928969	2.21023	0.9	-36	100	55.41947	43.60005	138.3084	105.5912	6
-46	100	76.92402	35.53036	8.171785	4.391265	1.25	-46	100	58.95743	31.75266	33.38642	29.75156	1.5
-107	100	103.7023	82.53759	41.37189	21.3119	2.4	-107	100	73.42594	59.40833	46.80297	24.76087	2.1
-118	100	97.33363	69.51187	23.08956	15.38056	2	-118	100	68.09097	45.42794	38.21377	19.44064	1.8
-131	100	101.8348	98.45688	38.49931	15.22486	2.4	-131	100	59.28384	51.22053	88.17186	19.84162	2.4
-150	100	92.35803	64.06988	28.21334	16.37925	2	-150	100	66.11863	46.92449	27.28589	16.35495	1.6
-163	100	63.4612	37.54623	19.43245	16.09697	1.4	-163	100	72.72229	49.76445	32.85015	19.09183	1.8
-168	100	65.42327	37.68703	17.45654	11.86897	1.3	-168	100	68.38208	41.76047	23.39272	16.16756	1.5
-191	100	84.36399	63.35945	24.5198	17.35052	1.9	-191	100	60.76706	40.06832	28.24556	15.85321	1.4
-196	100	84.13943	78.21984	32.21648	17.73483	2.1	-196	100	85.11429	60.99437	29.6638	16.20063	1.9
-202	100	53.30453	34.09789	15.56677	17.0608	1.1	-202	100	49.11172	29.31703	24.13078	17.25757	1.1
-214	100	88.43451	73.09988	41.39907	25.77981	2.4	-214	100	83.68963	66.40931	59.31279	17.58604	2.3
-229	100	110.7923	110.2916	92.353	41.72708	4	-229	100	78.13632	81.42193	90.10451	31.24315	3.2
-252	100	101.1827	110.0074	99.70926	50.1781	4.6	-252	100	96.12994	105.4028	92.56875	46.68601	4.3
-261	100	90.37169	87.06051	72.44889	44.21941	3.6	-261	100	76.77404	60.81455	73.93712	34.29073	2.9
-270	100	81.05901	93.09835	71.03012	21.94802	2.75	-270	100	62.9197	86.81733	76.5822	25.9749	3.8
-279	100	94.4273	87.55636	49.25535	18.9137	2.4	-279	100	76.84555	86.33408	44.51676	28.35709	2.4
-292	100	81.53971	49.53173	24.95968	19.42595	1.75	-292	100	62.29873	39.5804	29.65801	22.4418	1.6
-309	100	60.66136	39.59181	28.31498	16.26608	1.5	-309	100	70.4772	50.43474	35.72553	21.31148	1.8
-312	100	86.11619	48.83954	16.37527	11.52558	1.6	-312	100	80.74644	45.32477	26.8487	30.82881	1.9
-316	100	82.525	51.14928	28.44932	17.4704	1.75	-316	100	66.27379	53.75573	27.21955	22.93693	1.7
-320	100	89.72298	64.86124	35.65232	20.81949	2.1	-320	100	73.4343	48.54398	27.18249	28.1917	1.9
-339	100	59.07479	24.23832	14.25495	15.82258	1.1	-339	100	55.61477	33.86272	23.88645	28.18651	1.4
-343	100	54.06144	32.19406	16.29874	11.66167	1.1	-343	100	59.43837	35.72435	18.37263	19.23268	1.3
-346	100	51.49831	44.70935	22.58578	11.32792	1.25	-346	100	111.4525	61.7417	29.28592	37.14272	1.4
-351	100	108.1014	77.00583	30.23676	26.04571	2.4	-351	100	148.913	87.37868	46.54819	22.29464	1.6
-357	100	66.39484	52.85945	23.32181	13.77858	1.5	-357	100	86.85462	55.92504	28.31047	19.68317	1.9
-361	100	68.62521	44.29149	21.4522	17.80871	1.5	-361	100	69.4251	46.45112	21.38763	19.0668	1.6
-381	100	78.95368	57.72328	29.10926	18.55603	1.8	-381	100	74.10771	55.69172	29.29855	19.91238	1.8
-387	100	86.14945	69.71089	35.56811	17.73558	2	-387	100	83.2472	67.74995	34.45197	18.33416	2
-396	100	82.66815	72.79415	39.2295	18.89333	2.1	-396	100	86.74703	77.05962	41.39584	23.61272	2.3
Average	100	80.14698	59.94769	32.24194	18.54302	1.951471	Average	100	73.96245	55.52025	45.19736	27.98684	2.220588

A.IV.4.1 Tup1Δα TAM NTS

i) Band density values (peak areas)

CPD Position	Expt 1					CPD position	Expt 2				
	0	0.5	1	2	4		0	0.5	1	2	4
	158545	141250	162811	220310	251692		152055	135252	160179	204451	250837
	2	5	5	4	8		0	8	0	4	2
	55059.2	36701.8	24810.3	10772.8	2131.23		94161.6	76417.7	50134.4	21769.9	16165.2
-450	1	2	2	3	4	-450	6	7	6	7	1
	3737.56	1980.89	2430.95					20123.7	11556.6	4653.04	
-415	2	9	2	923.286	965.47	-415	26148.1	2	4	6	5062.49
	7394.61	4890.12	3368.57	1098.94	1379.70		12268.1	11588.8		1869.26	3544.67
-406	5	1	7	8	7	-406	3	3	4458.02	1	5
	31117.4	23817.7		10385.5	4739.25		32637.6	32058.6	22828.9	12230.9	5163.43
-369	4	1	22131	2	5	-369	9	8	3	6	9
	10062.8	7227.16	5730.29	2528.96	1122.29		13455.9	11470.1	8312.04	4128.84	
-334	6	1	5	6	3	-334	3	6	7	8	775.094
	5364.80		3914.03	2011.73			9726.18	8110.66		4138.88	1110.81
-319	5	3396.16	3	4	693.6	-319	9	5	6019.86	3	1
	45782.0	31389.1	25056.0	10202.9	8228.50		60713.4	45875.0	38494.7	16001.7	10919.1
-298	5	8	2	5	8	-298	3	4	6	1	7
	11303.2	12109.7	8267.76	3784.26	1871.46		35380.2	23731.7	18486.3	9575.81	5243.80
-264	4	5	4	2	1	-264	1	7	2	9	6
	10340.1	9298.62	12365.8	13523.8	8443.87		26247.4	21733.0	27088.4	22730.4	
-243	7	2	2	2	2	-243	1	5	1	9	16869.8
	8544.73		5371.03	3045.84	1353.16		20960.8	17249.2	16053.8	9437.05	3992.16
-239	9	5529.02	2	9	7	-239	3	6	6	6	7
	11414.8	5188.36	2418.61	2226.38	1719.62		12523.2	7268.63	6610.25	4299.91	3409.93
-149	8	7	4	4	7	-149	6	6	8	7	6
	19670.2	13906.3	9279.33	5587.24	5082.99		22182.0	16257.4	13209.2	7112.24	8299.04
-127	5	2	6	5	6	-127	9	2	9	1	4
	7699.97	4355.50		2925.17	1338.43		10025.6	7470.44	9352.99	7073.50	4593.88
-113	6	3	3069.88	7	4	-113	5	7	2	2	9
	18887.6	11919.3	7344.90	6446.63	5024.13		30186.8	14045.5	11539.6	7541.65	5769.17
-102	3	4	1	5	1	-102	8	8	8	7	7
	16679.6	10384.2	7914.41	3718.51	2919.13		30038.3	16109.1	12650.2	4808.62	4163.63
-97	9	1	1	1	7	-97	4	4	8	4	3
	2455.88	1077.90	1210.37				6422.03		1934.40	1159.46	
-87	6	6	7	665.262	940.711	-87	2	2804.2	9	7	896.92
	37278.8	21141.8	11823.5	6521.41	5003.43			24599.8	14359.1	5701.16	3437.48
-78	6	7	2	4	2	-78	46182.9	3	6	3	9
		7766.55	6056.14	3808.26	3439.13		10813.8	6624.32	5732.24	3175.91	1998.91
-63	13217.4	4	3	3	8	-63	3	1	1	2	4
	14533.8	11101.6	9052.73	5085.12	5984.61		16372.2	13255.3	8706.10	4989.29	
-50	9	6	1	9	3	-50	5	5	4	4	3376.91
	30594.4	25277.7	26210.1	14262.9	12323.4		28924.3	24348.2	27357.7	9470.38	8315.77
-40	8	9	3	6	3	-40	7	9	7	3	9
	15136.2	11054.9	9351.92	7430.71	4847.17		24626.0	19278.8	13779.2	11047.4	7649.35
-8	8	1	6	9	3	-8	7	2	3	2	7
	22517.7	21810.8	19284.0	17190.7	15938.1		46778.9	51685.1	25408.8	22788.1	
20	8	6	6	1	8	20	3	1	3	3	18381.3
	198424	169383	185457	233725	261241		213732	182463	195586	224021	264751
Total	6	1	7	1	7	Total	7	4	4	8	1
		0.85363	0.93465	1.17790	1.31657			0.85369	0.91509		1.23870
Ratio	1	9	1	4	9	Ratio	1	9	8	1.04814	2

ii) Adjusted band density values

CPD Position	Expt 1					CPD position	Expt 2				
	0	0.5	1	2	4		0	0.5	1	2	4
	55059.2	42994.5	26545.0	9145.76	1618.76		94161.6	89513.6	54785.8		13050.1
-450	1	2	2	2	6	-450	6	8	7	20770.1	2
	3737.56	2320.53		783.838				23572.3	12628.8	4439.33	4086.93
-415	2	4	2600.92	2	733.317	-415	26148.1	8	5	6	1
	7394.61	5728.55	3604.10	932.969	1047.94		12268.1	13574.8		1783.40	2861.60
-406	5	6	2	2	8	-406	3	4	4871.63	7	4
	31117.4	27901.3	23678.3	8816.95	3599.67		32637.6	37552.6	24946.9		4168.42
-369	4	7	6	3	3	-369	9	6	7	11669.2	7
	10062.8	8466.29	6130.94	2147.00	852.430		13455.9	13435.8	9083.22	3939.21	625.730
-334	6	2	8	5	9	-334	3	3	9	4	8
	5364.80	3978.44	4187.69	1707.89	526.819		9726.18	9500.61	6578.37	3948.78	
-319	5	8	6	3	7	-319	9	1	5	8	896.754
	45782.0		26807.8	8661.95	6249.91		60713.4	53736.7	42066.2	15266.7	8815.00
-298	5	36771	9	8	4	-298	3	6	5	6	7
	11303.2	14186.0	8845.83	3212.70	1421.45		35380.2	27798.7	20201.4		4233.30
-264	4	3	2	9	7	-264	1	4	5	9136.01	7
	10340.1	10892.9	13230.4	11481.2	6413.49		26247.4		29601.6		13618.9
-243	7	2	2	6	2	-243	1	25457.5	4	21686.5	3
	8544.73	6476.99	5746.56	2585.82			20960.8	20205.3	17543.3		3222.86
-239	9	7	5	1	1027.79	-239	3	2	1	9003.62	3
	11414.8	6077.93	2587.71	1890.12	1306.13		12523.2	8514.28		4102.42	
-149	8	7	9	4	2	-149	6	1	7223.55	6	2752.83
	19670.2	16290.6	9928.13		3860.75		22182.0	19043.4	14434.8	6785.58	
-127	5	2	1	4743.38	9	-127	9	9	3	2	6699.79
	7699.97	5102.27	3284.52	2483.37			10025.6	8750.67	10220.7	6748.62	3708.63
-113	6	5	1	5	1016.6	-113	5	7	5	2	1
	18887.6	13962.9	7858.44	5472.97	3816.04		30186.8		12610.3	7195.27	4657.43
-102	3	6	4	2	9	-102	8	16452.6	2	5	7
	16679.6	12164.6	8467.77	3156.88	2217.21		30038.3		13823.9	4587.76	3361.28
-97	9	3	3	8	3	-97	4	18869.8	6	8	7
	2455.88	1262.71	1295.00	564.784	714.511		6422.03	3284.76	2113.88	1106.21	724.080
-87	6	8	5	6	4	-87	2	3	1	4	5
	37278.8	24766.7		5536.45	3800.32			28815.5	15691.3	5439.31	2775.07
-78	6	4	12650.2	7	7	-78	46182.9	7	8	4	3
		9098.16	6479.57	3233.08	2612.17		10813.8	7759.54	6264.07	3030.04	1613.71
-63	13217.4	7	8	5	7	-63	3	8	1	5	6
	14533.8	13005.0	9685.68		4545.57		16372.2	15526.9	9513.84		2726.16
-50	9	9	3	4317.1	7	-50	5	5	6	4760.14	8
	30594.4	29611.7		12108.7	9360.18		28924.3	28520.9	29895.9	9035.41	
-40	8	9	28042.7	6	8	-40	7	3	9	7	6713.3
	15136.2	12950.3		6308.42	3681.64		24626.0	22582.6	15057.6	10540.0	
-8	8	3	10005.8	6	1	-8	7	8	5	2	6175.3
	22517.7	25550.4	20632.3	14594.3	12105.7		46778.9	60542.5	27766.2	21741.4	14839.1
20	8	3	6	2	5	20	3	3	3	9	6

iii) Signal remaining (%)

	Expt 1						Expt 2						
CPD Position	0	0.5	1	2	4	t50%	CPD position	0	0.5	1	2	4	t50%
-450	100	78.08779	48.21177	16.61078	2.940046	1.4	-450	100	95.06383	58.18278	22.05791	13.85927	1.8
-415	100	62.08682	69.58868	20.97191	19.62019	1.7	-415	100	90.14948	48.29737	16.97766	15.62993	1.7
-406	100	77.46929	48.73955	12.61687	14.17177	1.5	-406	100	110.6513	39.70964	14.53691	23.32551	1.9
-369	100	89.66472	76.09353	28.33444	11.56802	2	-369	100	115.0592	76.43608	35.75377	12.77182	2.2
-334	100	84.13406	60.92649	21.33594	8.47106	1.8	-334	100	99.85066	67.50356	29.27494	4.650225	1.9
-319	100	74.15829	78.05867	31.83514	9.819923	2	-319	100	97.68072	67.63569	40.59954	9.219993	2
-298	100	80.3175	58.55546	18.91999	13.65145	1.6	-298	100	88.50886	69.28657	25.14561	14.51904	1.9
-264	100	125.5041	78.25926	28.4229	12.57566	2.2	-264	100	78.57144	57.09817	25.82237	11.96518	1.7
-243	100	105.3457	127.9517	111.0355	62.02505	6	-243	100	96.99053	112.7793	82.6234	51.88676	4.4
-239	100	75.80099	67.25267	30.26215	12.02834	1.9	-239	100	96.39559	83.6957	42.9545	15.37565	2.2
-149	100	53.24574	22.6697	16.55842	11.44237	1	-149	100	67.98775	57.68107	32.75845	21.98174	1.8
-127	100	82.81858	50.47283	24.11449	19.6274	1.8	-127	100	85.85077	65.07425	30.59037	30.2036	2.2
-113	100	66.26351	42.65625	32.25172	13.20263	1.6	-113	100	87.28286	101.946	67.31354	36.99141	3.2
-102	100	73.9265	41.6063	28.97649	20.20396	1.7	-102	100	54.50249	41.77418	23.83577	15.42868	1.3
-97	100	72.93081	50.76696	18.92654	13.29289	1.6	-97	100	62.81906	46.02105	15.27304	11.18999	1.4
-87	100	51.41599	52.73064	22.99719	29.09383	1.7	-87	100	51.14835	32.91608	17.22529	11.27494	1.1
-78	100	66.43644	33.93399	14.85147	10.19432	1.2	-78	100	62.39446	33.97661	11.77777	6.008877	1.2
-63	100	68.83477	49.02309	24.46082	19.76317	1.6	-63	100	71.75576	57.92647	28.02008	14.92271	1.7
-50	100	89.48117	66.64208	29.70369	31.27572	2.2	-50	100	94.83702	58.10958	29.07444	16.65115	2
-40	100	96.78801	91.65935	39.57825	30.59437	2.5	-40	100	98.60519	103.3592	31.23808	23.20984	2.4
-8	100	85.55817	66.10471	41.67751	24.32328	2.2	-8	100	91.70232	61.14514	42.80026	25.07627	2.2
20	100	113.4678	91.627	64.81245	53.76086	3.9	20	100	129.4226	59.35628	46.4771	31.72189	2.6
Average	100	80.6244	62.43321	30.87521	20.16574	2.05	Average	100	87.60137	63.63231	32.36958	18.99384	2.036364

A.IV.4.3 CPD repair statistics

TS	*WT alpha TAM*	*Tup1 alpha TAM*
Mean	3.831897	2.071782
Variance	1.132436	0.446352
Observations	29	29
Pearson Correlation	0.684506	
Hypothesized Mean Difference	0	
df	28	
t Stat	12.18126	
P(T<=t) one-tail	5.23E-13	
t Critical one-tail	2.46714	
P(T<=t) two-tail	1.05E-12	
t Critical two-tail	2.763262	

TS mean = 1.76, SD = 0.78, CI(95%) = 0.3

NTS	*Wtalpha TAM*	*Tup1alpha TAM*
Mean	3.878	2.106667
Variance	0.473796	0.674456
Observations	20	20
Pearson Correlation	0.765939	
Hypothesized Mean Difference	0	
df	19	
t Stat	14.90955	
P(T<=t) one-tail	3.06E-12	
t Critical one-tail	2.539483	
P(T<=t) two-tail	6.12E-12	
t Critical two-tail	2.860935	

NTS mean = 1.77, SD = 0.53, CI (95%) = 0.25

A.IV.4.4 Endogenous repair data

TS

Nucleotide position	WT a T 50%	WTα T 50%	Tup1Δα T 50%
2	1.5	6	0.75
-16	1.5	3.5	0.6
-37	0.95	2.2	0.65
-48	1.6	1.8	0.7
-108	2.45	3.1	1.1
-119	2.15	3	0.75
-133	3.1	4.55	1
-155	2.2	2.8	0.75
-164	1.8	2.35	0.65
-174	2.1	2.7	0.65
-193	2.5	3	0.95
-198	2.6	2.65	0.8
-205	2.35	2.5	0.65
-215	2.95	3.8	1.7
-231	3.4	3.8	2
-255	4.3	3.8	2.15
-262	3.5	5.9	2.05
-293	2.7	2.35	1.95
-309	1.8	1.5	0.7
-316	3.1	3.05	1.55
-320	2.8	3	1.6
-346	2.1	2.2	0.8
-358	2.8	2.6	0.9
-362	2.4	2.85	0.75
-382	2.1	2.1	0.75
-431	2.8	2.85	0.9

NTS

Nucleotide position	WT a T 50%	WTα T 50%	Tup1Δα T 50%
-369	3.2	3.4	1.1
-330	2.65	3.7	1.05
-308	3.2	3.85	0.9
-275	3.1	2.8	0.9
-264	2.3	2.85	0.7
-240	3.9	3.45	2.3
-140	1.95	4.4	0.7
-137	1.6	3.65	0.65
-129	2.55	3.95	0.75
-98	2	3.4	0.7
-93	2.25	3.4	0.85
-88	2.45	3.5	1
-82	1.9	2.75	0.75
-72	2.45	3.15	1.25
-68	2.75	3	1.25
-60	2.65	2.3	0.8
-54	3.65	2.9	1.65
-51	1.85	1.25	0.8
-25	3.95	2.1	1.25

A.IV.5 rtPCR data

The data represent the H3 acetylation (K9 and K14) enrichment levels as determined by Bio-Rad icycler software, adjusted using the Input sample as an internal control, and normalised against the untreated WTα TAM adjusted IP sample.

a) TAM IP primers

WTα TAM		Input (IN)	Adjusted IN	IP	Adjusted IP (IP/IN)
Expt 1	U	0.12	1.00	0.56	0.56
	0	0.14	1.20	0.44	0.36
	1	0.13	1.15	0.53	0.46
	2	0.08	0.64	0.40	0.63
Expt 2	U	0.11	1.00	0.15	0.15
	0	0.09	0.84	0.15	0.18
	1	0.08	0.71	0.16	0.23
	2	0.08	0.68	0.19	0.28
Expt 3	U	0.12	1.00	0.37	0.37
	0	0.07	0.59	0.23	0.40
	1	0.09	0.75	0.22	0.29
	2	0.09	0.74	0.41	0.55

Tup1Δα TAM		Input (IN)	Adjusted IN	IP	Adjusted IP (IP/IN)
Expt 1	U	0.05	1.00	0.08	0.08
	0	0.04	0.83	0.07	0.08
	1	0.04	0.78	0.12	0.15
	2	0.03	0.64	0.16	0.25
Expt 2	U	0.09	1.00	0.10	0.10
	0	0.06	0.66	0.11	0.17
	1	0.06	0.67	0.02	0.03
	2	0.05	0.52	0.12	0.23
Expt 3	U	0.09	1.00	0.23	0.23
	0	0.08	0.92	0.15	0.17
	1	0.05	0.49	0.18	0.37
	2	0.05	0.53	0.20	0.38

		Average IP	Normalised	Adjusted	Standard deviation
WTα TAM	U	0.36	1.00		0.21
	0	0.31	0.87		0.12
	1	0.33	0.90		0.12
	2	0.49	1.35		0.18
Tup1Δα TAM	U	0.14	0.38	1.00	0.08
	0	0.14	0.39	1.03	0.05
	1	0.26	0.72	1.90	0.15
	2	0.29	0.80	2.11	0.08

b) *MFA2* N1 primers

WTα TAM		Input (IN)	Adjusted IN	IP	Adjusted IP (IP/IN)
Expt 1	U	0.11	1.00	0.08	0.08
	0	0.10	0.94	0.11	0.12
	1	0.08	0.76	0.09	0.12
	2	0.08	0.72	0.12	0.16
Expt 2	U	0.11	1.00	0.25	0.25
	0	0.13	1.15	0.18	0.15
	1	0.10	0.89	0.21	0.24
	2	0.07	0.60	0.18	0.30
Expt 3	U	0.10	1.00	0.15	0.15
	0	0.08	0.74	0.06	0.07
	1	0.08	0.74	0.07	0.10
	2	0.08	0.79	0.14	0.17

Tup1Δα TAM		Input (IN)	Adjusted IN	IP	Adjusted IP (IP/IN)
Expt 1	U	0.06	1.00	0.10	0.10
	0	0.03	0.59	0.09	0.16
	1	0.04	0.71	0.11	0.15
	2	0.03	0.53	0.14	0.26
Expt 2	U	0.08	1.00	0.12	0.12
	0	0.06	0.68	0.11	0.17
	1	0.07	0.79	0.00	0.00
	2	0.04	0.53	0.12	0.22
Expt 3	U	0.09	1.00	0.21	0.21
	0	0.09	1.03	0.14	0.13
	1	0.05	0.55	0.17	0.31
	2	0.05	0.60	0.21	0.34

		Average IP	Normalised	Adjusted	Standard deviation
WTα TAM	U	0.16	1.00		0.08
	0	0.11	0.71		0.04
	1	0.15	0.95		0.08
	2	0.21	1.34		0.08
Tup1Δα TAM	U	0.14	0.89	1.00	0.06
	0	0.15	0.96	1.08	0.02
	1	0.23	1.45	1.62	0.11
	2	0.28	1.72	1.93	0.06

c) *MFA2* coding region, N2 primers

	Input (IN)	Adjusted IN	IP	Adjusted IP (IP/IN)	Normalised	Adjusted
WTα TAM	0.15	1.00	0.10	0.10	1.00	
	0.12	0.79	0.08	0.11	1.08	
	0.12	0.79	0.09	0.12	1.21	
	0.10	0.66	0.12	0.18	1.79	
Tup1Δα TAM	0.08	1.00	0.07	0.07	0.67	1.00
	0.06	0.73	0.06	0.09	0.87	1.28
	0.06	0.77	0.11	0.14	1.40	2.08
	0.05	0.65	0.14	0.22	2.19	3.25

A.IV.6 Nucleosome eviction preliminary assay

Low resolution nucleosome mapping was carried out as described in Chapter 4. Briefly, chromatin was extracted from yeast cells and subject to limited digestion with MNase, which cuts preferentially at nucleosome linker regions. Samples were then subject to digestion with *Bgl*II restriction endonuclease, which creates a linear TAM fragment. The fragmented DNA was then run on an agarose gel, and transferred to a membrane following a southern blotting procedure. Following the standard nucleosome mapping procedure, a probe designed to detect the 5' end of linear TAM was hybridised to the membrane, detecting a ladder of fragments, representing the positions of MNase sensitive sites (not protected by positioned nucleosomes).

To determine whether nucleosomes are present across the *MFA2* promoter region in TAM, I designed a new primer set to create a probe located within the nucleosomes N-2 and N-1 (as positioned in the repressed gene). If the probe is able to hybridise to this sequence, it can be assumed that there are no positioned nucleosomes.

Primers for probe preparation

Evict FOR: TTAGAAAAGTTAAAGCAGCATGT
Evict REV: Biotin – ATACAAAATTACGTGGTAATGCA

MNase treated chromatin samples from various strains were run on a standard nucleosome mapping gel, and probed to produce a ladder of MNase sensitive sites. This membrane could then be stripped, and re-probed with the new radio-labelled fragment, designed to bind only to non-nucleosomal *MFA2*.

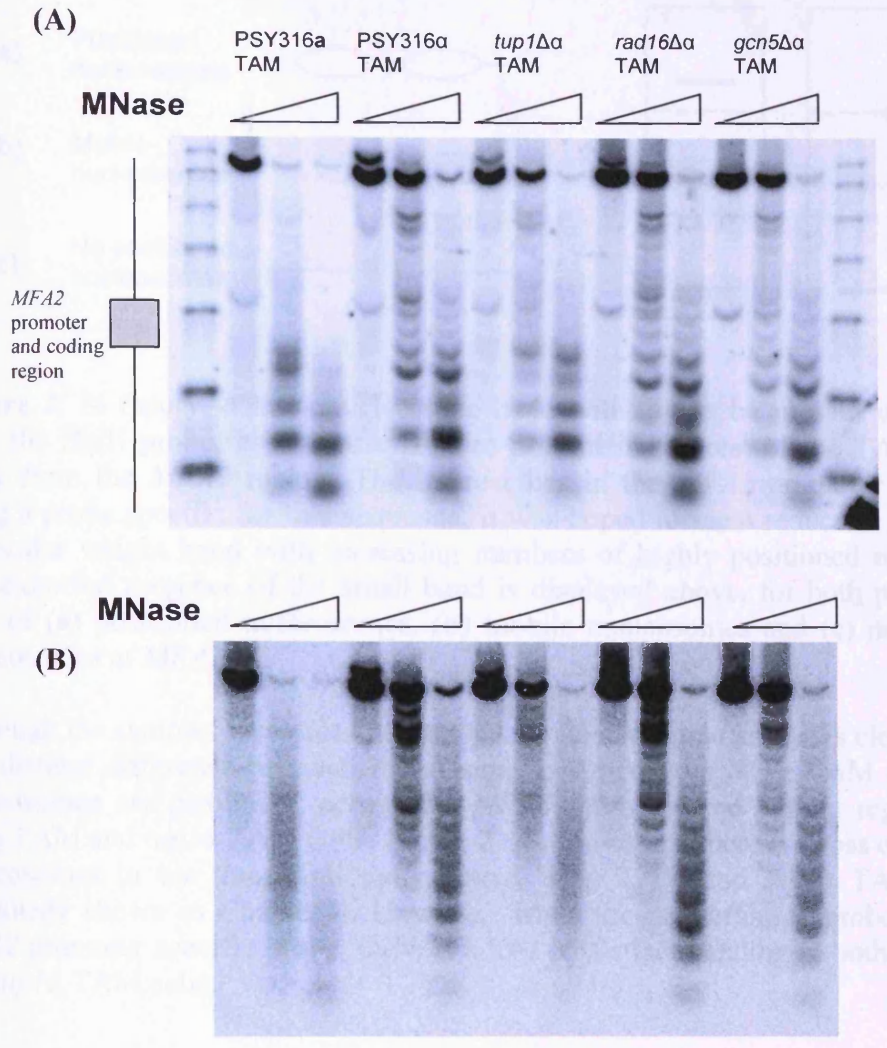

Figure 1: To determine whether nucleosomes were present in the *tup*1 mutant, a low resolution nucleosome mapping analysis was carried out. **(A)** Limited MNase digested chromatin samples were purified, digested with *Bgl*II to linearise the plasmid, then probed using a specifically designed radiolabelled probe to detect the 5' end of the linear sequence. **(B)** The same membrane could then be stripped, and re-probed using a probe designed to bind in the N-2, N-1 region.
The limited MNase digestion did not produce mononucleosome fragments, even with large amounts of MNase. Ideally this assay needed the presence of these mononucleosome fragments to determine if nucleosomes were present at the *MFA2* promoter.

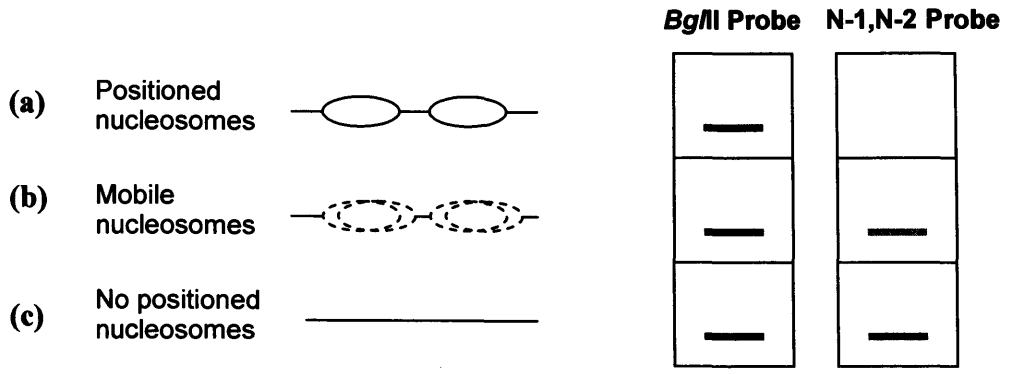

Figure 2: In theory, a mononucleosome band will always be present when probed with the *Bgl*II probe, as nucleosomes are present in the rest of the TAM plasmid, away from the *MFA2* region. The interest lies in the *MFA2* promoter region, and using a probe specific for this sequence, it was hoped to see a reduction in the small molecular weight band with increasing numbers of highly positioned nucleosomes. The expected presence of the small band is displayed above, for both probes in the case of **(a)** positioned nucleosomes, **(b)** mobile nucleosomes and **(c)** no positioned nucleosomes at *MFA2*.

Although the samples were not digested to mononucleosome size, it is clear that there is a distinct difference between the chromatin structure in WTα TAM cells, where nucleosomes are positioned across the *MFA2* promoter and coding region, and in WT**a** TAM and *tup1*α TAM cells. Figure 2 (A) shows that there is a loss of positioned nucleosomes in the transcriptionally active WT**a** TAM and *tup1*α TAM cells, as previously shown in Chapter 4. However, when the membrane is probed using the *MFA2* promoter specific probe, there is a loss of distinct banding in both WT**a** TAM and *tup1*α TAM cells.

Appendix V

Data from experiments presented in Chapter 6

A.V.1 UV survival

Gcn5αΔ TAM, 200 cells/100µl dilution

UV dose (J/m2)	0	10	30	50	100
Gcn5αTAM	256	189	179	82	5
	227	196	158	53	3
	146	196	108	104	9
Average	209.67	193.67	148.33	79.67	5.67
Standard deviation	57.01	4.04	36.47	25.58	3.06
% Survival	100	92.36884	70.74722	37.99682	2.702703

A.V.2 Southern blotting

The data represent the band intensities obtained using ImageQuant software, and the average ratios between $MFA2^{TAM}$ and g*MFA2* which provides an average copy number estimation.

Strain	TAM borne *MFA2*	g*MFA2*	Ratio
Gcn5αΔ TAM	319347869.1	14560245.7	21.9
	43171731.6	813392.9	
	107821684.9	3594462.2	30.0
Average			**26.0**
Standard deviation			5.7

Statistical analysis: Students t-test assuming equal variances (alpha value = 0.01).

	Gcn5Δα TAM	WTα TAM
Mean	25.965	29.4002538
Variance	32.56245	50.9869886
Observations	2	2
Pooled Variance	41.77471932	
Hypothesized Mean Difference	0	
df	2	
t Stat	-0.531498521	
P(T<=t) one-tail	0.324099304	
t Critical one-tail	6.964556734	
P(T<=t) two-tail	0.648198607	
t Critical two-tail	9.9248432	

A.V.3 Northern blotting

The data represent the relative band intensities quantified using ImageQuant software. Using *ACT1* as an internal control, relative *MFA2* mRNA levels were obtained. These figures were then normalised against mRNA levels in WTa cells to provide an average mRNA level.

Strain	ACT1	MFA2
Gcn5αΔ TAM	11503797	
	261775.1	573.184
	1.06E+08	

	WT a	WT a TAM	WTα TAM	Gcn5Δα TAM
	1.000	75.438	0.400	0.000
	1.000	12.166	0.000	0.000
	1.000	51.659	0.080	0.014
AVERAGE	1.000	46.421	0.160	0.005
ST DEV	0.000	31.960	0.211	0.008

A.V.4 CPD repair

A.V.4.1 Gcn5Δα TAM TS

i) Band density values

	Expt 1						Expt 2				
CPD Position	0	0.5	1	2	4	CPD position	0	0.5	1	2	4
Top bands	2447219	2386822	2365330	3004507	2880540	Top bands	114008818.07	124578022.82	111384720.71	124918526.52	135538833.55
1	9917.779	18350.58	9924.378	24655.02	27584.11	1	1026036.75	1556833.79	1389886.17	1594281.66	1418636.87
-20	14133.75	20355.75	12689.95	27306.18	23337.08	-20	1096782.76	1612547.57	1371088.05	1677808.08	1339338.1
-48	30714.91	36395.22	29138.94	38646.07	27210.83	-48	1452691.48	1832461.23	1655525.54	1490380.92	956777.86
-108	71153.3	82661.67	72057.2	129080.4	115323.6	-108	3016853.05	4470801.66	3678146.93	4811735.92	4474720.6
-119	35313.79	42740.23	36712.96	67590	58326.81	-119	1790418.78	2677655.61	2204800.62	2885307.5	2761878.94
-132	15724.94	17783.21	14844.56	29096.43	31870.55	-132	862315.85	1343726.69	1180416.37	1455471.89	1792410.12
-155	258567.1	295591.5	248986	474849.5	476637.4	-155	10677400.95	16216130.34	14107853.92	18834200.21	20806444.8
-164	88983.23	92894.14	82327.8	151837.2	123594.9	-164	3862645.21	5795986.96	4752140.73	5792131.18	5164217.6
-175	335912.5	387887.5	317232.9	609934.5	532232.5	-175	13410620.39	20671160.67	17752705.42	22382711.13	21761502.04
-192	84076.63	108580.1	90039.03	154802.4	116154.4	-192	3479720.83	5246833.07	4272346.21	5175118.23	4352370.63
-197	77474.21	95981.74	74551.21	146058.5	99670.59	-197	2759535.67	4252160.94	3665680.3	4513734.83	3481527.23
-204	129988.6	158398.2	125526.3	202439.8	134830.2	-204	5111383.33	7669928.23	6302687.17	6651005.95	4664569.91
-215	34794.6	45418.18	34958.15	64274.11	48369.88	-215	1259224.35	1925256.77	1574058.82	1777386.06	1285255.52
-232	52216.46	62224.62	50864.98	97473.4	85009.15	-232	2167340.31	3403420.83	2869771.01	3667278.95	3554504.4
-256	120709.2	164635.6	140235	260032.7	206815.1	-256	5207417.8	8158797.85	7057657.53	9046695.91	8142564.63
-262	37302.29	53999.19	40674.42	89998.23	72438.19	-262	1379094.18	2350754.96	2083040.76	2638814.23	2348380.09
-274	28039.51	38869.53	30644.61	68329.3	51810.34	-274	980290.5	1635969.68	1386614.48	1774972	1620069.33
-280	36263.31	45649.84	35283.15	61431.82	46087.8	-280	1138634.01	1673717.82	1473136.55	1725087.55	1281799.12
-293	30913.82	35268.26	22926.35	44186.2	31397.1	-293	984893.42	1427711.03	1190334.46	1182510.19	879442.04
-311	39862.02	45482.24	35274.41	58116.41	46873.13	-311	1011264.31	1645638.79	1376021.95	1482405.14	1082408.74
-316	33159.58	40208.07	32740.5	48728.17	38195.33	-316	968074.26	1482963.41	1161856.43	1346840.06	1069101.91
-320	64757.05	75456.41	61503.79	108650.1	85855.3	-320	1731099.85	2630943.64	2310158.43	2819157.82	2504873.81
-345	98023.93	113575.6	91508.07	156756.9	116760.4	-345	3786412.95	5211084.59	4642014.61	5251550.65	4600455.7
-352	36891.04	37634.32	32569.52	55265.23	49591.77	-352	1334579.62	1454859.75	1479160.82	1637582.37	3200642.64
-358	112889.8	114583.7	101193.8	182177.4	168879.3	-358	3426855.7	4892264.5	4305545.25	5525102.36	5848252.16
-362	89182.15	90055.39	68600.77	141068.9	129453.1	-362	2344587.57	3667732.4	3299582.07	4430322.28	4195452.04
-382	110963	132045.9	102429.3	201803.8	169298.6	-382	3564366.37	5344897.95	4565839.76	5506285.38	4231431.57
-390	218072.6	262040.4	210972.2	394287.9	348472.5	-390	7739258.73	11079729.07	9756632.35	11951180.1	9975419.41
-397	93890.91	111755.9	89135.52	171840.6	162674.5	-397	3138920.46	4370026.09	3644875.93	4665402.62	4159944.79
-402	21717.56	25872.55	18577.06	29831.95	26310.78	-402	666321.92	929693.2	724954.99	618284.38	439604.29
Total	4858828	5239217	4679452	7295056	6531605	Total	205383859.43	261209711.91	228619254.34	269229272.07	268932830.44
Ratio	1	1.078288	0.963083	1.501402	1.344276	Ratio	1	1.271812267	1.113131553	1.310858959	1.309415604

ii) Adjusted band density values

	Expt 1						Expt 2				
CPD Position	0	0.5	1	2	4	CPD position	0	0.5	1	2	4
1	9917.779	17018.25	10304.81	16421.33	20519.68	1	1026036.75	1224106.6	1248627.053	1216211.439	1083412.222
-20	14133.75	18877.84	13176.38	18187.12	17360.34	-20	1096782.76	1267913.207	1231739.453	1279930.285	1022851.794
-48	30714.91	33752.78	30255.91	25739.98	20242	-48	1452691.48	1440826.824	1487268.541	1136949.868	730690.7423
-108	71153.3	76660.09	74819.34	85973.2	85788.61	-108	3016853.05	3515299.998	3304323.663	3670674.018	3417341.74
-119	35313.79	39637.11	38120.26	45017.91	43389.01	-119	1790418.78	2105385.896	1980718.824	2201081.574	2109245.476
-132	15724.94	16492.07	15413.59	19379.5	23708.34	-132	862315.85	1056544.841	1060446.42	1110319.215	1368862.654
-155	258567.1	274130.3	258530.3	316270.6	354568.2	-155	10677400.95	12750411.96	12674022.12	14367831.17	15889870.82
-164	88983.23	86149.64	85483.64	101130.2	91941.63	-164	3862645.21	4557266.123	4269163.621	4418576.951	3943910.232
-175	335912.5	359725.3	329393.3	406243.2	395925	-175	13410620.39	16253311.28	15948434.29	17074843.17	16619247.52
-192	84076.63	100696.7	93490.46	103105.2	86406.64	-192	3479720.83	4125477.639	3838132.339	3947883.33	3323903.133
-197	77474.21	89013.07	77408.95	97281.41	74144.44	-197	2759535.67	3343387.267	3293124.062	3443341.33	2658840.492
-204	129988.6	146897.8	130338	134833.8	100299.5	-204	5111383.33	6030707.855	5662122.464	5073776.936	3562329.557
-215	34794.6	42120.63	36298.19	42809.38	35982.11	-215	1259224.35	1513790.061	1414081.576	1355894.201	981548.9564
-232	52216.46	57706.85	52814.77	64921.57	63237.87	-232	2167340.31	2676040.26	2578105.888	2797615.202	2714573.118
-256	120709.2	152682.3	145610.5	173193.2	153848.7	-256	5207417.8	6415096.049	6340362.478	6901349.57	6218472.273
-262	37302.29	50078.63	42233.57	59942.78	53886.4	-262	1379094.18	1848350.594	1871333.855	2013042.069	1793456.624
-274	28039.51	36047.44	31819.3	45510.32	38541.45	-274	980290.5	1286329.533	1245687.876	1354052.614	1237246.085
-280	36263.31	42335.47	36635.65	40916.29	34284.48	-280	1138634.01	1316010.124	1323416.398	1315997.834	978909.3055
-293	30913.82	32707.64	23805.17	29429.95	23356.14	-293	984893.42	1122580.012	1069356.499	902088.0411	671629.4177
-311	39862.02	42180.04	36626.57	38708.09	34868.68	-311	1011264.31	1293932.157	1236171.903	1130865.476	826634.9785
-316	33159.58	37288.8	33995.53	32455.1	28413.31	-316	968074.26	1166023.829	1043772.793	1027448.492	816472.5595
-320	64757.05	69977.96	63861.39	72365.71	63867.33	-320	1731099.85	2068657.229	2075368.742	2150618.723	1912970.795
-345	98023.93	105329.5	95015.81	104407	86857.44	-345	3786412.95	4097369.34	4170230.014	4006190.457	3513365.569
-352	36891.04	34901.91	33817.99	36809.07	36891.07	-352	1334579.62	1143926.496	1328828.4	1249243.757	2444329.08
-358	112889.8	106264.4	105072.8	121338.2	125628.4	-358	3426855.7	3846687.617	3867957.242	4214871.725	4466307.061
-362	89182.15	83516.99	71230.42	93958.08	96299.51	-362	2344587.57	2883863.047	2964233.708	3379709.351	3204064.489
-382	110963	122458.8	106355.7	134410.2	125940.4	-382	3564366.37	4202584.051	4101797.087	4200517.031	3231542.037
-390	218072.6	243015.2	219059.3	262613.1	259226.9	-390	7739258.73	8711764.586	8765030.806	9117060.247	7618222.493
-397	93890.91	103642	92552.32	114453.4	121012.7	-397	3138920.46	3436062.226	3274434.115	3559042.405	3176947.621
-402	21717.56	23994.09	19289.17	19869.39	19572.45	-402	666321.92	730998.7676	651275.2138	471663.5424	335725.5622

iii) Signal remaining (%)

	Expt 1							Expt 2					
CPD Position	0	0.5	1	2	4	t50%	CPD position	0	0.5	1	2	4	t50%
1	100	171.5933	103.9024	165.5747	206.8979	6	1	100	119.3043621	121.6941842	118.5348808	105.592	6
-20	100	133.5656	93.22636	128.6786	122.8289	6	-20	100	115.6029483	112.3047789	116.6986145	93.25929	6
-48	100	109.8905	98.50563	83.80289	65.90285	5.6	-48	100	99.1832639	102.3802068	78.26506067	50.2991	4.1
-108	100	107.7393	105.1523	120.8281	120.5687	6	-108	100	116.5220824	109.5288239	121.6722842	113.275	6
-119	100	112.2426	107.9472	127.4797	122.867	6	-119	100	117.5918126	110.6288007	122.9366894	117.8074	6
-132	100	104.8784	98.02002	123.2405	150.769	6	-132	100	122.5241124	122.976566	128.7601539	158.7426	6
-155	100	106.019	99.98578	122.3167	137.1281	6	-155	100	119.4149402	118.6995054	134.5630013	148.8178	6
-164	100	96.81559	96.06714	113.6509	103.3247	6	-164	100	117.9830369	110.5243528	114.3925137	102.1039	6
-175	100	107.089	98.05927	120.9372	117.8655	6	-175	100	121.1973109	118.9239112	127.3232906	123.926	6
-192	100	119.7678	111.1967	122.6324	102.7713	6	-192	100	118.5577189	110.3000076	113.4540247	95.52212	6
-197	100	114.8938	99.91577	125.5662	95.7021	6	-197	100	121.1576028	119.3361658	124.7797362	96.35101	6
-204	100	113.0082	100.2688	103.7274	77.16019	6	-204	100	117.9858263	110.774757	99.26426191	69.69404	6
-215	100	121.0551	104.3213	123.0346	103.4129	6	-215	100	120.2160728	112.2978265	107.6769363	77.9487	6
-232	100	110.5147	101.1458	124.3316	121.1072	6	-232	100	123.4711617	118.9525187	129.0805689	125.249	6
-256	100	126.4878	120.6292	143.4798	127.454	6	-256	100	123.191499	121.7563622	132.5292081	119.4157	6
-262	100	134.2508	113.2198	160.6946	144.4587	6	-262	100	134.0264226	135.6929702	145.9684261	130.046	6
-274	100	128.5595	113.4802	162.3078	137.4541	6	-274	100	131.2192185	127.0733396	138.1276891	126.2122	6
-280	100	116.7447	101.0268	112.8311	94.54317	6	-280	100	115.5779744	116.2284269	115.576895	85.97225	6
-293	100	105.8026	77.00497	95.20001	75.55244	6	-293	100	113.9798469	108.5758598	91.59245282	68.19311	6
-311	100	105.8151	91.8834	97.10519	87.47345	6	-311	100	127.9519255	122.2402384	111.8268948	81.74272	6
-316	100	112.4526	102.521	97.87549	85.68658	6	-316	100	120.447767	107.8194965	106.1332311	84.33987	6
-320	100	108.0623	98.6169	111.7496	98.62606	6	-320	100	119.4995903	119.8872926	124.2342389	110.5061	6
-345	100	107.4529	96.93124	106.5117	88.60841	6	-345	100	108.2124268	110.1366932	105.8043724	92.78876	6
-352	100	94.60812	91.66995	99.77781	100.0001	6	-352	100	85.71436867	99.5690613	93.60578703	183.1535	6
-358	100	94.13112	93.07553	107.4837	111.2841	6	-358	100	112.2512284	112.871903	122.9953081	130.3325	6
-362	100	93.64765	79.87071	105.3552	107.9807	6	-362	100	123.0008674	126.4287905	144.1494186	136.6579	6
-382	100	110.36	95.84789	121.1307	113.4977	6	-382	100	117.9055017	115.0778753	117.8475105	90.66245	6
-390	100	111.4378	100.4525	120.4246	118.8719	6	-390	100	112.5658786	113.2541386	117.8027582	98.43607	6
-397	100	110.3855	98.57432	121.9004	128.8865	6	-397	100	109.4663681	104.3172057	113.3842813	101.2115	6
-402	100	110.4824	88.81828	91.48995	90.12269	6	-402	100	109.7065466	97.74182633	70.78613629	50.38489	4
Average	100	113.3251	99.37791	118.704	111.9602	5.986667	Average	100	117.1809894	114.5997962	116.3255542	105.6214	5.87

A.V.4.2 Gcn5Δα TAM NTS

i) Band density values (peak areas)

	Expt 1						Expt 2				
CPD Position	0	0.5	1	2	4	**CPD position**	0	0.5	1	2	4
	28152	27199	24761	97364	27073		######	16547043	15581366	19321947	20860943
Top bands	72	99	97	9.2	18	Top bands	##	0.77	2.08	9.69	7.05
	22970	31891	24902	41460	19042		142584	12018301.	9557175.1	10692558.	7557211.3
-430	8.9	9.7	7.6	9.1	6.3	-430	65	98	4	71	1
	6380.8	8405.8	12674.	17237.	12333.		139982	2171203.3	1486350.6	1751708.4	
-408	78	14	85	46	99	-408	8	7	6	2	726924.21
	69615.	76257.	64582.	19072	64700.		519868	7438902.9	6344036.8	7454260.6	5837583.8
-371	73	55	14	3.1	5	-371	3	7	2	5	6
	22185.	73881.	62080.	73798.	46014.		152993	2440059.3			1965764.4
-330	04	69	29	54	05	-330	6	3	2100682.2	2586654.8	6
	21149.	34389.	47699.	68183.	26802.		130490	2700514.2	2207106.3	2876273.0	2269652.8
-317	36	48	4	75	7	-317	5	1	5	2	1
	20657	28281	25534	48200	17857		110234	16985366.	13834256.	16525639.	12889449.
-297	9.6	7.9	5.3	2.8	6.5	-297	68	78	34	45	53
	14305.	35210.	26758.	18794.	10236.		870309	1807828.4	1876076.8	1969012.9	1818724.6
-275	89	17	92	6	89	-275	.5	4	9	2	4
	14390	19183	13763	26801	11622		568679	9236760.3	7815348.5	9123305.8	5520057.1
-266	8.4	4.2	0.5	6.1	7.4	-266	2	5	3	9	8
	96384.	10258	82984.	18134	94554.		370565	5534812.7	4693066.8		4445505.6
-244	03	9.3	82	4.7	84	-244	7	5	8	5743893.9	6
	91219.	11003	85825.	18124	72534.		308288	5057128.0	3831917.2	3901340.0	2398265.0
-240	81	0.7	73	0.2	95	-240	6	4	9	5	1
	23120.	34108.	22989.	57727.	22574.		828407	1241054.7	1154701.4	1558218.2	
-227	3	6	2	85	68	-227	.6	8	8	5	707836.57
	44331.	44369.	25001.	43449.	19717.		995177	1476300.1	1170151.4	1042404.6	
-145	82	3	74	66	3	-145	.7	7	7	5	685827.43
	62953.	64654.	46699.	97046.	44441.		194029	2633067.6	2100574.7	2418015.2	2081939.8
-128	08	19	65	09	34	-128	7	6	8	8	8
	36097.	38936.	27206.	61166.	26699.		108772	1708403.2	1363666.4	1702247.2	1386086.6
-114	29	75	53	14	59	-114	5	7	9	6	6
	18378.	15951.	9645.7	19543.	10747.		536656				
-102	04	34	33	15	47	-102	.1	799099.62	637922.83	706868.43	566110.11
	10814	10627	77860.	12657	48869.		416074	5249069.3	3649225.5	3536487.6	2463215.3
-98	9.4	2.5	84	2.4	72	-98	9	5	3	1	8
	15992	16476	11617	19757	72246.		457716	8070816.9	5400409.9	5708760.7	4029946.4
-93	1.4	3.3	3.9	8.7	5	-93	2	3	5	6	3
	31895.	32212.	22382.	38216.	14629.		848477	1323576.5		1031517.3	
-88	91	39	11	63	75	-88	.7	9	970789.45	5	715294.42
	20737	21247	14376	24889	78935.		726029	11113713.	7747418.0	7105274.7	4266846.0
-83	0.3	5.7	5.7	8.7	27	-83	2	97	2	3	4
	91240.	91149.	64483.	11925	31535.		325517	3638651.0	2243693.6	2792409.4	1535828.9
-71	2	24	87	9.9	04	-71	2	7	1	2	8
	73000.	73523.	51909.	86845.	27374.		262080	4173692.8	2734370.1	2635069.7	1635449.5
-64	2	8	39	73	68	-64	4	6	5	1	9
	14808.	16484.	10329.	18925.	7376.7		654803				
-42	29	32	37	77	23	-42	.6	706057.41	586274.04	508933.03	381279.7
	11005	11431	84156.	15213	47878.		422481	4831442.0	3970756.6	3112711.2	
-27	7.9	6.8	76	1.7	1	-27	9	1	3	1	2457068.1
	8577.8	10547.	7399.1	18342.	5788.3						
-8	39	79	16	17	72						
	65797.	70648.	54321.	12203	39566.						
-4	37	23	7	5.3	4						
	23930.	17560.	14970.	35034.	11051.						
7	47	65	34	33	58						
	19910.	16200.	11890.	28347.	8246.4						
10	36	53	75	55	57						
	15953	16547	13792	27843	79246.						
20	1.3	6.8	2.8	3	14						
	49757	52439	44299	46191	41166		######	27782625	24328963	28970304	27695130
Total	81	87	16	54	51	**Total**	##	4.68	3.61	5.19	5.01
		1.0539	0.8902	0.9283	0.8273			1.2411380	1.0868520	1.2941954	1.2372293
Ratio	1	02	96	27	38	**Ratio**	1	71	22	64	93

ii) Adjusted band density values

CPD Position	Expt 1					CPD position	Expt 2				
	0	0.5	1	2	4		0	0.5	1	2	4
	22970	30260	27971	44661	23016		142584	9683291.	8793446.	8261934.	6108173.
-430	8.9	8.4	3.4	9.5	7.6	-430	65	697	531	927	109
	6380.8	7975.8	14236.	18568.	14908.		139982	1749364.	1367574.	1353511.	587541.9
-408	78	95	68	29	05	-408	8	894	086	481	821
	69615.	72357.	72540.	20544	78203.		519868	5993614.	5837075.	5759764.	4718271.
-371	73	32	11	8.1	26	-371	3	363	051	158	237
	22185.	70102.	69729.	79496.	55617.		152993	1965985.	1932813.	1998658.	1588843.
-330	04	97	97	24	01	-330	6	402	445	526	969
	21149.	32630.	53577.	73447.	32396.		130490	2175837.	2030733.	2222440.	1834464.
-317	36	61	03	95	32	-317	5	058	077	967	023
	20657	26835	28680	51921	21584		110234	13685316	12728739	12769044	10417994
-297	9.6	3	9.6	6.3	4.8	-297	68	.06	.57	.48	.92
	14305.	33409.	30056.	20245.	12373.		870309	1456589.	1726156.	1521418.	1469997.
-275	89	33	22	66	29	-275	.5	305	691	498	924
	14390	18202	15458	28870	14048		568679	7442169.	7190811.	7049403.	4461627.
-266	8.4	2.8	9.7	8.6	3.7	-266	2	864	972	386	9
	96384.	97342.	93210.	19534	11428		370565	4459465.	4318036.	4438196.	3593113.
-244	03	32	41	5.6	8.1	-244	7	775	666	592	52
	91219.	10440	96401.	19523	87672.		308288	4074589.	3525702.	3014490.	1938415.
-240	81	3.2	38	3	72	-240	6	409	868	591	805
	23120.	32364.	25821.	62184.	27285.		828407	999932.8	1062427.	1204005.	572114.2
-227	3	09	99	79	93	-227	.6	913	503	34	529
	44331.	42100.	28082.	46804.	23832.		995177	1189472.	1076642.	805446.0	554325.1
-145	82	01	51	24	22	-145	.7	956	861	695	993
	62953.	61347.	52454.	10453	53716.		194029	2121494.	1932714.	1868354.	1682743.
-128	08	42	09	8.6	08	-128	7	555	609	006	63
	36097.	36945.	30558.	65888.	32271.		108772	1376481.	1254693.	1315293.	1120315.
-114	29	31	98	55	69	-114	5	239	797	792	01
	18378.	15135.	10834.	21052.	12990.		536656	643844.2	586945.4	546183.6	457562.7
-102	04	5	3	01	43	-102	.1	576	325	712	714
	10814	10083	87455.	13634	59068.		416074	4229238.	3357610.	2732576.	1990912.
-98	9.4	7.2	04	4.5	65	-98	9	851	288	112	432
	15992	15633	13048	21283	87324.		457716	6502755.	4968854.	4411049.	3257234.
-93	1.4	6.4	9.1	3	08	-93	2	106	86	889	634
	31895.	30564.	25140.	41167.	17682.		848477	1066421.	893212.1	797033.6	578142.1
-88	91	87	09	19	92	-88	.7	715	674	617	165
	20737	20160	16148	26811	95408.		726029	8954454.	7128309.	5490109.	3448710.
-83	0.3	8.5	0.8	5.2	77	-83	2	164	894	435	533
	91240.	86487.	72429.	12846	38116.		325517	2931705.	2064396.	2157641.	1241345.
-71	2	37	72	7.5	29	-71	2	307	592	173	371
	73000.	69763.	58305.	93550.	33087.		262080	3362794.	2515862.	2036067.	1321864.
-64	2	39	78	76	68	-64	4	968	413	798	481
	14808.	15641.	11602.	20386.	8916.2		654803	568879.0	539423.9	393242.7	308172.1
-42	29	22	18	96	18	-42	.6	203	77	859	967
	11005	10847	94526.	16387	57870.		422481	3892751.	3653447.	2405132.	1985943.
-27	7.9	0	75	7.2	09	-27	9	437	342	22	846
	8577.8	10008.	8310.8	19758.	6996.3						
-8	39	32	53	3	84						
	65797.	67034.	61015.	13145	47823.						
-4	37	89	35	7.1	76						
	23930.	16662.	16815.	37739.							
7	47	5	02	2	13358						
	19910.	15371.	13355.	30536.	9967.4						
10	36	94	96	15	62						
	15953	15701	15491	29992	95784.						
20	1.3	3.4	8	9.8	51						

iii) Signal remaining (%)

CPD Position	Expt 1 0	0.5	1	2	4	t50%	CPD position	Expt 2 0	0.5	1	2	4	t50%
	10	131.7	121.7	194.4	100.1			10	67.9125	61.6717	57.9440	42.8389	
-430	0	356	686	285	997	6	-430	0	8402	6359	7185	2631	2.9
	10	124.9	223.1	290.9	233.6			10	124.969	97.6958	96.6912	41.9724	
-408	0	968	147	99	363	6	-408	0	9914	68	7279	4195	4
	10	103.9	104.2	295.1	112.3			10	115.291	112.279	110.792	90.7589	
-371	0	382	007	173	356	6	-371	0	0174	8833	7587	7423	6
	10	315.9	314.3	358.3	250.6			10	128.501	126.332	130.636	103.850	
-330	0	92	107	326	96	6	-330	0	1573	9648	7451	3585	6
	10	154.2	253.3	347.2	153.1			10	166.742	155.623	170.314	140.582	
-317	0	865	269	821	787	6	-317	0	8861	0016	3255	138	6
	10	129.9	138.8	251.3	104.4			10	124.147	115.469	115.835	94.5074	
-297	0	03	373	397	851	6	-297	0	107	4701	0982	2119	6
	10	233.5	210.0	141.5	86.49			10	167.364	198.338	174.813	168.905	
-275	0	354	968	197	087	6	-275	0	5282	2682	5101	2008	6
	10	126.4	107.4	200.6	97.62			10	130.867	126.447	123.960	78.4559	
-266	0	851	223	197	019	6	-266	0	634	6042	9897	7421	6
	10	100.9	96.70	202.6	118.5			10	120.342	116.525	119.768	96.9629	
-244	0	942	732	742	758	6	-244	0	1012	5283	136	2174	6
	10	114.4	105.6	214.0	96.11			10	132.168	114.363	97.7814	62.8766	
-240	0	523	803	248	15	6	-240	0	0221	7132	4958	6244	5.4
	10	139.9	111.6	268.9	118.0			10	120.705	128.249	145.339	69.0619	
-227	0	813	853	618	172	6	-227	0	4295	3748	7352	3128	6
	10	94.96	63.34	105.5	53.75			10	119.523	108.185	80.9349	55.7011	
-145	0	567	618	771	872	5.3	-145	0	6794	9957	0256	2972	4.4
	10	97.44	83.32	166.0	85.32			10	109.338	99.6091	96.2921	86.7260	
-128	0	943	253	58	718	6	-128	0	6285	9489	4651	6779	6
	10	102.3	84.65	182.5	89.40			10	126.546	115.350	120.921	102.996	
-114	0	493	726	304	198	6	-114	0	7856	2587	5184	1465	6
	10	82.35	58.95	114.5	70.68			10	119.973	109.370	101.775	85.2618	
-102	0	645	244	498	451	6	-102	0	3531	8778	3683	3043	6
	10	93.23	80.86	126.0	54.61			10	101.646	80.6972	65.6751	47.8498	
-98	0	876	503	706	764	6	-98	0	0928	5522	0014	5595	3.6
	10	97.75	81.59	133.0	54.60			10	142.069	108.557	96.3708	71.1627	
-93	0	831	58	86	438	6	-93	0	582	5454	4647	5416	5.9
	10	95.82	78.81	129.0	55.43			10	125.686	105.272	93.9369	68.1387	
-88	0	694	916	673	948	6	-88	0	4827	3271	0708	561	5.8
	10	97.22	77.87	129.2	46.00			10	123.334	98.1821	75.6182	47.5009	
-83	0	152	076	93	889	5.3	-83	0	6273	3682	9995	8893	3.8
	10	94.79	79.38	140.8	41.77			10	90.0629	63.4189	66.2834	38.1345	
-71	0	086	357	014	576	5.3	-71	0	8038	6279	6791	504	3
	10	95.56	79.87	128.1	45.32			10	128.311	95.9958	77.6886	50.4373	
-64	0	603	072	514	546	5.2	-64	0	5652	1515	6334	6006	4
	10	105.6	78.34	137.6	60.21			10	86.8778	82.3795	60.0550	47.0633	
-42	0	248	921	727	101	6	-42	0	1023	0818	7483	0287	3.4
	10	98.55	85.88	148.9	52.58			10	92.1400	86.4758	56.9286	47.0066	
-27	0	718	818	009	148	6	-27	0	7555	3067	4495	0163	3.4
	10	116.6	96.88	230.3	81.56								
-8	0	764	749	412	348	6							
	10	101.8	92.73	199.7	72.68								
-4	0	808	221	909	34	6							
	10	69.62	70.26	157.7	55.82								
7	0	88	613	035	004	6							
	10	77.20	67.08	153.3	50.06								
10	0	575	043	681	169	6							
	10	98.42	97.10	188.0	60.04								
20	0	169	82	069	121	6							
	10	117.7	112.2	190.5	89.33	5.896		10	120.196	108.977	101.580	75.5979	5.026
Average	0	078	909	81	047	429	Average	0	7009	963	8275	2588	087

A.V.4.3 CPD repair statistics

TS	*Wtalpha TAM*	*Gcn5alpha TAM*
Mean	3.813056	5.916667
Variance	1.104036	0.104885
Observations	30	30
Pearson Correlation	0.322086	
Hypothesized Mean Difference	0	
df	29	
t Stat	-11.5817	
P(T<=t) one-tail	1.07E-12	
t Critical one-tail	2.462021	
P(T<=t) two-tail	2.13E-12	
t Critical two-tail	2.756386	

TS mean = -2.1, SD = 0.99, CI (95%) = 0.37

NTS	*Wtalpha TAM*	*Gcn5alpha TAM*
Mean	3.857024	5.514286
Variance	0.483464	0.433698
Observations	28	28
Pearson Correlation	0.418624	
Hypothesized Mean Difference	0	
df	27	
t Stat	-12.003	
P(T<=t) one-tail	1.23E-12	
t Critical one-tail	2.47266	
P(T<=t) two-tail	2.47E-12	
t Critical two-tail	2.770683	

NTS mean = -1.65, SD = 0.73, CI (95%) = 0.28

A.V.5 rtPCR data

a) TAM primers

Gcn5Δα TAM		Input (IN)	Adjusted IN	IP	Adjusted IP (IP/IN)
Expt 1	**U**	0.21	1.00	0.16	0.16
	0	0.20	0.96	0.07	0.08
	1	0.16	0.75	0.04	0.05
	2	0.17	0.82	0.06	0.07
Expt 2	**U**	0.12	1.00	0.08	0.08
	0	0.14	1.16	0.04	0.04
	1	0.13	1.05	0.04	0.03
	2	0.12	1.05	0.03	0.03
Expt 3	**U**	0.07	1.00	0.06	0.06
	0	0.06	0.86	0.03	0.03
	1	0.07	0.94	0.00	0.00
	2	0.07	1.00	0.02	0.02

		Average IP	Normalised	Adjusted	Standard deviation
WTα TAM	**U**	0.36	1.00		0.21
	0	0.31	0.87		0.12
	1	0.33	0.90		0.12
	2	0.49	1.35		0.18
Gcn5Δα TAM	**U**	0.10	0.28	1.00	0.05
	0	0.05	0.14	0.49	0.02
	1	0.04	0.12	0.42	0.01
	2	0.04	0.11	0.39	0.03

b) *MFA2* N1

Gcn5Δα TAM		Input (IN)	Adjusted IN	IP	Adjusted IP (IP/IN)
Expt 1	U	0.02	1.00	0.14	0.14
	0	0.17	7.00	0.04	0.01
	1	0.14	5.92	0.02	0.00
	2	0.14	5.88	0.04	0.01
Expt 2	U	0.10	1.00	0.05	0.05
	0	0.12	1.20	0.03	0.02
	1	0.11	1.08	0.02	0.02
	2	0.11	1.02	0.02	0.02
Expt 3	U	0.07	1.00	0.05	0.05
	0	0.06	0.94	0.02	0.02
	1	0.06	0.98	0.00	0.00
	2	0.06	0.92	0.02	0.02

		Average IP	Normalised	Adjusted	Standard deviation
WTα TAM	U	0.16	1.00		0.08
	0	0.11	0.71		0.04
	1	0.15	0.95		0.08
	2	0.21	1.34		0.08
Gcn5Δα TAM	U	0.08	0.49	1.00	0.05
	0	0.02	0.10	0.20	0.01
	1	0.01	0.08	0.17	0.01
	2	0.01	0.09	0.19	0.01

A.V.6 Nucleosome mapping gel

Low resolution

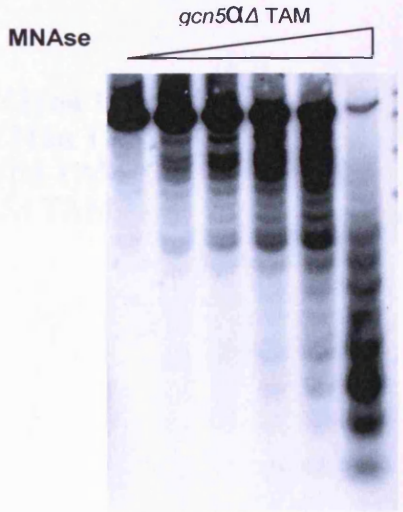

High resolution

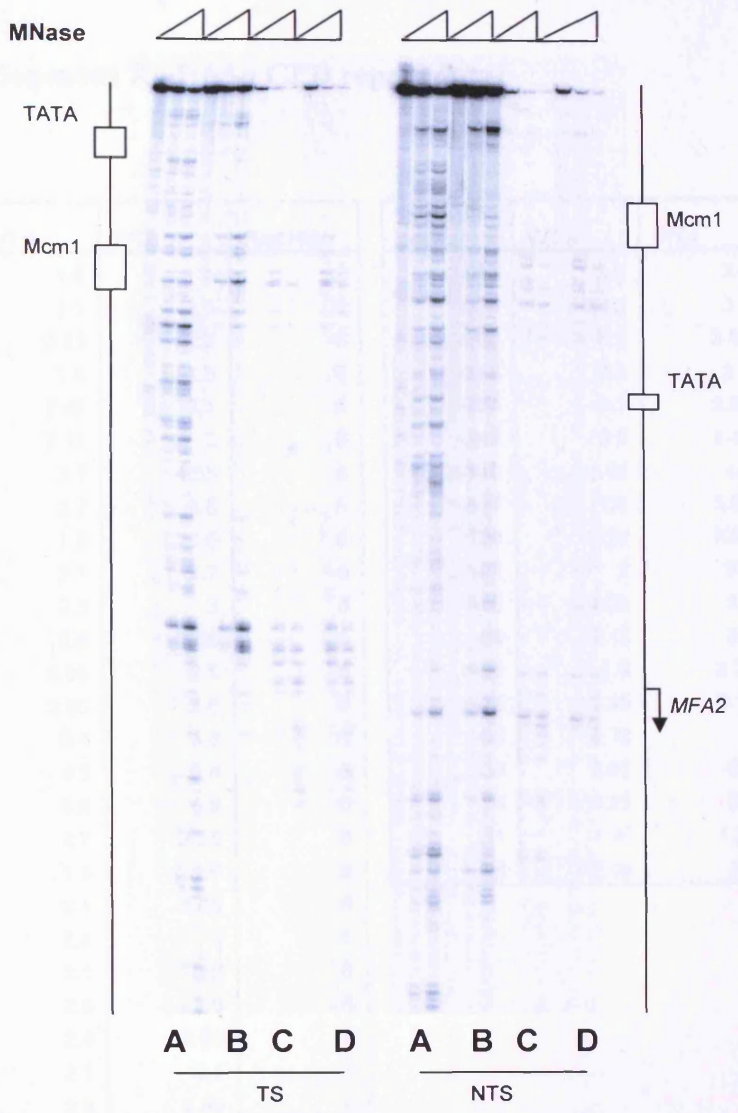

Where: A = PSY316**a** TAM
B = PSY316α TAM
C = *rad16Δ* TAM
D = *gcn5Δ* TAM

Appendix VI

Data from experiments presented in Chapter 7

A.VI.1 Endogenous Rad16Δα CPD repair data

TS

Nucleotide position	WT a	WTα	Rad16Δα
2	1.5	6	6
-16	1.5	3.5	6
-37	0.95	2.2	6
-48	1.6	1.8	6
-108	2.45	3.1	6
-119	2.15	3	6
-133	3.1	4.55	6
-155	2.2	2.8	6
-164	1.8	2.35	6
-174	2.1	2.7	6
-193	2.5	3	6
-198	2.6	2.65	6
-205	2.35	2.5	6
-215	2.95	3.8	6
-231	3.4	3.8	6
-255	4.3	3.8	6
-262	3.5	5.9	6
-293	2.7	2.35	6
-309	1.8	1.5	6
-316	3.1	3.05	6
-320	2.8	3	6
-346	2.1	2.2	6
-358	2.8	2.6	6
-362	2.4	2.85	6
-382	2.1	2.1	6
-431	2.8	2.85	6

NTS

Nucleotide position	WT a	WTα	Rad16Δα
-369	3.2	3.4	6
-330	2.65	3.7	6
-308	3.2	3.85	6
-275	3.1	2.8	6
-264	2.3	2.85	6
-240	3.9	3.45	6
-140	1.95	4.4	6
-137	1.6	3.65	6
-129	2.55	3.95	6
-98	2	3.4	6
-93	2.25	3.4	6
-88	2.45	3.5	6
-82	1.9	2.75	6
-72	2.45	3.15	6
-68	2.75	3	6
-60	2.65	2.3	6
-54	3.65	2.9	6
-51	1.85	1.25	6
-25	3.95	2.1	6

A.VI.2 UV survival

Rad16αΔ TAM, 200 cells/100µl dilution

UV dose (J/m2)	0	10	30	50	100
Rad16α TAM	334	124	6	0	0
	323	169	6	0	0
	350	102	2	0	0
Average	335.67	131.67	4.67	0.00	0.00
Standard deviation	13.58	34.15	2.31	0.00	0.00
% Survival	**100**	**39.22542**	**1.390268**	**0**	**0**

A.VI.3 Southern blotting

The data represent the band intensities obtained using ImageQuant software, and the average ratios between *MFA2*^{TAM} and g*MFA2* which provides an average copy number estimation.

Strain	TAM borne *MFA2*	g*MFA2*	Ratio
Rad16αΔ TAM	131885113.4	6778090.0	19.5
	26800221.9	390890.8	
	19950115.2	1070022.1	18.6
Average			**21.6**
Standard deviation			4.1

Statistical analysis: Students t-test assuming equal variances (alpha value = 0.01).

	Rad16Δα TAM	WTα TAM
Mean	21.57	29.4002538
Variance	17.1698	50.9869886
Observations	2	2
Pooled Variance	34.07839432	
Hypothesized Mean Difference	0	
df	2	
t Stat	-1.341331977	
P(T<=t) one-tail	0.155918094	
t Critical one-tail	6.964556734	
P(T<=t) two-tail	0.311836188	
t Critical two-tail	9.9248432	

A.VI.4 Northern blotting

The data represent the relative band intensities quantified using ImageQuant software. Using *ACT1* as an internal control, relative *MFA2* mRNA levels were obtained. These figures were then normalised against mRNA levels in WT**a** cells to provide an average mRNA level.

Strain	ACT1	MFA2
Rad16αΔ TAM	6572101	
	625322.7	476177.9
	48597136	

	WT a	WT a TAM	WTα TAM	Rad16Δα TAM
	1.000	75.438	0.400	0.000
	1.000	12.166	0.000	0.000
	1.000	51.659	0.080	0.003
AVERAGE	1.000	46.421	0.160	0.001
ST DEV	0.000	31.960	0.211	0.002

A.VI.5 CPD repair

A.VI.5.1 Rad16Δα TAM TS

i) Band density values

CPD Position	Expt 1					CPD position	Expt 2				
	0	0.5	1	2	4		0	0.5	1	2	4
Top bands	23484 04	26028 73	23005 67	22429 14	25561 00	Top bands	28333218 .30	37062210 .09	####### ###	####### ###	51905949 .1
1	14439. 23	15526. 61	13306. 59	10496. 86	6021.3 76	1	150004.5 8	38512.28 105132.4	175609.8 1	18622.15	75779.17
-20	15104. 18	17475. 59	14127. 99	8721.1 06	5366.9 43	-20	13780.04	1	43495.93	23086.84	21208.44
-48	28772. 86	25565. 16	18820. 77	10121. 18	9364.2 83	-48	291152.7 7	456272.9 8	335308.5 3	335599.1 5	321368.0 7
-108	52310. 77	57700. 36	50272. 55	39060. 89	24160. 83	-108	422741.6 7	637239.7 6	609840.0 1	639192.1 8	820964.8 2
-119	25373. 71	28952. 23	24171. 78	18922. 45	16662. 61	-119	249068.3 1	366903.9 7	364531.1	391788.3 2	458536.6 4
-132	9348.1 44	11262. 2	11390. 69	10284. 43	7828.2 03	-132	131553.8	159580.4 7	153301.6 4	154014.9 8	197233.1 6
-155	15273 6.4	17842 8.3	14750 8.5	12494 4.3	92075. 96	-155	952836.4 4	1643472. 74	1590800. 2	1702590. 94	2161028. 4
-164	57453. 1	53572. 88	47024. 6	30384. 32	16078. 98	-164	336352.7 9	559968.0 4	504800.7 1	634988.9 9	701918.6
-175	16486 8	17923 2.9	16041 9	11379 3.4	73209. 19	-175	1511527. 44	2222268. 19	2001452. 94	2190563. 87	2765691. 77
-192	37572. 76	53303. 6	35578. 98	24949. 36	13127. 08	-192	399351.5 2	690308.6 5	515983.1 2	590650.0 1	869185.8 5
-197	33419. 59	46544. 23	33059. 17	22592. 12	11010. 18	-197	390653.5 3	570196.6 9	489427.4 4	623462.0 8	671040.7
-204	58369. 72	71294. 21	43429. 04	26525. 19	15532. 99	-204	620603.1 7	919960.5 7	823767.6 7	953187.9 9	1177231. 7
-215	13961. 76	19042. 93	10347. 29	8984.7 72	6210.1 34	-215	188889.7 6	250353.7 1	206245.7 7	275143.8 3	346006.5 5
-232	35660. 33	42061. 29	27924. 69	32359. 27	17792. 31	-232	255292.0 3	390575.1 1	287891.9 6	361050.5 9	528291.7 4
-256	78450. 96	87088. 11	66478. 31	68712. 28	47824. 06	-256	776347.7	1149659. 3	975471.1 1	1069140. 88	1449500. 13
-262	35295. 88	36659. 88	29074. 33	27425. 18	18878. 61	-262	244563.2 9	362240.9	337914.3 7	356953.0 6	465398.2 5
-274	20390. 6	24388. 36	16964. 12	18370. 7	11549. 08	-274	211600.4 1	230569.7 1	242443.5 3	293314.6 3	320044.1 8
-280	22212. 4	23399. 91	17686. 11	14944. 58	9198.4 64	-280	197659.2 3	273780.9 3	220152.9 5	219866.2 7	313794.2 8
-293	17733. 46	18276. 54	11433. 38	7191.0 85	4598.7 65	-293	201855.4 9	264057.6 7	245503.5 4	260900.4 5	347322.1 6
-311	10436. 21	14341. 53	10057. 44	6760.8 64	3778.7 97	-311	207815.3	132077.1 4	289227.2 7	112601.4 1	218399.7 3
-316	15172. 91	18177. 71	11738. 65	8779.6 64	4502.1 66	-316	178397.3 8	350530.5 1	187900.4	191261.0 9	212847.8 5
-320	33774. 86	38747. 41	26468. 18	23634. 04	12084. 93	-320	305551.0 7	390491.3 5	353047.7 1	332273.0 3	346855.1 6
-345	62839. 08	67239. 97	42451. 98	41774. 94	24450. 12	-345	578678.6 2	806043.2 2	654725.9	735155.2	893033.3 2
-352	22477. 44	23843. 7	16159. 7	18227. 52	12720. 02	-352	147139.9 1	211615.4 3	193898.8 7	200690.0 5	233863.6 6
-358	56666. 42	60854. 94	43027. 5	48364. 93	36034. 6	-358	557471.5 9	615339.3 8	715662.3	833286.5 7	847459.0 6
-362	47170. 88	48156. 22	36835. 22	36884. 87	26175. 48	-362	529818.3 2	636586.1 4	640444.6 1	686119.5 5	920521.6 1
-382	70373. 36	71694. 32	48324. 56	49238	25785. 27	-382	607643.8 8	758715.1 7	717313.0 7	899076.2 5	1095788. 78
-390	10783 3.8	11499 2.1	79748. 25	82249. 01	43015. 76	-390	1210312. 09	1512320. 34	1358712. 52	1719623. 33	2093247. 03
-397	47835. 06	51491. 44	34060. 77	37644. 78	21724. 92	-397	432855.6 1	590910.4 6	528879.7	748272.6 7	869533.9 6
-402	5874.8 37	6858.1 08	4695.4 33	4407.7 44	2765.7 36	-402	166392.8 7	197052.9 2	148334.9 4	257904.4 7	319888.7 3
Total	37023 32	41090 46	34331 52	32196 64	31756 28	Total	40801128 .91	54554946 .23	####### ###	####### ###	73968932 .61
Ratio	1	1.1098 53	0.9272 95	0.8696 31	0.8577 37	Ratio	1.00	1.34	1.26	1.41	1.81

ii) Adjusted band density values

	Expt 1						Expt 2				
CPD Position	0	0.5	1	2	4	CPD position	0	0.5	1	2	4
	14439.	13989.	14349.	12070.	7020.0		150004.5		139408.0		
1	23	79	91	47	72	1	8	28802.97	0	13234.45	41799.65
	15104.	15745.	15235.	10028.	6257.0						
-20	18	86	71	51	96	-20	13780.04	78627.54	34529.28	16407.43	11698.54
	28772.	23034.	20296.	11638.	10917.		291152.7	341242.2	266184.9	238504.6	177266.0
-48	86	72	43	48	43	-48	7	5	6	5	4
	52310.	51989.	54214.	44916.	28168.		422741.6	476585.6	484122.0	454263.0	452842.7
-108	77	18	22	61	11	-108	7	0	1	9	0
	25373.	26086.		21759.	19426.		249068.3	274404.0	289383.3	278437.3	252927.9
-119	71	54	26067	17	25	-119	1	1	2	5	8
	9348.1	10147.	12283.	11826.	9126.5		131553.8	119348.7	121698.6	109455.8	108793.4
-132	44	47	79	2	77	-132	0	3	4	5	5
	152736	160767	159074	143675	107347		952836.4	1229137.	1262858.	1210002.	1192019.
-155	.4	.5	.1	.1	.5	-155	4	74	09	64	34
	57453.	48270.	50711.	34939.	18745.		336352.7	418794.8	400736.4	451275.9	387177.0
-164	1	23	61	32	82	-164	9	1	7	6	3
		161492	172996	130852	85351.		1511527.	1662013.	1588855.	1556796.	1525550.
-175	164868	.4	.9	.5	56	-175	44	39	12	77	56
	37572.	48027.	38368.	28689.	15304.		399351.5	516275.3	409613.6	419764.9	479441.3
-192	76	6	58	59	32	-192	2	2	4	9	4
	33419.	41937.	35651.	25978.	12836.		390653.5	426444.7	388532.3	443083.9	370144.8
-197	59	28	21	96	32	-197	3	2	9	8	3
	58369.	64237.	46834.	30501.	18109.		620603.1	688029.8	653948.6	677414.6	649358.8
-204	72	51	14	65	27	-204	7	2	7	2	7
	13961.	17158.	11158.	10331.	7240.1		188889.7	187237.1	163728.3	195540.0	190856.5
-215	76	06	58	7	37	-215	6	7	8	8	8
	35660.	37898.	30114.	37210.	20743.		255292.0	292107.4	228543.2	256592.5	291404.7
-232	33	06	16	34	32	-232	3	4	8	6	6
	78450.	78468.	71690.	79013.	55756.		776347.7	859819.3	774378.5	759820.3	799541.6
-256	96	13	61	12	09	-256	0	3	7	8	4
	35295.	33031.	31353.	31536.	22009.		244563.2	270916.5	268253.6	253680.5	256712.8
-262	88	28	93	56	78	-262	9	5	1	1	3
	20390.	21974.	18294.	21124.	13464.		211600.4	172440.9	192464.0	208453.7	176535.7
-274	6	4	21	7	59	-274	1	1	0	6	9
	22212.	21083.	19072.	17184.	10724.		197659.2	204758.1	174768.6	156255.2	173088.3
-280	4	78	81	96	11	-280	3	7	1	5	6
	17733.	16467.	12329.	8269.1	5361.5		201855.4	197486.2	194893.1	185417.5	191582.2
-293	46	52	82	2	09	-293	9	4	9	5	7
	10436.	12922.	10846.	7774.4	4405.5		207815.3		229603.3		120468.8
-311	21	01	01	03	42	-311	0	98779.25	1	80023.92	9
	15172.	16378.	12659.	10095.	5248.8		178397.3	262158.4	149164.8	135926.0	117406.4
-316	91	48	03	85	88	-316	8	6	9	3	9
	33774.	34912.	28543.	27177.	14089.		305551.0	292044.7	280267.2	236140.8	191324.6
-320	86	19	45	08	31	-320	7	9	3	3	8
	62839.	60584.	45780.	48037.	28505.		578678.6	602832.1	519754.7	522462.3	492595.5
-345	08	56	47	53	38	-345	2	1	1	9	6
	22477.	21483.	17426.	20960.	14829.		147139.9	158265.1	153926.7	142627.0	128998.7
-352	44	65	71	06	75	-352	1	8	8	3	7
	56666.	54831.	46401.	55615.	42011.		557471.5	460206.5	568129.1	592202.7	467456.8
-358	42	51	12	45	25	-358	9	1	3	0	8
	47170.	43389.	39723.	42414.	30516.		529818.3	476096.7	508417.5	487613.5	507758.0
-362	88	72	32	38	91	-362	2	6	0	8	5
	70373.	64598.	52113.	56619.	30061.		607643.8	567435.9	569439.5	638958.3	604435.1
-382	36	01	49	4	97	-382	8	1	9	2	0
	107833	103610	86000.	94579.	50150.		1210312.	1131050.	1078615.	1222107.	1154631.
-390	.8	.2	99	18	28	-390	09	10	09	28	26
	47835.	46394.	36731.	43288.	25328.		432855.6	441936.3	419851.6	531784.7	479633.3
-397	06	81	34	21	19	-397	1	5	0	6	5
	5874.8	6179.2	5063.5	5068.5	3224.4		166392.8	147374.0	117755.8	183288.3	176450.0
-402	37	92	83	21	57	-402	7	2	2	5	4

iii) Signal remaining (%)

CPD Position	Expt 1					t50%	CPD position	Expt 2					t50%
	0	0.5	1	2	4			0	0.5	1	2	4	
	10	96.887	99.381	83.594	48.618			10				27.865	
1	0	32	4	96	04	4.2	1	0	19.2014	92.9358	8.8227	6	1.5
	10	104.24	100.87	66.395	41.426			10	570.590	250.574	119.066	84.894	
-20	0	83	08	59	25	3.5	-20	0	0	6	6	8	4.6
	10	80.057	70.540	40.449	37.943			10	117.203			60.884	
-48	0	13	2	51	5	2.6	-48	0	8	91.4245	81.9174	2	4.8
	10	99.385	103.63	85.864	53.847			10	112.736	114.519	107.456	107.12	
-108	0	22	87	93	62	4.7	-108	0	8	6	4	04	6
	10	102.80	102.73	85.754	76.560			10	110.172	116.186	111.791	101.54	
-119	0	93	23	79	54	6	-119	0	2	3	6	96	6
	10	108.55	131.40	126.50	97.629			10				82.698	
-132	0	06	35	85	82	6	-132	0	90.7224	92.5086	83.2023	8	6
	10	105.25	104.14	94.067	70.282			10	128.997	132.536	126.989	125.10	
-155	0	81	95	36	9	6	-155	0	8	7	5	22	6
	10	84.016	88.266	60.813	32.628			10	124.510	119.141	134.167	115.11	
-164	0	76	1	63	03	3	-164	0	6	7	4	04	6
	10	97.952	104.93	79.368	51.769			10	109.955	105.115	102.994	100.92	
-175	0	52	05	01	62	4.3	-175	0	9	9	9	77	6
	10	127.82	102.11	76.357	40.732			10	129.278	102.569	105.111	120.05	
-192	0	56	81	42	48	3.6	-192	0	4	7	7	50	6
	10	125.48	106.67	77.735	38.409			10	109.161		113.421	94.750	
-197	0	71	76	73	55	3.6	-197	0	9	99.4570	2	2	6
	10	110.05	80.237	52.255	31.025			10	110.864	105.373	109.154	104.63	
-204	0	28	06	94	11	2.8	-204	0	7	1	2	35	6
	10	122.89	79.922	74.000	51.856			10			103.520	101.04	
-215	0	33	49	02	92	3.9	-215	0	99.1251	86.6793	7	13	6
	10	106.27	84.447	104.34	58.169			10	114.420		100.509	114.14	
-232	0	51	21	66	17	5.6	-232	0	9	89.5223	4	57	6
	10	100.02	91.382	100.71	71.071			10	110.751			102.98	
-256	0	19	71	66	27	6	-256	0	8	99.7464	97.8711	76	6
	10	93.583	88.831	89.349	62.357			10	110.775	109.686	103.728	104.96	
-262	0	96	69	11	93	5.7	-262	0	6	8	0	79	6
	10	107.76	89.718	103.60	66.033			10				83.428	
-274	0	73	85	02	33	6	-274	0	81.4937	90.9563	98.5129	8	6
	10	94.918	85.865	77.366	48.279			10	103.591			87.569	
-280	0	97	58	5	81	4	-280	0	5	88.4191	79.0528	1	6
	10	92.861	69.528	46.630	30.233			10				94.910	
-293	0	3	56	03	85	2.5	-293	0	97.8355	96.5509	91.8566	6	6
	10	123.81	103.92	74.494	42.213			10		110.484		57.969	
-311	0	89	66	48	99	3.7	-311	0	47.5322	3	38.5072	2	3.9
	10	107.94	83.431	66.538	34.593			10	146.952			65.811	
-316	0	55	77	63	81	3.1	-316	0	0	83.6138	76.1928	8	4.8
	10	103.36	84.510	80.465	41.715			10				62.616	
-320	0	74	93	42	38	3.7	-320	0	95.5797	91.7252	77.2836	3	5.2
	10	96.412	72.853	76.445	45.362			10	104.173			85.124	
-345	0	24	51	32	5	3.7	-345	0	9	89.8175	90.2854	2	6
	10	95.578	77.529	93.249	65.976			10	107.561	104.612		87.670	
-352	0	73	81	32	15	6	-352	0	0	5	96.9329	8	6
	10	96.761	81.884	98.145	74.137			10		101.911	106.230	83.853	
-358	0	91	68	33	81	6	-358	0	82.5525	8	1	0	6
	10	91.984	84.211	89.916	64.694			10				95.836	
-362	0	11	54	45	38	6	-362	0	89.8604	95.9607	92.0341	3	6
	10	91.793	74.052	80.455	42.717			10			105.153	99.471	
-382	0	27	87	72	83	3.6	-382	0	93.3830	93.7127	4	9	6
	10	96.083	79.753	87.708	46.507			10			100.974	95.399	
-390	0	22	29	3	02	4.1	-390	0	93.4511	89.1188	6	5	6
	10	96.989	76.787	90.494				10	102.097		122.855	110.80	
-397	0	14	48	74	52.949	4.6	-397	0	9	96.9958	0	68	6
	10	105.18	86.191	86.275	54.885			10			110.154	106.04	
-402	0	24	04	09	89	4.6	-402	0	88.5699	70.7698	0	42	6
	10	102.22	89.659	81.645	52.487	4.4366		10	116.770	103.754	96.5250	92.174	5.6266
Average	0	57	21	47	65	67	Average	0	117	251	279	91	67

A.VI.5.2 Rad16Δα TAM NTS

i) Band density values

CPD Position	Expt 1					CPD position	Expt 2				
	0	0.5	1	2	4		0	0.5	1	2	4
	311013	310253	297635	361160	367178		403591	498288	459573	498299	641923
	3	3	7	0	9		62	94	83	92	63
	235823.	201739.	161996.	152343.	75364.4		238974	324688	232970	290233	317547
-430	6	3	7	8	7	-430	9	4	0	7	0
	19995.8		4115.96	2574.77	3757.18		251543.	372840.		391050.	
-408	2	14972.3	9	6	7	-408	6	9	382739	3	361483
	83262.9	77699.7	76742.5	72349.6	30664.8		701145.	992699.	103820	967660.	992936.
-371	1	2	9	3	1	-371	4	6	7	8	8
	28462.4	27162.9	34259.1		14270.9		249836.	363515.	293780.	267564.	345087.
-330	8	1	9	27991.9	3	-330	5	2	8	9	2
	25217.3	24956.5	32936.6	29200.0	13339.2		354714.	398089.	320974.	304311.	373287.
-317	2	1	1	6	2	-317	6	1	2	7	8
	213675.	179449.	191312.		92795.0		143931	199407	183185	166537	206986
-297	3	3	4	187265	3	-297	7	7	4	6	9
	14115.5	12479.2					111973.	77063.5	128659.	113641.	104593.
-275	9	3	13557.8	15949.9	4267.12	-275	3	9	4	9	7
	80481.8	64071.7	62631.2		16138.9		877050.	101851		785579.	981889.
-266	6	4	5	49852.3	7	-266	7	0	868355	8	5
	63728.3	62103.6	67823.4	66386.1	36283.4		461612.	613813.	536653.		551835.
-244	2	2	9	7	7	-244	5	6	4	503270	4
	70870.3	60741.0		56863.7	25195.6		561740.	669758.	549342.	460600.	442717.
-240	1	5	58187.5	2	5	-240	9	3	2	3	7
	8515.76	7328.27	8090.00	8330.39	2922.00		89233.1	100751.	75599.0	89583.1	96860.5
-227	9	9	3	2	4	-227	4	6	5	2	3
	21630.4	20446.8	15428.8	8565.85	6016.79		134230.	186391.	165840.	144149.	153237.
-145	7	2	4	5	8	-145	7	1	6	3	7
	42711.5	39404.0	39877.3		21811.3		320251.	380381.	327011.	256193.	297400.
-128	3	4	6	35947.4	1	-128	9	6	1	8	2
	24493.4	21552.0	22952.3	20622.8	10036.3		148852.	190691.	131705.	119409.	134358.
-114	9	6	6	7	4	-114	8	1	4	1	7
	8675.99	7984.63	8328.88		3118.69		90991.4	36949.6	59660.7	50694.9	57700.4
-102	5	3	9	3839.19	5	-102	8	4	8	6	5
	73509.8	61494.0	51617.2	33563.9	15214.8		643230.	785650.	580877.	213127.	295228.
-98	3	6	4	9	5	-98	7	8	2	7	4
	94295.6		72688.0	48629.3	21621.0		651384.	768093.	670225.	337658.	527944.
-93	4	82733.9	5	1	1	-93	5	7	7	8	6
	20961.4		14474.2	9593.72	3385.70		180497.	227971.	150683.	128830.	141847.
-88	9	16924.9	5	2	1	-88	3	6	2	5	3
	123157.		79976.6	47089.2	15802.3		113934	132030	900928.	728849.	679587.
-83	3	96602	1	9	8	-83	2	8	5	6	5
	57719.6	48682.9	41426.1	27462.4	10997.5		404863.	696354.	446732.	327572.	285332.
-71	4	2	8	8	6	-71	1	9	5	2	6
	55042.0	44830.5		24057.4	12505.9		395725.	519498.	330080.	262160.	279144.
-64	9	2	37215.7	3	1	-64	4	9	2	5	4
	9462.03		10126.6	5624.56	3970.94		167502.	201622.	110407.	163162.	42285.6
-42	9	10742.6	2	7	1	-42	8	7	8	6	7
	94693.6	89658.6	75992.7	45414.1	26782.3		635255.	110682	810101.	338308.	893337.
-27	6	1	1	2	4	-27	4	9	5	3	2
	4930.49	4784.39	4507.09	3354.22	2783.32		42216.9	149032.		100178.	105146.
-8	4	5	2	4	9	-8	5	4	172230	8	4
	7889.37	8027.42	7379.01	5940.93	3628.18		443646.	616205.	511338.		645347.
-4	9	1	8	8	2	-4	8	6	1	392142	9
	50020.9	48157.4	46549.1	35503.5	22067.9		204083.	109845.	122301.	157553.	84524.5
7	1	1	9	2	6	7	1	6	2	8	6
							63389.5	63303.2	63724.1	17619.3	29460.5
						10	6	5	9	6	4
							914480.	884810.	717533.	559978.	334624.
						20	6	4	9	8	4
	464347	443726	421655	463591	416653		######	######	######	######	######
Total	6	3	1	7	1	Total	##	##	##	##	##
		0.95559	0.90805	0.99837	0.89728			1.24792	1.11313		1.44551
Ratio	1	1	9	2	7	Ratio	1	5	5	1.14977	2

ii) Adjusted band density values

CPD Position	Expt 1					CPD position	Expt 2				
	0	0.5	1	2	4		0	0.5	1	2	4
-430	235823.6	211114.7	178398.9	152592.2	83991.48	-430	238974.9	260182.6	209291.8	252427.6	219677.9
-408	19995.82	15668.11		2578.974	4187.274	-408	251543.6	298768.7	343838.7	340111.8	250072.7
-371	83262.91	81310.66	84512.77		34175.03	-371	701145.4	795480.2	932687.2	841612.5	686910.2
-330	28462.48	28425.26	37727.93	28037.54	15904.54	-330	249836.5	291295.8	263922	232711.7	238730.1
-317	25217.32	26116.32	36271.44	29247.67	14866.17	-317	354714.6	319000.8	288351.5	264671.8	258239.2
-297	213675.3	187788.8	210682.8	187570.4	103417.3	-297	143931.7	159791.4	164567.1	144844.3	143192.8
-275	14115.59	13059.17	14930.53	15975.91	4755.586	-275	111973.3	61753.39	115582.9	98838.86	72357.56
-266	80481.86	67049.35	68972.65	49933.59	17986.41	-266	877050.7	816162.9	780098.5	683249.5	679267.7
-244	63728.32	64989.76	74690.62	66494.42	40436.86	-244	461612.5	491867.4	482109.9	437713.6	381757.8
-240	70870.31	63563.87	64078.94	56956.41	28079.81	-240	561740.9	536697.6	493509.1	400602.6	306270.6
-227	8515.769	7668.846	8909.115	8343.975	3256.487	-227	89233.14	80735.32	67915.45	77913.95	67007.78
-145	21630.47	21397.04	16991	8579.822	6705.544	-145	134230.7	149360.9	148985.2	125372.3	106009.3
-128	42711.53	41235.26	43914.94	36006.02	24308.06	-128	320251.9	304811.3	293774.8	222821.7	205740.4
-114	24493.49	22553.65	25276.28	20656.51	11185.21	-114	148852.8	152806.6	118319.3	103854.8	92948.89
-102	8675.995	8355.705	9172.188	3845.454	3475.694	-102	90991.48	29608.87	53597.07	44091.39	39916.97
-98	73509.83	64351.87	56843.47	33618.72	16956.55	-98	643230.7	629565.8	521838.9	185365.5	204238
-93	94295.64	86578.79	80047.71	48708.68	24095.98	-93	651384.5	615496.8	602106.4	293675.1	365230.2
-88	20961.49	17711.45	15939.79	9609.369	3773.269	-88	180497.3	182680.6	135368.3	112048.9	98129.47
-83	123157.3	101091.4	88074.23	47166.08	17611.28	-83	113934.2	105800.3	809361.3	633909.1	470136.3
-71	57719.64	50945.37	45620.57	27507.26	12256.46	-71	404863.1	558010.3	401328.2	284902.4	197392.1
-64	55042.09	46913.93	40983.79	24096.66	13937.46	-64	395725.4	416290.2	296532	228011.3	193111.1
-42	9462.039	11241.84	11151.99	5633.739	4425.499	-42	167502.8	161566.3	99186.33	141908.9	29253.08
-27	94693.66	93825.31	83686.96	45488.17	29848.13	-27	635255.4	886935.6	727765.7	294240	618007.6
-8	4930.494	5006.744	4963.434	3359.693	3101.938	-8	42216.95	119424.1	154725.2	87129.45	72739.89
-4	7889.379	8400.479	8126.149	5950.625	4043.509	-4	443646.8	493784.2	459367.5	341061.3	446449.4
7	50020.91	50395.43	51262.29	35561.41	24594.09	7	204083.1	88022.64	109870.4	137030.9	58473.87
10						10	63389.56	50726.81	57247.49	15324.25	20380.75
20						20	914480.6	709025.3	644606.3	487035.5	231492

iii) Signal remaining (%)

CPD Position	Expt 1 0	0.5	1	2	4	t50%	CPD position	Expt 2 0	0.5	1	2	4	t50%
	10	89.522	75.649	64.706	35.616			10	108.87	87.578	105.62	91.925	
-430	0	33	31	11	24	3	-430	0	45	99	94	12	6
	10	78.356	22.668	12.897	20.940			10	118.77	136.69	135.20	99.415	
-408	0	92	29	57	75	1.4	-408	0	41	15	99	23	6
	10	97.655	101.50	87.034	41.044			10	113.45	133.02	120.03	97.969	
-371	0	31	11	67	72	4	-371	0	44	34	4	73	6
	10	99.869	132.55	98.507	55.878			10	116.59	105.63	93.145	95.554	
-330	0	23	32	04	96	5.3	-330	0	46	79	61	55	6
	10	103.56	143.83	115.98	58.952			10	89.931	81.291	74.615	72.801	
-317	0	5	54	25	21	6	-317	0	7	14	42	96	6
	10	87.885	98.599	87.782	48.399			10	111.01	114.33	100.63	99.486	
-297	0	13	51	9	29	4.3	-297	0	89	69	4	63	6
	10	92.515	105.77	113.17	33.690			10	55.150	103.22	88.269	64.620	
-275	0	96	33	92	27	4.1	-275	0	11	37	99	38	6
	10	83.309	85.699	62.043	22.348			10	93.057	88.945	77.903	77.449	
-266	0	89	63	28	4	2.7	-266	0	67	65	08	08	6
	10	101.97	117.20	104.34	63.451			10	106.55	104.44	94.822	82.700	
-244	0	94	16	05	95	6	-244	0	42	04	73	92	6
	10	89.690	90.417	80.367	39.621			10	95.541	87.853	71.314	54.521	
-240	0	41	24	13	4	3.6	-240	0	84	5	39	68	4.2
	10	90.054	104.61	97.982	38.240			10	90.476	76.110	87.315	75.092	
-227	0	65	9	64	67	4	-227	0	83	1	04	93	6
	10	98.920	78.551	39.665	31.000			10	111.27	110.99	93.400	78.975	
-145	0	85	26	45	46	2.6	-145	0	17	18	6	44	6
	10	96.543	102.81	84.300	56.912			10	95.178	91.732	69.577	64.243	
-128	0	63	75	45	17	4.9	-128	0	61	43	03	32	5
	10	92.080	103.19	84.334	45.666			10	102.65	79.487	69.770	62.443	
-114	0	2	59	67	05	4.1	-114	0	61	43	1	48	4.7
	10	96.308	105.71	44.322	40.061			10	32.540	58.903	48.456	43.868	
-102	0	3	91	87	04	3	-102	0	26	4	62	91	2.3
	10	87.541	77.327	45.733	23.066			10	97.875	81.127	28.817	31.751	
-98	0	86	73	63	99	2.4	-98	0	58	8	89	9	2.4
	10	91.816	84.890	51.655	25.553			10	94.490	92.434	45.084	56.069	
-93	0	32	15	21	65	2.6	-93	0	54	86	75	83	3.6
	10	84.495	76.043	45.842	18.000			10	101.20	74.997	62.077	54.366	
-88	0	19	12	96	94	2.3	-88	0	96	43	91	18	3.8
	10	82.083	71.513	38.297	14.299			10	92.860	71.037	55.638	41.263	
-83	0	15	62	43	83	2.1	-83	0	88	6	17	84	3
	10	88.263	79.038	47.656	21.234			10	137.82	99.126	70.370	48.755	
-71	0	49	21	67	47	2.4	-71	0	69	89	05	27	3.8
	10	85.232		43.778	25.321			10	105.19	74.933	57.618	48.799	
-64	0	83	74.459	6	47	2.4	-64	0	67	78	56	26	3.4
	10		117.85	59.540	46.771			10	96.455	59.214	84.720	17.464	
-42	0	118.81	97	43	07	3.7	-42	0	9	73	29	23	2.6
	10	99.082	88.376	48.037	31.520			10	139.61	114.56	46.318	97.284	
-27	0	99	52	19	72	2.8	-27	0	88	27	38	91	6
	10	101.54	100.66	68.141	62.913			10	282.88	366.50	206.38	172.30	
-8	0	64	81	11	34	4.9	-8	0	2	01	5	02	6
	10	106.47	103.00	75.425	51.252			10	111.30	103.54	76.876	100.63	
-4	0	83	1	77	48	4.2	-4	0	12	35	77	17	6
	10	100.74	102.48	71.093	49.167			10	43.130	53.836	67.144	28.651	
7	0	87	17	09	62	4	7	0	79	37	58	96	2.2
								10	80.023	90.310	24.174	32.151	
							10	0	92	6	72	51	2.3
								10	77.533	70.488	53.258	25.314	
							20	0	12	79	16	04	2.4
	10	94.013	94.017	68.178	38.497	3.5692		10	103.62	100.44	78.877	68.424	4.6321
Average	0	71	71	81	2	31	Average	0	43	15	96	08	43

A.VI.5.3 CPD repair statistics

TS	*Wtalpha TAM*	*Rad16alpha TAM*
Mean	3.813056	5.354444
Variance	1.104036	0.322413
Observations	30	30
Pearson Correlation	0.692491	
Hypothesized Mean Difference	0	
df	29	
t Stat	-10.898	
P(T<=t) one-tail	4.53E-12	
t Critical one-tail	2.462021	
P(T<=t) two-tail	9.06E-12	
t Critical two-tail	2.756386	

TS mean = -154, SD = 0.77, CI (95%) = 0.29

NTS	*Wtalpha TAM*	*Rad16alpha TAM*
Mean	3.857024	4.467857
Variance	0.483464	1.060287
Observations	28	28
Pearson Correlation	0.358356	
Hypothesized Mean Difference	0	
df	27	
t Stat	-3.18387	
P(T<=t) one-tail	0.001822	
t Critical one-tail	2.47266	
P(T<=t) two-tail	0.003644	
t Critical two-tail	2.770683	

NTS mean = -0.61, SD = 1.01, CI (95%) = 0.39

A.VI.5.2 Global repair analysis

Having treated repair samples with *ML endo* for 1 hour at 37°C, run samples in a denaturing gel overnight at a low voltage. Smaller DNA fragments migrate further on the gel, therefore *ML endo* cut damaged DNA has a lower molecular weight. As samples repair with time after UV, the samples are repaired, therefore present as higher molecular weight bands.

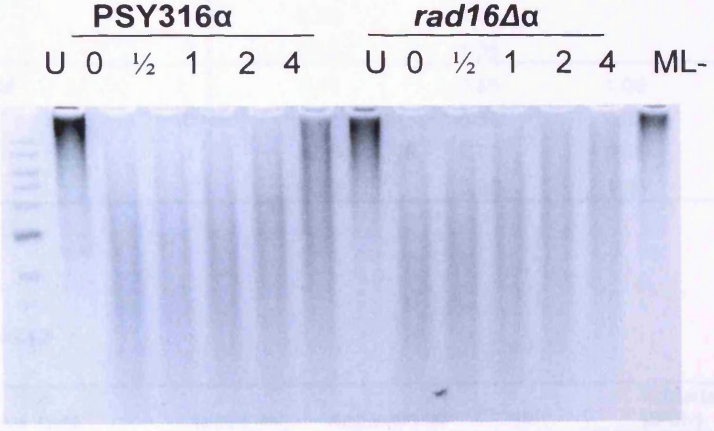

A.VI.6 rtPCR

a) TAM primers

Rad16Δα TAM		Input (IN)	Adjusted IN	IP	Adjusted IP (IP/IN)
Expt 1	U	0.08	0.66	0.25	0.39
	0	0.08	0.69	0.19	0.28
	1	0.07	0.64	0.24	0.38
	2	0.07	0.57	0.26	0.45
Expt 2	U	0.12	1.00	0.21	0.21
	0	0.13	1.08	0.16	0.14
	1	0.15	1.24	0.18	0.14
	2	0.12	0.99	0.19	0.19
Expt 3	U	0.10	1.00	0.32	0.32
	0	0.08	0.80	0.16	0.20
	1	0.12	1.22	0.28	0.23
	2	0.10	0.97	0.33	0.34

		Average IP	Normalised	Adjusted	Standard deviation
WTα TAM	U	0.36	1.00		0.21
	0	0.31	0.87		0.12
	1	0.33	0.90		0.12
	2	0.49	1.35		0.18
Rad16Δα TAM	U	0.31	0.85	1.00	0.09
	0	0.21	0.58	0.67	0.07
	1	0.25	0.70	0.83	0.12
	2	0.33	0.90	1.06	0.13

b) MFA2 primers

Rad16Δα TAM		Input (IN)	Adjusted IN	IP	Adjusted IP (IP/IN)
Expt 1	U	0.09	1.00	0.12	0.12
	0	0.08	0.93	0.07	0.07
	1	0.07	0.81	0.10	0.12
	2	0.06	0.67	0.11	0.16
Expt 2	U	0.12	1.00	0.08	0.08
	0	0.13	1.08	0.04	0.04
	1	0.13	1.15	0.06	0.05
	2	0.11	0.94	0.07	0.07
Expt 3	U	0.12	1.00	0.15	0.15
	0	0.12	1.00	0.07	0.07
	1	0.13	1.13	0.12	0.11
	2	0.10	0.82	0.15	0.18

		Average IP	Normalised	Adjusted	Standard deviation
WTα TAM	U	0.16	1.00		0.08
	0	0.11	0.71		0.04
	1	0.15	0.95		0.08
	2	0.21	1.34		0.08
Rad16Δα TAM	U	0.12	0.73	1.00	0.04
	0	0.06	0.38	0.52	0.02
	1	0.09	0.59	0.81	0.04
	2	0.14	0.87	1.18	0.06

A.VI.7 Nucleosome mapping gel

Low resolution

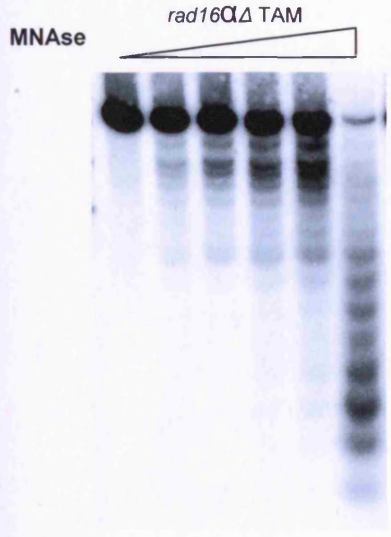

High resolution: see A.V.6

The construction and employment of a system for the *in vivo* and *in vitro* analysis of NER in chromatin.

Rebecca Johnson

School of Medicine,
Cardiff University

Thesis submitted in partial fulfilment of the requirements for the degree of Doctor of Philosophy

DECLARATION

This work has not previously been accepted in substance for any degree and is not concurrently submitted in candidature for any degree.

Signed ..... (candidate) Date .....

STATEMENT 1

This thesis is being submitted in partial fulfillment of the requirements for the degree of PhD.

Signed ..... (candidate) Date .....

STATEMENT 2

This thesis is the result of my own independent work/investigation, except where otherwise stated.
Other sources are acknowledged by explicit references.

Signed ..... (candidate) Date .....

STATEMENT 3

I hereby give consent for my thesis, if accepted, to be available for photocopying and for inter-library loan, and for the title and summary to be made available to outside organisations.

Signed ..... (candidate) Date .....

STATEMENT 4: PREVIOUSLY APPROVED BAR ON ACCESS

I hereby give consent for my thesis, if accepted, to be available for photocopying and for inter-library loans **after expiry of a bar on access previously approved by the Graduate Development Committee.**

Signed ..... (candidate) Date .....

Acknowledgements

I would firstly like to thank my supervisor Professor Ray Waters for his continued support and positive words of advice throughout this study. Many thanks go to Dr. Yumin Teng for his patience in the laboratory, and his invaluable advice and support. I would also like to thank the inspirational group of researchers within the laboratory for their professional help and support throughout the last few years, including Dr. Shirong Yu, Dr. Yachuan Yu, Dr. Huayun Zhang-Jackson, and Dr. Simon Reed. Also thanks go to all at the Department of Pathology, Cardiff School of Medicine for their friendship and encouragement. Thank you especially to Dr. Neil Humphryes and Katie Evans for making my time in the laboratory so enjoyable.

Special thanks go to Alex, whose continued love and support throughout this process has been invaluable. I would also like to thank my family and friends, without which this study would have been made far more difficult. A special mention should be made for my Grandad, who above all has believed in me, and encouraged me throughout.

Thank you to all who have supported me throughout the past few years, helping me achieve as much as I have.

Summary

NER is vital for the integrity of the genome, with defects in NER giving rise to the rare human disorder Xeroderma Pigmentosum. The NER mechanism has been largely elucidated in naked DNA, however the complexities of efficient repair in a chromatin substrate are yet to be unravelled. Metabolic processes in chromatin require the concerted actions of both histone modification agents and ATP-dependant chromatin remodelling complexes to afford access to DNA.

This study has seen the construction of a mini-chromosome containing *MFA2* as a model gene. The TAM plasmid model provides a chromatin environment analogous to that seen at the endogenous *MFA2* gene, and the nucleosome positions have been determined along with the repair profile in wild type cells, and in cells lacking the general repressor Tup1p. When *TUP1* is deleted, repair of CPDs occurs at a faster rate in both the TS and NTS of the *MFA2* promoter. Repair was studied in respect to the HAT Gcn5p, a factor responsible for the H3 acetylation (K9 and K14) of *MFA2,* a prerequisite for efficient transcription initiation and repair. The TAM model showed diminished repair and a reduction in H3 acetylation at the *MFA2* gene when *GCN5* was absent, confirming the role for Gcn5p in repair at this gene, regardless of the chromosomal context. Repair was also investigated in the absence of the GG-NER factor Rad16p. Rad16p has been implicated with roles in chromatin remodelling, as well as the UV-induced occupancy of Gcn5p to promote H3 acetylation. In TAM, the absolute requisite for Rad16p in GG-NER was overcome, suggesting the chromatin environment within the plasmid differs from that seen at the endogenous *MFA2*.

The TAM plasmid has provided a tool to study NER both *in vivo*, as reported here, and *in vitro*, enabling the biochemistry behind the complex mechanism of NER in chromatin to be realised.